SUSTAINABLE SYNTHESIS OF GRAPHENE-BASED MATERIALS AND APPLICATIONS

Thesis submitted by

Muhammad Adeel Zafar

For the Degree of Doctor of Philosophy

College of Science and Engineering

May 2023

Supervisors: Prof. Mohan V. Jacob, Dr. Yang Liu & Prof. Ronald White

DECLARATION

I hereby declare that the work presented in this thesis entitled "*Sustainable synthesis of graphene-based materials and applications*" is my own work and has not been submitted in any form for another degree or diploma at any university or institute of territory education. Information derived from the published and unpublished works of others have been acknowledged in the text and a list of references is given.

Muhammad Adeel Zafar

January 2023

STATEMENT OF ACCESS TO THIS THESIS

I, the undersigned, the author of this work, understand that James Cook University will make this workavailable for use within the University, and via the Australian Digital Thesis Network, for use elsewhere.

I understand that as an unpublished work, a thesis has significant protection under the Copyright Act. Ido not wish to place any restriction on access to this thesis. However, any use of its content must be acknowledged and could be potentially be restricted by future patents.

Muhammad Adeel Zafar

May 2023

ACKNOWLEDGMENTS

Firstly, I would like to thank my primary supervisor, Prof. Mohan V. Jacob for entrusting me with this project and facilitating throughout the course to accomplish my work within the given period. I also want to appreciate him for being considerate and most importantly providing a conducive and healthy research environment to enhance students' creativity. I also cherish my co-supervisor Dr. Yang Liu for teaching me her lifelong learning of electrochemical sensors in a short period and evoking in me an inclination for this field. I also truly acknowledge both of my supervisors for their guidance, feedback, and editing of the writings.

I am grateful to Prof. Oomman K Varghese and Prof. Francisco Hernandez, University of Houston, USA, for collaborating with us and performing part of the characterizations of the samples as well as providing valuable suggestions. Thank you to my senior, Ahmed Al-Jumaili for giving a kick-start to my Ph.D. Special thanks to the technician, John Renehan for his assistance in troubleshooting the apparatuses.

I would like to acknowledge the financial support from James Cook University and Australian Government, through the International training program stipend (IRTPS) and Graduate Research School funding.

I also want to thank my friends and colleagues for their treasured company during my Ph.D. Special thanks to my wife Mehwish for her unwavering support during this journey. Finally, I express gratitude to my parents for their teachings, training, and prayers, which enabled me to accomplish my goals in life.

STATEMENT OF CONTRIBUTION OF OTHERS

This thesis involved the following contributions from others:

Financial assistance: The financial assistance to cover the tuition fees and stipend for this course was provided by James Cook University, Australia, through the International research training program stipend (IRTPS). The funding for the procurement of consumables, sample characterizations, and to attend conferences was received from the Graduate Research School and College of Science and Engineering.

Experimental assistance and data analysis: Prof. Mohan V. Jacob assisted in planning the experiments and arranging all the hardware required for the synthesis experiments. Dr. Yang Liu helped with the experiments and analysis of electrochemical investigations.

Editorial assistance: Prof. Mohan V. Jacob provided editorial assistance for all journal articles and the thesis. Dr. Yang Liu helped in a similar way for all the electrochemical studies.

Contribution to co-authored publications: The assistance in terms of access to advanced characterizations, and partial assistance in editing (chapter 3) was given by Prof. Oomman K Varghese and Prof. Francisco Hernandez, University of Houston, USA.

ABSTRACT

Graphene received lots of attention during the last two decades due to its unique and outstanding characteristics, which will be useful for developing many applications in a wide range of scientific fields. Several graphene synthesis techniques, which include top-down and bottom-up approaches have been developed in the past. Nonetheless, most of the methods have certain drawbacks, such as solvent-assisted multistep procedures, long processing time, involvement of hazardous chemicals, and the need for a catalyst, pre-heating, and vacuuming. Moreover, the vast majority of the practices use expensive and non-renewable precursors for the synthesis. Thus, the present study was aimed at using sustainable atmospheric pressure microwave plasma for synthesis, which circumvented most of the shortcomings observed in the previous processes. The development of sustainable routes, the use of renewable precursors for synthesis, and the demonstration of the applications of as-synthesized material are the dedicated aspects of this study. The project not only included the synthesis of pristine graphene but also involved other graphene-based materials such as graphene-silver nanocomposite, and nitrogen-doped graphene oxide (N-GO).

In this thesis 2 natural precursors namely, *melaleuca alternifolia*, commonly known as tea tree and tangerine, and a synthetic chemical Aniline was used for developing graphene comprising different properties. The key point of this investigation was the synthesis of graphene in one step at a considerably low microwave power. Modern characterization methods, such as Raman spectroscopy, X-ray diffraction, transmission electron microscopy, electrochemical impedance spectroscopy, etc., were used to examine the morphology, structure, and electrochemical characteristics of graphene. The images from transmission electron microscopy revealed graphene comprised of few to multi-layer. The tea tree-derived graphene showed excellent sensing characteristics for the detection of diuron herbicide.

Taking advantage of the ability of the atmospheric pressure microwave plasma process to synthesize nanomaterials in a chemical-free environment, the production of the graphene-Ag nanocomposite was also accomplished. For this purpose, tea tree oil and silver nitrate ($AgNO_3$) vapors were used as source materials. The notable feature in this study was the observation of a relationship between the concentration of $AgNO_3$ in the precursor and the aggregation and the size of the produced Ag nanoparticles. The as-synthesized graphene-Ag nanocomposite was used in the electrochemical detection of methyl paraben by modifying the screen-printed electrode which displayed superior electrochemical sensing outcomes.

In another study, the synthesis of graphene from tangerine peel oil was also investigated. The tangerine peel-derived graphene used in a chemiresistive sensor displayed an extraordinary response for the recognition of vapors of ethanol, insecticide, and herbicide in the atmosphere.

Aniline, which served as a single source of both nitrogen and carbon, was used to synthesize N-GO in a single step. It was shown that microwave power, as low as 80 W can synthesize N-GO having nitrogen retention greater than 3 %. The interlayer spacing in N-GO nanosheets was determined to be lower than that of graphene oxide, which suggested a lower content of oxygen and other species present in between N-GO layers. The as-synthesized N-GO exhibited enhanced algicidal and anti-scaling properties that are essential for water purification applications.

CONTENTS

SUSTAINABLE SYNTHESIS OF GRAPHENE-BASED MATERIALS AND APPLICATIONS **1**

DECLARATION ***1***

STATEMENT OF ACCESS TO THIS THESIS ***2***

ACKNOWLEDGMENTS ***3***

STATEMENT OF CONTRIBUTION OF OTHERS ***4***

ABSTRACT ***5***

CONTENTS **1**

LIST OF FIGURES **7**

LIST OF TABLES **14**

LIST OF PUBLICATIONS **15**

Chapter 1: Introduction **17**

1.1 Rational 17

1.2 Research objectives 18

1.3 Document organization 19

References 21

Chapter 2: Literature Review **22**

2.1 Introduction 24

2.1.1 Carbon nanostructures *26*

2.1.2 Zero-dimensional carbon nanostructures *27*

2.1.3 One-dimensional carbon nanostructures *28*

2.1.4 Two-dimensional carbon nanostructures *28*

2.2 PECVD synthesis of graphene 29

2.2.1 Input parameters *30*

2.2.2 Radiofrequency PECVD *35*

2.2.3 Microwave PECVD *37*

2.2.4 Growth mechanism of graphene *38*

2.3 Atmospheric pressure microwave plasma synthesis of graphene 40

2.3.1 Plasma reactors *41*

2.3.2 Precursors and their role in graphene formation *43*

2.3.3 Microwave power *46*

2.3.4 Comparison of the graphene structure and morphology *47*

2.3.5 Synthesis of nitrogen-doped graphene *50*

2.4 Other plasma sources for the synthesis of graphene 51

2.5 Plasma for the synthesis of graphene-based composites 52

2.6 Plasma-based processing of graphene structure 54

2.7 Applications of graphene 56

2.7.1 Applications of PECVD grown graphene 56

2.7.2 Applications of atmospheric pressure microwave plasma-synthesized graphene 62

2.8 Conclusion and future outlook 66

References 70

Chapter 3: Synthesis of graphene from tea tree extract for sensing application.... 96

3.1 Introduction 98

3.2 Materials and method 100

3.2.1 Materials 100

3.3 Results and discussions 103

3.4 Application of graphene in an electrochemical sensor 109

3.5 Conclusion 113

References 114

Chapter 4: Synthesis of graphene-Ag nanocomposite and its application in detection 123

4.1 Introduction 124

4.2 Materials and method 127

4.3 Results and discussions 130

4.4 Electrochemical detection of methyl paraben 140

4.5 Conclusion 144

References 152

Chapter 5: Synthesis of graphene from tangerine peel oil for chemiresistive sensor 159

5.1 Introduction 161

5.2 Experimental 163

5.3 Results and discussions 165

5.4 Chemiresistive sensing behavior of graphene 172

5.5 Conclusion 173

References 176

Chapter 6: Synthesis of nitrogen-doped graphene oxide and its application.....181

6.1 Sustainable approach for the synthesis of nitrogen-doped graphene oxide 182

6.1.1 Introduction.....183

6.1.2 Experimental.....185

6.1.3 Results and discussions.....188

6.1.4 Performance of N-GO membrane in water purification system.....198

6.1.5 Conclusion.....201

References.....209

6.2 Application of nitrogen-doped graphene oxide.....218

6.2.1 Introduction.....219

6.2.2 Materials and method.....220

6.2.3 Results and discussion.....223

6.2.4 Electrochemical analysis of electrode.....226

6.2.5 Conclusion.....231

References.....232

Chapter 7: Conclusion.....238

7.1 Synthesis of graphene.....238

7.2 Synthesis of nitrogen-doped graphene oxide 239

7.3 Synthesis of graphene-Ag nanocomposite 239

7.4 Overall conclusion 240

7.5 Recommendations for future work 241

LIST OF FIGURES

Fig 2.1: Top-down and bottom-up synthesis techniques of graphene 26

Fig 2.2: Types of Carbon nanostructures [26] 27

Fig 2.3: An overview of the PECVD process to synthesize graphene.....30

Fig 2.4: (a) Three stages of graphene nucleation and growth [102], (b) Three-step growth mechanism of graphene [98], (c) High-resolution SEM images of graphene [98].....40

Fig 2.5: (a) Schematic illustrations of plasma reactors used by Dato's et al. [63] (b) Tatarova et al. [106] (c) Munzer et al. [108] (d) Toman et al. [20] 43

Fig 2.6: Effect of ethanol flux and microwave power on carbon nanostructure [112].....47

Fig 2.7: Raman spectra and corresponding TEM images showing the effect of chamber wall temperatures [112] 49

Fig 2.8: (a) Raman spectra of samples showing the effect of ethanol precursor flow rate, (b) I_D/I_G (black circles) and I_{2D}/I_G (red squares) values of the Raman spectrum obtained at different flow rate of ethanol [115] 49

Fig 2.9: Cyclic voltammetry (CV) curves of VGNS grown at (a) 40% and (b) 80% H_2 at varied scan rates [87] 57

Fig 2.10: (a) Wearable temperature sensor showing response/recovery time [182] (b) Cyclic voltametric response of different graphene-based sensors for lactate detection [183].....59

Fig 2.11: (a) Dye-sensitized solar cell configuration (b) J-V curves of graphene/polyaniline curves [197] 61

Fig 2.12: (a) Cyclic voltammograms of N-doped graphene at various scan rates (b) Galvanic charge-discharge at various current densities [118].....62

Fig 2.13: Cyclic voltmmograms of modified working electrodes for oxalic acid detection in a phosphate buffer solution [198].....64

Fig 2.14: (a) Schematic demonstration of the nitrogen-doped graphene oxide -coated-polyamide membrane, (b) water contact angle of the polyamide and (c) nitrogen-doped graphene oxide-coated polyamide membranes, and (d) flux recovery ratio after number of cycles of water filtration [199].....64

Fig 3.1: (a) A diagrammatic representation of atmospheric pressure microwave plasma reactor (b) Schematic illustration of steps involved in the synthesis of graphene inside the reactor 102

Fig 3.2: (a) Raman spectra and (b) peaks' intensity ratios of graphene samples synthesized at different microwave powers 104

Fig 3.3: (a) Survey scan XPS spectrum of 200 W graphene sample, and deconvoluted peaks of high-resolution (b) C1s and (c) O1s XPS spectra.....105

Fig 3.4: SEM images of 200 W graphene sample at (a) lower and (b) higher magnification106

Fig 3.5: Transmission Electron Microscopy of graphitic particles (a) low magnification, (b-e) HRTEM.....107

Fig 3.6: XRD pattern of 200 W graphene.....108

Fig 3.7: EIS of bare and graphene-modified GCE in 0.1 M KCl containing 5 mM $K_3[Fe(CN)_6]$. Frequency range 0.1 Hz to 100 kHz 110

Fig 3.8: Cyclic voltammograms of bare and graphene-modified GCE in 0.1 M PBS containing 2 mM diuron, and graphene/GCE in blank 0.1 M PBS, the scan rate is 10 mV/sec 111

Fig 3.9: (a) DPV curves at graphene/GCE for different concentrations (20, 80, 120, 180, 300, 400, 500, 600, 700, 800, 900, 1000 µM) of diuron in 0.1 M PBS (b) Calibration plot from the DPV measurements.....112

Fig 4.1: Schematic illustration of the synthesis of graphene-Ag nanocomposite in atmospheric pressure microwave plasma 129

Fig 4.2: (a) Raman spectra of graphene-Ag nanocomposites (b) I_D/I_G of graphene-Ag nanocomposites synthesized at different concentrations of $AgNO_3$.....131

Fig 4.3: SEM images of graphene and graphene-Ag nanocomposites synthesized from different concentrations of $AgNO_3$.....132

Fig 4.4: XRD pattern of 0.10 M graphene-Ag nanocomposite.....133

Fig 4.5: XPS of (a) 0.10 M graphene-Ag nanocomposite and (b) Ag 3d, High-resolution spectra of (c) C1s and (d) O1s.....135

Fig 4.6: TEM images of 0.10 M graphene-Ag nanocomposite at (a) lower and (b) higher magnification (c) TEM image of carbon nano-onion (d) SAED pattern of 0.10 M graphene-Ag nanocomposite 137

Fig 4.7: OES spectra of (a) pure Ar (b) Ar with tea tree oil vapours and (c) Ar with 0.1 M $AgNO_3$ vapours 139

Fig 4.8: Cyclic voltammograms of (a) bare SPE, (b) graphene/SPE, (c) graphene-Ag nanocomposite/SPE in 0.1 M PBS (pH 7.01) containing 10 µM MP 140

Fig 4.9: (a) Differential pulse voltammogramms of different concentrations of MP (20, 30, 40, 50, 60, 80, 100, 120, 140, 160, 180, 200, 220, 240, 260 µM) in 0.1 M PBS (pH 7.01) and (b) corresponding calibration curve.....141

Fig 4.10: (a) Repeatability study of one graphene-Ag nanocomposite/SPE in 0.1 M PBS containing 20 µM MP. (b) Reproducibility study of five graphene-Ag nanocomposite/SPEs in 0.1 M PBS containing 20 µM MP 143

Fig 5.1: (a) Schematic illustration of atmospheric pressure microwave plasma synthesis of graphene (b) quartz tube covered with graphene after the synthesis **(c)** appearances of plasma before and after exposure to tangerine peel oil vapours at different microwave powers 164

Fig 5.2: (a) Raman spectra and (b) the intensity ratios of D and 2D bands to the G band in the graphene samples, demonstrating the effect of plasma power on a synthesis.....167

Fig 5.3: XRD pattern of graphene samples.....167

Fig 5.4: (a) Survey spectra of graphene samples (b) Percentages of carbon and oxygen vs microwave power. High-resolution C 1s XPS spectra of (c) 200 W (d) 600 W and (e) 1000 W graphene samples.....169

Fig 5.5: SEM images of tangerine peel oil-derived graphene nanosheets (600 W sample) at lower and higher magnifications.....170

Fig 5.6: TEM images of 600 W tangerine peel oil-derived graphene sample 171

Fig 5.7: Response of tangerine peel oil-derived graphene chemiresistive device toward various chemical substances.....173

Fig 6.1: Schematic illustration of downstream microwave plasma setup and top-view of the tube showing N-GO deposited on walls 187

Fig 6.2: Appearance of plasma (a) in the absence of aniline and (b) after exposure to aniline 187

Fig 6.3: (a) Raman spectra and (b) the intnesity ratios of 2D and D peaks with respect to the G peak in the N-GO samples, representing the effect of plasma power on synthesis.....190

Fig 6.4: FTIR spectrum of N-GO sample synthesized at 80 W.....191

Fig 6.5: XPS survey spectra of N-GO samples synthesized at (a) 80 W (b) 150 W (c) 200 W. The deconvoluted high-resolution (d) C1s and (e) N1s peaks arising from 80W sample and (f) a schematic representation of types of N-bonding in N-GO samples are also shown. 193

Fig 6.6: SEM images of N-GO samples synthesized at different plasma powers 194

Fig 6.7: TEM images of the (a-b) 80 W and (c) 150 W films grown on silicon. The high resolution images of the regions marked in the left-side images are given in the right side of each part of the figure 196

Fig 6.8: The electrochemical impedance spectroscopy (EIS) of (a) bare GCE (b) N-GO coated GCE in 0.1 M KCl aqueous solution containing 5 mM $K_3Fe(CN)_6$. The inset shows the Randles equivalent circuit model.....197

Fig 6.9: (a) Schematic presentation of N-GO coated-PA membrane (b) water contact angle of control and (c) N-GO coated-PA membrane (d) graph showing flux recovery ratio against the number of water filtration cycles.....198

Fig 6.10: Microscopic images showing the degree of algal growth on (a) N-GO coated and (b) control polyamide membranes.....198

Fig 6.11: Schematic illustration of N-GO synthesis in atmospheric pressure microwave plasma 222

Fig 6.12: Ag-Nps/N-GO/GCE modified electrode preparation scheme.....223

Fig 6.13: (a) Raman spectrum and (b) SEM image of N-GO sample.....225

Fig 6.14: (a) SEM image (high resolution in inset) and (b) EDS of Ag-Nps/N-GO/GCE modified electrode 226

Fig 6.15: EIS spectra for (a) bare GCE (b) N-GO/GCE (c) Ag-Nps/N-GO/GCE in a solution of 0.1 M KCl and 5 mM $K_3[Fe(CN)_6]$ with the frequencies swept from 0.1 Hz to 100 kHz.....227

Fig 6.16: CVs of bare GCE, N-GO/GCE, and Ag-Nps/N-GO/GCE in 0.1 M PBS (pH 7) containing 0.1 mM OA, scan rate 50 mV/s 228

Fig 6.17: (a) Amperometric response of the Ag-Nps/N-GO/GCE in stirred 0.1 M PBS with sequential injections of OA at 1.2 V potential (b) Calibration curve showing OA current response against its concentration.....229

Fig 6.18: Amperometric response of Ag-Nps/N-GO/GCE towards OA (50 µM), ascorbic acid (100 µM), glucose (50 µM) and uric acid (100 µM) in 0.1 M PBS at 1.2 V.....231

LIST OF TABLES

Table 2.1 Overview of past works on atmospheric pressure microwave plasma synthesis of graphene 68

Table 3.1: Comparison of tea tree oil-derived graphene with others synthesized in atmospheric pressure microwave plasma 109

Table 3.2: Comparison of different carbon-based modified electrodes for electrochemical detection of diuron 112

Table 4.1: Details of synthesis conditions of graphene-Ag nanocomposite 129

Table 4.2: Comparison of electrochemical performance of sensor for methyl paraben detection 142

Table 5.1: Comparison of tangerine peel oil-derived graphene with others synthesized in atmospheric pressure microwave plasma..... 171

Table 6.1: Comparison of the analytical performance of the electrochemical OA sensors... 229

LIST OF PUBLICATIONS

Candidate prepared the following publications during the course of this thesis:

1. Zafar, M. A., & Jacob, M. V. (2022). Plasma-based synthesis of graphene and applications: a focused review. Reviews of Modern Plasma Physics, 6(1), 1-38.

2. Zafar, M. A., Yang Liu, Francisco C. Robles Hernandez, Oomman K. Varghese, Mohan V Jacob, “Plasma-based synthesis of freestanding graphene from a natural resource for a sensing application”. Advanced materials interfaces.

3. Zafar, M. A., & Jacob, M. V. “Rapid and sustainable synthesis of graphene for its application in the chemiresistive sensor”. *(To be submitted).*

4. Zafar, M. A., Varghese, O. K., Robles Hernandez, F. C., Liu, Y., & Jacob, M. V. (2022). Single-Step Synthesis of Nitrogen-Doped Graphene Oxide from Aniline at Ambient Conditions. ACS Applied Materials & Interfaces, 14(4), 5797-5806.

5. Zafar, M. A., Liu, Y., Allende, S., & Jacob, M. V. (2022). Electrochemical sensing of oxalic acid using silver nanoparticles loaded nitrogen-doped graphene oxide. Carbon Trends, 8, 100188.

6. Zafar, M. A., Liu, Y., & Jacob, M. V. Rapid and sustainable synthesis of graphene-Ag nanocomposite for the detection of methyl paraben. *(To be submitted).*

Candidate contributed to additional publications that is not related to this thesis:

7. Zafar, M. A., & Jacob, M. V. (2022). Synthesis of free-standing graphene in atmospheric pressure microwave plasma for the oil-water separation application. Applied Surface Science Advances, 11, 100312.

8. Al-Jumaili, A., Zafar, M. A., Bazaka, K., Weerasinghe, J., & Jacob, M. V. (2022). Bactericidal vertically aligned graphene networks derived from renewable precursor. Carbon Trends, 7, 100157.

Chapter 1: Introduction

1.1 Rational

Nanotechnology and the use of nanomaterials in various state-of-the-art technologies not only enhanced the performance of the devices many-fold but also paved the way for its miniaturization. Graphene, a novel nanomaterial has the highest potential to revolutionize the modern developments due to its extraordinary properties. Superior charge transport properties, high tensile strength, record-high thermal conductivity, excellent visible light transmittance, ultrahigh specific surface area, and nearly perfect impermeability to all gases are just a few of its impressive characteristics [1]. Graphene has potential applications in various fields, including electronic and photonic devices, energy generation or storage, optical devices, water purification, renewable energy conversion, and chemical/biological sensors [2]. This led to a huge increase in the demand for graphene. It is expected that the global graphene market will increase to US $349 million by 2025 which was just US $12 million in 2013 [3, 4]. To meet the growing demand, serious attention to the scalable, sustainable, and economical synthesis of graphene should be given.

Graphene synthesis has undergone a number of efforts in the past. Each technique used in past has its own merits and demerits. Epitaxial growth and thermal or plasma-enhanced chemical vapor deposition (PECVD) require numerous formalities to synthesize high quality graphene that comprises minimal defects [5]. For instance, a widely used technique i.e. PECVD involved pre-heating, high vacuuming, subsequent cooling, and transfer of graphene. In this way, it includes a lengthy procedure in addition to the several phases of synthesis [6].

A beneficial bottom-up PECVD alternative that avoids the aforementioned problems is atmospheric pressure microwave plasma (APMP) technology. APMP does not require heating,

vacuuming, or cooling for the synthesis. The synthesis method is facile, scalable, and substrate-free [7]. Multiple layers of graphene has been previously synthesized using this method. However, the method is still evolving for the synthesis of graphene and graphene-based materials such as doping and nanocomposites. Most importantly sustainable aspect of the synthesis of graphene is not explored to the full extend [8].

In an attempt to replace previously used toxic and nonrenewable precursors, a sustainable, environmentally benign, and less energy-intensive approach is introduced in this work. Pristine graphene is synthesized from natural resources i.e. tea tree and tangerine peel extracts separately. The nitrogen-doping of graphene is made in a single step at a remarkably low microwave power. Furthermore, the synthesis approach for the nanocomposite of graphene and silver metal using microwave plasma which does not involve toxic chemicals and multiple steps, is developed. Lastly, the application of as-synthesized nanomaterials in advanced applications such as environmental sensing is reported in this work.

1.2 Research objectives

The goal of this research was to provide sustainable, rapid, and economically viable approaches for the synthesis of graphene-based materials i.e. pristine graphene, nitrogen-doped graphene oxide, and graphene-metal nanocomposites. Moreover, showcasing the applications of these materials in environmental sensing is also intended in this work. The following set of objectives were defined in order to fulfill these:

- Synthesize graphene from a natural source for its use in the electrochemical detection of diuron herbicide.
- Investigate rapid and chemical-free synthesis of graphene-Ag nanocomposite for the detection of endocrine disruptor chemical, i.e. methyl paraben.

- Develop a sustainable approach for the synthesis of nitrogen-doped graphene oxide and demonstrate its application for the detection of oxalic acid, a hazardous substance.

Achieving these objectives would considerably contribute to the sustainable, facile, and environmentally-friendly fabrication of graphene-based materials. Moreover, it would be a great step towards the UN sustainable development goals of 2030 [9].

1.3 Document organization

This thesis contains seven chapters, each of which addresses the aforementioned research objectives.

Chapter 1 gives a brief background and the research context of this work. The research gaps and objectives of this project are also outlined in this chapter.

Chapter 2 provides a literature review on the recent history of the plasma-based synthesis of graphene and its applications. The chapter discusses the process parameters and their effects on the production and properties of graphene in detail.

Chapter 3 presents investigations on the synthesis of graphene from the extract of tea tree. The effects of microwave power on the properties of graphene are discussed comprehensively. The traits of produced graphene have been investigated using laser Raman spectroscopy, X-ray photoelectron spectroscopy (XPS), scanning electron microscopy (SEM), and transmission electron microscopy (TEM). The application of graphene for the detection of diuron herbicide has been discussed in detail in this chapter.

Chapter 4 explains the synthesis approach for fabricating the graphene-Ag nanocomposite using atmospheric pressure microwave plasma. The confirmation of the formation of nanocomposite has been made through X-ray diffraction (XRD), XPS, and TEM. An optical

emission spectrum illustrating the plasma environment during different stages of synthesis is also provided. Lastly, the application of the graphene-Ag nanocomposite is demonstrated for the electrochemical sensing of an endocrine disruptor i.e. methyl paraben.

Chapter 5 discusses the synthesis of graphene from the tangerine peel oil. The influence of microwave power on the properties of graphene are investigated in detail. The characteristics of as-synthesized graphene have been studied using laser Raman spectroscopy, X-ray photoelectron spectroscopy (XPS), scanning electron microscopy (SEM), and transmission electron microscopy (TEM). The application of graphene for the detection of toxic vapors is also discussed in this chapter.

The method utilized to produce nitrogen-doped graphene oxide (N-GO) sustainably is described in full in Chapter 6. It is demonstrated how nitrogen-doped graphene oxide may be produced in a single step with a single precursor using remarkably low microwave power. This chapter also includes information on the N-GO characterizations performed using Raman, XPS, SEM, and TEM as well as Fourier transform infrared (FTIR) spectroscopy. It is also shown how N-GO could be used as an electrochemical sensor to detect oxalic acid.

Chapter 7 gives a general summary of the work carried out to achieve the objectives of the project. This chapter also highlighted the key results and future recommendations.

References

1. Zafar, M.A., O.K. Varghese, F.C. Robles Hernandez, Y. Liu, and M.V. Jacob, *Single-Step Synthesis of Nitrogen-Doped Graphene Oxide from Aniline at Ambient Conditions.* ACS Applied Materials & Interfaces, 2022. **14**(4): p. 5797-5806.
2. Jacob, M.V., R.S. Rawat, B. Ouyang, K. Bazaka, D.S. Kumar, D. Taguchi, M. Iwamoto, R. Neupane, and O.K. Varghese, *Catalyst-free plasma enhanced growth of graphene from sustainable sources.* Nano letters, 2015. **15**(9): p. 5702-5708.
3. Peplow, M., *Graphene booms in factories but lacks a killer app.* Nature, 2015. **522**(7556): p. 268.
4. Siow, K.S., *Graphite Exfoliation to Commercialize Graphene Technology.* Sains Malays, 2017. **46**: p. 1047-1059.
5. Bo, Z., Y. Yang, J. Chen, K. Yu, J. Yan, and K. Cen, *Plasma-enhanced chemical vapor deposition synthesis of vertically oriented graphene nanosheets.* Nanoscale, 2013. **5**(12): p. 5180-204.
6. Yeh, N.C., C.C. Hsu, J. Bagley, and W.S. Tseng, *Single-step growth of graphene and graphene-based nanostructures by plasma-enhanced chemical vapor deposition.* Nanotechnology, 2019. **30**(16): p. 162001.
7. Zafar, M.A. and M.V. Jacob, *Plasma-based synthesis of graphene and applications: a focused review.* Reviews of Modern Plasma Physics, 2022. **6**(1): p. 1-38.
8. Dato, A., *Graphene synthesized in atmospheric plasmas—A review.* Journal of Materials Research, 2019. **34**(1): p. 214-230.
9. Costanza, R., L. Daly, L. Fioramonti, E. Giovannini, I. Kubiszewski, L.F. Mortensen, K.E. Pickett, K.V. Ragnarsdottir, R. De Vogli, and R. Wilkinson, *The UN Sustainable Development Goals and the dynamics of well-being.* 2016.

Chapter 2: Literature Review

This chapter summarizes the literature relevant to the plasma-based synthesis of graphene. Additionally, the applications of graphene-based materials synthesized through plasma techniques are also provided. Mainly, the review focuses on two areas: PECVD growth of graphene and atmospheric pressure microwave plasma-assisted synthesis of graphene. The first section 2.1, introduces various carbon nanostructures. The second section 2.2 comprises a detailed analysis of the key parameters for the growth of graphene. The third section signifies the atmospheric pressure plasma for the synthesis of pristine as well as doped graphene. Especially, the role of various plasma process parameters on the properties and structure of graphene is discussed in detail. Furthermore, an overview of the applications of graphene in various fields is given. The chapter is concluded with a summary, conclusions, and future recommendations.

This Chapter is given as published in “Reviews of Modern plasma Physics”.

Zafar, M. A., & Jacob, M. V. (2022). Plasma-based synthesis of graphene and applications: a focused review. Reviews of Modern Plasma Physics, 6(1), 1-38.

Plasma-based synthesis of graphene and applications: A focused review

Abstract

Graphene is a highly sought-after material for a wide range of applications, particularly in areas such as energy harvesting and storage, electronics, electrochemical sensors, biomedical, composites, and coatings. The synthesis of high-quality graphene is a precondition for its real-time application. However, conventional synthesis methods have certain drawbacks including laborious procedures and structural defects in graphene nanosheets. Plasma-based synthesis techniques such as plasma-enhanced chemical vapour deposition and atmospheric pressure microwave plasma are high-tech synthesis practices that can produce graphene without any solvents in a few seconds. This article reviews these state-of-the-art techniques emphasizing mainly their process parameters for the synthesis of high-grade graphene, which is defect-free, and comprises mono to few layers, great carrier mobility, and high purity. The applications of as-synthesized graphene in various fields are also provided. Moreover, the potential breakthroughs and the prospect of these techniques are also discussed in this work.

Keywords

Plasma-enhanced chemical vapour deposition, atmospheric pressure microwave plasma, process parameters, growth of graphene

2.1 Introduction

The astonishing discovery in the field of materials science in the last two decades is indeed graphene. Graphene was synthesized by Professor Andre Geim and Konstantin Novoselov in 2004 who won a noble prize for this [1]. Although graphene was under investigation before 2004 under different names, however, due to the lack of suitable synthesis techniques, graphene failed to appear in the limelight. Prof. Geim and Novoselov used a simple approach of mechanical exfoliation, which involved using scotch tape on graphite [2]. Eventually, the exfoliated single layer of graphite, comprising a thickness between 0.4-1.7 nm was termed graphene [3].

Graphene is a 2-dimensional monolayer of carbon atoms arranged in a honeycomb structure. It is basically composed of sp^2 hybridized carbon atoms. Just like other allotropes of carbon i.e. diamond, graphite, fullerenes (C_{60}), and carbon nanotube, graphene is also an allotrope of carbon [4]. Graphene has a large theoretical specific area [5] and possesses extraordinary mechanical, electrical, optical, thermal, etc. properties [6]. It is the thinnest as well as the strongest known material, surpassing diamond [7]. Owing to all these properties, Prof. Geim called it a “wonder material” [8]. Also referred to as “magic material” in some writings by others [9].

The main challenge towards the practical application of any material comes during its synthesis process. A variety of synthesis techniques have been used to produce pristine graphene. Mainly, it can be divided into bottom-up and top-down approaches, which are further divided into various techniques based on the synthesis approach. Each synthesis method has its own merits and demerits [10]. Fig 2.1 gives the division of techniques.

The methods which involve the break-down of the bulk material, such as graphite to acquire a single or few layers of graphene are regarded as top-down methods. Based on how exfoliation

is carried out, various techniques have been reported as top-down methods. It includes, mechanical exfoliation [11], chemical synthesis, liquid-phase exfoliation [12] etc. However, these techniques lack a good production rate, give poor quality of graphene [13], or require the reaction of graphite with strong oxidizers such as sulphuric acid, potassium chlorate, nitric acid and potassium permanganate which produce toxic gases [14]. Conversely, bottom-up approaches use molecules or atoms as building blocks of a complex structure and are considered very promising since these involve no wastage of materials [15]. The processes include epitaxial growth [16], chemical vapour deposition (CVD) [17], plasma-enhanced chemical vapour deposition (PECVD) [18, 19] and atmospheric pressure microwave plasma synthesis [20].

In vapour deposition techniques, a precursor in the form of gases is sent into a reaction chamber set at a higher temperature. When gases are exposed to the substrate, a reaction occurs and a monolayer to a few layers of graphene are created on the surface of the substrate. CVD, also known as thermal CVD, involves a high temperature of about 1000°C [21]. However, with the assistance of plasma, graphene can be grown at lower temperatures ranging from 600°C to 800°C. The plasma generates an enormous chemical environment, producing a mixture of molecules, radicals and ions from hydrocarbon precursors, as a result facilitates lower formation temperatures and a faster synthesis process than thermal CVD [22]. The atmospheric pressure plasma is the state-of-art technique in which synthesis is carried out at atmospheric pressure**;** rendering it a substrate-free process without the need for high vacuum or temperature. This literature review focuses on PECVD and atmospheric pressure microwave plasma synthesis of graphene. Particularly, the parameters involved in the synthesis of graphene and their role in the structure of the graphene are addressed. Lastly, a detailed outlook on these techniques is provided as well.

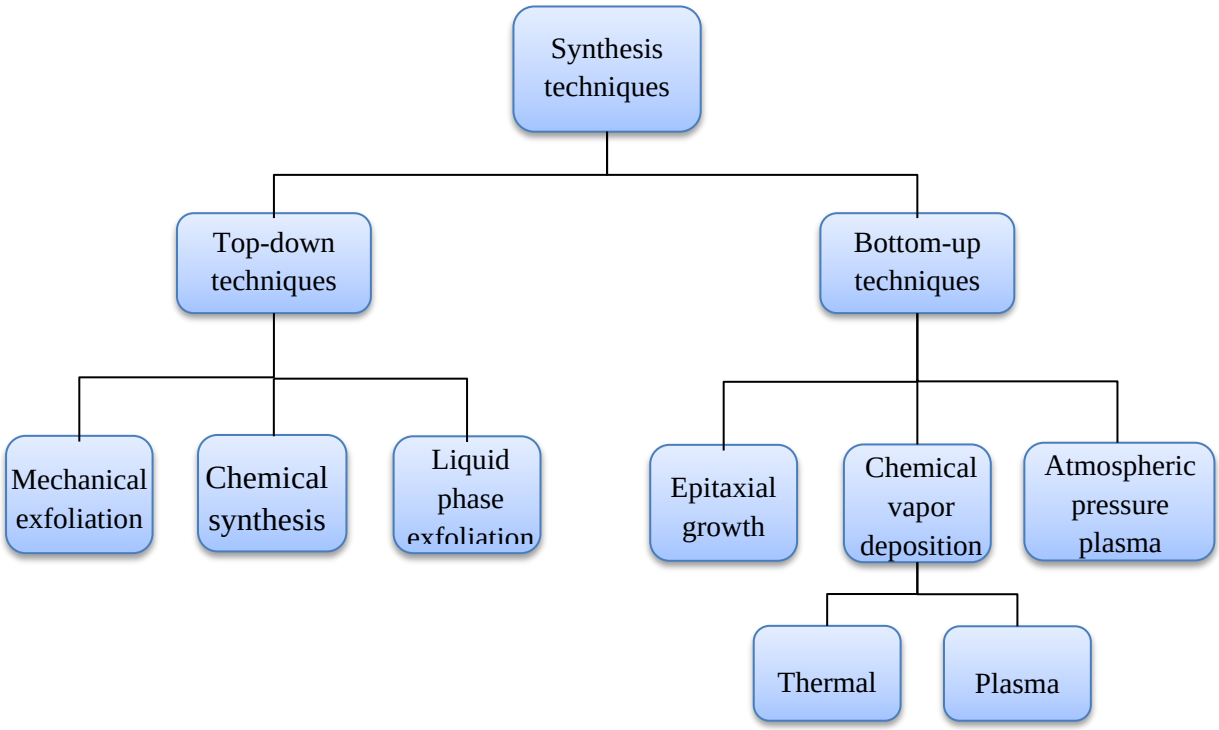

Fig 2.1: Top-down and bottom-up synthesis techniques of graphene

2.1.1 Carbon nanostructures

The carbon allotropes of the nano-sizes comprising different shapes, sizes and dimensionality are widely sought-after research materials. This is due to their diverse properties, structural diversity and myriad of applications [23-26]. Until now variety of carbon nanostructures have been developed, and many efforts have been made to tailor the properties of those materials for targeted applications [27]. These nanoscale carbon structures can be classified based on their dimensionality i.e. zero, one and two-dimensional carbon nanostructures. Their division is shown in Fig 2.2.

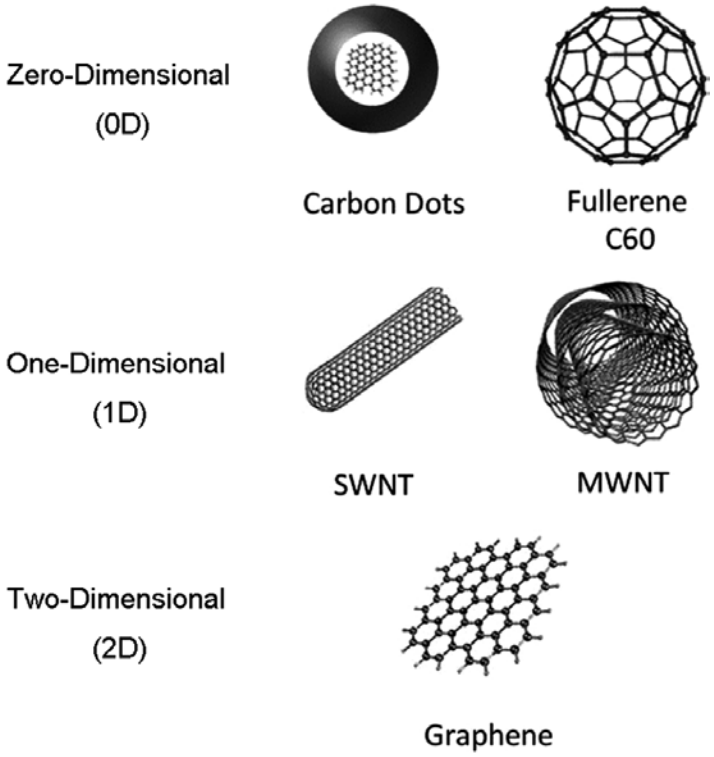

Fig 2.2: Types of Carbon nanostructures [26]

2.1.2 Zero-dimensional carbon nanostructures

Zero-dimensional carbon nanostructures include fullerenes, carbon dots or graphene quantum dots. The first synthesis of fullerenes was reported in 1990, where it was prepared by evaporation and recondensation of graphite [28]. Now fullerenes is prepared massively and thus easily available. Fullerenes have many interesting characteristics. For instance, the delocalization of charges within spherical carbon network and aromatic p-sphere are important for stabilizing charged units [29].

Carbon dots or graphene quantum dots are the recent addition in zero-dimensional carbon nanostructures. The very first reported fabrications of these materials were from candle soot [30] and laser ablation method [31]. However, now a variety of techniques have developed to synthesize carbon dots which include hydrothermal and electrochemical

methods, and pyrolysis or microwave conversion of waste materials [32]. The luminescence of carbon dots spans into the visible spectrum [33].

2.1.3 One-dimensional carbon nanostructures

Carbon nanotube is a one-dimensional allotrope of carbon. Carbon nanotube is basically a cylindrically tube which can be obtained by rolling the graphene film [34-36]. Carbon nanotubes are two types, single-wall carbon nanotube (SWCNT) [37] and multiwall carbon nanotube (MWCNT) [38]. Carbon nanotube offers interesting properties such as semiconductor, semi-metallic and metallic which make them an ideal material for sensing applications [39-41]. The synthesis of carbon nanotube is usually obtained through chemical vapour deposition method due to great merits of this method [42, 43].

2.1.4 Two-dimensional carbon nanostructures

The newest example of two-dimensional carbon nanostructure is graphene [8]. Graphene is basically an atomically thin single-layer of carbon hexagonal structure [44]. Graphene has myriad of applications due to its extraordinary properties, such as highest electron mobility, high surface area, and excellent conductivity, stronger than diamond etc. [45]. Owing to this, extensive research has been devoted on developing the preparation methods of graphene. CVD [21, 46], PECVD [47], epitaxial growth [48], Hummers method [49] and mechanical exfoliation [50] are widely used methods to produce this two-dimensional material.

In addition to pristine graphene, various surface-treated forms of graphene i.e. graphene oxide, reduced-graphene oxide, photoluminescent graphene oxide, nitrogen-doped graphene/graphene oxide have also been developed [26]. Graphene oxide is rich with oxygen functional groups such as hydroxyl, carboxyl, and epoxy groups [51]. Due to

these oxygen functional groups, a negative charge is developed on the surface of the graphene. The non-altered areas of graphene contains free p-electrons, allowing p-interactions. The charge, surface chemistry, and hydrophilicity of graphene oxide add interesting properties in the graphene [52, 53].

2.2 PECVD synthesis of graphene

The PECVD process for the synthesis of graphene can be divided into three parts, i.e. precursor delivery, decomposition, and graphene formation. A precursor in the form of gas is supplied into the plasma region, where it breaks down into smaller reactive reagents i.e. C, H, H_2, or CO, etc. depending on the composition of the precursor. Carbon in the form of graphene is deposited on the substrate, whereas, the residual gases flow out from the plasma region. The entire process is completed within a few seconds [27, 54]. Upon cooling, graphene deposited substrates are collected from the chamber and are well-kept for further investigations.

The PECVD reaction process is fast and efficient; however, it involves several factors influencing the process. For example, process parameters such as plasma power, precursor flow rate, chamber pressure, substrate temperature, etc. affect the synthesis method significantly [45, 55]. An overview of the method is shown in Fig 2.3. The next section will address these factors, explaining how they have been used in the past and their impact on the quality of graphene.

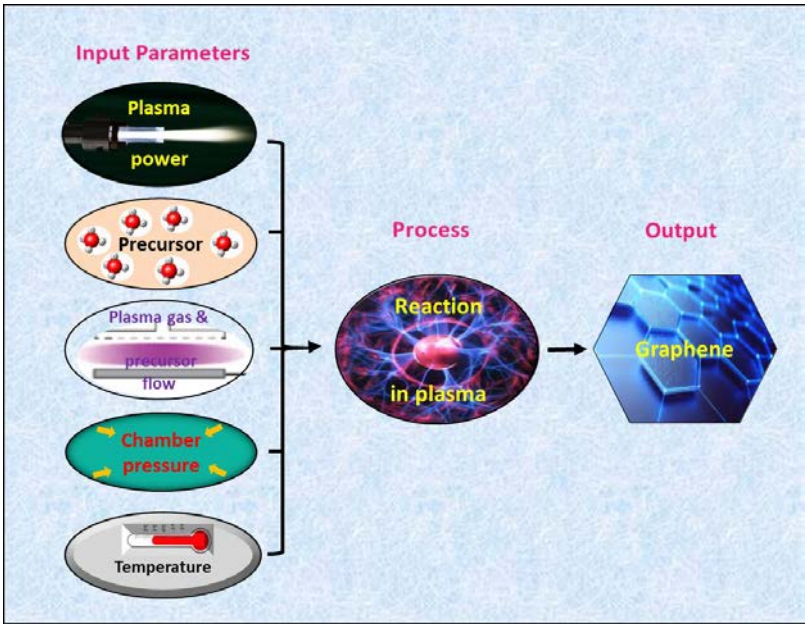

Fig 2.3: An overview of the PECVD process to synthesize graphene

2.2.1 Input parameters

i. Plasma power

Plasma sources such as radio frequency (RF) and microwave (MW) in the frequency range of 1 to 500 MHz and 0.5 to 10 GHz respectively, and direct current (dc) plasma are commercially available to be utilized in different applications. For the synthesis of graphene, most researchers prefer using RF and MW at the frequencies of 13.56 MHz and 2.45 GHz respectively [55]. These are standard industrial frequencies and are considered optimum values for the quality of the product [56]. Both types of plasmas have been optimized for different powers and have shown quality results.

Nang and Kim [57] studied the effect of RF power on the synthesis of graphene on Cu substrate from CH_4 precursor. For this purpose, the substrate was first preheated at 950°C. Then among 50 W, 200 W, 400 W, and 600 W they reported 200 W, as a suitable power for quality production of graphene. Unlike RF plasma, high power of the microwave, typically above 1 kW was used to synthesize the graphene [58-62]. However,

it should be noted that contrary to RF plasma, no substrate pre-heating is involved in microwave plasma. In the substrate-free synthesis of graphene using microwave plasma, Dato and Fraenklach [63] varied the plasma power from 350 W to 1100 W and determined that the change in power had no substantial effect on graphene synthesis. It was noted that the low power of plasma was sufficient to produce the required quality of graphene.

ii. Precursor

Precursor, also known as monomer or feedstock plays a vital role in the synthesis and properties of graphene. It has been found that the properties of synthesized graphene are not only affected by the composition of the precursor but also the flow rate of the precursor [54]. Therefore, scientists have investigated varieties of precursors. The key point in all precursors is that they must contain carbon compounds [64]. The fragmentation of a precursor is the primary step in all PECVD processes. The fragmentation process of a hydrocarbon precursor is highly endothermic and thus require a high temperature. Because of this process, the carbon will form graphene on the substrate. The by-products in the reaction are H_2 and CO, depending on the composition of the precursor. Some have used carbon-based chemicals, which are fossil fuels. These include but are not limited to methane (CH_4) [65-67], toluene (C_7H_8) [68], xylene (C_8H_{10}) [69], hexane(C_6H_{14}) [70], ethylene (C_2H_4) [71], ethanol (CH_3OH) , methanol (C_2H_5OH) [65], acetylene(C_2H_2) [72] etc. The hydrocarbons are usually mixed with hydrogen before they are supplied into the chamber. These precursors, mostly produced by fossil decomposition are highly toxic as well as prone to depletion over time.

Lately, renewable hydrocarbon-based precursors have been used which are found in enormous amounts on earth. The prime benefits of using these precursors are that they are easily accessible and can keep the reaction process green. To date, following precursors have been used; sesame oil [69], *Melaleuca alternifolia* is commonly known as tea tree [18], camphor [73], turpentine [74], geranium [45], eucalyptus [75], palm [76], and soybean oil [77]. Moreover, eatable products such as honey, biscuits, sugar, milk, and cheese have excitedly shown the viability of being potential precursors for the synthesis of graphene [78].

Overall, it has been found that the used precursors can be in solid, liquid, and gaseous forms. Nonetheless, the results have shown that the quality of graphene is far better in gaseous precursors compared with solids or liquids [46].

iii. Gas and precursor flow

Hydrogen (H_2) gas in combination with a precursor is generally used in the synthesis of graphene. Only a few have used argon (Ar) without H_2, however, the quality of graphene is compromised in this method [79, 80]. The proportion of gas relative to that of the precursor also has a significant effect on the synthesis process. Not only does it determine the final product, i.e. carbon nanotube (CNT), graphite, and/or graphene but also plays a role in shaping the morphology and structure of the graphene [81]. Wu et al. [82] studied the effect of the H_2/CH_4 ratio in synthesis on gold (Au) substrate. Using the MW-PECVD at temperatures between 650-700°C, and varying only H_2 concentration, they found considerable impact of H_2 gas on synthesis. A higher concentration of H_2 i.e. H_2/CH_4 ratio of 100, which is used for diamond film formation, showed no observable outcomes. Decreasing the ratio to 30 showed some columnar structures, further decrease showed a mixture of fibers/tubes and graphite nanosheets. Additional lowering of the ratio to reach

the range of 4-8 produced vertical graphene nanosheets. Wang et al. [83] studied the effects of CH_4 concentration by varying it from 10 % to 100 % in H_2 atmosphere. They used an RF plasma system at the power of 900 W while changing substrate temperatures from 600 to 900°C. All specimens yielded the same vertically standing graphene flakes of similar thicknesses. However, with the increase of CH_4 concentration, the size of sheet decreased; meanwhile the density of graphene decreased as well. Generally, gas ratio of CH_4/H_2 higher than 1:20 is depicted as optimum for vertical graphene synthesis in PECVD [81].

Hydrogen, either mixed with inert gasses (argon or helium) or in pristine form, play a vital role in the synthesis of graphene film on a substrate. Hydrogen acts as a catalyst and controls the grain size and shape by etching away the weak carbon bonds. Hydrogen partial pressure also affects the number of layers of graphene. It also has been noted that in the absence of hydrogen, graphene might not form [84].

iv. Chamber pressure

The chamber pressure has shown remarkable influences on the production rate of graphene. For instance, sub-atmospheric pressure has a low production rate while high vacuum pressure is favourable to attain a high production rate in microwave plasma. It happens, because the collisions between electrons and heavy particles which causes high temperature, is a key part of the process. Sub-atmospheric plasma does not favor this collisional phenomenon, hence a rise in temperature does not occur which eventually slows down the graphene synthesis [54]. However, to get high-quality graphene, without any impurities, it is important to vacuum the chamber. In literature, a wide range of chamber pressures has been used. It includes high vacuum pressure, low pressure (0.01-0.02 mbar), and atmospheric pressure (1014 mbar) [21].

v. Temperature

Temperature is an essential factor in any graphene synthesis process. Depending on C-H bonding energy, temperature also varies from one precursor to another. Compared with thermal and CVD processes, the PECVD process can be performed at lower temperatures. It is due to the presence of active ions and energetic electrons which can assist in breaking down the chains of molecules [54]. Based on the plasma source, some PECVD processes require precursor and/or substrate heating. In dc glow discharge, the substrate as well as the precursor must be heated. MW and RF-PECVD also require substrate heating. However, some of the MW plasma systems do not rely on the heating of the precursor or the substrate [81].

The substrate is heated externally, thus an additional heating element is coupled with the quartz tube. The heating temperature of the substrate depends on the conditions of other parameters. In most of the studies, substrate temperature usually differs from 600°C and 1000°C. Rao et al. [85] have shown a very low substrate temperature i.e. 400°C for the synthesis of carbon nanostructures. In another study, it was revealed that graphene could not be produced at a temperature below 600°C. In addition, the substrate temperature happens to have an effect on the density of the synthesized graphene. Higher temperatures, for example, more than 730°C produced high-density graphene [81]. Apart from substrate temperature, plasma generation also causes some increase in the temperature. Therefore, at the time of reaction, the temperature inside the chamber is always higher than the measured substrate temperature [86].

RF and MW plasma are widely studied plasma sources. The main role of plasma is twofold, i.e. heat transfer and transfer of momentum to breakdown the chains of precursor molecules. This role helps to lower the pre-heating temperature of the substrate. Here,

the past work on RF and MW-PECVD, categorizing them based on different substrate temperatures, will be analysed.

2.2.2 Radiofrequency PECVD

i. Low temperature (<600 °C)

Seo et al. [87] produced graphene without any substrate by heating butter on Ni foam; where butter was used as a precursor. They used a high 1000 W plasma power, which can build a temperature from 400 to 450°C. The Raman spectroscopy results showed evidence of some graphene. However, the quality of graphene was compromised, as the D peak, which indicates the number of defects, was quite high. Chen et al. [88] attempted to synthesize graphene at a quite low temperature of 300°C and studied the effects of deposition time on the thickness of graphene. Their results presented graphene of thickness varying from 10 to 600 nm, which is higher than most reported thicknesses of graphene. The Raman spectra also did not produce the desired outcome as the D peak was quite higher and the 2D peak was quite lower than the G peak. Moreover, the lengthy synthesis time of 60 min also renders this approach unsuitable for graphene synthesis.

ii. Medium temperature (600 – 750 °C)

Qi et al. [89] produced 1 to 3 layers of graphene on a Si/SiO_2 with Ni film-substrate at low temperatures. It can be attributed to the fact that the plasma power leads to the formation of a high concentration of radicals on the surface of Ni, which in turn promotes carbon growth on the surface. Likewise, Wang et al. [90] adopted the same parametric approach using relatively medium temperatures. They used Cobalt (Co) as a substrate. In their results, they mentioned that Co has a vital role in synthesizing better quality graphene.

Vizireanu et al. [91] performed a parametric study and found that the gas mixture $Ar/H_2/C_2H_2$ flow rate has a noteworthy influence on the morphology of graphene. In addition, temperatures greater than 600 °C, plasma power between 250 and 400 W, and the argon mass flow rate greater than 500 sccm are important factors for graphene growth. Song et al. [92] produced graphene on different substrates i.e. Si, SiO_2, Quartz, gallium arsenide (GaAs), germanium (Ge), and carbon fiber (C_f). They successfully accomplished a homogeneous vertical graphene distribution on all substrates. Good quality graphene at medium temperatures is reported by Zhu et al. [93], who used RF plasma at 680°C and deposited nanosheets directly on a Ni wire.

iii. High temperature (> 750 °C)

Kato et al. [94] performed high-temperature PECVD process and analyzed the effect of temperature on graphene nucleation and growth rate. High-density graphene grains were observed at 750°C, which start growing with the increase in temperature. At a temperature of 950°C, they found a single graphene grain. However, unlike the ones observed at 800°C and 850°C, the graphene grain at 950°C was not hexagonal.

Terasawa and Saiki [95] found that the substrate temperature has a great impact on ~~the~~ graphene layers. The substrate temperature of 500°C produced multilayer graphene, whereas they detected a monolayer at 900°C. Moreover, crystallinity is higher at temperatures greater than 900°C. Ma et al. [96] studied the effect of gas pressure on graphene synthesis at a higher temperature. For instance, the growth rate of graphene at 950°C temperature and 1.2 torr pressure is slower than that at 570 mTorr. It is mainly due to the slower carbon supply from the gas phase to the substrate.

Ma et al. [97] studied the effects of plasma power source and growth temperatures on the morphology of vertically grown graphene. Varying the power source from 80 to 280 W,

they noticed vertical graphene flakes forming a bush-like shape. They named it a tree-like structure as it appeared like one when seen from above in SEM microscope. Similarly, varying the temperature of the substrate from 700 to 850°C greatly influenced the tree-like morphology. When the temperatures are lowered, the distance between each tree is reduced prominently, while the height of tree-like structure increases. The flakes of graphene in tree-like structure become interlinked. Resultantly, porous films of graphene are obtained at lower temperatures.

Among low, medium, and high-temperature, it is believed that irrespective of precursor type, medium temperature range, i.e. 600 – 750°C is appropriate for graphene synthesis. Low temperatures require either high plasma power or demand a long processing time. Higher temperature ranges do not make the process suitable for the substrates, which have low melting temperatures. Thus, a medium temperature range assisted with medium plasma power is adequately suitable for graphene synthesis.

2.2.3 Microwave PECVD

Malesevic et al. [98] produced highly crystalline graphene on various substrates such as quartz, silicon, nickel, steel, titanium, etc. Overall, similar results were observed on all substrates. However, different flakes adhesion was indicated which could be attributed to the carbide formation on the substrate. Yamada et al. [99] also used the MW-PECVD process to synthesize graphene at a low temperature such as 320°C accompanied by no substrate heating. They displayed successful graphene synthesis for optoelectronic applications due to the high optical transmittance and sheet resistance. The production of graphene at this lowest temperature on a non-catalytic aluminum substrate was an extraordinary achievement.

Yuan et al. [100] also synthesized graphene using MW-PECVD; however, they used higher temperature by heating the substrate with an inductive heater. In their results, they found crystalline graphene with some defective morphology. Vitchev et al. [101] studied the growth of graphene on different substrates, produced using MW-PECVD. On the initial synthesis stage, they found SiC formation on a silicon substrate, which was not seen on quartz, or platinum (Pt) substrates. At later stages of growth, they observed a similar formation phenomenon in which layers of graphene flakes were developed. Kalita et al. [59] prepared graphene film at the lowest temperature of 240°C. The results, however, showed some defects, which render this lower temperature unsuitable for synthesis.

Kim et al. [60] studied the synthesis of graphene at various temperatures. Consequently, they found monolayer graphene in the temperature range of 450°C to 750°C. The outcome was the creation of centimeter-scale graphene with the characteristics of high transparency and low sheet resistance i.e. 590 Ω/sq. However, graphene formed below 450°C had numerous defects, making it undesirable for applications.

MW-PECVD has also been used to dope the graphene sheets. For instance, Kumar et al. [61] produced an N-doped graphene film up to the concentration of 2 atomic percent. For this purpose, an additional supply of nitrogen gas was provided in a microwave plasma system. Nitrogen gas was released for a minute when precursor (CH_4) was released. This fast and efficient process of N-doping showed the potential to produce p-doped graphene as well.

2.2.4 Growth mechanism of graphene

The growth of vertical graphene using RF-PECVD process has been studied by Wang et al. [102]. In their findings, they delineated a three-step formation process, i.e. (i)

nucleation and island formation of carbon film, (ii) initial growth of graphene sheets, and (iii) further growth and net-like formation of graphene sheets. A schematic representation of graphene growth processes and SEM images taken during the growth process are shown in Fig 2.4a.

Similarly, Malesevic et al. [98] also identified the three-step graphene growth process as shown in Fig 2.4 (b, c). Firstly, a graphite layer is made parallel to the substrate surface and seen as a crack on the surface. In the second stage, freestanding graphene nucleation starts from these cracks in the vertical direction. The growth of these vertical graphene continues due to the accumulation of carbon radicals on the edges of these graphene.

A recent study by Zhang et al. [103] also mentioned the similar three stages of graphene growth on Si substrate. However, they observed the growth of the buffer layer (SiC) parallel to the substrate's surface before the nucleation of vertical graphene flakes from the defects. However, the defect formation such as cracks on the surface of the substrate is beneficial for graphene growth as it provides highly active sites for nucleation.

Nevertheless, it should be noted that the final quality of graphene highly depends on the process conditions such as type of plasma source, process parameters, growth and cooling time, etc. The process conditions bring about differences in graphene morphology, density, and microstructure. As evident from the different names given to the final morphology of graphene, it can be referred to as petal, bush or tree-like, turnstile, cauliflower, and maze-like structure [104].

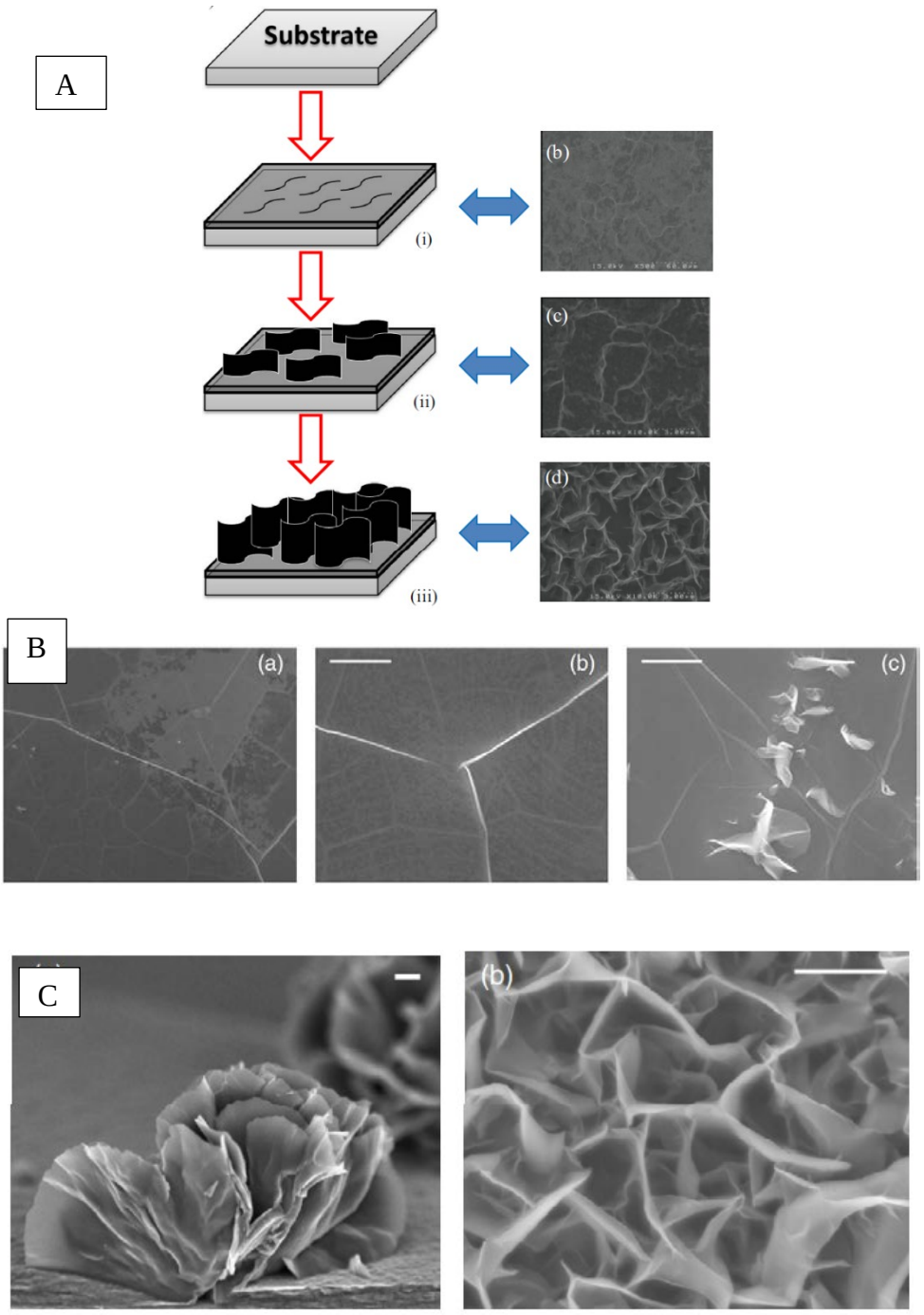

Fig 2.4: (a) Three stages of graphene nucleation and growth [102], (b) Three-step growth mechanism of graphene [98], (c) High-resolution SEM images of graphene [98]

2.3 Atmospheric pressure microwave plasma synthesis of graphene

Atmospheric pressure plasma synthesis is a substrate-free synthesis in which freestanding graphene is produced on a gram scale within a few seconds. The formed graphene is collected

downstream on membrane filters or from the walls of the reaction chamber [16, 54, 105]. In the following discussion, salient features of this process (summarised in table 2.1) will be discussed.

2.3.1 Plasma reactors

Atmospheric pressure microwave plasma has been previously used to synthesize boron nitride or aluminium nanoparticles. For graphene, Dato et al. [54] were the first to show the possibility of synthesis of free-standing graphene in a similar reactor. They used a quartz chamber, which has an alumina tube concentred in a quartz tube. The alumina tube was used to deliver carbon precursor i.e. ethanol, directly into the plasma stream. The schematic illustration of their system is shown in Fig 2.5a. The dissociation of ethanol vapors and their conversion into solid matters occurred in a short interval, and a 2 mg/min production rate was recorded.

Tatarova et al. [105] used surface wave-induced microwave plasma to synthesize free-standing graphene. Considering the crucial role of outlet plasma stream, they modified the system with a cryostat to control the temperature at the nucleation zone. With small modifications, they used the same system for the synthesis of N-doped graphene as well. Briefly, it consists of a 2.45 GHz generator, which is connected with the waveguide, quartz tubes, and hurricane cyclone system followed by a methanol trap. They actively controlled the gas flow rates and temperature by MKS247 Readout and infrared irradiation of the wall respectively. Vaporization was performed by passing argon gas through an ethanol tank [106]. The system is shown in Fig 2.5b.

Melero et al. [107] used a special microwave plasma torch, named as TIAGO (Torche a Injection Axiale sur Guide d'Ondes, in French) torch. It is a one-nozzle component, providing a single flame of plasma. The torch supplied with argon gas opens inside a

quartz chamber and forms plasma having the appearance of a jet conical flame. They adjusted the system with efficient argon and precursor input i.e. ethanol mixer system, which allowed the control of ethanol vapors supply. The Controlled Evaporator Mixer (CEM, Bronkhorst) along with the ethanol vaporization system is superior to bubblers in terms of stability and accuracy.

Munzer et al. [108] used the same approach as Dato et al. [54] and Tatarova et al. [105] as shown in Fig 2.5c. However, they supplied ethanol using an external syringe pump at an optimized flow rate. Moreover, they also investigated the effect of reactor's pressure by varying it from 1000 to 1500 mbar.

Toman et al. [20] synthesized graphene in a dual-channel microwave plasma torch at atmospheric conditions. The setup is shown in Fig 2.5d. The system was fixed with two supply channels i.e. central and secondary channels for argon and argon-ethanol mixture respectively. The advantage of this specific design is that the system can also be fed with oxygen and/or hydrogen gasses through the central or secondary channel. The precursor flow was controlled by the mass-loss method, which may not have had a precise and active control on ethanol vapors. Nonetheless, an efficient method for the collection of graphene nanosheets is needed, as the collection from the walls of the container is tiresome for upscaling of the method.

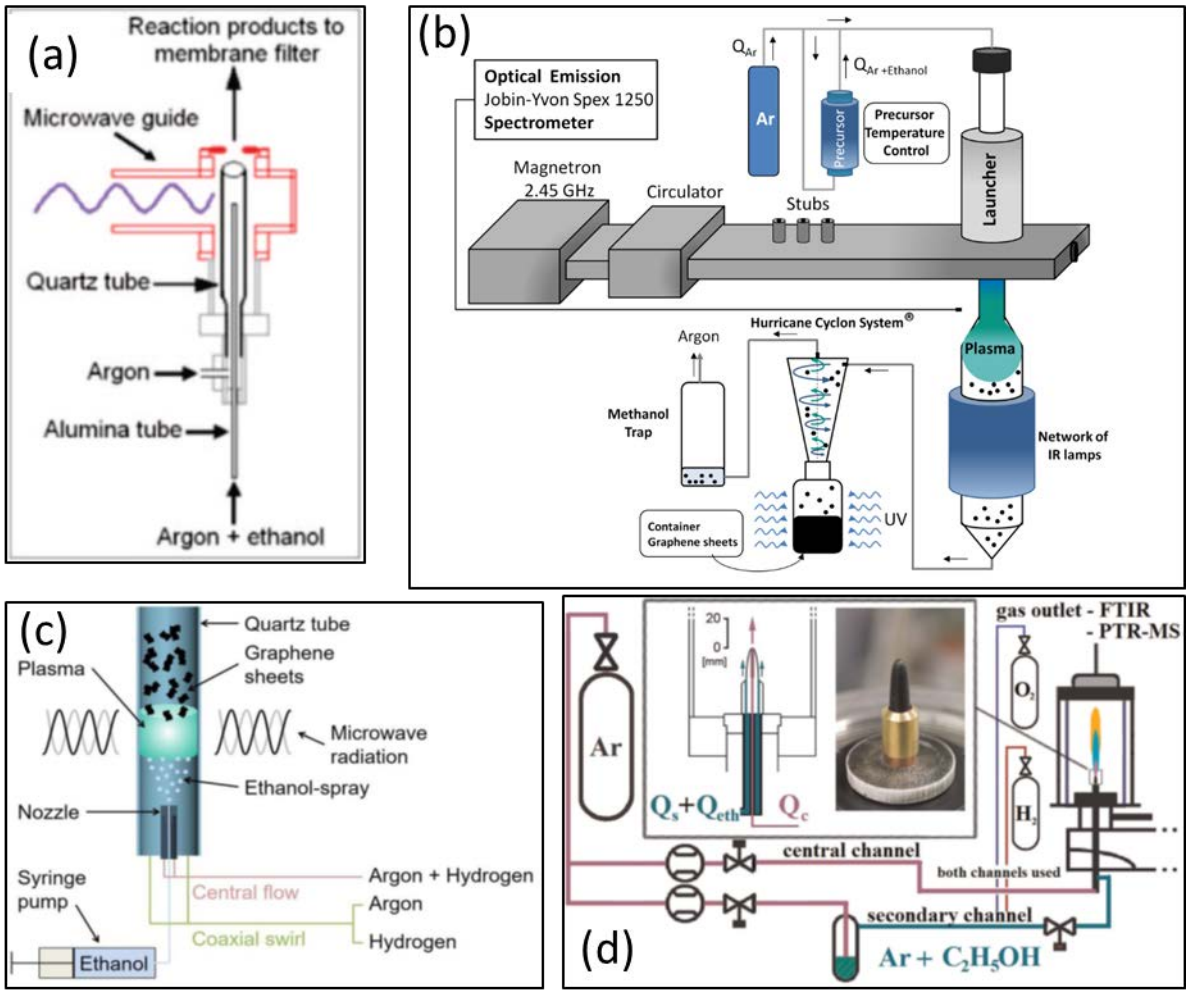

Fig 2.5: (a) Schematic illustrations of plasma reactors used by Dato's et al. [63] (b) Tatarova et al. [106] (c) Munzer et al. [108] (d) Toman et al. [20]

2.3.2 Precursors and their role in graphene formation

Few precursors have been explored for microwave plasma synthesis of freestanding graphene. Dato et al. [63, 109] employed different precursors and investigated their role in shaping the final morphology of graphene. They supplied precursors into the plasma in an aerosol form. Their main study was on investigating ethanol as a precursor, however, they also studied methanol, isopropyl alcohol (IPA), dimethyl ether (DME). The methanol feed showed no apparent formation of substances. It could be due to two possibilities; either plasma power was not enough to breakdown the methanol into its

constituents or only gas substances were formed which escaped the outlet of the reaction chamber. On the other hand, IPA formed carbon soot, whereas, DME showed encouraging results for graphene synthesis.

Ethanol is the most commonly used precursor in the gas-phase synthesis of graphene. In Dato et al.'s [63] work, ethanol formed single and bilayers graphene nanosheets at a microwave power of 250 W at the rate of 2 mg/min. Tatarova et al. [105] made graphene having 1 to 5 number of layers from ethanol at a microwave power of 900 W. Similarly, Melero et al. [107] observed 2 to 7 layers of graphene from ethanol at a microwave power of 300 W. In their work, ethanol produced 1.33 mg/min of graphene from 33 mg/min of ethanol consumption, which is comparable with the findings of Dato et al. [63], where they obtained 2 mg/min graphene but at the cost of 3 times higher ethanol consumption.

The composition of the precursor especially C/O ratio has a profound effect on graphene formation [109]. It was noted that in order to develop C-C bonding in graphene, a suitable amount of carbon is necessary. Since the C/O ratio in methanol (CH_3OH) is one, it is more likely to produce CO instead of C-C bonding. On the other hand, a higher C/O ratio as in the case of IPA (C_3H_8O) will form carbon soot. The C/O ratio in ethanol (C_2H_5OH) has been reported to be appropriate to initiate C-C bonding. DME (C_2H_6O), which has the same C/O ratio as ethanol, showed promising results for graphene synthesis. A single carbon is deemed insufficient to give forth C-C bonding, instead it may form CO. The above description also highlights the significance of the presence of oxygen in the formation of graphene as well as overall production rate.

Encouraging results on graphene formation have been reported using methane (CH_4) as the only source of carbon at a microwave power of ~1 kW [110, 111]. Interestingly,

methane, which carries only one unit of carbon negates the fact that carbon should be in C-C form to produce graphene. However, it should also be noted that the O in methane is absent and CO formation might not happen.

The influence of the flow rate of ethanol and plasma gas on the structure of synthesized products has also been analyzed. Tatarova et al. [105, 112, 113] studied the effect of aerosol flow rate ranging from 0.5 to 3.5 sccm. A flow rate of 0.6 sccm for ethanol and 250 sccm for Ar showed the highest quality graphene. In another study, Tatarova [106] raised the ethanol flow rate to 30 sccm, and Ar to 1200 sccm to synthesize graphene. It was suggested by them that a short precursor residence time would avoid the agglomeration of graphene into graphite. They observed ethanol decomposing into C, H, H_2, C_2, and CO [112]. Dato et al. [63, 109] mentioned the formation of CO, C_2, and H_2 as well. However, they linked C_2 formation with the C/O ratio of the precursor. In mass spectrometeric analysis, Rincon et al. [86] observed CO, H_2, and traces of acetylene and methane as a by-product. Munzer et al. [108] synthesized high quality and largest quantity of graphene at 1 mL/min flow rate of ethanol. Singh et al. [111] added hydrogen in the precursor to study the influence of hydrogen on graphene structure. They found that higher the ratio of H/C, greater would be the yield of graphene.

The role of oxygen in the synthesis of freestanding graphene using microwave plasma has also been investigated. It was found that the reactant concentration has a great influence on the graphene formation. The low content of the reactant concentration reduces the soot formation, and promotes the graphene production. The amount of water in the precursor promotes CO formations, and hence the graphene formation [114].

2.3.3 Microwave power

Microwave power plays an important part in dissociating the precursor and raising the electron temperature in the plasma chamber [109]. A range of microwave powers, for instance, as low as 250 W [63] and as high as 2 kW [106] have been investigated to synthesize graphene. It has been noted that for ethanol precursors, the microwave power does not significantly affect the structure of graphene. Graphene was formed at all microwave powers. However, other alcoholic compounds, such as isopropyl alcohol, start forming soot-like carbonaceous particles at higher microwave power [109].

In another study on the synthesis of graphene from ethanol, Tatarova et al. [112] observed that decreasing the power below 500 W formed carbon nanoparticles instead of graphene (Fig 2.6). They ascribed this to supersaturation occurring inside the chamber due to the decrease in gas temperature. However, the TIAGO torch operating at a low microwave power of 300 W revealed the formation of pure graphene consisting of a few layers [107]. Thus, it can be stated that the design of the plasma reactors also carries a strong influence on the final structure of the carbon material.

Bundaleska et al. [110] synthesized graphene from methane at a microwave power of 1 kW. Interestingly, the same microwave power of 1 kW but with higher methane and Ar flow rates formed diamond-like structures. They also developed a theoretical model, which indicated the formation of solid carbon compounds at higher microwave powers such as 1.5 kW. Toman et al. [20] have studied the influence of the microwave power on the structure of graphene. They reported that the transition of material from amorphous to crystalline form depends on the microwave power, ethanol flow rate, and molecules mixture.

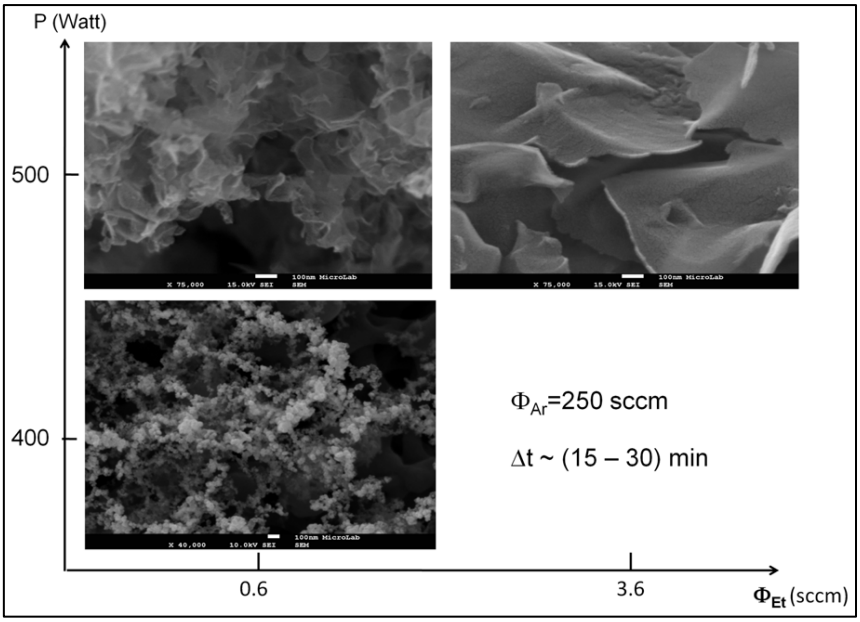

Fig 2.6: Effect of ethanol flux and microwave power on carbon nanostructure [112]

2.3.4 Comparison of the graphene structure and morphology

Tatarova et al. [112] controlled the wall temperature of the plasma chamber using a cryostat and studied its influence on the quality of graphene. It was noted that external heating or cooling does have some effect on the structure of graphene. For instance, low wall temperatures form carbon nanoparticles, whereas temperatures above 60°C promote graphene formation. Also, the samples showed lower numbers of monolayers when the wall temperatures were kept above 60°C. However, the Raman spectra shown in Fig 2.7 displayed an intense peak for the wall temperature of 60°C as compared to that of 80°C. This can be attributed to the structural defects in the samples created at 60 °C. The low-resolution images shown in Fig 2.7 showed monolayers and a few layers of graphene nanosheets. In addition, it can be observed that some of the sheets are overlapping and folded at the edges.

The effect of precursor flow rate on the quality and production amount of graphene has also been investigated thoroughly. In a work presented by Casanova et al. [115], they

found that varying the ethanol flow rate from 2 g/hr to 3.4 g/hr, increases graphene production steadily. However, a further rise in ethanol flow rate not only reduces the quantity of graphene but also starts forming carbonaceous particles. This can be illustrated through the Raman spectra (shown in Fig 2.8 a, b) which also shows the intensity ratios i.e. I_{2D}/I_G and I_{2D}/I_G at different ethanol flow rates. Only 4 g/hr flow rate of ethanol showed I_{2D}/I_G value of less than one, which is indicative of multilayer graphene. However, a 3.4 g/hr flow rate of ethanol can be considered optimum parameter in this synthesis since the value of I_D/I_G, which suggest the defects in the structure, is the lowest. Overall, all the samples of different ethanol flow rates showed evidence of graphene formation. The D (~1350 cm^{-1}), G (~1580 cm^{-1}) and 2D (~2700 cm^{-1}) bands can be observed in Fig 2.8. The low values of I_D/I_G, ranging between 0.2 and 0.35 indicated the low number of defects in the sample. The shoulder peak in G band arises due to intra valley transition [116] and corresponds to weak disorder-induced feature [117].

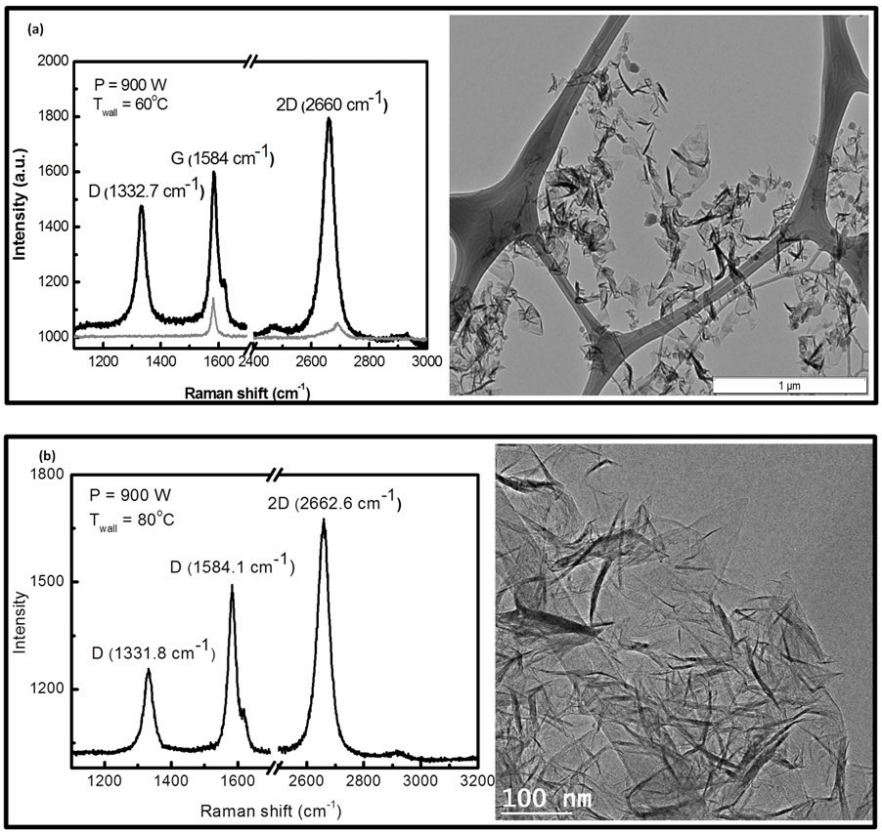

Fig 2.7: Raman spectra and corresponding TEM images showing the effect of chamber wall temperatures [112]

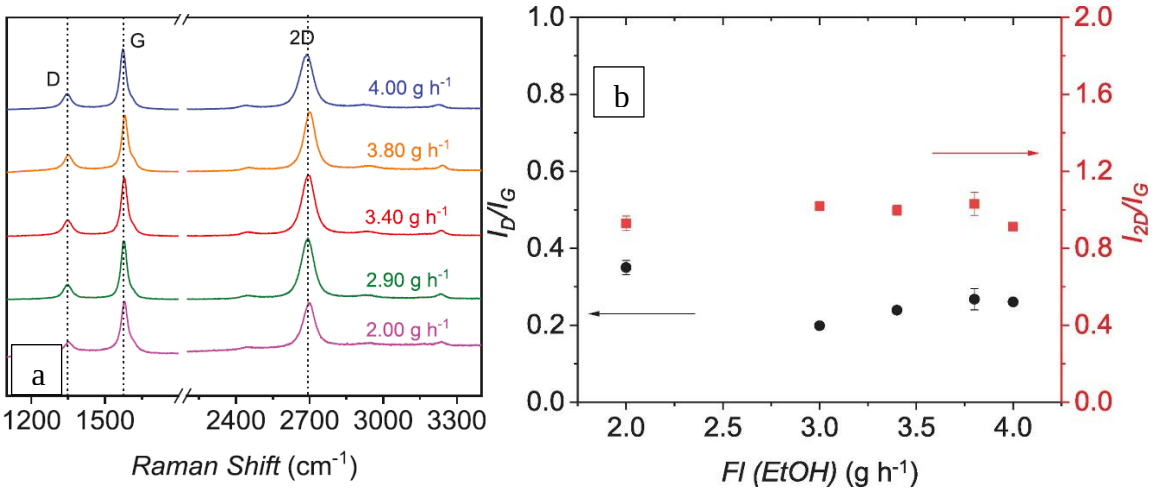

Fig 2.8: (a) Raman spectra of samples showing the effect of ethanol precursor flow rate, (b) I_D/I_G (black circles) and I_{2D}/I_G (red squares) values of the Raman spectrum obtained at different flow rate of ethanol [115]

2.3.5 Synthesis of nitrogen-doped graphene

The scope of atmospheric pressure microwave plasma has now been extended to the synthesis of nitrogen-doped graphene (N-graphene). It has been proven that it is possible to synthesize a good quality N-graphene in a single-step using an atmospheric pressure microwave plasma system. However, the high-resolution N1s spectra of these materials have revealed that the pyrollic N that is considered important for some applications was absent. Moreover, the procedure involved the usage of an additional nitrogen gas supply along with the consumption of a 2 kW high microwave power. This practice makes the process energy-intensive [106]. In another attempt to synthesize in-situ N-graphene, Bundaleska et al. [118] used ammonia instead of nitrogen along with ethanol. The high-resolution N1s results showed the presence of pyridinic, pyrrolic, and graphitic nitrogen. However, they also used a high microwave power of 2 kW. Moreover, ammonia being a toxic chemical is not an appropriate choice for the synthesis.

Tsyganov et al. [119] synthesized N-graphene by injecting ammonia directly into different zones of plasma. They found that the injection position plays a role in determining the doping level of nitrogen in graphene and the yield of N-graphene. Recently, another approach for single-step synthesis of nitrogen-doped graphene oxide (N-GO) has been reported [120]. They eliminated the usage of any additional gas or precursor and synthesized the N-GO from aniline as a sole precursor. Also, they brought down the microwave power to 80 W, which was a substantial reduction in the usage of the energy. Moreover, their results exhibited the presence of nitrogen in the form of pyridinic, pyrrolic, and graphitic nitrogen. However, applications N-GO needs to be converted into N-graphene using additional steps such as reduction.

2.4 Other plasma sources for the synthesis of graphene

Various other plasma techniques depending upon the sources of plasma have also been employed to synthesize graphene. It includes DC plasma [121, 122], cathodic vacuum arc plasma [123], thermal jet plasma [124, 125], and hot filament/hot wire plasma [126, 127]. Although the product of theses plasma sources i.e. graphene have nearly same characteristics, but the setup to produce graphene involves different parts and procedures. For instance, DC plasma setup consisted of graphite rod anode to hold the substrate, tungsten cathode, DC power supply, and quartz chamber [128]. DC plasma system are also two types, i.e. pin to plate and parallel plate type. In DC plasma, it has also been reported that the distance between plasma source and substrate significantly affects the final structure of the graphene [129, 130].

In hot-filament process two Tantalum filaments (0.5 mm diameter) fitted above the substrate, heated to 2000°C are used to dissociate the gasses and to convert it into the graphene. Zhai et al. [131] synthesized B-doped graphene directly on glass substrate using hot-filament CVD method. The synthesized graphene consisted of nanocrystalline graphene grains and was uniform on the large scale of glass substrate. Radio-frequency thermal plasma jet system consisted of plasma torch, generator, quartz reactor, and a precursor delivery system. Fronczak et al. [132, 133] showed continuous synthesis of graphene from different carbon sources in RF-thermal plasma. The proposed system produced a comparable graphene nanostructure.

Microplasma, a recently emerging technique is also a promising technique for the synthesis of graphene. Microplasma, featuring micro-scale dimensions is a low-temperature plasma, which comprises non-equilibrium reactive environment and high-energy density [134]. Microplasma has been employed to synthesize graphene quantum dots in colloidal form. The synthesis was carried out at atmospheric conditions. The graphene quantum dots had the average diameter of 4.9 nm, and showed photoluminescence around 448 nm [135].

An inductively coupled plasma was used to synthesize and coat graphene on the stainless steel. In this novel approach, it was demonstrated how graphene can be sprayed on the substrate by employing a two-translation axis robotized arm. This system also allows a precise control over the distance between substrate and plasma torch, and substrate's plasma exposure time [136].

2.5 Plasma for the synthesis of graphene-based composites

Wei et al. [137] synthesized graphene oxide and silver nanoparticles nanocomposite in dielectric barrier discharge plasma at ambient conditions. A reduction method was used for this purpose, where plasma worked as a reductant on a graphene oxide substrate. Briefly, first a mixture of graphene oxide and Ag nanoparticles powders were mixed ultrasonically for 12 hours. After drying the mixture, it was reduced using hydrogen plasma for 1 hour. However, it was a long procedure for the synthesis of nanocomposite, overall it was a green and dry process since it did not require any surfactants and solutions. The nanocomposite formation was confirmed through XRD, XPS and EDS elemental analysis. The as-fabricated nanocomposite was quite effective against escherichia coli bacteria.

In another study, rGO/Mn_3O_4 composite was prepared in dielectric barrier discharge plasma. First, Mn and GO were produced through Hummers method. Subsequently, they were converted into rGO/Mn_3O_4 composite using air oxidation and dielectric barrier discharge plasma deoxygenation. XPS, XRD and TEM confirmed the formation of nanocomposite. The synergistic effect of both rGO and Mn_3O_4 showed remarkable results in supercapacitor application. For instance, 193 F/g specific capacitance was noted when the amount of Mn_3O_4 was 90 % in the composite [138].

Microwave plasma was used to synthesize Pt/graphene composite from the mixture of Pt and ethanol. The experiment was employed at ambient conditions. Raman, XRD and TEM were used to characterize the composite. The TEM images showed Pt nanoparticles of 2.6 nm sizes

uniformly dispersed on graphene having wrinkled-paper like sheets. The Pt/Graphene composite had high surface area, which made it promising material for catalysts applications [139].

TiC/graphene nanocomposite was produced by Kim et al. [140] in thermal plasma. The results showed that TiC were less than 50 nm sizes, and well dispersed. In another study, graphene nanocomposite with anatase TiO has also been produced using the plasma. The synthesis was carried out in three steps, i.e. thermal plasma, dielectric barrier discharge (DBD) and heat treatment. In thermal plasma, TiC-graphene composite was synthesized from isopropoxide. Afterwards, it was converted to anatase TiO_2 in dielectric barrier discharge plasma, followed by heat treatment to remove amorphous carbon and contaminants. The TEM images revealed 50 nm or below sizes of TiO_2 nanoparticles. Moreover, the dispersion of the TiO_2 nanoparticles were quite uniform on the graphene nanosheets [141].

Tanaka et al. [142] synthesized graphene-encapsulated silicon nanoparticles using pulse-modulated induction thermal plasma with a controlled feedstock. Graphene was synthesized from methane in the induction plasma. Micro-sized Si particles were sent intermittently into the plasma. The formation of graphene-encapsulated Si nanoparticles was confirmed through SEM, XRD and TEM. This approach of synthesizing the graphene composite is commendable especially for its high production rate.

Another unique approach i.e. solution plasma process was used to synthesize GO-MnO_2 composite for a supercapacitor application. The process involves the generation of plasma in the beaker containing the mixture of GO and MnO_2. The plasma was generated by bipolar-DC power supply at ambient conditions. The as-synthesized GO/MnO_2 composite was used for a supercapacitor application which showed specific capacitance of 218 F/g [143].

2.6 Plasma-based processing of graphene structure

In order to achieve desirable properties in synthesized graphene, the structure of graphene can be altered using radio frequency or microwave plasma. The structure alterations include doping, intentional creation of pores, defects and/or functionalization. Depending on the exposure time, reactive radicals and ions in the plasma are responsible for the development of point and line defects in the graphene layers and thinning the reactive edges of the graphene [144, 145]. The defects such as grain boundary and topological defects give rise to high strength in tilted graphene boundaries [146] and improved electronic properties [147] respectively.

Plasma can be used for in-situ functionalization of graphene by introducing different gases in the reaction chamber. Hydrogenated graphene gives improved p-type conduction and physical properties. Also, it converts the semi-metallic graphene to insulator [148], and impart magnetic properties [149]. Increasing the doping amount of hydrogen ions in graphene layer, also increases electrical resistance and lowers the holes mobility. Consequently, an increase in the band gap of the layers is noticed. It is also important to mention here that plasma-based hydrogen functionalization requires certain order of frequencies i.e. kilohertz (kHz). Higher order of frequencies i.e. MHz etches the graphene layers [150].

Similar to hydrogenation, oxygen functionalization also imparts significant changes in electrical properties of graphene. Plasma-based oxygen functionalization is much appreciated approach owing to its simplicity and environment-friendly approach. For instance, Liu et al. [151] functionalized graphene using controlled water-vapors supplied in the plasma chamber, operated at 100 W. In another approach graphene has been functionalized using oxygen/argon gas mixtures in electron beam generated plasma. The oxygen functional groups increased the covalent bonds in graphene structure, and hence the surface-energy. Consequently, oxygen-functionalized graphene become reactive and very feasible for strong bonding between

graphene and metals [152]. CVD synthesized graphene has been modified in atmospheric pressure microwave plasma using O_2 gas. This approach of oxygen functionalization was quite useful to enhance the graphene semiconducting properties and chemical reactivity [153].

Nitrogen functionalization using amine (NH_2) in plasma reactor has shown significant changes in graphene electrical and chemical properties, particularly used in biosensors. Such a functionalized graphene shows n-type conductive behavior. At lower plasma powers nitrogen functionalization occurs only at the edges of the graphene layers, whereas, at higher powers nitrogen bonds at complete basal plane. Consequently, higher powers functionalized graphene show a high decrease in the conductivity of the graphene [154-156]. Fluorination of graphene has shown great improvement in optical properties. For instance, one-sided fluorinated graphene has shown high optical transmittance and resistivity, which consisted of an optical band gap of 2.93 eV [157].

Alosaimi et al. [158] demonstrated a graphene oxide modification technique using the atmospheric pressure plasma. The modification showed changes in the multiple properties such as chemistry, surface charge, electrical, wettability, thermal conductivity and the morphology of the graphene. These properties were obtained by exposing the graphene oxide to atmospheric pressure plasma. The process involves the reduction of graphene oxide into partially reduced-graphene oxide and reduced-graphene oxide. The procedure is advantageous because of its environmentally friendly nature and being very economical. Moreover, it can be performed on various substrates including metals, glass, semiconductors, Si, plastic etc.

The usage of microwave plasma to reduce the graphene oxide for the potential applications has been investigated. Polyethylene terephthalate (PET) coated with graphene oxide on its both sides has been successfully reduced to conductive reduced-graphene oxide. It was also shown

that the addition of nitrogen gas into the reactor chamber converts the graphene oxide into a nitrogen-doped graphene oxide [159].

2.7 Applications of graphene

2.7.1 Applications of PECVD grown graphene

i. Applications in supercapacitor

Owing to fast charge/discharge rate, high power density, and long cycle life in supercapacitors (pseudocapacitors and electric double-layer capacitors) have attracted great interest of scientists as a new energy storage device [160-162]. Fast charge-discharge rate, long-life, high power and energy density are few characteristics which make supercapacitors different and advanced from conventional capacitors. Supercapacitors are of two types, i.e. electric double-layer capacitors (EDLC) and pseudocapacitor. In EDLC electrical energy is stored by intercalating charges at electrolyte-electrode interface by making the double layer of charges. In this, charges are deposited physically due to the electrostatic attraction. Here graphene is used as an electrode material to store charges. Pseudocapacitor involve faradic reactions to store the electrical energy [163-165]. Graphene has been considered as a new alternative supercapacitor material due to its high conductivity and surface area. Moreover, vertical morphology of graphene is very suitable for the diffusion of ions [166, 167].

PECVD grown graphene grown on different substrates has also been investigated for supercapaciotrs applications using electrochemical studies. The graphene grown on Ni foam has shown excellent specific capacitance of 230 F/g at a scan rate of 10 mV/s. The results are shown in Fig 2.9. The supercapacitor showed insignificant capacitance after 1500 cycles at high current density. It should also be noted that the capacitive behavior

of graphene can be modified by controlling the plasma process parameters such as gas type and plasma power [47, 87].

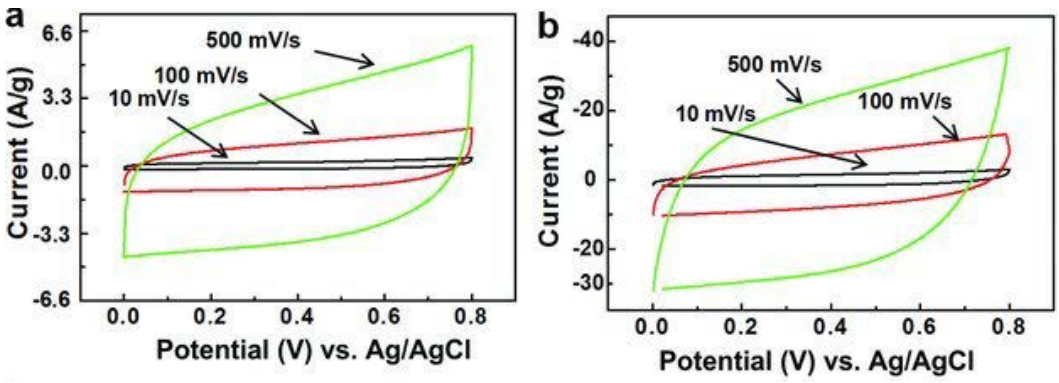

Fig 2.9: Cyclic voltammetry (CV) curves of VGNS grown at (a) 40% and (b) 80% H_2 at varied scan rates [87]

Miller et al. [168] synthesized graphene from methane using RF-PECVD on Ni substrate. The as-synthesized graphene was utilized as an electrode in supercapacitor. In another study Bo et al. [169] synthesized graphene in PECVD for an electric double layer capacitor. The binder-free electrode showed improved wettability and offered improved ion access. Resultantly, remarkable electrochemical properties were observed in aqueous and binder-free electrolytes.

ii. Applications in sensors

Graphene materials are also widely used in variety of sensors owing to their remarkable sensitive properties [170, 171]. PECVD synthesized graphene was directly grown on Au/Si to form the heterojunction for its application in infrared photodetector. The deposited graphene formed strong van der Waals bond. Resultantly, a photo to dark ratio and responsivity was noted up to 2 x 10^4 and 138 mA/W respectively [172]. Comparing with CVD grown graphene, it was found that CVD graphene showed impurities and mismatching between graphene and Au/Si [173]. Yang et al. [174] made graphene-based

electrode for tunable and sensitive capacitive pressure sensor. The sensor showed fast response, low detection limit, tunable sensitivity, high sensitivity, stability and flexibility. This is a great example of graphene application in wearable health-monitoring devices. PECVD synthesized graphene-based sensors have also been used in various electrochemical sensors [175-177].

Wearable sensors with high sensitivity and stretch-ability are highly desirable. Graphene is now becoming an important part in wearable sensors and electronics. Compressing, stretching and flexibility are the important characteristics of wearable electronics. Graphene is combined with elastic materials in real applications to form wearable electronics. Robotics and wearable smart electronics are particularly using graphene as wearable sensor materials owing to graphene excellent properties of stretchability and sensitivity [178, 179].

Wu et al. [180] developed a strain sensor made of graphene sandwiched between polydimethylsiloxane (PDMS). The sensor was non-corrosive to human sweat and insensitive to temperature. They found that the basal plane of vertical graphene is crucial in obtaining the high gauge factor in the strain sensor. Also, it was observed that the stretch-ability and sensitivity can be modified by altering the height of the vertical graphene.

In another stretchable sensors study Yang et al. [181] made electronic skin (E-skin) which showed very sensitive response to vocal cord vibration, joint and eye movement. The sensor demonstrated a gauge factor up to 65.9 with a 100 % of maximum stretch-ability. The sensor is quite promising for its applications in wearable healthcare devices.

A temperature sensor based on graphene and polydimethylsiloxane (PDMS) was also developed. The sensor showed a temperature coefficient of $0.214°C^{-1}$, three times higher

than that of conventional temperature sensors. It was due to the outstanding thermal sensitivity and stretchability of graphene. The sensor showed promising results for human body temperature sensing. Moreover, the recovery time of the sensor was quite efficient. It is shown in Fig 2.10a [182]. An electrochemical biosensor for lactate sensing has also been developed which showed wide linear range and low limit of detection. The cyclic voltametric response of detection is shown in Fig 2.10b [183].

Huang et al. [184] fabricated parallelly aligned vertical graphene for wearable strain vector sensor. Due to the electrically anisotropic nature, the sensor was able to detect strain and amplitude of the strain vectors simultaneously. The human-sensor interface was investigated in real-time application for finger-joint movements.

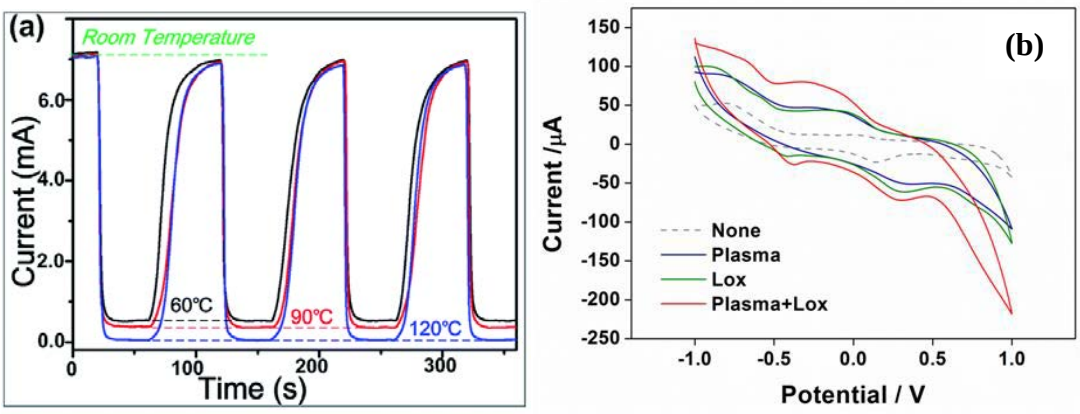

Fig 2.10: (a) Wearable temperature sensor showing response/recovery time [182] (b) Cyclic voltametric response of different graphene-based sensors for lactate detection [183]

iii. Applications in photovoltaic devices

A photovoltaic device converts sunlight energy into the electricity. Though much progresses have been made in photovoltaic devices, high production cost and low efficiency of the devices are still some of the challenges which require scientist's attention [185]. Benefitting from graphene's low sheet resistance and high transparency,

graphene is now considered an ideal material to be used in current photovoltaic devices. For instance, graphene transparent electrodes have been used in organic photovoltaic devices [186-188] and dye-sensitized solar cells [189, 190]. Previously used CVD techniques require the transferring of the synthesized graphene on required substrates for photovoltaic devices. The transferring process produces cracks or wrinkles in the graphene, which affect the quality of the graphene. PECVD has the ability to directly synthesize graphene on variety of substrates and which at the same time has low sheet resistance and high transparency [191].

Carbon-based heterostructure junctions are now widely appreciated in solar cells. P-N and Schottky junction are some examples of it. Graphene Schottky junction is more valued due to its excellent charge separation efficiency and large built-in field [192, 193]. The power conversion efficiency in graphene still needs scientist's attentions. An example of that is the fabrication of graphene-graphitic film on silicon substrate. However, this graphene/silicon schottky junction solar cell showed poor efficiency of 0.078 %.

PECVD fabricated graphene nanowalls are another example of graphene-based materials, employed in solar cells. Their use include as a counter electrode in dye-sensitized solar cells [194]. The dye-sensitized solar cells made of as-synthesized and hydrogen plasma treated graphene nanowalls showed improved power conversion efficiency. The power conversion efficiency in plasma treated solar cell was higher than as-synthesized graphene. It is attributed to the reduction in sheet resistance of graphene material [195]. The power conversion efficiency can be increased even more by fabricating graphene nanowalls directly on silicon substrate. For instance, Liu et al. [196]

reported 5.1 % of power conversion efficiency of such a heterojunction material. It was attributed to the high surface area of vertical graphene nanowalls.

Bayram et al. [197] synthesized graphene/polyaniline nanocomposite using the PECVD setup for the dye-sensitized solar cell application. Graphene/polyaniline nanocomposite was used as a counter electrode. Nanocomposite was prepared in multi-steps. It includes single and multilayer graphene films fabrication on fluorine-doped tin oxide substrate. Subsequently, polyaniline films were produced on graphene films. The dye-sensitized solar cell comprised of N719 dye, iodolyte liquid electrolyte, titanium dioxide (TiO_2) nanotube photoanode, and graphene/PANI nanocomposite. It is shown in Fig 2.11a. Current-voltage characterization given in Fig 2.11b showed that photo-conversion efficiency varied between 0.56 and 1.36 % depending upon the number of layers of graphene. The photovoltaic performance of dye-sensitized solar cell was recorded as 1.1 %.

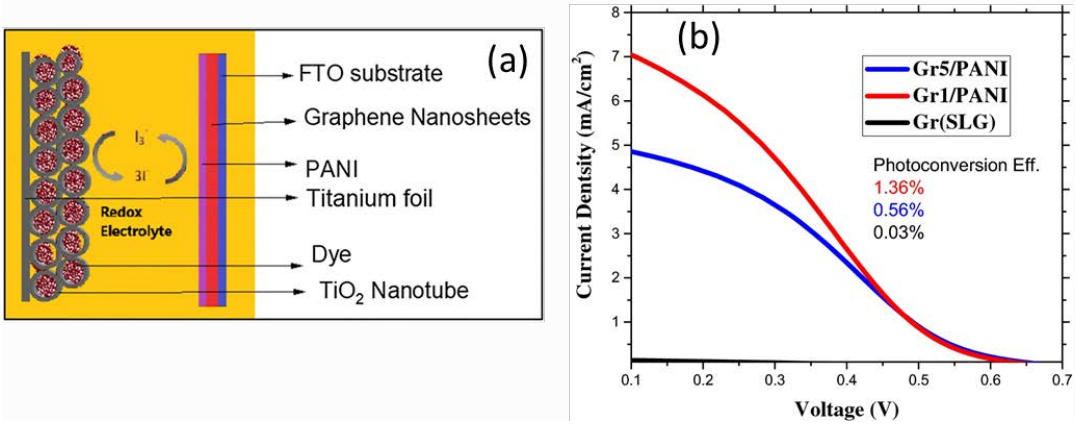

Fig 2.11: (a) Dye-sensitized solar cell configuration (b) J-V curves of graphene/polyaniline curves [197]

2.7.2 Applications of atmospheric pressure microwave plasma-synthesized graphene

i. Applications in supercapacitor

Nitrogen-doped graphene synthesized in atmospheric pressure plasma was used as an electrode in supercapacitor application. Electrochemical methods i.e. cyclic voltammetry, electrochemical impedance spectroscopy, and galvanostatic charge-discharge were used for this purpose. As expected from a charge storing material, N-graphene showed perfect rectangular structure. It is shown in Fig 2.12a. The cathodic and anodic current responses showed an increase with the increase of scan rate, and a rectangular shape was observed even at 400 mV/s scan rate. Galvanostatic charge-discharge measurement were conducted at current densities ranging between 0.1 and 1 A/g. It is shown in Fig 2.12b. The results showed linear charge and discharge behavior at all current densities which prove the electric double layer capacitance behavior. Moreover, specific capacitance of 8.87 F/g was attained at 0.1 A/g current density. The specific capacitance retained its value even at increased amount of currents [118].

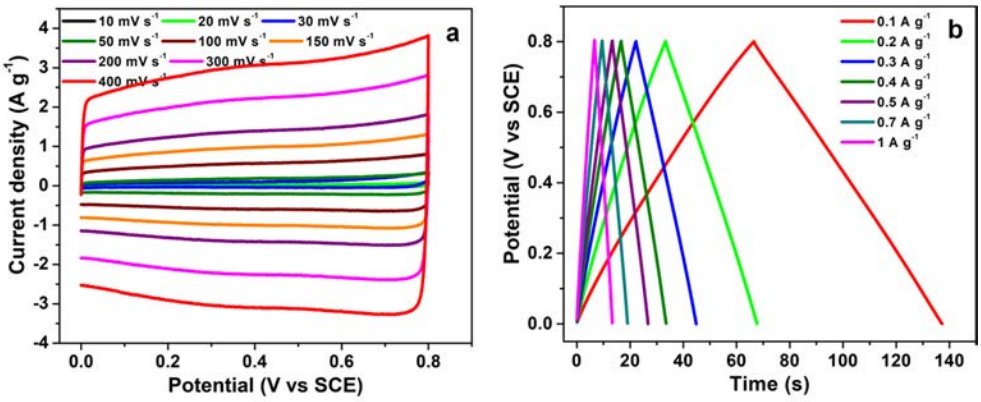

Fig 2.12: (a) Cyclic voltammograms of N-doped graphene at various scan rates (b) Galvanic charge-discharge at various current densities [118]

ii. Applications in sensors

The atmospheric pressure microwave plasma synthesized nitrogen-doped graphene oxide has also shown remarkable results in electrochemical sensing of oxalic acid [198]. Oxalic acid could have adverse effects on human health if consumed excessively. Thus, it is very important to detect oxalic acid in foods. Ag-Nps loaded nitrogen-doped graphene oxide drop-casted on glassy carbon electrode was used as a working electrode in this study. The electrode was used for oxalic acid detection in a phosphate buffer solution. Compared with bare or nitrogen-doped graphene oxide showed prominent peak current in cyclic voltammetry measurements. The cyclic voltammetry results are shown in Fig 2.13. Furthermore, characterized through chronoamperometry, the electrochemical sensor showed a lower limit of detection and a wide linear range i.e. 2 µM and 10 – 300 µM respectively. Attributed to the anti-fouling properties of nitrogen-doped graphene oxide, the proposed sensor demonstrated excellent stability and repeatability results. Graphene synthesized using the microwave plasma has proven its excellency in herbicide detection. A wide linear range and a remarkable limit of detection was noted for diuron detection.

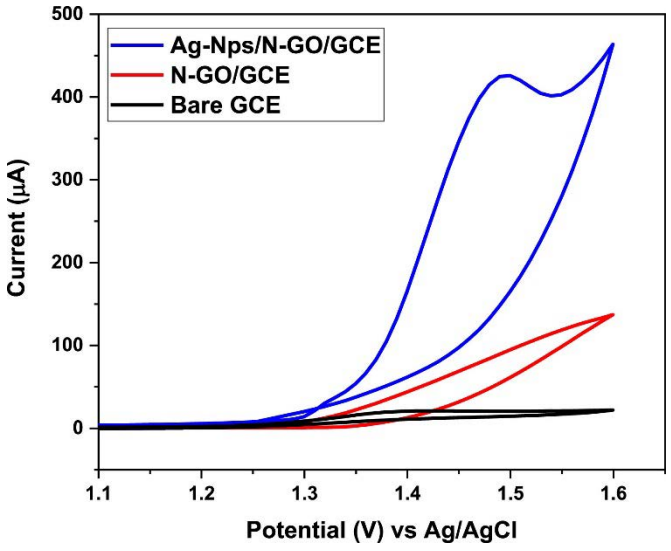

Fig 2.13: Cyclic voltmmograms of modified working electrodes for oxalic acid detection in a phosphate buffer solution [198]

iii. Application in water desalination

Nitrogen-doped graphene oxide, synthesized in atmospheric pressure microwave plasma from a single source i.e. aniline was used in a demonstration application of desalination. A lab scale developed desalination system was used for this purpose. Commercially available polyamide membrane was used in this application. The membrane was coated with nitrogen-doped graphene oxide using the drop-casting method. It is shown schematically in Fig 2.14a. The nitrogen-doped graphene oxide coating did not affect much hydrophilicity of the membrane, shown through water contact angle in Fig 2.14b, c. However, nitrogen-doped graphene oxide coating improved the flux recovery ratio (Fig 2.14 d), which can be attributed to the excellent anti-scaling properties of the nitrogen-doped graphene oxide material [199].

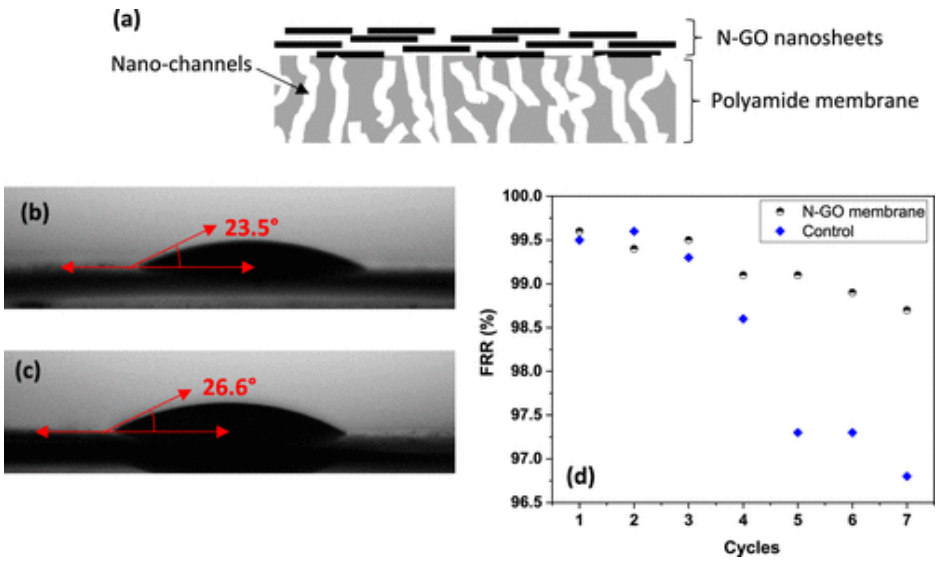

Fig 2.14: (a) Schematic demonstration of the nitrogen-doped graphene oxide -coated-polyamide membrane, (b) water contact angle of the polyamide and (c) nitrogen-doped graphene oxide-coated polyamide membranes, and (d) flux recovery ratio after number of cycles of water filtration [199]

iv. Applications in catalysis and battery

The dispersion of nanoparticles on base materials is critical for catalysis applications. It is highly desired that the catalytic nanoparticles should have high surface area, and avoid any aggregation [200, 201]. Graphene for dispersion of nanoparticles can play an important role. In a study, gold nanoparticles of varying diameters were spread on graphene synthesized through atmospheric pressure microwave plasma. The study revealed that the small sizes nanoparticles i.e. less than 10 nm tend to locate on the edges of the graphene nsnosheets, and avoided aggregations. It means, nanoparticles less than 10 nm dispersed on graphene nanosheets can be useful in catalysis applications [202].

In another study by Jo et al. [139] Pt/graphene nanocomposite was prepared in microwave plasma. The nanocomposite was investigated for its application in electrocatalysis. Investigated through cyclic voltammetry, the Pt/graphene nanocomposite showed excellent electrocatalytic activity for the methanol oxidation. Compared with other Pt composites with carbon and graphene, this study revealed that the electrocatalytic results were superior. It can be attributed to the high dispersion of Pt on graphene, and graphene's high electrocatalytic properties.

Graphene nanosheets synthesized in atmospheric pressure microwave plasma has also been used for its application in battery. For instance, graphene nanosheets and Si nanocomposite was used in Li-ion battery. Compared with other reported Si composites, graphene/Si nanocomposite anode outperformed all those and showed superior Coulomb efficiency and longer stability [108, 203, 204].

2.8 Conclusion and future outlook

The production of superior quality graphene in a fast and efficient way is one of the merits of Plasma-based synthesis method. PECVD synthesis of graphene is a widely adopted bottom-down approach capable of producing monolayer to few-layers graphene. In comparison to top-down methods where graphite is the main resource for graphene, PECVD is a versatile approach as it can synthesize graphene from a diverse range of precursors, such as natural gas, botanical hydrocarbons, food products, polymers, wastes, etc. Furthermore, shorter processing time and absence of additional chemical requirements are two more benefits of PECVD. However, the need for high vacuum and low chamber pressure makes the process tiresome. In addition, the requisite for a substrate and the subsequent transfer of graphene for further applications are some issues needed to be addressed in this procedure. Moreover, the biggest challenge for this technique is the scalable preparation of graphene. Therefore, to convert this system into an industrial-scale process, more attention must be given to the scalable synthesis of graphene.

Atmospheric pressure microwave plasma synthesis of graphene is another state-of-the-art technique to synthesize graphene. This method certainly has some advantages over PECVD-as it does not require high vacuum or low chamber pressure conditions to produce graphene. In contrast to PECVD, it offers scalable graphene; however, the amount synthesized is still not adequate for large-scale production. Besides, the process is generally reliant on the usage of non-sustainable precursors. Thus, it is pivotal to substitute these unrenewable precursors with environmental-friendly and sustainable resources. It is extremely critical to demonstrate the real application of any material; however, the practical usage of graphene synthesized through atmospheric pressure microwave plasma has scarcely been reported. Therefore, it is highly crucial to demonstrate the potential applications of graphene produced through this method.

Furthermore, a theoretical study of the complex growth environment of the atmospheric pressure plasma, as well as PECVD, should be carried out for a complete understanding of the process. The above-mentioned processes have used only a continuous mode of plasma. Varying the plasma source to pulse mode may vary the chamber environment substantially. Thus, its effects on the synthesis should be investigated. Remarkable work on the synthesis of nanocomposite of graphene with other nanomaterials using wet chemical methods is widely reported. However, the synthesis in a dry and chemical-free environment of plasma still lacks. Scale-up of the laboratory-scale reaction chambers is essential for the industrialization of the technologies. Although, applications of plasma-synthesized graphene in electrochemical sensors, batteries, supercapacitors, membranes, etc. have been demonstrated at a lab scale. It is also very important to showcase its broad use in potential future applications such as transistors, semiconductors, bendable phones, medical science, wearable electronics and sensors, metals recovery, crop protection and growth, etc.

Table 2.1 Overview of past works on atmospheric pressure microwave plasma synthesis of graphene

Power	**Precursor**			**Plasma gas and flow rate**	**Production rate ($mg.min^{-1}$)**	**References**
	Type	Flow rate	Feeding mechanism			
250 W	Ethanol	4 x 10^{-4} L/min	Aerosol	Ar, 1.71 L/min	2	[63, 205]
250 to 1050 W	Ethanol, methanol, isopropyl alcohol (IPA), dimethyl ether (DME)	4 x 10^{-4} L/min	Aerosol	Ar, 6.8 L/min	-	[109]
250 to 1050 W	Ethanol	4 x 10^{-4} L/min	Aerosol	Ar, 3.4 & 1.71 L/min	6	[109]
400 to 900 W	Ethanol	0.5 – 3.5 sccm	Aerosol	Ar, 250 to 2000 sccm	2	[105]
500 to 900 W	Ethanol	0.6 – 3.5 sccm	Aerosol	Ar 250 sccm	-	[112]
400 to 1000 W	Ethanol, methane	0.6 – 10 sccm	Aerosol	Ar, 250-1500 sccm	-	[113]
500 to 2000 W	Ethanol	5 - 30 sccm	Aerosol	Ar, 1000 to 1500 sccm	2	[106]
200 W	Ethanol	0.22 g/h	Aerosol	Ar, 0.75 L/min	0.07	[86]

300 W	Ethanol	2 g/hour	Aerosol	Ar, 1 L/min	1.33	[107]
-	Ethanol	1 mL/min	Direct spray	Ar, 5 slm	-	[206]
1 kW	Methane	2 – 8 sccm	-	Ar, 600 – 2000 sccm	-	[110]
700 – 900 W	Ethanol	0.6 sccm	Aerosol	Ar, 250 sccm	-	[207]
-	Ethanol	0.1 – 1.5 mL/min	Direct spray	Ar (5 – 14 slm) + H2 (1 – 1.5 slm)	-	[108]
1.2-1.4 kW	Methane	-	-	Ar	-	[111]
250 W	Ethanol	2×10^{-4} L/min	Aerosol	Ar, 1.71 L/min	-	[208]
300 W	Ethanol	48.3 mg/min	Aerosol	Ar, 1 L/min	1.45	[115]

References

1. Hancock, Y., *The 2010 Nobel Prize in physics—ground-breaking experiments on graphene.* Journal of Physics D: Applied Physics, 2011. **44**(47): p. 473001.
2. Allen, M.J., V.C. Tung, and R.B. Kaner, *Honeycomb carbon: a review of graphene.* Chemical reviews, 2009. **110**(1): p. 132-145.
3. Shearer, C.J., A.D. Slattery, A.J. Stapleton, J.G. Shapter, and C.T. Gibson, *Accurate thickness measurement of graphene.* Nanotechnology, 2016. **27**(12): p. 125704.
4. Shunhong, Z., Z. Jian, W. Qian, C. Xiaoshuang, K. Yoshiyuki, and J. Puru, *Penta-graphene: A new carbon allotrope.* Радиоэлектроника. Наносистемы. Информационные технологии, 2015. **7**(2).
5. Wei, W. and X. Qu, *Extraordinary physical properties of functionalized graphene.* Small, 2012. **8**(14): p. 2138-2151.
6. Iqbal, A.A., N. Sakib, A.P. Iqbal, and D.M. Nuruzzaman, *Graphene-based nanocomposites and their fabrication, mechanical properties and applications.* Materialia, 2020. **12**: p. 100815.
7. Wagner, S., T. Dieing, A. Centeno, A. Zurutuza, A.D. Smith, M. Östling, S. Kataria, and M.C. Lemme, *Noninvasive scanning Raman spectroscopy and tomography for graphene membrane characterization.* Nano letters, 2017. **17**(3): p. 1504-1511.
8. Geim, A.K., *Graphene: status and prospects.* science, 2009. **324**(5934): p. 1530-1534.
9. Aliofkhazraei, M., *Advances in Graphene Science*. 2013: BoD–Books on Demand.
10. Bhuyan, M.S.A., M.N. Uddin, M.M. Islam, F.A. Bipasha, and S.S. Hossain, *Synthesis of graphene.* International Nano Letters, 2016. **6**(2): p. 65-83.

11. Park, S., H.C. Floresca, Y. Suh, and M.J. Kim, *Electron microscopy analyses of natural and highly oriented pyrolytic graphites and the mechanically exfoliated graphenes produced from them.* Carbon, 2010. **48**(3): p. 797-804.

12. Lee, H.C., W.-W. Liu, S.-P. Chai, A.R. Mohamed, A. Aziz, C.-S. Khe, N.M. Hidayah, and U. Hashim, *Review of the synthesis, transfer, characterization and growth mechanisms of single and multilayer graphene.* RSC advances, 2017. **7**(26): p. 15644-15693.

13. Whitener Jr, K.E. and P.E. Sheehan, *Graphene synthesis.* Diamond and related materials, 2014. **46**: p. 25-34.

14. Lotya, M., Y. Hernandez, P.J. King, R.J. Smith, V. Nicolosi, L.S. Karlsson, F.M. Blighe, S. De, Z. Wang, and I. McGovern, *Liquid phase production of graphene by exfoliation of graphite in surfactant/water solutions.* Journal of the American Chemical Society, 2009. **131**(10): p. 3611-3620.

15. Biswas, A., I.S. Bayer, A.S. Biris, T. Wang, E. Dervishi, and F. Faupel, *Advances in top–down and bottom–up surface nanofabrication: Techniques, applications & future prospects.* Advances in Colloid and Interface Science, 2012. **170**(1): p. 2-27.

16. Lee, X.J., B.Y.Z. Hiew, K.C. Lai, L.Y. Lee, S. Gan, S. Thangalazhy-Gopakumar, and S. Rigby, *Review on graphene and its derivatives: Synthesis methods and potential industrial implementation.* Journal of the Taiwan Institute of Chemical Engineers, 2019. **98**: p. 163-180.

17. Wang, J.-b., Z. Ren, Y. Hou, X.-l. Yan, P.-z. Liu, H. Zhang, H.-x. Zhang, and J.-j. Guo, *A review of graphene synthesisatlow temperatures by CVD methods.* New Carbon Materials, 2020. **35**(3): p. 193-208.

18. Jacob, M.V., R.S. Rawat, B. Ouyang, K. Bazaka, D.S. Kumar, D. Taguchi, M. Iwamoto, R. Neupane, and O.K. Varghese, *Catalyst-free plasma enhanced growth of graphene from sustainable sources.* Nano letters, 2015. **15**(9): p. 5702-5708.

19. Alancherry, S., K. Bazaka, I. Levchenko, A. Al-Jumaili, B. Kandel, A. Alex, F.C. Robles Hernandez, O.K. Varghese, and M.V. Jacob, *Fabrication of Nano-Onion-Structured Graphene Films from Citrus sinensis Extract and Their Wetting and Sensing Characteristics.* ACS Applied Materials & Interfaces, 2020.

20. Toman, J., O. Jašek, M. Šnírer, D. Pavliňák, Z. Navrátil, J. Jurmanová, S. Chudják, F. Krčma, V. Kudrle, and J. Michalička, *On the transition of reaction pathway during microwave plasma gas-phase synthesis of graphene nanosheets: From amorphous to highly crystalline structure.* Plasma Processes and Polymers, 2021: p. e2100008.

21. Muñoz, R. and C. Gómez-Aleixandre, *Review of CVD synthesis of graphene.* Chemical Vapor Deposition, 2013. **19**(10-11-12): p. 297-322.

22. Boyd, D., W.-H. Lin, C.-C. Hsu, M. Teague, C.-C. Chen, Y.-Y. Lo, W.-Y. Chan, W.-B. Su, T.-C. Cheng, and C.-S. Chang, *Single-step deposition of high-mobility graphene at reduced temperatures.* Nature communications, 2015. **6**: p. 6620.

23. Peng, J., W. Gao, B.K. Gupta, Z. Liu, R. Romero-Aburto, L. Ge, L. Song, L.B. Alemany, X. Zhan, and G. Gao, *Graphene quantum dots derived from carbon fibers.* Nano letters, 2012. **12**(2): p. 844-849.

24. Hahm, M.G., A. Leela Mohana Reddy, D.P. Cole, M. Rivera, J.A. Vento, J. Nam, H.Y. Jung, Y.L. Kim, N.T. Narayanan, and D.P. Hashim, *Carbon nanotube–nanocup hybrid structures for high power supercapacitor applications.* Nano letters, 2012. **12**(11): p. 5616-5621.

25. Novoselov, K.S., V. Fal, L. Colombo, P. Gellert, M. Schwab, and K. Kim, *A roadmap for graphene.* nature, 2012. **490**(7419): p. 192-200.

26. Liu, H., L. Zhang, M. Yan, and J. Yu, *Carbon nanostructures in biology and medicine.* Journal of Materials Chemistry B, 2017. **5**(32): p. 6437-6450.

27. Hatakeyama, R., *Nanocarbon materials fabricated using plasmas.* Reviews of Modern Plasma Physics, 2017. **1**(1): p. 7.

28. Krätschmer, W. and L. Lamb, *K. Fostiropoulos, and DR Huffman.* Nature, 1990. **347**: p. 354.

29. Al-Jumaili, A., S. Alancherry, K. Bazaka, and M.V. Jacob, *Review on the antimicrobial properties of carbon nanostructures.* Materials, 2017. **10**(9): p. 1066.

30. Liu, H., T. Ye, and C. Mao, *Fluorescent carbon nanoparticles derived from candle soot.* Angewandte chemie, 2007. **119**(34): p. 6593-6595.

31. Sun, Y.-P., B. Zhou, Y. Lin, W. Wang, K.S. Fernando, P. Pathak, M.J. Meziani, B.A. Harruff, X. Wang, and H. Wang, *Quantum-sized carbon dots for bright and colorful photoluminescence.* Journal of the American Chemical Society, 2006. **128**(24): p. 7756-7757.

32. Gao, X., C. Ding, A. Zhu, and Y. Tian, *Carbon-Dot-Based Ratiometric Fluorescent Probe for Imaging and Biosensing of Superoxide Anion in Live Cells.* Analytical Chemistry, 2014. **86**(14): p. 7071-7078.

33. Baker, S.N. and G.A. Baker, *Luminescent carbon nanodots: emergent nanolights.* Angewandte Chemie International Edition, 2010. **49**(38): p. 6726-6744.

34. Zhang, M. and J. Li, *Carbon nanotube in different shapes.* Materials today, 2009. **12**(6): p. 12-18.

35. Iijima, S., *Helical microtubules of graphitic carbon.* Nature, 1991. **354**(6348): p. 56-58.

36. Avouris, P., Z. Chen, and V. Perebeinos, *Carbon-based electronics.* Nature Nanotechnology, 2007. **2**(10): p. 605-615.

37. Niyogi, S., M. Hamon, H. Hu, B. Zhao, P. Bhowmik, R. Sen, M. Itkis, and R. Haddon, *Chemistry of single-walled carbon nanotubes.* Accounts of Chemical Research, 2002. **35**(12): p. 1105-1113.

38. Lehman, J.H., M. Terrones, E. Mansfield, K.E. Hurst, and V. Meunier, *Evaluating the characteristics of multiwall carbon nanotubes.* Carbon, 2011. **49**(8): p. 2581-2602.

39. Yang, W., K.R. Ratinac, S.P. Ringer, P. Thordarson, J.J. Gooding, and F. Braet, *Carbon nanomaterials in biosensors: should you use nanotubes or graphene?* Angewandte Chemie International Edition, 2010. **49**(12): p. 2114-2138.

40. Allen, B.L., P.D. Kichambare, and A. Star, *Carbon nanotube field-effect-transistor-based biosensors.* Advanced Materials, 2007. **19**(11): p. 1439-1451.

41. Kauffman, D.R. and A. Star, *Carbon nanotube gas and vapor sensors.* Angewandte Chemie International Edition, 2008. **47**(35): p. 6550-6570.

42. Li, X.-Q., S. Jiang, L. Zhang, M.-K. Zou, Y. Jian, D.-M. Sun, P.-X. Hou, H.-M. Cheng, and C. Liu, *Preparation of isolated semiconducting single-wall carbon nanotubes by oxygen-assisted floating catalyst chemical vapor deposition.* Chemical Engineering Journal, 2022: p. 137861.

43. Wu, S.-L., C.-M. Chen, J.-H. Kuo, and M.-Y. Wey, *Synthesis of carbon nanotubes with controllable diameter by chemical vapor deposition of methane using Fe@ Al2O3 core–shell nanocomposites.* Chemical Engineering Science, 2020. **217**: p. 115541.

44. Huang, S., C. Song, G. Zhang, and H. Yan, *Graphene plasmonics: physics and potential applications.* Nanophotonics, 2017. **6**(6): p. 1191-1204.

45. Al-Jumaili, A., M.A. Zafar, K. Bazaka, J. Weerasinghe, and M.V. Jacob, *Bactericidal Vertically Aligned Graphene Networks Derived from Renewable Precursor.* Carbon Trends, 2022: p. 100157.

46. Deng, B., Z.F. Liu, and H.L. Peng, *Toward Mass Production of CVD Graphene Films.* Advanced Materials, 2019. **31**(9).

47. Yang, C., H. Bi, D. Wan, F. Huang, X. Xie, and M. Jiang, *Direct PECVD growth of vertically erected graphene walls on dielectric substrates as excellent multifunctional electrodes.* Journal of Materials Chemistry A, 2013. **1**(3): p. 770-775.

48. Hass, J., W. De Heer, and E. Conrad, *The growth and morphology of epitaxial multilayer graphene.* Journal of Physics: Condensed Matter, 2008. **20**(32): p. 323202.

49. Yu, H., B. Zhang, C. Bulin, R. Li, and R. Xing, *High-efficient synthesis of graphene oxide based on improved hummers method.* Scientific reports, 2016. **6**(1): p. 1-7.

50. Martinez, A., K. Fuse, and S. Yamashita, *Mechanical exfoliation of graphene for the passive mode-locking of fiber lasers.* Applied Physics Letters, 2011. **99**(12): p. 121107.

51. Chen, C., L. Jia, J. Li, L. Zhang, L. Liang, E. Chen, Z. Kong, X. Wang, W. Zhang, and J.-W. Shen, *Understanding the effect of hydroxyl/epoxy group on water desalination through lamellar graphene oxide membranes via molecular dynamics simulation.* Desalination, 2020. **491**: p. 114560.

52. Dreyer, D.R., S. Park, C.W. Bielawski, and R.S. Ruoff, *The chemistry of graphene oxide.* Chemical society reviews, 2010. **39**(1): p. 228-240.

53. Mao, H.Y., S. Laurent, W. Chen, O. Akhavan, M. Imani, A.A. Ashkarran, and M. Mahmoudi, *Graphene: Promises, Facts, Opportunities, and Challenges in Nanomedicine.* Chemical Reviews, 2013. **113**(5): p. 3407-3424.

54. Dato, A., *Graphene synthesized in atmospheric plasmas—A review.* Journal of Materials Research, 2019. **34**(1): p. 214-230.

55. Li, M., D. Liu, D. Wei, X. Song, D. Wei, and A.T. Wee, *Controllable Synthesis of Graphene by Plasma-Enhanced Chemical Vapor Deposition and Its Related Applications.* Adv Sci (Weinh), 2016. **3**(11): p. 1600003.

56. Vollath, D., *Plasma synthesis of nanopowders.* Journal of Nanoparticle Research, 2008. **10**(1): p. 39-57.

57. Van Nang, L. and E.-T. Kim, *Controllable synthesis of high-quality graphene using inductively-coupled plasma chemical vapor deposition.* Journal of the Electrochemical Society, 2012. **159**(4): p. K93-K96.

58. Hiramatsu, M., M. Naito, H. Kondo, and M. Hori, *Fabrication of Graphene-Based Films Using Microwave-Plasma-Enhanced Chemical Vapor Deposition.* Japanese Journal of Applied Physics, 2013. **52**(1).

59. Kalita, G., K. Wakita, and M. Umeno, *Low temperature growth of graphene film by microwave assisted surface wave plasma CVD for transparent electrode application.* Rsc Advances, 2012. **2**(7): p. 2815-2820.

60. Kim, Y., W. Song, S. Lee, C. Jeon, W. Jung, M. Kim, and C.-Y. Park, *Low-temperature synthesis of graphene on nickel foil by microwave plasma chemical vapor deposition.* Applied physics letters, 2011. **98**(26): p. 263106.

61. Kumar, A., A.A. Voevodin, R. Paul, I. Altfeder, D. Zemlyanov, D.N. Zakharov, and T.S. Fisher, *Nitrogen-doped graphene by microwave plasma chemical vapor deposition.* Thin Solid Films, 2013. **528**: p. 269-273.

62. Malesevic, A., R. Vitchev, K. Schouteden, A. Volodin, L. Zhang, G. Van Tendeloo, A. Vanhulsel, and C. Van Haesendonck, *Synthesis of few-layer graphene via microwave plasma-enhanced chemical vapour deposition.* Nanotechnology, 2008. **19**(30).

63. Dato, A., V. Radmilovic, Z. Lee, J. Phillips, and M. Frenklach, *Substrate-free gas-phase synthesis of graphene sheets.* Nano letters, 2008. **8**(7): p. 2012-2016.

64. Kumar, R., R.K. Singh, and D.P. Singh, *Natural and waste hydrocarbon precursors for the synthesis of carbon based nanomaterials: Graphene and CNTs.* Renewable & Sustainable Energy Reviews, 2016. **58**: p. 976-1006.

65. Guermoune, A., T. Chari, F. Popescu, S.S. Sabri, J. Guillemette, H.S. Skulason, T. Szkopek, and M. Siaj, *Chemical vapor deposition synthesis of graphene on copper with methanol, ethanol, and propanol precursors.* Carbon, 2011. **49**(13): p. 4204-4210.

66. Wassei, J.K., M. Mecklenburg, J.A. Torres, J.D. Fowler, B. Regan, R.B. Kaner, and B.H. Weiller, *Chemical vapor deposition of graphene on copper from methane, ethane and propane: Evidence for bilayer selectivity.* Small, 2012. **8**(9): p. 1415-1422.

67. Zafar, M.A. and M.V. Jacob, *Synthesis of free-standing graphene in atmospheric pressure microwave plasma for the oil-water separation application.* Applied Surface Science Advances, 2022. **11**: p. 100312.

68. Zhang, B., W.H. Lee, R. Piner, I. Kholmanov, Y. Wu, H. Li, H. Ji, and R.S. Ruoff, *Low-temperature chemical vapor deposition growth of graphene from toluene on electropolished copper foils.* ACS nano, 2012. **6**(3): p. 2471-2476.

69. Kumar, R., R.K. Singh, P. Kumar, P.K. Dubey, R. Tiwari, and O. Srivastava, *Clean and efficient synthesis of graphene nanosheets and rectangular aligned-carbon nanotubes bundles using green botanical hydrocarbon precursor: sesame oil.* Science of Advanced Materials, 2014. **6**(1): p. 76-83.

70. Gao, H., Z. Liu, L. Song, W. Guo, W. Gao, L. Ci, A. Rao, W. Quan, R. Vajtai, and P.M. Ajayan, *Synthesis of S-doped graphene by liquid precursor.* Nanotechnology, 2012. **23**(27): p. 275605.

71. Somekh, M., E. Shawat, and G.D. Nessim, *Fully reproducible, low-temperature synthesis of high-quality, few-layer graphene on nickel via preheating of gas precursors using atmospheric pressure chemical vapor deposition.* Journal of Materials Chemistry A, 2014. **2**(46): p. 19750-19758.

72. Qi, M., Z. Ren, Y. Jiao, Y. Zhou, X. Xu, W. Li, J. Li, X. Zheng, and J. Bai, *Hydrogen kinetics on scalable graphene growth by atmospheric pressure chemical vapor*

deposition with acetylene. The Journal of Physical Chemistry C, 2013. **117**(27): p. 14348-14353.

73. Sharma, S., G. Kalita, R. Hirano, Y. Hayashi, and M. Tanemura, *Influence of gas composition on the formation of graphene domain synthesized from camphor.* Materials Letters, 2013. **93**: p. 258-262.

74. Awasthi, K., R. Kumar, R. Tiwari, and O. Srivastava, *Large scale synthesis of bundles of aligned carbon nanotubes using a natural precursor: turpentine oil.* Journal of Experimental Nanoscience, 2010. **5**(6): p. 498-508.

75. Li, C., Z. Zhuang, X. Jin, and Z. Chen, *A facile and green preparation of reduced graphene oxide using Eucalyptus leaf extract.* Applied Surface Science, 2017. **422**: p. 469-474.

76. Nasir, S., M. Hussein, N. Yusof, and Z. Zainal, *Oil palm waste-based precursors as a renewable and economical carbon sources for the preparation of reduced graphene oxide from graphene oxide.* Nanomaterials, 2017. **7**(7): p. 182.

77. Seo, D.H., S. Pineda, J. Fang, Y. Gozukara, S. Yick, A. Bendavid, S.K.H. Lam, A.T. Murdock, A.B. Murphy, and Z.J. Han, *Single-step ambient-air synthesis of graphene from renewable precursors as electrochemical genosensor.* Nature communications, 2017. **8**: p. 14217.

78. Seo, D.H., A.E. Rider, Z.J. Han, S. Kumar, and K. Ostrikov, *Plasma Break-Down and Re-Build: Same Functional Vertical Graphenes from Diverse Natural Precursors.* Advanced Materials, 2013. **25**(39): p. 5638-5642.

79. Peng, K.-J., C.-L. Wu, Y.-H. Lin, Y.-J. Liu, D.-P. Tsai, Y.-H. Pai, and G.-R. Lin, *Hydrogen-free PECVD growth of few-layer graphene on an ultra-thin nickel film at the threshold dissolution temperature.* Journal of Materials Chemistry C, 2013. **1**(24): p. 3862-3870.

80. Wang, Z., M. Shoji, and H. Ogata, *Carbon nanosheets by microwave plasma enhanced chemical vapor deposition in CH4–Ar system.* Applied Surface Science, 2011. **257**(21): p. 9082-9085.

81. Bo, Z., Y. Yang, J. Chen, K. Yu, J. Yan, and K. Cen, *Plasma-enhanced chemical vapor deposition synthesis of vertically oriented graphene nanosheets.* Nanoscale, 2013. **5**(12): p. 5180-204.

82. Wu, Y., B. Yang, B. Zong, H. Sun, Z. Shen, and Y. Feng, *Carbon nanowalls and related materials.* Journal of Materials Chemistry, 2004. **14**(4): p. 469-477.

83. Wang, J., M. Zhu, R.A. Outlaw, X. Zhao, D.M. Manos, and B.C. Holloway, *Synthesis of carbon nanosheets by inductively coupled radio-frequency plasma enhanced chemical vapor deposition.* Carbon, 2004. **42**(14): p. 2867-2872.

84. Vlassiouk, I., M. Regmi, P. Fulvio, S. Dai, P. Datskos, G. Eres, and S. Smirnov, *Role of hydrogen in chemical vapor deposition growth of large single-crystal graphene.* ACS nano, 2011. **5**(7): p. 6069-6076.

85. Purna Chandra Rao, B., R. Maheswaran, S. Ramaswamy, O. Mahapatra, C. Gopalakrishanan, and D. John Thiruvadigal, *Low Temperature Growth of Carbon Nanostructures by Radio Frequency-Plasma Enhanced Chemical Vapor Deposition (Low Temperature Growth of Carbon Nanostructures by RF-PECVD).* Fullerenes, Nanotubes and Carbon Nanostructures, 2009. **17**(6): p. 625-635.

86. Rincón, R., C. Melero, M. Jiménez, and M. Calzada, *Synthesis of multi-layer graphene and multi-wall carbon nanotubes from direct decomposition of ethanol by microwave plasma without using metal catalysts.* Plasma Sources Science and Technology, 2015. **24**(3): p. 032005.

87. Seo, D.H., Z.J. Han, S. Kumar, and K. Ostrikov, *Structure-Controlled, Vertical Graphene-Based, Binder-Free Electrodes from Plasma-Reformed Butter Enhance Supercapacitor Performance.* Advanced Energy Materials, 2013. **3**(10): p. 1316-1323.

88. Chen, S.M., M. Gao, R.N. Cao, H.W. Du, J. Yang, L. Zhao, and Z.Q. Ma, *Hydrogen-free synthesis of graphene-graphitic films directly on Si substrate by plasma enhanced chemical vapor deposition.* Journal of Materials Science-Materials in Electronics, 2015. **26**(3): p. 1485-1493.

89. Qi, J., W. Zheng, X. Zheng, X. Wang, and H. Tian, *Relatively low temperature synthesis of graphene by radio frequency plasma enhanced chemical vapor deposition.* Applied Surface Science, 2011. **257**(15): p. 6531-6534.

90. Wang, S., Y. Pei, X. Wang, H. Wang, Q. Meng, H. Tian, X. Zheng, W. Zheng, and Y. Liu, *Synthesis of graphene on a polycrystalline Co film by radio-frequency plasma-enhanced chemical vapour deposition.* Journal of Physics D: Applied Physics, 2010. **43**(45): p. 455402.

91. Vizireanu, S., L. Nistor, M. Haupt, V. Katzenmaier, C. Oehr, and G. Dinescu, *Carbon Nanowalls Growth by Radiofrequency Plasma-Beam-Enhanced Chemical Vapor Deposition.* Plasma Processes and Polymers, 2008. **5**(3): p. 263-268.

92. Song, X., J. Liu, L. Yu, J. Yang, L. Fang, H. Shi, C. Du, and D. Wei, *Direct versatile PECVD growth of graphene nanowalls on multiple substrates.* Materials Letters, 2014. **137**: p. 25-28.

93. Zhu, M., J. Wang, B.C. Holloway, R.A. Outlaw, X. Zhao, K. Hou, V. Shutthanandan, and D.M. Manos, *A mechanism for carbon nanosheet formation.* Carbon, 2007. **45**(11): p. 2229-2234.

94. Kato, R., S. Minami, Y. Koga, and M. Hasegawa, *High growth rate chemical vapor deposition of graphene under low pressure by RF plasma assistance.* Carbon, 2016. **96**: p. 1008-1013.

95. Terasawa, T.-o. and K. Saiki, *Growth of graphene on Cu by plasma enhanced chemical vapor deposition.* Carbon, 2012. **50**(3): p. 869-874.

96. Ma, C., H. Yu, and K. Yu, *Plasma-enhanced chemical vapor deposition of graphene optimized by pressure.* Materials Research Express, 2019.

97. Ma, Y., W. Jiang, J. Han, Z. Tong, M. Wang, J. Suhr, X. Chen, L. Xiao, S. Jia, and H. Chae, *Experimental Investigation on Vertically Oriented Graphene Grown in a Plasma-Enhanced Chemical Vapor Deposition Process.* ACS applied materials & interfaces, 2019. **11**(10): p. 10237-10243.

98. Malesevic, A., R. Vitchev, K. Schouteden, A. Volodin, L. Zhang, G. Van Tendeloo, A. Vanhulsel, and C. Van Haesendonck, *Synthesis of few-layer graphene via microwave plasma-enhanced chemical vapour deposition.* Nanotechnology, 2008. **19**(30): p. 305604.

99. Yamada, T., J. Kim, M. Ishihara, and M. Hasegawa, *Low-temperature graphene synthesis using microwave plasma CVD.* Journal of Physics D: Applied Physics, 2013. **46**(6): p. 063001.

100. Yuan, G., W. Zhang, Y. Yang, Y. Tang, Y. Li, J. Wang, X. Meng, Z. He, C. Wu, and I. Bello, *Graphene sheets via microwave chemical vapor deposition.* Chemical Physics Letters, 2009. **467**(4-6): p. 361-364.

101. Vitchev, R., A. Malesevic, R.H. Petrov, R. Kemps, M. Mertens, A. Vanhulsel, and C. Van Haesendonck, *Initial stages of few-layer graphene growth by microwave plasma-enhanced chemical vapour deposition.* Nanotechnology, 2010. **21**(9): p. 095602.

102. Wang, Z., M. Shoji, K. Baba, T. Ito, and H. Ogata, *Microwave plasma-assisted regeneration of carbon nanosheets with bi-and trilayer of graphene and their application to photovoltaic cells.* Carbon, 2014. **67**: p. 326-335.

103. Zhang, L., Z. Sun, J.L. Qi, J. Shi, T. Hao, and J. Feng, *Understanding the growth mechanism of vertically aligned graphene and control of its wettability.* Carbon, 2016. **103**: p. 339-345.

104. Chen, J., Z. Bo, and G. Lu, *The Properties of Vertically-Oriented Graphene*, in *Vertically-Oriented Graphene*. 2015, Springer. p. 11-18.

105. Tatarova, E., J. Henriques, C. Luhrs, A. Dias, J. Phillips, M. Abrashev, and C. Ferreira, *Microwave plasma based single step method for free standing graphene synthesis at atmospheric conditions.* Applied Physics Letters, 2013. **103**(13): p. 134101.

106. Tatarova, E., A. Dias, J. Henriques, M. Abrashev, N. Bundaleska, E. Kovacevic, N. Bundaleski, U. Cvelbar, E. Valcheva, and B. Arnaudov, *Towards large-scale in free-standing graphene and N-graphene sheets.* Scientific reports, 2017. **7**(1): p. 1-16.

107. Melero, C., R. Rincón, J. Muñoz, G. Zhang, S. Sun, A. Perez, O. Royuela, C. González-Gago, and M. Calzada, *Scalable graphene production from ethanol decomposition by microwave argon plasma torch.* Plasma Physics and Controlled Fusion, 2017. **60**(1): p. 014009.

108. Münzer, A., L. Xiao, Y.H. Sehlleier, C. Schulz, and H. Wiggers, *All gas-phase synthesis of graphene: Characterization and its utilization for silicon-based lithium-ion batteries.* Electrochimica Acta, 2018. **272**: p. 52-59.

109. Dato, A. and M. Frenklach, *Substrate-free microwave synthesis of graphene: experimental conditions and hydrocarbon precursors.* New Journal of Physics, 2010. **12**(12): p. 125013.

110. Bundaleska, N., D. Tsyganov, A. Dias, E. Felizardo, J. Henriques, F. Dias, M. Abrashev, J. Kissovski, and E. Tatarova, *Microwave plasma enabled synthesis of free standing carbon nanostructures at atmospheric pressure conditions.* Physical Chemistry Chemical Physics, 2018. **20**(20): p. 13810-13824.

111. Singh, M., A. Sengupta, K. Zeller, G. Skoptsov, and R.L. Vander Wal, *Effect of hydrogen concentration on graphene synthesis using microwave-driven plasma-mediated methane cracking.* Carbon, 2019. **143**: p. 802-813.

112. Tatarova, E., A. Dias, J. Henriques, A.B. do Rego, A. Ferraria, M. Abrashev, C.C. Luhrs, J. Phillips, F. Dias, and C. Ferreira, *Microwave plasmas applied for the synthesis of free standing graphene sheets.* Journal of Physics D: Applied Physics, 2014. **47**(38): p. 385501.

113. Tatarova, E., A. Dias, E. Felizardo, N. Bundaleski, M. Abrashev, J. Henriques, Z. Rakocevic, and L. Alves, *Microwave Plasmas Applied for Synthesis of Free-Standing Carbon Nanostructures at Atmospheric Pressure Conditions.* Journal of Magnetohydrodynamics and Plasma Research, 2016. **21**(2): p. 185.

114. Fortugno, P., S. Musikhin, X. Shi, H. Wang, H. Wiggers, and C. Schulz, *Synthesis of freestanding few-layer graphene in microwave plasma: The role of oxygen.* Carbon, 2022. **186**: p. 560-573.

115. Casanova, A., R. Rincón, J. Muñoz, C. Ania, and M. Calzada, *Optimizing high-quality graphene nanoflakes production through organic (bio)-precursor plasma decomposition.* Fuel Processing Technology, 2021. **212**: p. 106630.

116. Sukumaran, S.S., C. Rekha, A. Resmi, K. Jinesh, and K. Gopchandran, *Raman and scanning tunneling spectroscopic investigations on graphene-silver nanocomposites.* Journal of Science: Advanced Materials and Devices, 2018. **3**(3): p. 353-358.

117. Toth, P.S., M. Velický, Q.M. Ramasse, D.M. Kepaptsoglou, and R.A. Dryfe, *Symmetric and Asymmetric Decoration of Graphene: Bimetal-Graphene Sandwiches.* Advanced Functional Materials, 2015. **25**(19): p. 2899-2909.

118. Bundaleska, N., J. Henriques, M. Abrashev, A.B. do Rego, A. Ferraria, A. Almeida, F. Dias, E. Valcheva, B. Arnaudov, and K. Upadhyay, *Large-scale synthesis of free-standing N-doped graphene using microwave plasma.* Scientific reports, 2018. **8**(1): p. 1-11.

119. Tsyganov, D., N. Bundaleska, A. Dias, J. Henriques, E. Felizardo, M. Abrashev, J. Kissovski, A.B. do Rego, A. Ferraria, and E. Tatarova, *Microwave plasma-based direct synthesis of free-standing N-graphene.* Physical Chemistry Chemical Physics, 2020. **22**(8): p. 4772-4787.

120. Zafar, M.A., O.K. Varghese, F.C. Robles Hernandez, Y. Liu, and M.V. Jacob, *Single-Step Synthesis of Nitrogen-Doped Graphene Oxide from Aniline at Ambient Conditions.* ACS Applied Materials & Interfaces, 2022.

121. Tu, C.-h., W. Chen, H.-C. Fang, Y. Tzeng, and C.-P. Liu, *Heteroepitaxial nucleation and growth of graphene nanowalls on silicon.* Carbon, 2013. **54**: p. 234-240.

122. Tzeng, Y., W.L. Chen, C. Wu, J.-Y. Lo, and C.-Y. Li, *The synthesis of graphene nanowalls on a diamond film on a silicon substrate by direct-current plasma chemical vapor deposition.* Carbon, 2013. **53**: p. 120-129.

123. Shen, B., J. Ding, X. Yan, W. Feng, J. Li, and Q. Xue, *Influence of different buffer gases on synthesis of few-layered graphene by arc discharge method.* Applied Surface Science, 2012. **258**(10): p. 4523-4531.

124. Kim, J., S.B. Heo, G.H. Gu, and J.S. Suh, *Fabrication of graphene flakes composed of multi-layer graphene sheets using a thermal plasma jet system.* Nanotechnology, 2010. **21**(9): p. 095601.

125. Lee, M.W., H.-Y. Kim, H. Yoon, J. Kim, and J.S. Suh, *Fabrication of dispersible graphene flakes using thermal plasma jet and their thin films for solar cells.* Carbon, 2016. **106**: p. 48-55.

126. Singh, M., H.S. Jha, and P. Agarwal, *Synthesis of vertically aligned carbon nanoflakes by hot-wire chemical vapor deposition: Influence of process pressure and different substrates.* Thin Solid Films, 2019. **678**: p. 26-31.

127. Wang, B., K. Zheng, Q. Cheng, and K. Ostrikov, *Plasma effects in aligned carbon nanoflake growth by plasma-enhanced hot filament chemical vapor deposition.* Applied Surface Science, 2015. **325**: p. 251-257.

128. Yu, K., Z. Bo, G. Lu, S. Mao, S. Cui, Y. Zhu, X. Chen, R.S. Ruoff, and J. Chen, *Growth of carbon nanowalls at atmospheric pressure for one-step gas sensor fabrication.* Nanoscale research letters, 2011. **6**(1): p. 1-9.

129. Ghosh, S., S.R. Polaki, N. Kumar, S. Amirthapandian, M. Kamruddin, and K.K. Ostrikov, *Process-specific mechanisms of vertically oriented graphene growth in plasmas.* Beilstein journal of nanotechnology, 2017. **8**(1): p. 1658-1670.

130. Sahoo, S., G. Sahoo, S.M. Jeong, and C.S. Rout, *A review on supercapacitors based on plasma enhanced chemical vapor deposited vertical graphene arrays.* Journal of Energy Storage, 2022. **53**: p. 105212.

131. Zhai, Z., H. Shen, J. Chen, X. Li, and Y. Li, *Metal-Free Synthesis of Boron-Doped Graphene Glass by Hot-Filament Chemical Vapor Deposition for Wave Energy Harvesting.* ACS Applied Materials & Interfaces, 2020. **12**(2): p. 2805-2815.

132. Fronczak, M., A.M. Keszler, M. Mohai, B. Jezsó, A. Farkas, and Z. Károly, *Facile and continuous synthesis of graphene nanoflakes in RF thermal plasma.* Carbon, 2022. **193**: p. 51-67.

133. Fronczak, M., P. Fazekas, Z. Károly, B. Hamankiewicz, and M. Bystrzejewski, *Continuous and catalyst free synthesis of graphene sheets in thermal plasma jet.* Chemical Engineering Journal, 2017. **322**: p. 385-396.

134. Chiang, W.H., D. Mariotti, R.M. Sankaran, J.G. Eden, and K. Ostrikov, *Microplasmas for advanced materials and devices.* Advanced Materials, 2020. **32**(18): p. 1905508.

135. Yang, J.-S., D.Z. Pai, and W.-H. Chiang, *Microplasma-enhanced synthesis of colloidal graphene quantum dots at ambient conditions.* Carbon, 2019. **153**: p. 315-319.

136. Aissou, T., N. Braidy, and J. Veilleux, *A new one-step deposition approach of graphene nanoflakes coating using a radio frequency plasma: Synthesis, characterization and tribological behaviour.* Tribology International, 2022. **167**: p. 107406.

137. Wei, Y., X. Zuo, X. Li, S. Song, L. Chen, J. Shen, Y. Meng, Y. Zhao, and S. Fang, *Dry plasma synthesis of graphene oxide–Ag nanocomposites: A simple and green approach.* Materials Research Bulletin, 2014. **53**: p. 145-150.

138. Jiangying, Q., G. Feng, Z. Quan, W. Zhiyu, H. Han, L. Beibei, W. Wubo, W. Xuzhen, and Q. Jieshan, *Highly atom-economic synthesis of graphene/Mn 3 O 4 hybrid composites for electrochemical supercapacitors.* Nanoscale, 2013. **5**(7): p. 2999-3005.

139. Jo, E.H., H. Chang, S.K. Kim, J.-H. Choi, S.-R. Park, C.M. Lee, and H.D. Jang, *One-Step Synthesis of Pt/Graphene Composites from Pt Acid Dissolved Ethanol via Microwave Plasma Spray Pyrolysis.* Scientific Reports, 2016. **6**(1): p. 33236.

140. Kim, D.-W., U.S. Heo, K.-S. Kim, and D.-W. Park, *One-step synthesis of TiC/multilayer graphene composite by thermal plasma.* Current Applied Physics, 2018. **18**(5): p. 551-558.

141. Heo, U.S., D.-W. Kim, K.-S. Kim, and D.-W. Park, *A facile synthesis of anatase TiO2-Graphene nanocomposites using plasma and heat treatment.* Applied Surface Science, 2019. **474**: p. 118-126.

142. Tanaka, Y., K. Shimizu, K. Akashi, K. Onda, Y. Uesugi, T. Ishijima, S. Watanabe, S. Sueyasu, and K. Nakamura, *High rate synthesis of graphene-encapsulated silicon nanoparticles using pulse-modulated induction thermal plasmas with intermittent feedstock feeding.* Japanese Journal of Applied Physics, 2020. **59**(SH): p. SHHE07.

143. Pimklang, T., A. Watthanaphanit, and P. Pakawatpanurut, *Novel green synthesis of graphene oxide-manganese dioxide using solution plasma process for energy storage.* Chemical Engineering Journal, 2022. **442**: p. 136244.

144. Ostrikov, K., E. Neyts, and M. Meyyappan, *Plasma nanoscience: from nano-solids in plasmas to nano-plasmas in solids.* Advances in Physics, 2013. **62**(2): p. 113-224.

145. Jagodar, A., J. Berndt, E. von Wahl, T. Strunskus, T. Lecas, E. Kovacevic, and P. Brault, *Nitrogen incorporation in graphene nanowalls via plasma processes: Experiments and simulations.* Applied Surface Science, 2022. **591**: p. 153165.

146. Wei, Y., J. Wu, H. Yin, X. Shi, R. Yang, and M. Dresselhaus, *The nature of strength enhancement and weakening by pentagon–heptagon defects in graphene.* Nature materials, 2012. **11**(9): p. 759-763.

147. Botello-Méndez, A.R., X. Declerck, M. Terrones, H. Terrones, and J.-C. Charlier, *One-dimensional extended lines of divacancy defects in graphene.* Nanoscale, 2011. **3**(7): p. 2868-2872.

148. Elias, D.C., R.R. Nair, T. Mohiuddin, S. Morozov, P. Blake, M. Halsall, A.C. Ferrari, D. Boukhvalov, M. Katsnelson, and A. Geim, *Control of graphene's properties by reversible hydrogenation: evidence for graphane.* Science, 2009. **323**(5914): p. 610-613.

149. Zhou, J., Q. Wang, Q. Sun, X.S. Chen, Y. Kawazoe, and P. Jena, *Ferromagnetism in Semihydrogenated Graphene Sheet.* Nano Letters, 2009. **9**(11): p. 3867-3870.

150. Nandanapalli, K.R., D. Mudusu, and S. Lee, *Functionalization of graphene layers and advancements in device applications.* Carbon, 2019. **152**: p. 954-985.

151. Liu, L., D. Xie, M. Wu, X. Yang, Z. Xu, W. Wang, X. Bai, and E. Wang, *Controlled oxidative functionalization of monolayer graphene by water-vapor plasma etching.* Carbon, 2012. **50**(8): p. 3039-3044.

152. Hopkins, P.E., M. Baraket, E.V. Barnat, T.E. Beechem, S.P. Kearney, J.C. Duda, J.T. Robinson, and S.G. Walton, *Manipulating thermal conductance at metal–graphene contacts via chemical functionalization.* Nano letters, 2012. **12**(2): p. 590-595.

153. Tincu, B., M. Avram, A. Avram, V. Tucureanu, G. Mihai, M. Popa, P. Osiceanu, I. Demetrescu, and M. Enachescu, *Investigation of plasma-assisted functionalization of pristine single layer graphene.* Chemical Physics Letters, 2022. **789**: p. 139330.

154. Baraket, M., R. Stine, W.K. Lee, J.T. Robinson, C.R. Tamanaha, P.E. Sheehan, and S.G. Walton, *Aminated graphene for DNA attachment produced via plasma functionalization.* Applied Physics Letters, 2012. **100**(23): p. 233123.

155. Kato, T., L. Jiao, X. Wang, H. Wang, X. Li, L. Zhang, R. Hatakeyama, and H. Dai, *Room-temperature edge functionalization and doping of graphene by mild plasma.* Small, 2011. **7**(5): p. 574-577.

156. Stine, R., J.W. Ciszek, D.E. Barlow, W.-K. Lee, J.T. Robinson, and P.E. Sheehan, *High-density amine-terminated monolayers formed on fluorinated CVD-grown graphene.* Langmuir, 2012. **28**(21): p. 7957-7961.

157. Robinson, J.T., J.S. Burgess, C.E. Junkermeier, S.C. Badescu, T.L. Reinecke, F.K. Perkins, M.K. Zalalutdniov, J.W. Baldwin, J.C. Culbertson, and P.E. Sheehan, *Properties of fluorinated graphene films.* Nano letters, 2010. **10**(8): p. 3001-3005.

158. Alosaimi, F.K., T.T. Tung, V.-D. Dao, N.K. Huyen, M.J. Nine, K. Hassan, J. Ma, and D. Losic, *Graphene-based multifunctional surface and structure gradients engineered by atmospheric plasma.* Applied Materials Today, 2022. **27**: p. 101486.

159. Kalita, G., B.P. Jaisi, and M. Umeno, *Effective reduction and doping of graphene oxide films at near-room temperature by microwave-excited surface-wave plasma process.* Diamond and Related Materials, 2022. **126**: p. 109066.

160. Zhu, Y., S. Murali, M.D. Stoller, K.J. Ganesh, W. Cai, P.J. Ferreira, A. Pirkle, R.M. Wallace, K.A. Cychosz, and M. Thommes, *Carbon-based supercapacitors produced by activation of graphene.* science, 2011. **332**(6037): p. 1537-1541.

161. Purkait, T., G. Singh, M. Singh, D. Kumar, and R.S. Dey, *Large area few-layer graphene with scalable preparation from waste biomass for high-performance supercapacitor.* Scientific reports, 2017. **7**(1): p. 1-14.

162. Wang, Y., Z. Shi, Y. Huang, Y. Ma, C. Wang, M. Chen, and Y. Chen, *Supercapacitor devices based on graphene materials.* The Journal of Physical Chemistry C, 2009. **113**(30): p. 13103-13107.

163. Jiang, Y. and J. Liu, *Definitions of pseudocapacitive materials: a brief review.* Energy & Environmental Materials, 2019. **2**(1): p. 30-37.

164. Tomboc, G.M. and H. Kim, *Derivation of both EDLC and pseudocapacitance characteristics based on synergistic mixture of NiCo2O4 and hollow carbon nanofiber: an efficient electrode towards high energy density supercapacitor.* Electrochimica Acta, 2019. **318**: p. 392-404.

165. Choi, C., D.S. Ashby, D.M. Butts, R.H. DeBlock, Q. Wei, J. Lau, and B. Dunn, *Achieving high energy density and high power density with pseudocapacitive materials.* Nature Reviews Materials, 2020. **5**(1): p. 5-19.

166. Seo, D.H., Z.J. Han, S. Kumar, and K. Ostrikov, *Structure-controlled, vertical graphene-based, binder-free electrodes from plasma-reformed butter enhance supercapacitor performance.* Advanced Energy Materials, 2013. **3**(10): p. 1316-1323.

167. Seo, D.H., S. Yick, Z.J. Han, J.H. Fang, and K. Ostrikov, *Synergistic fusion of vertical graphene nanosheets and carbon nanotubes for high-performance supercapacitor electrodes.* ChemSusChem, 2014. **7**(8): p. 2317-2324.

168. Miller, J.R., R. Outlaw, and B. Holloway, *Graphene double-layer capacitor with ac line-filtering performance.* Science, 2010. **329**(5999): p. 1637-1639.

169. Bo, Z., Z. Wen, H. Kim, G. Lu, K. Yu, and J. Chen, *One-step fabrication and capacitive behavior of electrochemical double layer capacitor electrodes using vertically-oriented graphene directly grown on metal.* Carbon, 2012. **50**(12): p. 4379-4387.

170. Yi, K., X. Chen, Z. Jin, C. Zhang, D. Wei, and Y. Liu, *A two-dimensional cross-linked polythiophene network.* Journal of Materials Chemistry C, 2019. **7**(30): p. 9362-9368.

171. Wang, Z., K. Yi, Q. Lin, L. Yang, X. Chen, H. Chen, Y. Liu, and D. Wei, *Free radical sensors based on inner-cutting graphene field-effect transistors.* Nature communications, 2019. **10**(1): p. 1-10.

172. Liu, X., Q. Zhou, S. Luo, H. Du, Z. Cao, X. Peng, W. Feng, J. Shen, and D. Wei, *Infrared photodetector based on the photothermionic effect of graphene-nanowall/silicon heterojunction.* ACS applied materials & interfaces, 2019. **11**(19): p. 17663-17669.

173. Lupina, G., J. Kitzmann, I. Costina, M. Lukosius, C. Wenger, A. Wolff, S. Vaziri, M. Ostling, I. Pasternak, and A. Krajewska, *Residual metallic contamination of transferred chemical vapor deposited graphene.* ACS nano, 2015. **9**(5): p. 4776-4785.

174. Yang, J., S. Luo, X. Zhou, J. Li, J. Fu, W. Yang, and D. Wei, *Flexible, Tunable, and Ultrasensitive Capacitive Pressure Sensor with Microconformal Graphene Electrodes.* ACS Applied Materials & Interfaces, 2019. **11**(16): p. 14997-15006.

175. Chen, F., Z. Fan, Y. Zhu, H. Sun, J. Yu, N. Jiang, S. Zhao, G. Lai, A. Yu, and C.-T. Lin, *β-Cyclodextrin-Immobilized Ni/Graphene Electrode for Electrochemical Enantiorecognition of Phenylalanine.* Materials, 2020. **13**(3): p. 777.

176. Li, Y., J. Liu, M. Liu, F. Yu, L. Zhang, H. Tang, B.-C. Ye, and L. Lai, *Fabrication of ultra-sensitive and selective dopamine electrochemical sensor based on molecularly imprinted polymer modified graphene@ carbon nanotube foam.* Electrochemistry Communications, 2016. **64**: p. 42-45.

177. Huang, B., J. Liu, L. Lai, F. Yu, X. Ying, B.-C. Ye, and Y. Li, *A free-standing electrochemical sensor based on graphene foam-carbon nanotube composite coupled with gold nanoparticles and its sensing application for electrochemical determination of dopamine and uric acid.* Journal of Electroanalytical Chemistry, 2017. **801**: p. 129-134.

178. Deng, C., P. Gao, L. Lan, P. He, X. Zhao, W. Zheng, W. Chen, X. Zhong, Y. Wu, and L. Liu, *Ultrasensitive and highly stretchable multifunctional strain sensors with timbre-recognition ability based on vertical graphene.* Advanced Functional Materials, 2019. **29**(51): p. 1907151.

179. Zheng, W., X. Zhao, and W. Fu, *Review of Vertical Graphene and its Applications.* ACS Applied Materials & Interfaces, 2021. **13**(8): p. 9561-9579.

180. Wu, S., S. Peng, Z.J. Han, H. Zhu, and C.H. Wang, *Ultrasensitive and stretchable strain sensors based on mazelike vertical graphene network.* ACS applied materials & interfaces, 2018. **10**(42): p. 36312-36322.

181. Yang, J., Q. Ran, D. Wei, T. Sun, L. Yu, X. Song, L. Pu, H. Shi, and C. Du, *Three-dimensional conformal graphene microstructure for flexible and highly sensitive electronic skin.* Nanotechnology, 2017. **28**(11): p. 115501.

182. Yang, J., D. Wei, L. Tang, X. Song, W. Luo, J. Chu, T. Gao, H. Shi, and C. Du, *Wearable temperature sensor based on graphene nanowalls.* Rsc Advances, 2015. **5**(32): p. 25609-25615.

183. Chen, Q., T. Sun, X. Song, Q. Ran, C. Yu, J. Yang, H. Feng, L. Yu, and D. Wei, *Flexible electrochemical biosensors based on graphene nanowalls for the real-time measurement of lactate.* Nanotechnology, 2017. **28**(31): p. 315501.

184. Huang, S., G. He, C. Yang, J. Wu, C. Guo, T. Hang, B. Li, C. Yang, D. Liu, and H.-J. Chen, *Stretchable strain vector sensor based on parallelly aligned vertical graphene.* ACS applied materials & interfaces, 2018. **11**(1): p. 1294-1302.

185. Kim, J.P., H. Lim, J.H. Song, Y.J. Chang, and C.H. Jeon, *Numerical analysis on the thermal characteristics of photovoltaic module with ambient temperature variation.* Solar Energy Materials and Solar Cells, 2011. **95**(1): p. 404-407.

186. Liu, Z., J. Li, Z. Sun, G. Tai, S. Lau, and F. Yan, *Package-free flexible organic solar cells with graphene top electrodes the application of highly doped single-layer graphene as the top electrodes of semitransparent organic solar cells.* ACS Nano, 2012. **6**: p. 810-818.

187. Park, H., P.R. Brown, V. Bulović, and J. Kong, *Graphene as transparent conducting electrodes in organic photovoltaics: studies in graphene morphology, hole transporting layers, and counter electrodes.* Nano letters, 2012. **12**(1): p. 133-140.

188. Park, H., R.M. Howden, M.C. Barr, V. Bulovic, K. Gleason, and J. Kong, *Organic solar cells with graphene electrodes and vapor printed poly (3, 4-ethylenedioxythiophene) as the hole transporting layers.* ACS nano, 2012. **6**(7): p. 6370-6377.

189. Das, S., P. Sudhagar, V. Verma, D. Song, E. Ito, S.Y. Lee, Y.S. Kang, and W. Choi, *Amplifying charge-transfer characteristics of graphene for triiodide reduction in dye-sensitized solar cells.* Advanced Functional Materials, 2011. **21**(19): p. 3729-3736.

190. Wang, X., L. Zhi, and K. Müllen, *Transparent, conductive graphene electrodes for dye-sensitized solar cells.* Nano letters, 2008. **8**(1): p. 323-327.

191. Yang, W., C. He, L. Zhang, Y. Wang, Z. Shi, M. Cheng, G. Xie, D. Wang, R. Yang, and D. Shi, *Growth, characterization, and properties of nanographene.* Small, 2012. **8**(9): p. 1429-1435.

192. Chen, S., M. Gao, R. Cao, H. Du, J. Yang, L. Zhao, and Z. Ma, *Hydrogen-free synthesis of graphene–graphitic films directly on Si substrate by plasma enhanced chemical vapor deposition.* Journal of Materials Science: Materials in Electronics, 2015. **26**(3): p. 1485-1493.

193. Li, X., H. Zhu, K. Wang, A. Cao, J. Wei, C. Li, Y. Jia, Z. Li, X. Li, and D. Wu, *Graphene-on-silicon Schottky junction solar cells.* Advanced materials, 2010. **22**(25): p. 2743-2748.

194. McClure, J.P., J.D. Thornton, R. Jiang, D. Chu, J.J. Cuomo, and P.S. Fedkiw, *Oxygen reduction on metal-free nitrogen-doped carbon nanowall electrodes.* Journal of the Electrochemical Society, 2012. **159**(11): p. F733.

195. Jung, Y.H., W.S. Choi, and B. Hong, *Post-plasma treatment of a carbon nanowall for use as a counter electrode in a dye-sensitized solar cell.* Journal of the Korean Physical Society, 2014. **65**(3): p. 291-296.

196. Liu, J., W. Sun, D. Wei, X. Song, T. Jiao, S. He, W. Zhang, and C. Du, *Direct growth of graphene nanowalls on the crystalline silicon for solar cells.* Applied Physics Letters, 2015. **106**(4): p. 043904.

197. Bayram, O., E. Igman, H. Guney, Z. Demir, M.T. Yurtcan, C. Cirak, U.C. Hasar, and O. Simsek, *Graphene/polyaniline nanocomposite as platinum-free counter electrode material for dye-sensitized solar cell: its fabrication and photovoltaic performance.* Journal of Materials Science: Materials in Electronics, 2020. **31**(13): p. 10288-10297.

198. Zafar, M.A., Y. Liu, S. Allende, and M.V. Jacob, *Electrochemical sensing of oxalic acid using silver nanoparticles loaded nitrogen-doped graphene oxide.* Carbon Trends, 2022. **8**: p. 100188.

199. Zafar, M.A., O.K. Varghese, F.C. Robles Hernandez, Y. Liu, and M.V. Jacob, *Single-Step Synthesis of Nitrogen-Doped Graphene Oxide from Aniline at Ambient Conditions.* ACS Applied Materials & Interfaces, 2022. **14**(4): p. 5797-5806.

200. Zhu, Q.-L. and Q. Xu, *Immobilization of ultrafine metal nanoparticles to high-surface-area materials and their catalytic applications.* Chem, 2016. **1**(2): p. 220-245.

201. Gao, Y., L. Zhang, A.J.F. van Hoof, H. Friedrich, and E.J.M. Hensen, *A Robust Au/ZnCr2O4 Catalyst with Highly Dispersed Gold Nanoparticles for Gas-Phase Selective Oxidation of Cyclohexanol to Cyclohexanone.* ACS Catalysis, 2019. **9**(12): p. 11104-11115.

202. Jeon, K.-J. and Z. Lee, *Size-dependent interaction of Au nanoparticles and graphene sheet.* Chemical Communications, 2011. **47**(12): p. 3610-3612.

203. Tan, D.H., Y.-T. Chen, H. Yang, W. Bao, B. Sreenarayanan, J.-M. Doux, W. Li, B. Lu, S.-Y. Ham, and B. Sayahpour, *Carbon free high loading silicon anodes enabled by sulfide solid electrolytes for robust all solid-state batteries.* arXiv preprint arXiv:2103.04230, 2021.

204. Xu, Z.-L., B. Zhang, and J.-K. Kim, *Electrospun carbon nanofiber anodes containing monodispersed Si nanoparticles and graphene oxide with exceptional high rate capacities.* Nano Energy, 2014. **6**: p. 27-35.

205. Dato, A., Z. Lee, K.-J. Jeon, R. Erni, V. Radmilovic, T.J. Richardson, and M. Frenklach, *Clean and highly ordered graphene synthesized in the gas phase.* Chemical Communications, 2009(40): p. 6095-6097.

206. Bertin, E., A. Münzer, S. Reichenberger, R. Streubel, T. Vinnay, H. Wiggers, C. Schulz, S. Barcikowski, and G. Marzun, *Durability study of platinum nanoparticles supported on gas-phase synthesized graphene in oxygen reduction reaction conditions.* Applied Surface Science, 2019. **467**: p. 1181-1186.

207. Tsyganov, D., N. Bundaleska, E. Tatarova, A. Dias, J. Henriques, A. Rego, A. Ferraria, M. Abrashev, F. Dias, and C.C. Luhrs, *On the plasma-based growth of 'flowing'graphene sheets at atmospheric pressure conditions.* Plasma Sources Science and Technology, 2015. **25**(1): p. 015013.

208. Nakahara, K., J. Knego, T. Sloop, C. Bisquera, N. Subler, and A. Dato, *Enhanced mechanical properties of epoxy-matrix nanocomposites reinforced with graphene synthesized in atmospheric plasmas.* Plasma Processes and Polymers, 2020. **17**(5): p. 1900244.

Chapter 3: Synthesis of graphene from tea tree extract for sensing application

In order to achieve the goal of sustainable manufacturing, it is crucial that the parent material or precursor involved in synthesis is sustainable. This chapter shows the fabrication of graphene from naturally occurring resource i.e. the extract of tea tree. This chapter shows the feasibility of the synthesis of graphene from natural precursor using the atmospheric pressure microwave plasma. In addition, the characterization of the synthesized graphene using state-of-the-art techniques is discussed. The application of as-synthesized graphene is showcased for sensing application. The outcomes of the study were reported in the following publication.

This Chapter is given as submitted to journal "Advanced materials interfaces" and accepted for publication.

M. Adeel Zafar, Yang Liu, Francisco C. Robles Hernandez, Oomman K. Varghese, Mohan V Jacob, "Plasma-based synthesis of freestanding graphene from a natural resource for a sensing application". Advanced materials interfaces

Plasma-based synthesis of freestanding graphene from a natural resource for sensing application

Abstract

Atmospheric pressure microwave plasma has the lead in synthesizing freestanding and scalable graphene within seconds without the need for high vacuum and temperature. However, the process has been limited in utilizing chemical sources for synthesis, such as methane and ethanol. Herein, we first time report the usage of an extract of a sustainable precursor, i.e. *melaleuca alternifolia*, commonly known as tea tree to synthesize graphene nanosheets in atmospheric pressure microwave plasma. The synthesis has been carried out in a single step at a remarkably low microwave power of 200 W. The morphology, structure, and electrochemical properties of graphene have been studied using state-of-the-art characterization techniques like Raman spectroscopy, X-ray diffraction, transmission electron microscopy, electrochemical impedance spectroscopy, etc. The TEM images revealed the presence of the combination of nanostructures such as nano-horns, nano-rods, or nano-onions consisting of multi-layer graphitic architectures. An excellent sensing capability of as-synthesized graphene has been demonstrated through the detection of diuron herbicide. A commendable linear range of 20 μM to 1 mM and a limit of detection of 5 μM of diuron have been recorded.

Keywords

Graphene nanosheets, atmospheric pressure microwave plasma, sustainable precursor, tea tree oil, herbicide detection

3.1 Introduction Graphene has been greatly applauded in academia and industry owing to its extraordinary properties and countless applications [1, 2]. Characterized by a single layer of graphite, graphene is composed of sp^2-bonded carbon atoms arranged in a honeycomb lattice structure [3]. Multiple techniques have been developed to synthesize graphene, mainly classified as top-down and bottom-up approaches. The bottom-up approach i.e. modified Hummers' method, is a well-established chemical synthesis technique to synthesize graphene. However, this technique, not only utilizes strong acids and oxidants [4, 5] but also entails numerous steps of synthesis such as dilution, mixing, oxidation, reduction, washing, centrifuging, and intense stirring [6]. On the other hand, some of the bottom-up methods, in particular, chemical vapour deposition (CVD) and plasma-enhanced chemical vapour deposition (PE-CVD) are expensive and laborious methodologies comprising pre-synthesis and post-synthesis requirements i.e. high vacuum, pre-heating, and subsequent transfer of graphene to other substrates [7-9]. Recently, a new bottom-up approach, so-called atmospheric pressure microwave plasma (APMP) is gaining popularity as it synthesizes graphene without the hassles of pre-heating, high vacuuming, and the need for a substrate. Most importantly, the graphene obtained through this method happens to be free-standing and scalable [10, 11].

The precursors used for producing graphene have a significant role in determining the sustainability of the synthesis process. Often graphene is produced from commercially available graphite [12], graphene oxide (GO) [13], methane, or other unreplenishable hydrocarbons [14]. These resources are generally non-renewable, expensive, and/or produce

toxic chemicals during synthesis practice. This has driven scientists to replace these precursors with economical, regenerative, and environment-friendly raw materials. Considerable attempts have been made to derive graphene from a wide range of natural resources, for example, food materials, botanical hydrocarbons, and biomass [15]. These include table sugar, honey, butter [16], cookies, chocolate [17], camphor [18], tea tree essential oil [19], *Citrus sinensis* oil [20], soybean oil [21], waste cooking palm oil [22], nutshells [21], *Colocasia esculenta* and *Nelumbo nucifera* leaves [23], etc. However, the usage of these feedstocks is limited to certain methods, such as modified Hummers' method, pyrolysis, and CVD or PE-CVD techniques. On the other hand, for APMP, the use of sustainable precursors has not been reported yet. The APMP technique is mainly associated with ethanol [24-29] and methane resources [30]. These precursors are extracted from non-renewable bases and are mostly explosive or toxic. Additionally, it has been observed that the increase in the feed of ethanol above a certain quantity causes an extinction of plasma flame [31], which eventually limits the production rate of graphene.

A hydrocarbon-rich and naturally occurring resource, *Melaleuca alternifolia*, has the potential to be an excellent alternative precursor for graphene synthesis. Commonly known as tea tree, it is an abundant and cost-effective resource. It comprises more than 100 compounds, which include~~s~~ terpinen-4-ol ($C_{10}H_{18}O$, 30−48%), γ-terpinene ($C_{10}H_{16}$, 10−28%), α-terpinene ($C_{10}H_{16}$, 5−13%), and 1, 8-cineole ($C_{10}H_{18}O$, 0−15%) as primary constituents and some other compounds in trace amounts [19]. The chemical formula i.e. $C_{28}H_{60}O_4P_2S_4Zn$, given by PubChem also shows the presence of an ample amount of hydrocarbons. Previously, this resource has been used for graphene synthesis in the PE-CVD technique; though the actual synthesis was quick, the overall synthesis was time-consuming due to the heating and cooling required, and was substrate-dependant [19].

This study aimed to synthesize graphene through a facile, rapid, viable, and environmentally benign process. We synthesized free-standing graphene from *Melaleuca alternifolia* extract using APMP. To the best of our knowledge, this is the first report on the APMP synthesis of graphene from a sustainable parent material. The graphene was synthesized at a remarkably low microwave power of 200 W in ambient air. Since the practical use of graphene, synthesized through APMP is scarcely reported, herein we also demonstrate the employment of as-fabricated graphene for diuron herbicide detection.

3.2 Materials and method

3.2.1 Materials

Melaleuca alternifolia was purchased from Australian Botanical Products (ABP, Victoria, Australia). Sodium dihydrogen orthophosphate ($NaH_2PO_4.2H_2O$), disodium hydrogen orthophosphate (Na_2HPO_4), sodium hydroxide (NaOH), potassium hexacyanoferrate (III) $K_3[Fe(CN)_6]$, potassium chloride (KCl), and diuron were obtained from Sigma Aldrich, Australia. All chemicals were of analytical grade, and were used as received. Ultrapure water was used throughout all the experiments.

3.2.2 Synthesis of graphene

The graphene nanosheets were synthesized using a downstream APMP, schematically shown in Fig 3.1a. A 2.45 GHz microwave with a variable output power of max 2 kW was used to generate plasma. The discharge takes place inside a quartz tube having an external diameter of 30 mm. The investigated microwave powers were set at the values of 200 W, 400 W and 600 W. A custom-made precursor delivery system was made to transport the carbon precursor, i.e. tea tree oil vapours into the quartz chamber. The tea tree oil vapours were conveyed into the chamber along with argon gas (plasma gas) at the optimum flow rate of 3 slm. Upon exposure

to the plasma, the tea tree vapours first decomposed into constituent elements and then started arranging in graphene structure. The synthesis stages are shown schematically in Fig 3.1b. The graphene nanosheets were directly deposited on the silicon substrate for characterizations.

The graphene's morphology, structural investigation were carried out using scanning electron microscopy (SEM) (Hitachi SU 5000), and confocal laser Raman spectroscopy (Witec, 532 nm laser). Rigaku Smart Lab x-ray diffractometer was used for X-ray diffraction (XRD). The x-ray photoelectron spectroscopy (XPS) studies were performed using a Kratos Axis Ultra XPS with an Al Kα x-ray source. The JEOL 2100 F machine operated at 200 kV was used for transmission electron microscopy (TEM) images.

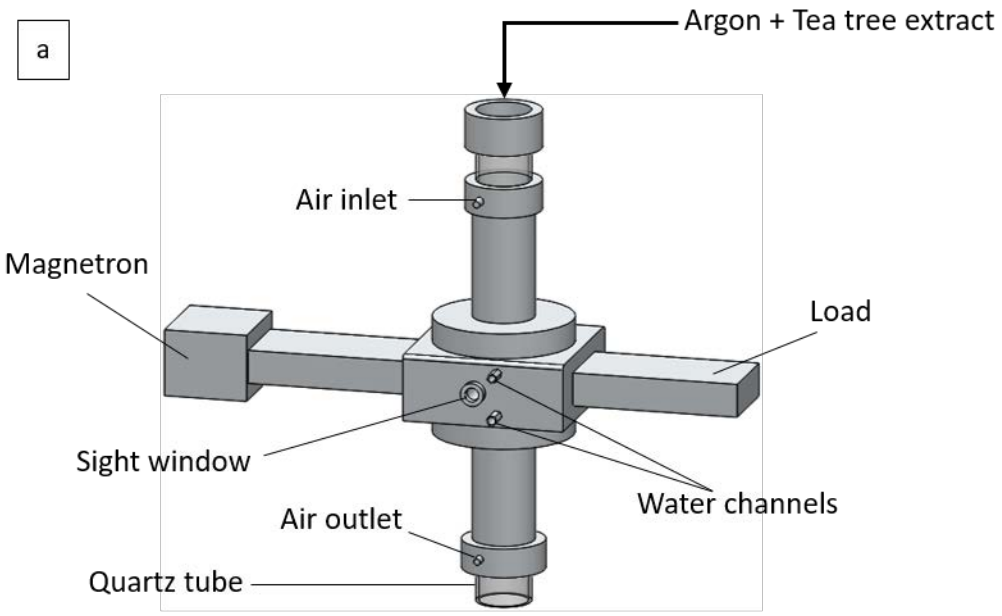

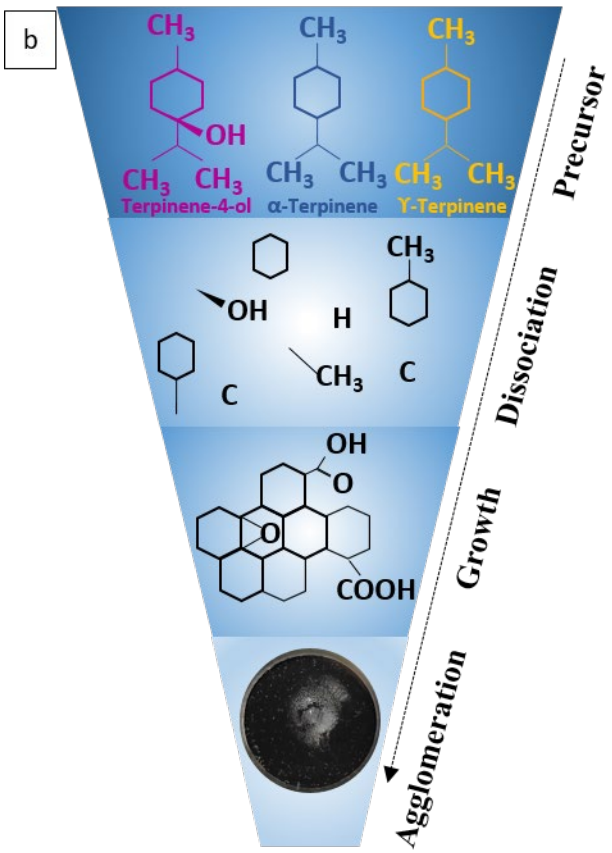

Fig 3.1: (a) A diagrammatic representation of atmospheric pressure microwave plasma reactor (b) Schematic illustration of steps involved in the synthesis of graphene inside the reactor

3.2.3 Electrochemical measurements

Electrochemical measurements were performed on Palm Sense 4 (Palm Instruments, Netherlands) potentiostat using the three-electrode system with a glassy carbon electrode (GCE) as a working electrode, a platinum wire as the counter electrode and an Ag/AgCl as the reference electrode. Before each testing or modification, the bare GCE was first mechanically polished with 0.3 and 0.05 μM alumina slurry, followed by ultrasonic cleaning in ethanol and ultrapure water respectively. To prepare a modified electrode, 10 μL of graphene (1 mg/mL) aliquot was drop-casted on GCE and dried at room temperature. Such an electrode is denoted as graphene/GCE. The electrochemical impedance spectroscopy (EIS) experiment was

conducted in 0.1 M KCl containing 5 mM $K_3[Fe(CN)_6]$ solution in the frequency swept from 0.1 Hz to 100 kHz. Cyclic voltammetry (CV) and differential pulse voltammetry (DPV) were carried out in 0.1 M phosphate buffer solution (PBS) (pH 7.0) containing certain amount of diuron.

3.3 Results and discussions

Raman spectroscopy is a non-destructive tool for the structural elucidation of carbon materials. Therefore, graphene samples prepared at 200W, 400W, and 600W were analysed using Raman spectroscopy. All Raman results showed three vibrational modes related to graphene materials. D peak at ~1335 cm^{-1} corresponds to the defect mode, G peak at ~1570 cm^{-1} implicates vertical vibration mode, and a 2D peak at ~2677 cm^{-1} indicates two-phonon vibration mode [32].

The Raman results exhibited in Fig 3.2a showed the increase in the intensity of the D peak with the increase of microwave power. The D peak reflects the structural imperfections in the graphene materials. Mainly it is associated with the functional groups attached to the basal plane of graphene [33]. However, it is also ascribed to the defects such as vacancies, edge defects, bond-angle disorder, and bond-length disorder [34]. In the current work, the lowest power i.e. 200 W showed a comparatively smaller value of I_D/I_G in the sample (shown in Fig 3.2b); hence indicating a fewer disorder or higher oxygen content attached to the 200 W graphene structure.

Generally, the 2D peak is considered a significant feature in the Raman spectra of graphene-related materials. The intensity ratio between 2D and G peaks i.e. I_{2D}/I_G and full width at half-maximum (FWHM) of the 2D peak is normally associated with the number of layers in graphene. In literature, the I_{2D}/I_G ratio of 1 to 1.5 with FWHM ~50 cm^{-1}, and I_{2D}/I_G of 2 or higher with FWHM ~30 cm^{-1} are usually linked with the bilayer and monolayer structures,

respectively [35, 36]. In this study, the 200 W sample exhibited I_{2D}/I_G and FWHM values of 1.04 and 56 cm^{-1} respectively, suggestive of few to multi-layers graphene. Whereas slightly broader 2D peaks of 400 W and 600 W samples, having FWHM of 62 cm^{-1} and 65 cm^{-1} respectively, and relatively smaller I_{2D}/I_G values are indicative of the higher number of layers in comparison to the 200 W sample. Thus, the remaining investigations and applications were studied using a 200 W graphene sample.

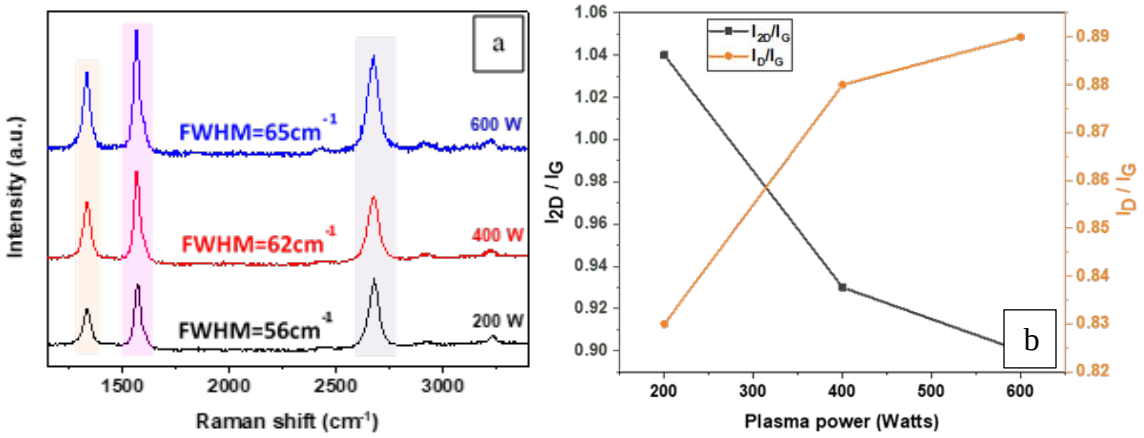

Fig 3.2: (a) Raman spectra and (b) peaks' intensity ratios of graphene samples synthesized at different microwave powers

XPS was performed on the 200 W graphene sample to unravel their elemental composition and functional group species. The XPS survey scans given in Fig 3.3a, clearly exhibit the presence of C and O in the sample having the composition of ~87% and ~10% respectively. The peaks centered at 284 eV and 531.5 eV ascribed to C1s and O1s respectively. To understand the bonding structures of C and O elements, the high-resolution spectra of C1s and O1s were analysed comprehensively.

The high-resolution spectrum of C1s with deconvoluted peaks is given in Fig 3.3b. Overall, four component peaks were identified in the spectrum. The key peaks at 284.3 eV and 285 eV correspond to sp^2-C and sp^3-C, respectively. The peak at 286.4 eV reflects C=O, whereas the

smallest peak at 289 eV represents C-OH bonding. The occurrence of sp^2-C is suggestive of the conjugated honeycomb lattice arrangement of graphene, while sp^3-C indicates substitution defects in graphene or the edges of the graphene nanosheets [37]. The high-resolution spectra of O1s (Fig 3.3c) showed contributions at 531 eV and 532.1 eV arising from C=O and C-OH respectively. Comparing our XPS results with that of Lambert et al. [38], where they also used atmospheric pressure microwave plasma, it is found that they obtained a fairly low amount of oxygen i.e. 3 %. However, their synthesis was from graphene oxide at a quite high power of 900 W.

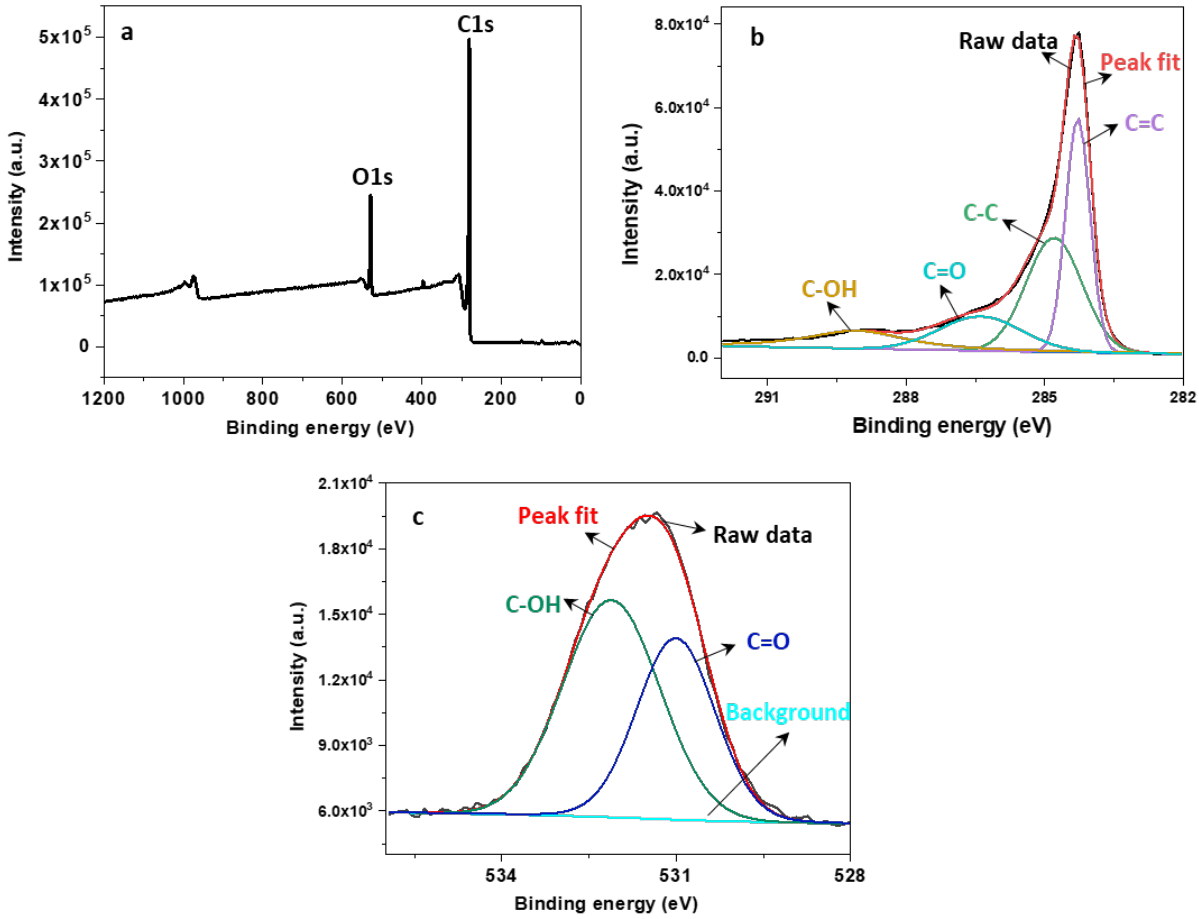

Fig 3.3: (a) Survey scan XPS spectrum of 200 W graphene sample, and deconvoluted peaks of high-resolution (b) C1s and (c) O1s XPS spectra

SEM images of the 200 W graphene sample taken at lower and higher magnifications are given in Fig 3.4. Fig 3.4a shows the dense accumulation of graphene nanosheets at varying places, where nanosheets coalesce together to form an aggregate. The aggregation can be attributed to the continuous synthesis process in which nanosheets after formation tend to reside on existing graphene nanosheets. A higher magnification image in Fig 3.4b reveals a typical vertically standing petal-like structure where graphene nanosheets are curled, wrinkled, and overlapped. The size of individual nanosheets varies between 50-150 nm.

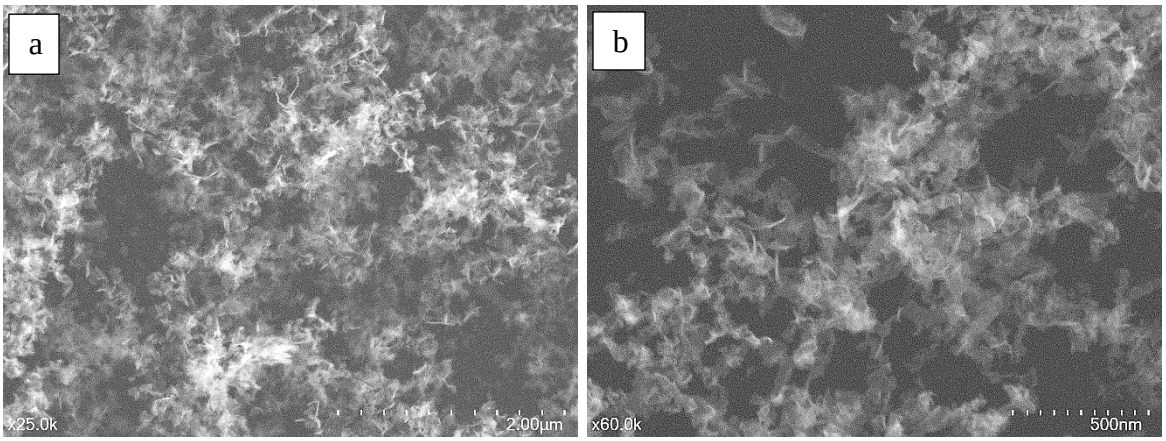

Fig 3.4: SEM images of 200 W graphene sample at (a) lower and (b) higher magnification

The low magnification TEM images show a mix of regular nanoparticles and sheets. The TEM results agree with the idea of agglomerations of carbon nanostructures. The nanosheets in the TEM image (Fig 3.5a) are supporting the SEM results presented in Fig 3.4. The sheets are potentially agglomerations of single or multi-layered graphitic structures formed during the plasma synthesis, which turns into multi-layer architectures as seen in high-resolution TEM (HRTEM) (Fig 3.5c). In the case of Fig 3.5c the graphitic particles observed has approximately 20 layers. Graphene sheets with less number of layers were also observed. But in most cases the graphene sheets are multi-layered. The particles showing regular structures are multi-layer graphitic architectures with a variety of structures such as nano-horns, nano-rods (Fig 3.5b) or nano-onions (Fig 3.5d-e). The d-spacing in all the structures is larger than the typical 0.33 nm

[39-41]. The measured d-spacing varies from 0.37 nm to 0.4 nm. This larger d-spacing has already been reported in other structures such as morphed graphene [42-44]. In the present work, the rather smaller d-spacing is commonly seen in the graphitic sheets, while the larger d-spacing is typical of the regular structures such as nano-horns, nano-rods and nano-onions. Potentially the nano-sheets with d-spacing of approximately 0.37 nm is due to potential agglomerations of graphene sheets. However, the d-spacing on the regular structures is attributed to potential bending of the graphene sheets or the functional groups (C-OH, C=O etc.) detected with XPS.

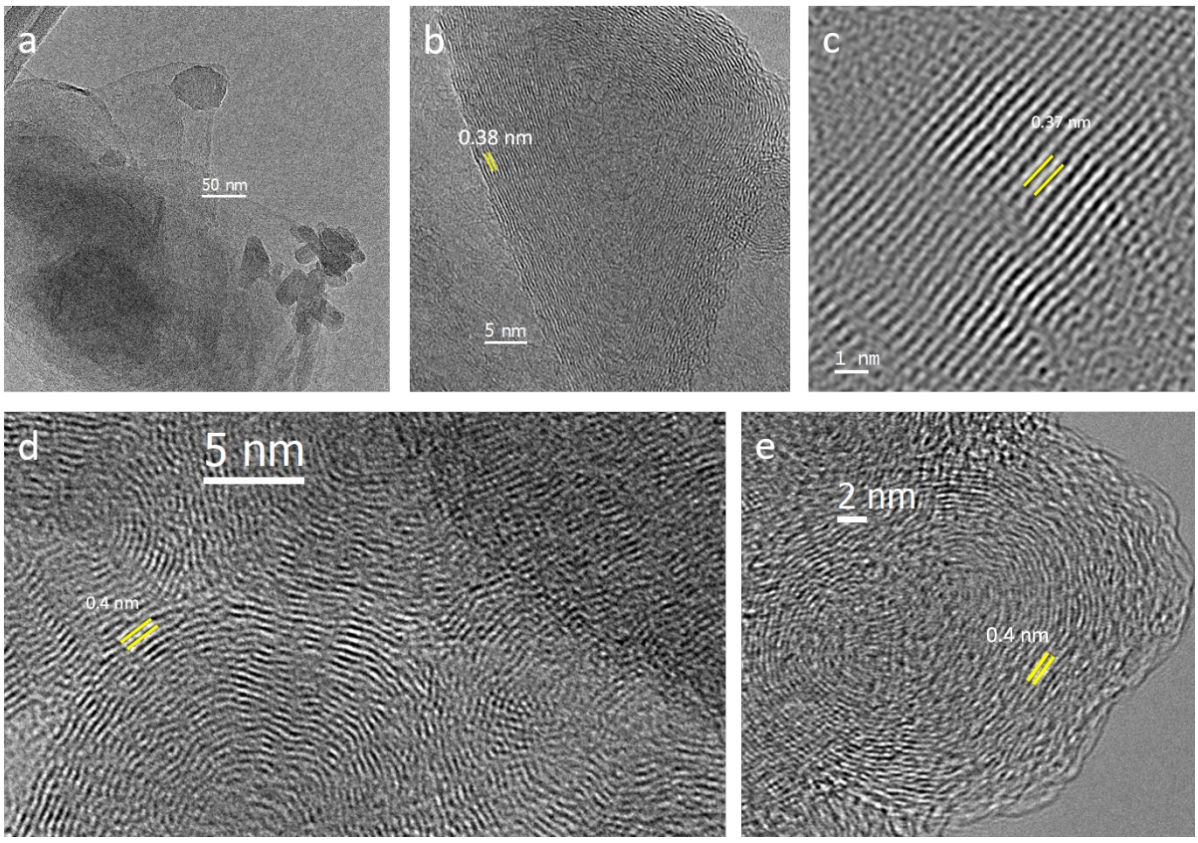

Fig 3.5: Transmission Electron Microscopy of graphitic particles (a) low magnification, (b-e) HRTEM

Crystalline materials have a unique XRD pattern that can be used as a fingerprint for materials identification. The distinctive peak centered at a diffraction angle (2θ) of 23.6° in Fig 3.6 XRD

pattern, confirms the successful formation of graphitic lattice. The peak position is associated with the (002) basal plane and corresponds to an interlayer spacing of 0.37 nm which is also verified by TEM. The interlayer spacing is higher compared to the typical 0.33 nm reported for graphene [39-41, 45]. We attribute this to intercalated C=O, C-OH functional groups within the layers. Our XRD results are in good agreement with the other reports [46, 47], where they synthesized graphene using ultra-sonic exfoliation or hydrothermal method. The comparable properties of tea tree-derived graphene (given in table 3.1) makes our synthesis approach a viable, cost-effective, and environmentally friendly strategy to replace unsustainable and harmful parent-materials.

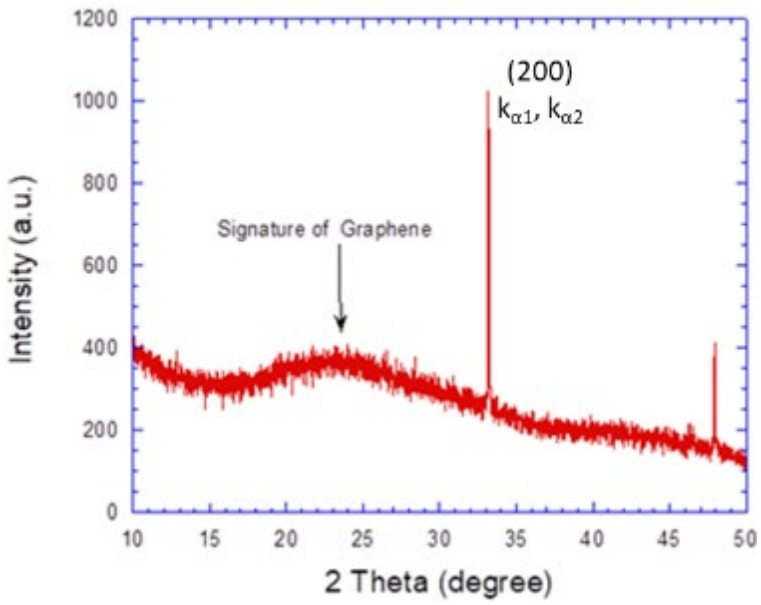

Fig 3.6: XRD pattern of 200 W graphene

Table 3.1: Comparison of tea tree oil-derived graphene with others synthesized in atmospheric pressure microwave plasma

Precursor	Microwave power (W)	Precursor flow rate (sccm)	I_D/I_G	Number of layers	Production rate (mg/min)	Ref.
Ethanol	250	0.3	-	Mono-and bi-layers	2	[10, 25]
Ethanol	900	0.5 – 3.5	-	Few layers	2	[48]
Ethanol	200	0.0036	0.6	Multilayers	0.07	[49]
Ethanol	300	0.33	0.24	Few layers	1.33	[24]
Ethanol	300	0.048	0.35	Few to multilayers	1.45	[50]
Methane	1000	2 – 8	0.62	Multilayers	-	[30]
Methane	1200-1400	-	1.57 or 1.77	Few to multilayers	-	[51]
Tea tree oil	200	0.3	0.83	Multilayers	1.37	Current work

3.4 Application of graphene in an electrochemical sensor

The electron-transfer kinetics of the graphene/GCE was investigated by comparing it with bare GCE using the EIS method. Fig 3.7shows the typical Nyquist plots of both electrodes. A semicircle region at higher frequencies attributed to the charge-transfer resistance (R_{ct}) and the linear region at lower frequencies corresponding to the diffusion process was observed for both electrodes. The Rct values can be estimated by fitting the plot with an equivalent Randles

circuit (inset, Fig 3.7), which were 206 Ω and 79 Ω on the bare GCE and graphene/GCE, respectively. The substantial decrease in the R_{ct} of graphene/GCE by a factor of ~2.6 times, suggests the fast electron-transfer kinetics due to the excellent electrical conductivity of the graphene material.

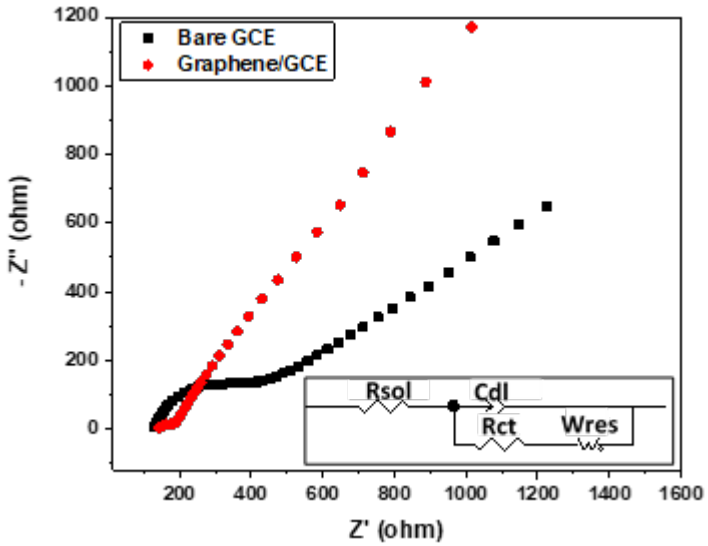

Fig 3.7: EIS of bare and graphene-modified GCE in 0.1 M KCl containing 5 mM $K_3[Fe(CN)_6]$. Frequency range 0.1 Hz to 100 kHz

The electrocatalytic activity of the graphene material for the detection of diuron was investigated in 0.1 M PBS (pH 7.0) containing 2 mM diuron using CV. Fig 3.8 indicates that the electrochemical reaction of diuron at the bare GCE undergo sluggish charge-transfer kinetic process. Whereas, the graphene/GCE electrode improved the peak current substantially. The diuron undergoes an irreversible chemical reaction and forms a dimmer resultantly [52]. The graphene/GCE performance in the absence of diuron showed a different voltammogram with no peak formation. Similar cyclic voltammograms were observed by Wong et al. [53] and Morita et al. [54] in separate studies for diuron detection.

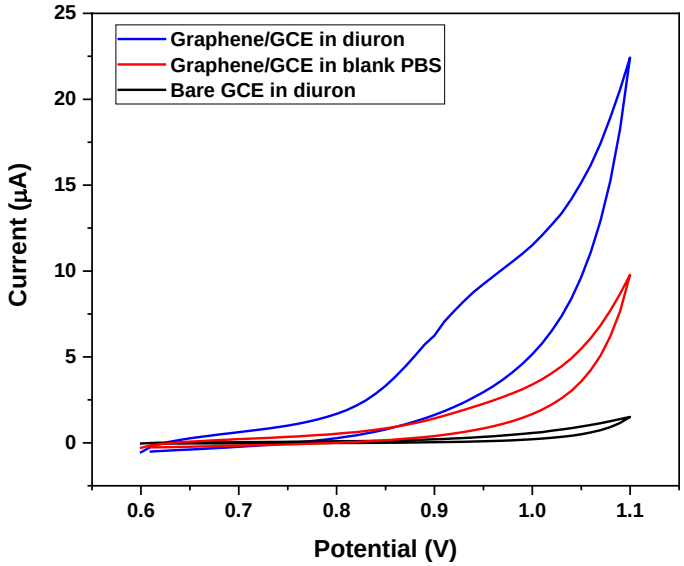

Fig 3.8: Cyclic voltammograms of bare and graphene-modified GCE in 0.1 M PBS containing 2 mM diuron, and graphene/GCE in blank 0.1 M PBS, the scan rate is 10 mV/sec

Differential pulse voltammetry (DPV) has the lead in high sensitivity due to low capacitive current [55]. DPV of graphene/GCE was carried out in 0.1 M PBS to obtain the calibration curve of diuron. It can be observed that the peak currents increase upon increasing the concentration of diuron (Fig 3.9). A linear range (LR) was obtained in the range of 20 µM to 1000 µM with a regression equation of y = 0.0062x + 4.1039, (R^2=0.998). A low limit of detection (LOD) i.e. 5 µM was also recorded, which is comparable with values reported in literature. As compared with the analytical performance of carbon-based diuron sensors reported previously (Table 3.2), our electrode has promising outcomes with the wider LR and comparable LOD. Moreover, it is noteworthy that we used graphene without any further modifications.

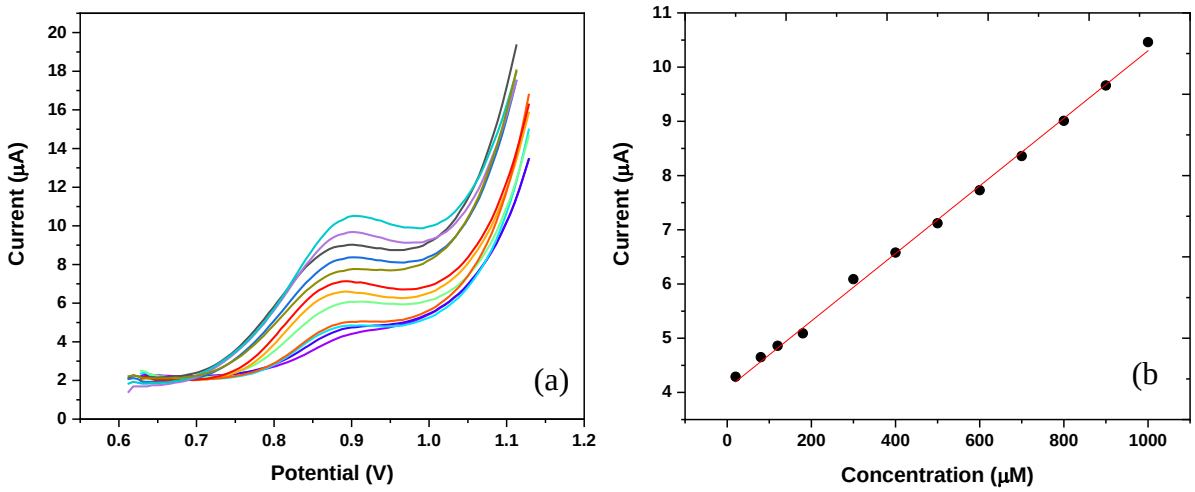

Fig 3.9: (a) DPV curves at graphene/GCE for different concentrations (20, 80, 120, 180, 300, 400, 500, 600, 700, 800, 900, 1000 µM) of diuron in 0.1 M PBS (b) Calibration plot from the DPV measurements

Table 3.2: Comparison of different carbon-based modified electrodes for electrochemical detection of diuron

Electrode	**Linear range**	**Limit of detection (µM)**	**Ref.**
Nanocrystalline cellulose carbon paste electrode	4.2 µM − 47 µM	0.35	[52]
Nafion/AuNPs/RGO/GCE	1.0×10^{-6} µM − 0.001 µM	4.1×10^{-7}	[56]
ITO-ppy-MWCNT-PSS polypyrrole	–	0.26	[57]
rGO–AuNPs/Nafion/GCE	0.001 µM − 0.1 µM	0.0003	[58]
MWCNT-COOH/GCE	0.215 µM − 2.15 × µM	0.0688	[54]

MWCNT-COOH-MIP/Carbon paste electrode	0.052 μM – 1.25 μM	0.009	[59]
Organometallic complexes and graphene oxide	50 μM – 1000 μM	20	[60]
GO-MWCNT/GCE	9 μM – 380 μM	1.49	[61]
Graphene/GCE	20 μM – 1000 μM	5	This work

The graphene/GCE exhibited excellent repeatability in four successive measurements with a relative standard deviation (RSD) of 3.82 % calculated using peak currents. Similarly, the electrode offered good reproducibility by showing 5.17 % of RSD, investigated on three different electrodes. The stability test of the electrode was conducted for period of 2 weeks, which showed 4.21 % RSD, indicating a satisfactory outcome for the stability of the electrode.

3.5 Conclusion

This work presents the synthesis of graphene from a tea tree essential oil vapours in atmospheric pressure microwave plasma. The synthesis has been carried out in one-step at a reasonably low microwave power of 200 W. The Raman spectra showed the effect of power increase in higher I_D/I_G ratio and FWHM values of the 2D peak. XPS results revealed ~87 % of carbon and ~10 % of oxygen content, where oxygen is attached with the carbon in the form of hydroxyl and carbonyl functional groups. The signature of graphene was obtained using an XRD pattern, which showed 2θ at 23.6° and interlayer spacing of 0.37 nm. This is confirm on HRTEM. The impedance of graphene appeared to be less than half of bare GCE, indicating fast electron-transfer kinetics of graphene/GCE electrode. The graphene sensing performance

for diuron herbicide was investigated by drop-casting it's aliquot on GCE. The graphene/GCE sensor showed a linear range from 20 μM to 1 mM, and a limit of detection of 5 μM.

Collectively, the synthesized graphene nanosheets possess comparable properties to any other graphene-based materials, synthesized through different methods. Our synthesis pathway, paves the way for a green, energy-efficient, and fast synthesis of graphene.

References

1. Novoselov, K.S., V. Fal, L. Colombo, P. Gellert, M. Schwab, and K. Kim, *A roadmap for graphene.* nature, 2012. **490**(7419): p. 192-200.
2. Ferrari, A.C., F. Bonaccorso, V. Fal'Ko, K.S. Novoselov, S. Roche, P. Bøggild, S. Borini, F.H. Koppens, V. Palermo, and N. Pugno, *Science and technology roadmap for graphene, related two-dimensional crystals, and hybrid systems.* Nanoscale, 2015. **7**(11): p. 4598-4810.
3. Bu, Y., Z. Chen, W. Li, and B. Hou, *Highly efficient photocatalytic performance of graphene–ZnO quasi-shell–core composite material.* ACS applied materials & interfaces, 2013. **5**(23): p. 12361-12368.
4. Brisebois, P. and M. Siaj, *Harvesting graphene oxide–years 1859 to 2019: a review of its structure, synthesis, properties and exfoliation.* Journal of Materials Chemistry C, 2020. **8**(5): p. 1517-1547.
5. Wang, H., Q. Fu, and C. Pan, *Green mass synthesis of graphene oxide and its MnO2 composite for high performance supercapacitor.* Electrochimica Acta, 2019. **312**: p. 11-21.
6. Smith, A.T., A.M. LaChance, S. Zeng, B. Liu, and L. Sun, *Synthesis, properties, and applications of graphene oxide/reduced graphene oxide and their nanocomposites.* Nano Materials Science, 2019. **1**(1): p. 31-47.

7. McEvoy, N., H. Nolan, N.A. Kumar, T. Hallam, and G.S. Duesberg, *Functionalisation of graphene surfaces with downstream plasma treatments.* Carbon, 2013. **54**: p. 283-290.

8. Felten, A., A. Eckmann, J. Pireaux, R. Krupke, and C. Casiraghi, *Controlled modification of mono-and bilayer graphene in O2, H2 and CF4 plasmas.* Nanotechnology, 2013. **24**(35): p. 355705.

9. Hadish, F., S. Jou, B.-R. Huang, H.-A. Kuo, and C.-W. Tu, *Functionalization of CVD grown graphene with downstream oxygen plasma treatment for glucose sensors.* Journal of The Electrochemical Society, 2017. **164**(7): p. B336.

10. Dato, A. and M. Frenklach, *Substrate-free microwave synthesis of graphene: experimental conditions and hydrocarbon precursors.* New Journal of Physics, 2010. **12**(12): p. 125013.

11. Tatarova, E., A. Dias, J. Henriques, M. Abrashev, N. Bundaleska, E. Kovacevic, N. Bundaleski, U. Cvelbar, E. Valcheva, and B. Arnaudov, *Towards large-scale in free-standing graphene and N-graphene sheets.* Scientific reports, 2017. **7**(1): p. 1-16.

12. Hansora, D., N. Shimpi, and S. Mishra, *Graphite to graphene via graphene oxide: an overview on synthesis, properties, and applications.* Jom, 2015. **67**(12): p. 2855-2868.

13. Agarwal, V. and P.B. Zetterlund, *Strategies for reduction of graphene oxide–A comprehensive review.* Chemical Engineering Journal, 2021. **405**: p. 127018.

14. Yan, Y., F.Z. Nashath, S. Chen, S. Manickam, S.S. Lim, H. Zhao, E. Lester, T. Wu, and C.H. Pang, *Synthesis of graphene: Potential carbon precursors and approaches.* Nanotechnology Reviews, 2020. **9**(1): p. 1284-1314.

15. Kumar, R., R.K. Singh, and D.P. Singh, *Natural and waste hydrocarbon precursors for the synthesis of carbon based nanomaterials: Graphene and CNTs.* Renewable and Sustainable Energy Reviews, 2016. **58**: p. 976-1006.

16. Seo, D.H., A.E. Rider, Z.J. Han, S. Kumar, and K. Ostrikov, *Plasma Break-Down and Re-Build: Same Functional Vertical Graphenes from Diverse Natural Precursors.* Advanced Materials, 2013. **25**(39): p. 5638-5642.

17. Ruan, G., Z. Sun, Z. Peng, and J.M. Tour, *Growth of graphene from food, insects, and waste.* ACS nano, 2011. **5**(9): p. 7601-7607.

18. Sharma, S., G. Kalita, R. Hirano, Y. Hayashi, and M. Tanemura, *Influence of gas composition on the formation of graphene domain synthesized from camphor.* Materials Letters, 2013. **93**: p. 258-262.

19. Jacob, M.V., R.S. Rawat, B. Ouyang, K. Bazaka, D.S. Kumar, D. Taguchi, M. Iwamoto, R. Neupane, and O.K. Varghese, *Catalyst-Free Plasma Enhanced Growth of Graphene from Sustainable Sources.* Nano Letters, 2015. **15**(9): p. 5702-5708.

20. Alancherry, S., K. Bazaka, I. Levchenko, A. Al-Jumaili, B. Kandel, A. Alex, F.C. Robles Hernandez, O.K. Varghese, and M.V. Jacob, *Fabrication of Nano-Onion-Structured Graphene Films from Citrus sinensis Extract and Their Wetting and Sensing Characteristics.* ACS Applied Materials & Interfaces, 2020.

21. Purkait, T., G. Singh, M. Singh, D. Kumar, and R.S. Dey, *Large area few-layer graphene with scalable preparation from waste biomass for high-performance supercapacitor.* Scientific reports, 2017. **7**(1): p. 1-14.

22. Malek, M., M. Robaiah, A. Suriani, M. Mamat, M. Ahmad, T. Soga, M. Rusop, S. Abdullah, Z. Khusaimi, and M. Aslam, *The utilization of waste cooking palm oil as a green carbon source for the growth of multilayer graphene.* Journal of the Australian Ceramic Society, 2021. **57**(2): p. 347-358.

23. Mohan, A.N. and M. . B, *Extraction of graphene nanostructures from Colocasia esculenta and Nelumbo nucifera leaves and surface functionalization with tin oxide:*

Evaluation of their antibacterial properties. Chemistry–A European Journal, 2020. **26**(36): p. 8105-8114.

24. Melero, C., R. Rincón, J. Muñoz, G. Zhang, S. Sun, A. Perez, O. Royuela, C. González-Gago, and M. Calzada, *Scalable graphene production from ethanol decomposition by microwave argon plasma torch.* Plasma Physics and Controlled Fusion, 2017. **60**(1): p. 014009.

25. Dato, A., V. Radmilovic, Z. Lee, J. Phillips, and M. Frenklach, *Substrate-free gas-phase synthesis of graphene sheets.* Nano letters, 2008. **8**(7): p. 2012-2016.

26. Münzer, A., L. Xiao, Y.H. Sehlleier, C. Schulz, and H. Wiggers, *All gas-phase synthesis of graphene: Characterization and its utilization for silicon-based lithium-ion batteries.* Electrochimica Acta, 2018. **272**: p. 52-59.

27. Nakahara, K., J. Knego, T. Sloop, C. Bisquera, N. Subler, and A. Dato, *Enhanced mechanical properties of epoxy-matrix nanocomposites reinforced with graphene synthesized in atmospheric plasmas.* Plasma Processes and Polymers, 2020. **17**(5): p. 1900244.

28. Tsyganov, D., N. Bundaleska, A. Dias, J. Henriques, E. Felizardo, M. Abrashev, J. Kissovski, A.B. do Rego, A. Ferraria, and E. Tatarova, *Microwave plasma-based direct synthesis of free-standing N-graphene.* Physical Chemistry Chemical Physics, 2020. **22**(8): p. 4772-4787.

29. Jašek, O., J. Toman, J. Jurmanová, M. Šnírer, V. Kudrle, and V. Buršíková, *Study of graphene layer growth on dielectric substrate in microwave plasma torch at atmospheric pressure.* Diamond and Related Materials, 2020. **105**: p. 107798.

30. Bundaleska, N., D. Tsyganov, A. Dias, E. Felizardo, J. Henriques, F. Dias, M. Abrashev, J. Kissovski, and E. Tatarova, *Microwave plasma enabled synthesis of free*

standing carbon nanostructures at atmospheric pressure conditions. Physical Chemistry Chemical Physics, 2018. **20**(20): p. 13810-13824.

31. Jimenez, M., R. Rincon, A. Marinas, and M. Calzada, *Hydrogen production from ethanol decomposition by a microwave plasma: influence of the plasma gas flow.* International journal of hydrogen energy, 2013. **38**(21): p. 8708-8719.

32. Liu, B., Z. Liu, I.-S. Chiu, M. Di, Y. Wu, J.-C. Wang, T.-H. Hou, and C.-S. Lai, *Programmable synaptic metaplasticity and below femtojoule spiking energy realized in graphene-based neuromorphic memristor.* ACS applied materials & interfaces, 2018. **10**(24): p. 20237-20243.

33. Krishnamoorthy, K., M. Veerapandian, K. Yun, and S.-J. Kim, *The chemical and structural analysis of graphene oxide with different degrees of oxidation.* Carbon, 2013. **53**: p. 38-49.

34. Shen, L., L. Zhang, K. Wang, L. Miao, Q. Lan, K. Jiang, H. Lu, M. Li, Y. Li, and B. Shen, *Analysis of oxidation degree of graphite oxide and chemical structure of corresponding reduced graphite oxide by selecting different-sized original graphite.* RSC advances, 2018. **8**(31): p. 17209-17217.

35. Boas, C.R.S.V., B. Focassio, E. Marinho, D.G. Larrude, M.C. Salvadori, C.R. Leão, and D.J. Dos Santos, *Characterization of nitrogen doped graphene bilayers synthesized by fast, low temperature microwave plasma-enhanced chemical vapour deposition.* Scientific reports, 2019. **9**(1): p. 1-12.

36. Hao, Y., Y. Wang, L. Wang, Z. Ni, Z. Wang, R. Wang, C.K. Koo, Z. Shen, and J.T. Thong, *Probing layer number and stacking order of few-layer graphene by Raman spectroscopy.* small, 2010. **6**(2): p. 195-200.

37. Al-Gaashani, R., A. Najjar, Y. Zakaria, S. Mansour, and M. Atieh, *XPS and structural studies of high quality graphene oxide and reduced graphene oxide prepared by*

different chemical oxidation methods. Ceramics International, 2019. **45**(11): p. 14439-14448.

38. Lambert, T.N., C.C. Luhrs, C.A. Chavez, S. Wakeland, M.T. Brumbach, and T.M. Alam, *Graphite oxide as a precursor for the synthesis of disordered graphenes using the aerosol-through-plasma method.* Carbon, 2010. **48**(14): p. 4081-4089.

39. Toman, J., O. Jašek, M. Šnírer, D. Pavliňák, Z. Navrátil, J. Jurmanová, S. Chudják, F. Krčma, V. Kudrle, and J. Michalička, *On the transition of reaction pathway during microwave plasma gas-phase synthesis of graphene nanosheets: From amorphous to highly crystalline structure.* Plasma Processes and Polymers, 2021: p. e2100008.

40. Zafar, M.A. and M.V. Jacob, *Plasma-based synthesis of graphene and applications: a focused review.* Reviews of Modern Plasma Physics, 2022. **6**(1): p. 37.

41. Al-Jumaili, A., M.A. Zafar, K. Bazaka, J. Weerasinghe, and M.V. Jacob, *Bactericidal vertically aligned graphene networks derived from renewable precursor.* Carbon Trends, 2022. **7**: p. 100157.

42. Bao, J., S. Xing, Y. Wang, W. Wu, F. Robles-Hernandez, and S.S. Pei. *Fabrication of large-area twisted bilayer graphene for high-speed ultra-sensitive tunable photodetectors*. in *Proceedings of SPIE - The International Society for Optical Engineering*. 2013.

43. Chilkoor, G., N. Shrestha, A. Kutana, M. Tripathi, F.C. Robles Hernández, B.I. Yakobson, M. Meyyappan, A.B. Dalton, P.M. Ajayan, M.M. Rahman, and V. Gadhamshetty, *Atomic Layers of Graphene for Microbial Corrosion Prevention.* ACS Nano, 2020.

44. Wang, Y., Z. Su, W. Wu, S. Nie, X. Lu, H. Wang, K. McCarty, S.S. Pei, F. Robles-Hernandez, V.G. Hadjiev, and J. Bao, *Four-fold Raman enhancement of 2D band in*

twisted bilayer graphene: Evidence for a doubly degenerate Dirac band and quantum interference. Nanotechnology, 2014. **25**(33).

45. Calderon, H.A., F. Alvarez Ramirez, D. Barber, V.G. Hadjiev, A. Okonkwo, R. Ordoñez Olivares, I. Estrada Guel, and F.C. Robles Hernandez, *Enhanced elastic behavior of all-carbon composites reinforced by in-situ synthesized morphed graphene.* Carbon, 2019. **153**: p. 657-662.

46. Calderon, H.A., I. Estrada-Guel, F. Alvarez-Ramírez, V.G. Hadjiev, and F.C. Robles Hernandez, *Morphed graphene nanostructures: Experimental evidence for existence.* Carbon, 2016. **102**: p. 288-296.

47. Calderon, H.A., A. Okonkwo, I. Estrada-Guel, V.G. Hadjiev, F. Alvarez-Ramírez, and F.C. Robles Hernández, *HRTEM low dose: the unfold of the morphed graphene, from amorphous carbon to morphed graphenes.* Advanced Structural and Chemical Imaging, 2016. **2**(1): p. 10.

48. Wang, G., X. Shen, B. Wang, J. Yao, and J. Park, *Synthesis and characterisation of hydrophilic and organophilic graphene nanosheets.* Carbon, 2009. **47**(5): p. 1359-1364.

49. Asgar, H., K. Deen, U. Riaz, Z.U. Rahman, U.H. Shah, and W. Haider, *Synthesis of graphene via ultra-sonic exfoliation of graphite oxide and its electrochemical characterization.* Materials Chemistry and Physics, 2018. **206**: p. 7-11.

50. Chen, W., D. Li, L. Tian, W. Xiang, T. Wang, W. Hu, Y. Hu, S. Chen, J. Chen, and Z. Dai, *Synthesis of graphene quantum dots from natural polymer starch for cell imaging.* Green chemistry, 2018. **20**(19): p. 4438-4442.

51. Tatarova, E., J. Henriques, C. Luhrs, A. Dias, J. Phillips, M. Abrashev, and C. Ferreira, *Microwave plasma based single step method for free standing graphene synthesis at atmospheric conditions.* Applied Physics Letters, 2013. **103**(13): p. 134101.

52. Rincón, R., C. Melero, M. Jiménez, and M. Calzada, *Synthesis of multi-layer graphene and multi-wall carbon nanotubes from direct decomposition of ethanol by microwave plasma without using metal catalysts.* Plasma Sources Science and Technology, 2015. **24**(3): p. 032005.

53. Casanova, A., R. Rincón, J. Muñoz, C. Ania, and M. Calzada, *Optimizing high-quality graphene nanoflakes production through organic (bio)-precursor plasma decomposition.* Fuel Processing Technology, 2021. **212**: p. 106630.

54. Singh, M., A. Sengupta, K. Zeller, G. Skoptsov, and R.L. Vander Wal, *Effect of hydrogen concentration on graphene synthesis using microwave-driven plasma-mediated methane cracking.* Carbon, 2019. **143**: p. 802-813.

55. Zafar, M.A., Y. Liu, S. Allende, and M.V. Jacob, *Electrochemical sensing of oxalic acid using silver nanoparticles loaded nitrogen-doped graphene oxide.* Carbon Trends, 2022. **8**: p. 100188.

56. Serge, M., B.R. KarangaYssouf, T. Issa, S. Fadilatou, S.I. KoulibalyBazoumana, T. Ignas, and N. Emmanuel, *Electrochemical Determination of Diuron in Soil Using a Nanocrystalline Cellulose Modified Carbon Paste Electrode.*

57. Wong, A., M.R. de Vasconcelos Lanza, and M.D.P.T. Sotomayor, *Sensor for diuron quantitation based on the P450 biomimetic catalyst nickel (II) 1, 4, 8, 11, 15, 18, 22, 25-octabutoxy-29H, 31H-phthalocyanine.* Journal of Electroanalytical Chemistry, 2013. **690**: p. 83-88.

58. Morita, I.M., G.M. Araújo, L. Codognoto, and F.R. Simões, *Functionalised multi-walled carbon nanotubes-modified electrode for sensitive determination of Diuron in seawater samples.* International Journal of Environmental Analytical Chemistry, 2019. **99**(15): p. 1565-1574.

59. Brazaca, L.C., L. Ribovski, B.C. Janegitz, and V. Zucolotto, *10 - Nanostructured materials and nanoparticles for point of care (POC) medical biosensors*, in *Medical Biosensors for Point of Care (POC) Applications*, R.J. Narayan, Editor. 2017, Woodhead Publishing. p. 229-254.

60. Qin, J., Y. Qin, X. Jiang, Y. Du, C.-Z. Yao, X. Wang, and H. Yang, *Electrochemical Sensor Based on Nafion/Gold Nanoparticle/Electrochemically Reduced Graphene Oxide Composite-Modified Glassy Carbon Electrode for the Detection of Diuron.* Int. J. Electrochem. Sci, 2020. **15**: p. 11203-11214.

61. de Araújo, G.M. and F.R. Simões, *Self-assembled films based on polypyrrole and carbon nanotubes composites for the determination of Diuron pesticide.* Journal of Solid State Electrochemistry, 2018. **22**(5): p. 1439-1448.

62. Zarei, K. and A. Khodadadi, *Very sensitive electrochemical determination of diuron on glassy carbon electrode modified with reduced graphene oxide–gold nanoparticle–Nafion composite film.* Ecotoxicology and environmental safety, 2017. **144**: p. 171-177.

63. Wong, A., M.V. Foguel, S. Khan, F.M. de Oliveira, C.R.T. Tarley, and M.D. Sotomayor, *Development of an electrochemical sensor modified with MWCNT-COOH and MIP for detection of diuron.* Electrochimica Acta, 2015. **182**: p. 122-130.

64. Wong, A. and M.D.P.T. Sotomayor, *Determination of carbofuran and diuron in FIA system using electrochemical sensor modified with organometallic complexes and graphene oxide.* Journal of Electroanalytical Chemistry, 2014. **731**: p. 163-171.

65. Mani, V., R. Devasenathipathy, S.-M. Chen, T.-Y. Wu, and K. Kohilarani, *High-performance electrochemical amperometric sensors for the sensitive determination of phenyl urea herbicides diuron and fenuron.* Ionics, 2015. **21**(9): p. 2675-2683.

Chapter 4: Synthesis of graphene-Ag nanocomposite and its application in detection

This chapter demonstrates the rapid and sustainable methodology for the synthesis of graphene-Ag nanocomposite. It is presented that the nanocomposite can now be synthesized in atmospheric pressure microwave plasma. The confirmation of synthesis of nanocomposite, made through various state-of-the-art characterization techniques, is described in detail in this chapter. Furthermore, the application of as-synthesized graphene-Ag nanocomposite that was drop casted on screen-printed-electrode is shown for the detection of methyl paraben.

This Chapter as following will be submitted to the journal.

Zafar, M. A., Liu, Y., & Jacob, M. V. (2023). Rapid and sustainable synthesis of graphene-Ag nanocomposite for the detection of methyl paraben.

Rapid and sustainable synthesis of graphene-Ag nanocomposite for the detection of methyl paraben

Abstract

The synthesis of graphene-based nanocomposites using wet chemical techniques entails a number of time-consuming and laborious synthesis stages in addition to the use of potentially dangerous substances. The present article provides a novel approach to green and in-situ synthesis that employs no hazardous chemicals and synthesizes graphene and silver nanoparticles (Ag NPs) nanocomposite from the tea tree oil and silver nitrate ($AgNO_3$) vapours respectively. The synthesis happens in a matter of seconds in microwave plasma at ambient conditions. Images from the scanning and transmission electron microscopy revealed that graphene nanosheets act as the most favoured sites for the Ag NPs to anchor and form a nanocomposite. The investigations revealed a correlation between the concentration of $AgNO_3$ in the precursor and the size and aggregation of Ag NPs. The results of X-ray photoelectron spectroscopy demonstrated a negative shifting of the Ag-doublet, which suggested a strong interaction between Ag NPs and graphene. Additionally, the graphene-Ag nanocomposite drop-casted on screen-printed electrode demonstrated good electrochemical sensing capability for methyl paraben, with a superior linear range of 20 to 260 µM and a commendable limit of detection of 2.5 µM.

4.1 Introduction

A new class of hybrid materials i.e. graphene-based nanocomposites offers significantly enhanced and multifarious properties. In this regard, various graphene-based nanocomposites comprising different metal oxides and nanoparticles have been developed [1]. The synergy of Ag NPs and graphene nanosheets offered superior properties that have applications in various

fields such as catalysis, antimicrobial coatings, sensors etc. [2-5]. Ag NPs composite with pristine graphene, graphene oxide (GO), and reduced-graphene oxide (r-GO) are used in electrochemical sensors [6, 7], catalysis [8], biomaterials [9], and chemical detection processes [10]. This promising material, however, still needs attention for its facile and sustainable synthesis.

The production of graphene-Ag nanocomposites has received considerable research interest. Traditional wet chemical methods to synthesize graphene-Ag nanocomposites entail two stages. First, GO is synthesized using the Hummers method, and then it is converted to r-GO or pristine graphene. The Hummers method comprises multiple steps such as stirring, heating, purifying, and drying [8, 11]. In the second stage, the composite with Ag is created through another solution-based chemical method, which involves reductants, oxidants, and surfactants [10, 12, 13]. This two-stage traditional approach is time-consuming and includes the use of hazardous chemicals, which are not only toxic to the environment but also difficult to remove from the nanocomposite. Some of the reductants and surfactants persist as pollutants within the nanocomposite, further affecting the inherent antibacterial activity of the Ag nanoparticles [14]. The use of hazardous compounds at several subsequent phases and laborious synthesis processes are still not addressed, despite attempts by some researchers to investigate green-reducing agents [6, 9, 15-17].

In the past, plasma has been used in the synthesis to speed up the procedure and reduce overall chemical usage [8, 18]. However, since the wet chemical technique of producing graphene is still in use, the plasma was only used for the reduction and did not succeed in making the process chemical-free. Interestingly, later on, plasma was used to synthesize graphene as well as metal nanoparticles. For this purpose, a single precursor which contains carbon and metal, for instance, titanium isopropoxide ($C_{12}H_{28}O_4Ti$) is used to synthesize TiO_2-

graphene nanocomposite in a single-step [19]. Unfortunately, the requirement of this unique combination of both elements in the same precursor limits the scope of the method to very few nanocomposites. In addition, the technique produces the nanocomposite, which has a fixed amount of metal in the product.

Lately, Jo et al. [20] presented the idea of mixing a metal salt into ethanol and decomposing them in the atmospheric pressure microwave plasma to synthesize Pt-graphene nanocomposite. This approach broadens the choice of metal nanoparticles and gives the freedom to experiment with the proportion of metal and graphene in the nanocomposite. However, not all metal salts fulfil the requirement of the good solubility of metal salt in ethanol. On the other hand, the usage of ethanol vapours above a certain level increases the chances of the plasma undergoing extinction, thereby affecting the overall production rate of the graphene [21].

There is a high demand for the rapid synthesis of graphene-based nanocomposite using green and sustainable precursors. Herein, we report a facile, dry, and sustainable approach to synthesizing the graphene-Ag nanocomposites using atmospheric pressure microwave plasma (APMP). The APMP method comprises two stages. In the first stage, the graphene is synthesized from a natural source, i.e. tea tree extract, and in the second step, Ag NPs are produced over graphene from $AgNO_3$ vapours. The reasons why APMP is a groundbreaking approach that outperforms all other traditional synthesis methods include: (i) the advantage of reduced synthesis time. Both the graphene and the Ag NPs can be fabricated within just a fraction of a second. (ii) The post-synthesis formalities of washing, drying, etc. are not necessary with this process, nor are any chemicals. Table S1 presents a comparative analysis of the APMP with the previously used methodologies. The APMP offers to use sustainable precursors in milder conditions of plasma (low microwave power, ambient conditions) ensuring that the process is eco-friendly and energy saving. This report also presented the

application of as-synthesized graphene-Ag nanocomposite for the detection of methyl paraben (MP), which is an endocrine disruptor chemical.

4.2 Materials and method

4.2.1 Raw materials

The essential oil of *melaleuca alternifolia*, commonly known as tea tree was purchased from Australian Botanical Products (ABP, Victoria, Australia). Silver nitrate ($AgNO_3$) and methyl paraben (MP) in ultrapure form were procured from Sigma Aldrich, Australia. Lastly, ultrapure water was used to make the solutions.

4.2.2 Instrumentations

Confocal laser Raman spectroscopy (Witec, 532 nm laser), scanning electron microscopy (SEM) (Hitachi SU 5000), and x-ray photoelectron spectroscopy (XPS) (Kratos Axis Ultra XPS with an Al Kα x-ray source) were used to investigate the structure, morphology, and elemental analysis. X-ray diffraction (XRD) (Bruker, D8-Advance X-ray diffractometer, Cu Kα, $\lambda = 0.154$ nm) was used for crystallographic information. A transmission electron microscope (Hitachi HF5000) was used for transmission electron microscopy (TEM) images. Optical emission spectroscopy was recorded using Avantes equipment.

Electrochemical experimentations were carried out on a PalmSens 4 (Palm Instruments BV, Netherlands) potentiostat. Screen-printed electrodes (SPE) were also purchased from Palm Instruments BV, Netherlands.

4.2.3 Synthesis of graphene-Ag nanocomposite

Fig. 4.1 illustrates the synthesis scheme of the graphene-Ag nanocomposite using the APMP. The plasma system composed of a microwave power supply (2.45 GHz), a tuner, a reaction tube made of quartz, and an ultrasonic vaporizer has been used for the experiment. A vaporizer was used to deliver the $AgNO_3$ into the reaction tube as a gas phase, whereas, oil vapours were sent by passing the argon gas through the container carrying tea tree oil.

Table 4.1 presents the operating condition used for the synthesis. Three different samples, synthesized from different concentrations of $AgNO_3$ i.e. 0.05 M, 0.10 M, and 0.15 M, named 0.05 M graphene-Ag, 0.10 M graphene-Ag, and 0.15 M graphene-Ag were prepared. The synthesis was carried out in two stages. At first, graphene was synthesized on the walls of the quartz tube for 15 minutes by adding the tea tree oil vapours. After that, the oil supply was stopped and $AgNO_3$ vapours were released for 7 minutes by switching on the vaporizer. The formation of graphene-Ag nanocomposite happened on the walls of the quartz tube. The walls of the quartz tube were where the graphene-Ag nanocomposite was formed. As-synthesized graphene-Ag nanocomposite was also collected on Si substrate for evaluation.

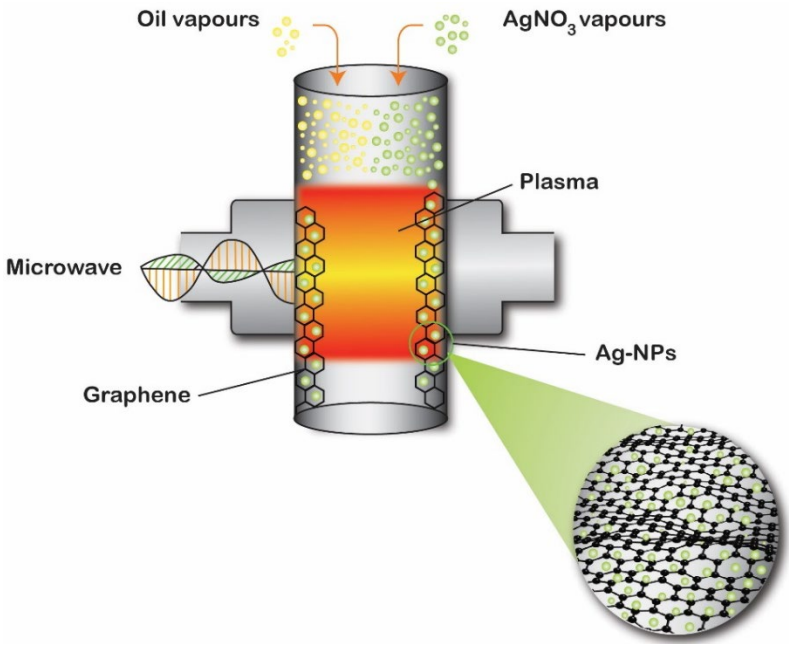

Fig 4.1: Schematic illustration of the synthesis of graphene-Ag nanocomposite in atmospheric pressure microwave plasma

Table 4.1: Details of synthesis conditions of graphene-Ag nanocomposite

Factors	Synthesis of graphene	Synthesis of Ag NPs
Precursor	Tea tree essential oil	$AgNO_3$ (0.05 M, 0.10 M, 0.15 M)
Microwave power	250 W	300 W
Argon flow rate	2.5 slm	2.5 slm
Precursor residence time	Few seconds	Few seconds
Synthesis duration	15 min	7 min

4.2.4 Analytical methods

A disposable screen-printed electrode (SPE) consisting of working, reference, and counter electrodes was used for the electrochemical study. The working electrode (diameter of 3 mm) was modified by drop-casting 5 µL of graphene-Ag nanocomposite followed by drying under

room temperature conditions. The modification solution consisted of 1mg/mL of graphene-Ag nanocomposite in ethanol. The stock solution of methyl paraben (MP) was prepared in methanol. Cyclic voltammetry and differential pulse voltammetry were used for electrochemical investigations. River water that was gathered from Ross River, Townsville, Australia, was used for real application. Before the experimentation, the river water was treated according to the procedure reported previously [22]. Concisely, the river water was first filtered through a 0.45 µm filter membrane, before it was diluted with 0.1 M PBS (pH 7.01) at a ratio of 1:9. Its pH was reassessed after dilution.

4.3 Results and discussions

4.3.1 Morphology and structural analysis of graphene-Ag nanocomposite

The Raman spectra of the graphene-Ag nanocomposite samples synthesized at different concentrations of $AgNO_3$ are given in Fig. 4.2a. The nanocomposites at all concentrations showed prominent D and G peaks along with a signature peak of 2D related to graphene-based materials [23].The peak D represents the A_{1g} vibration of the C_6 assembly of atoms appearing after the defects and disorders in the structure [24]. Additionally, it is also related to the functional groups and doping in the graphene [25, 26]. The G peak is attributed to the E_2g vibrational mode of sp^2 carbon [27]. The 2D band is the second order of zone-boundary phonons [28].

Each of the three concentrations had distinct D peaks. This is attributed to the oxygen functional groups found in the graphene's basal plane, which were further validated by XPS. Moreover, Ag NPs might also contribute to these intense D peaks. The degree of imperfection in graphene structure is usually determined by the intensity ratio of the D and G bands [29]. Fig. 4.2b presents the graph between intensity ratios (I_D/I_G) vs different concentrations of $AgNO_3$.

Although negligible differences are found in the values of I_D/I_G, a slight increase with the increase of $AgNO_3$ concentration was found. The number of layers in the graphitic structure may be estimated using full width half maximum (FWHM) along with I_{2D}/I_G [30]. The samples displayed nearly the same FWHM and I_{2D}/I_G values i.e. ~59 cm^{-1} and ~1.04 respectively. These values are indicative of a few layers of graphene, which has been confirmed through the TEM analysis discussed in the later section.

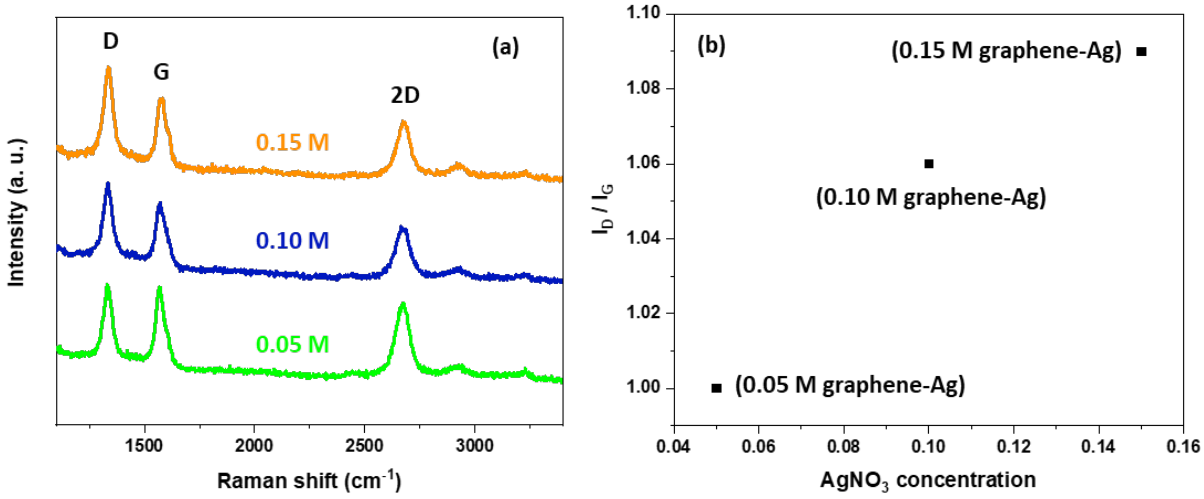

Fig 4.2: (a) Raman spectra of graphene-Ag nanocomposites (b) I_D/I_G of graphene-Ag nanocomposites synthesized at different concentrations of $AgNO_3$

The structure and morphology of graphene-Ag nanocomposites were investigated using SEM. The SEM images are given in Fig. 4.3 and Fig. S1 at lower magnification. The images of the samples on Si-substrates showed isolated nanoislands that were amalgamated in a disordered manner. The graphene displayed wrinkled sheet-like morphology similar to that of in the previous reports [31, 32]. SEM pictures also show the Ag NPs in close proximity to the graphene nanosheets. The Ag NPs were randomly distributed on the surface of the graphene nanosheets. It appeared that the overall quantity and size of the Ag NPs were affected by the concentration of $AgNO_3$ in the feeding solution. At 0.05 M concentration of $AgNO_3$, the produced amount of Ag NPs was minimal. The 0.10 M concentration of Ag NO_3 showed

increased content of the Ag NPs with the varying sizes of the particles. Also, the accumulation of Ag NPs can be observed in the 0.10 M $AgNO_3$ SEM image. However, increased aggregation and the average size of the Ag NPs was observed in case of the 0.15 M graphene-Ag sample. Similar observations have been reported by Yuan et al. [9]. They found that the size and shape of Ag NPs were affected by the varied concentration of $AgNO_3$ precursor.

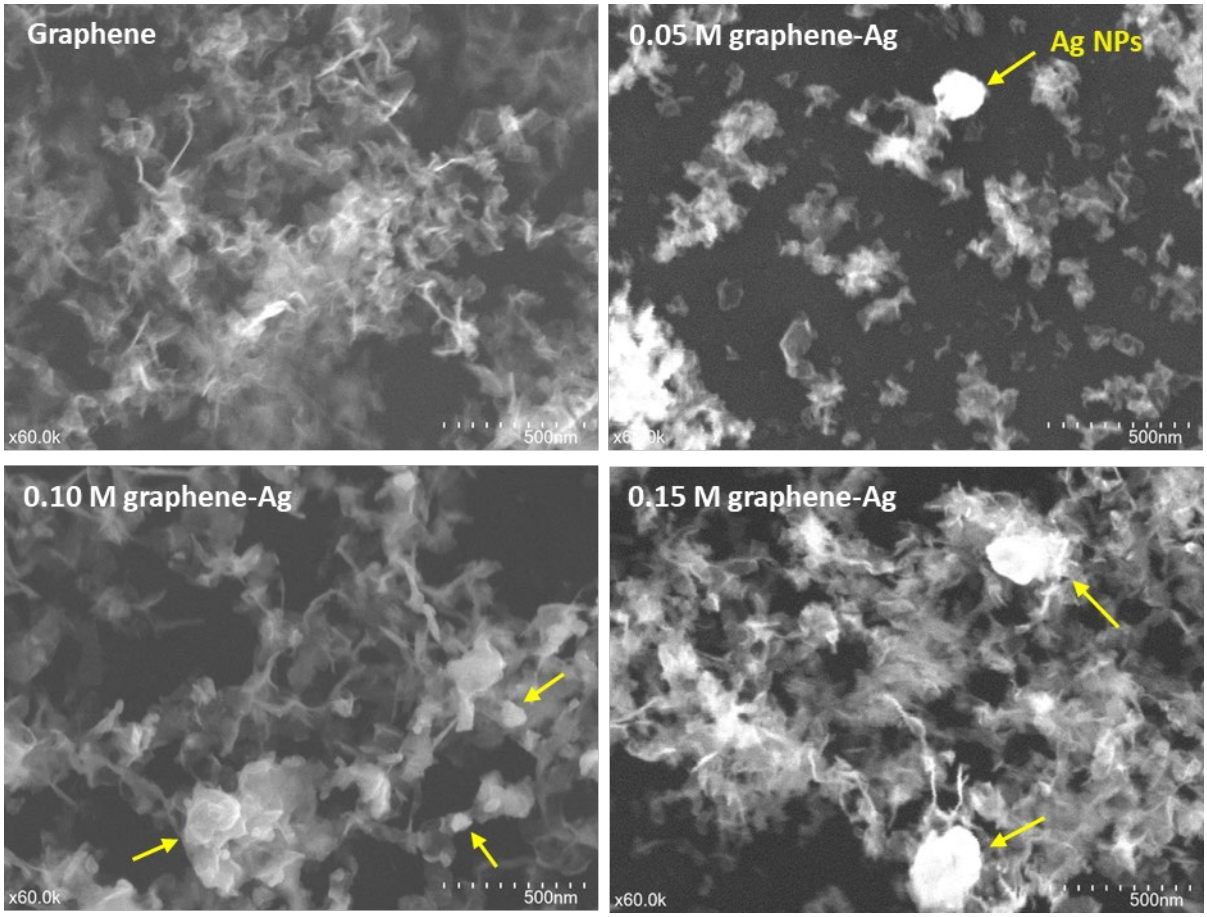

Fig 4.3: SEM images of graphene and graphene-Ag nanocomposites synthesized from different concentrations of $AgNO_3$

The 0.10 M graphene-Ag nanocomposite samples were characterized by XRD. The XRD analysis was performed to investigate the crystalline nature of the material. The XRD pattern given in Fig. 4.4 exhibited four peaks. The characteristic peak of graphene (magnified in the inset image) can be observed at a 2θ value of 25.8° corresponding to the (002) plane [33]. The

interlayer spacing of 0.34 nm, calculated through Bragg's law, roughly matches the value of the same in TEM results. The distinctive peaks at 38.14°, 44.36°, and 64.5° corresponding to (111), (200), and (220) planes respectively, are ascribed to the crystalline planes of Ag NPs [3].

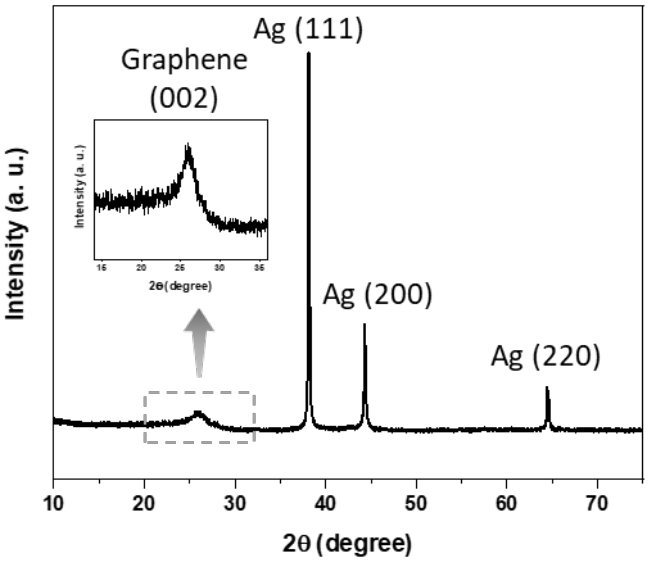

Fig 4.4: XRD pattern of 0.10 M graphene-Ag nanocomposite

The 0.10 M graphene-Ag nanocomposite sample was subjected to XPS analysis in order to reveal the elemental composition and functional group species. The survey scan XPS of pristine graphene presented in Fig. S2 showed the presence of carbon (C) and oxygen (O); whereas the XPS of 0.10 M graphene-Ag nanocomposite in Fig. 4.5a revealed silver (Ag) beside the C and O, centred at 284.2, 531.5, and 370 eV respectively. The compositions of the C, O, and Ag elements were found as ~86, ~8, and 6 % respectively. High-resolution spectra of C1s, O1s, and Ag were also analysed to investigate the bonding structure.

C1s high-resolution spectrum was deconvoluted into its respective peaks. It is given in Fig 4.5c. The deconvolution discovered four component peaks. The main C=C peak related to sp^2-C which appeared at 248.4 eV, is a signature of graphene material. In addition, the structure

contained C-C (sp^3-C), C=O, and C-OH located at 285.1, 286.3, and 289.1 eV respectively. The presence of sp^2-C is indicative of the honeycomb lattice structure of graphene. Whereas, the sp^3-C peak was attributed to the edges of the graphene or the substitutional defects in the structure [34]. The O1s, given in Fig. 4.5d demonstrated contributions from C=O and C-OH peaks at 531 and 532 eV respectively.

A magnified image of the XPS of the Ag 3d in Fig. 4.5b revealed the doublet of the Ag NPs. Ag $3d_{5/2}$ and Ag $3d_{3/2}$ were allocated to the peaks with centres at 367.9 and 374 eV, respectively. When compared to the typical peaks for Ag metal at 368.2 and 374.2 eV, these peaks are located at lower binding energies [35]. Similar findings were made in earlier research, where the negative shifting was attributed to the transport of electrons from metallic Ag to the graphene sheets as well as an interaction between the Ag and the carboxylic groups (C=O) in the graphene structure [8, 36].

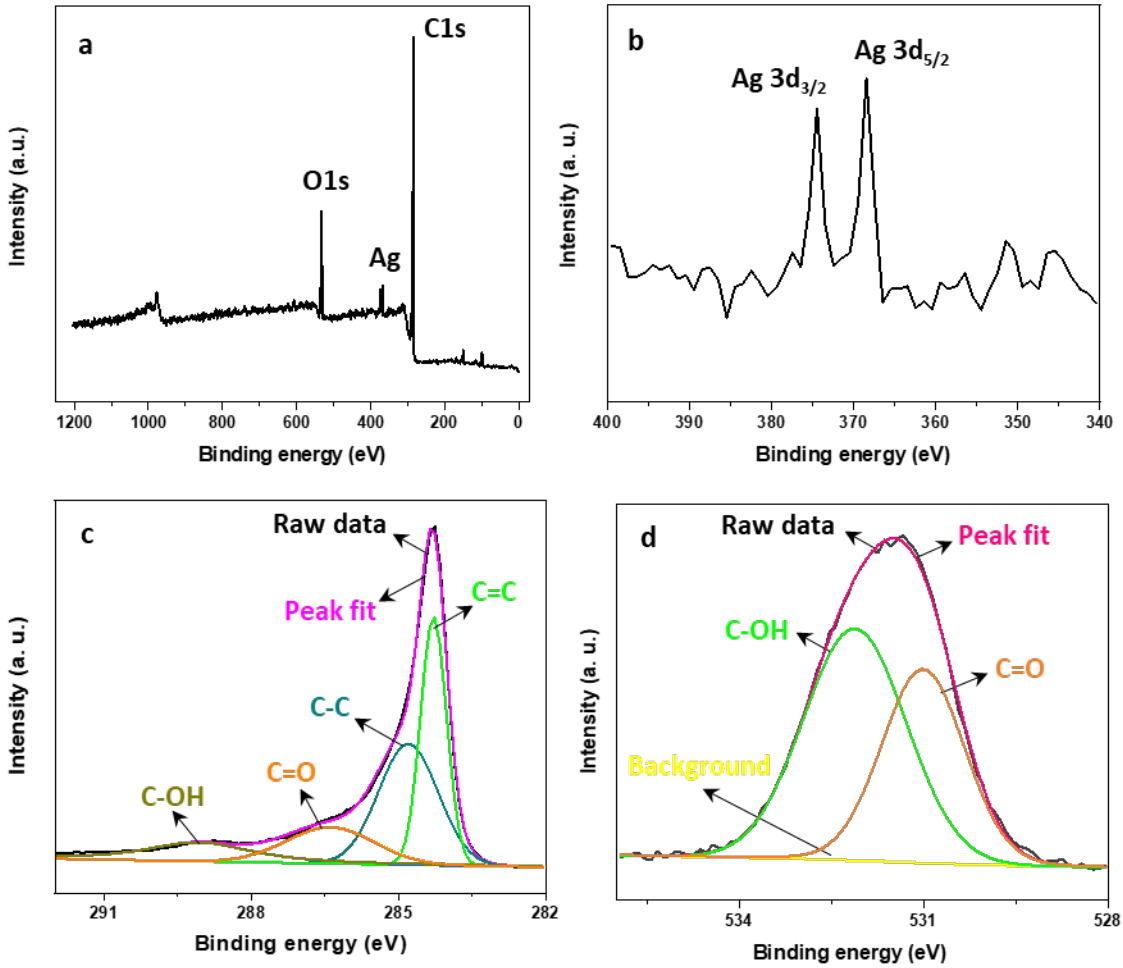

Fig 4.5: XPS of (a) 0.10 M graphene-Ag nanocomposite and (b) Ag 3d, High-resolution spectra of (c) C1s and (d) O1s

Additionally, TEM was used to characterize the 0.10 M graphene-Ag nanocomposite. A low-resolution TEM image shown in Fig. 4.6a displays graphene nanosheets well-loaded with Ag NPs. The graphene is made up of a few to several layers of folded and wrinkled sheets. The interlayer gap of 0.35 nm was observed, and this value almost matches the one determined by employing XRD. An interesting feature of carbon nano-onion shown in Fig. 4.6c, was also observed in the TEM images. The carbon nano-onions are pentagonal or quasi-spherical-shaped concentric graphitic layers. These are regarded as a precursor to graphene [37].

Heterogeneous distribution of Ag NPs on graphene nanosheets has been observed in Fig. 4.6a. The Ag NPs are spherical and have varying sizes ranging between a few nanometres to 60 nm. A high-resolution image in Fig. 4.6b shows that most of the Ag NPs are well embedded with the graphene nanosheets. A magnified inset image in Fig. 4.6b displays the implantation of the Ag nanoparticle into graphene. This finding shows that graphene is a preferred location for Ag NPs to accumulate and form a robust connection. This phenomenon also advocates the shifting of the Ag doublet to lower binding energies (XPS Fig. 4.5b), where it was attributed to the electron transfer from Ag to graphene and/or interaction between the Ag and the carboxylic groups (C=O) in the graphene structure. The large and thick dark nanoparticles are due to the aggregation of smaller Ag NPs. The particle size and aggregation are more in the 0.15 M $AgNO_3$ sample due to the higher concentration of $AgNO_3$ in the solution. It is shown in Fig. S3. The SAED pattern presented in Fig. 4.6d demonstrates the characteristic rings for the (111), (200), and (220) planes of the face-centred cubic Ag structure.

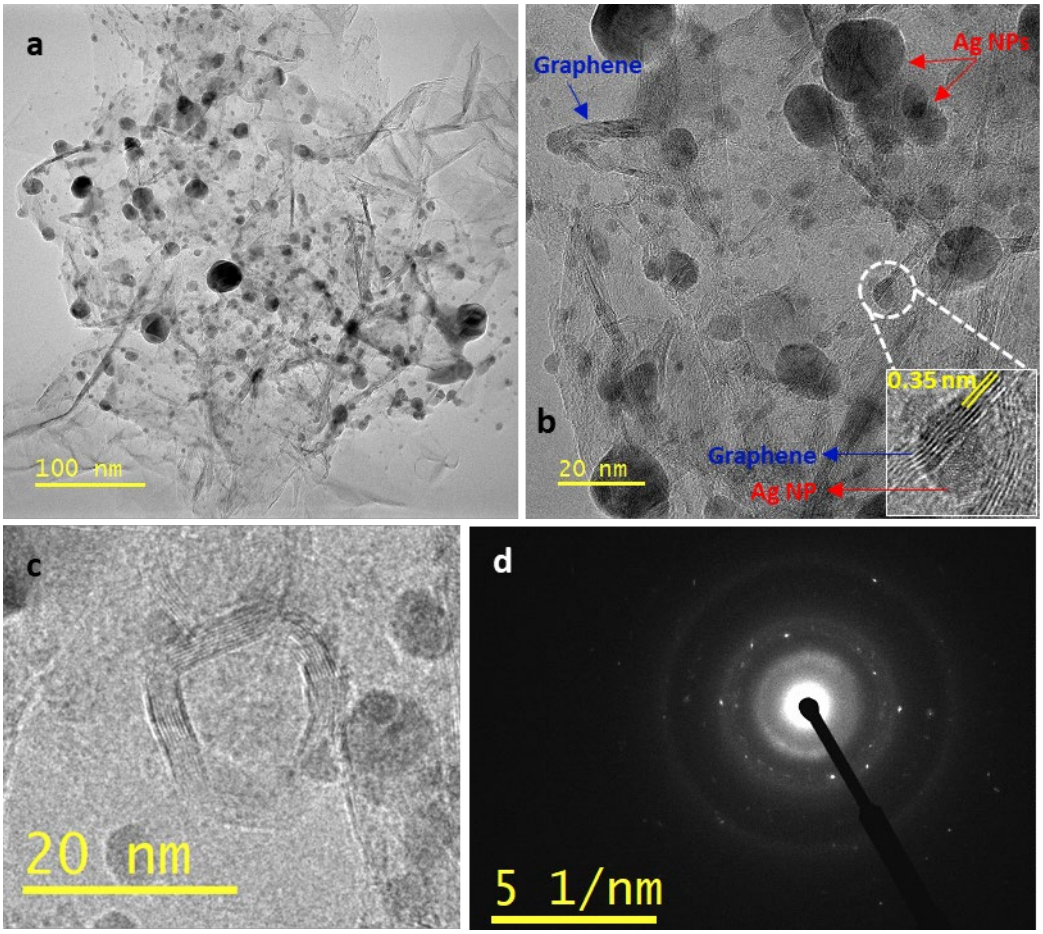

Fig 4.6: TEM images of 0.10 M graphene-Ag nanocomposite at (a) lower and (b) higher magnification (c) TEM image of carbon nano-onion (d) SAED pattern of 0.10 M graphene-Ag nanocomposite

4.3.2 Optical emission spectroscopy measurements

Optical emission spectroscopy (OES) was used to determine the light-emitting species by pointing the optical fibre to the plasma through a viewing window. The images of the plasma and OES spectrums were recorded by using three distinct states of plasma, i.e. pure Ar plasma (Fig. 4.7a), Ar plasma with tea tree oil vapours (Fig. 4.7b), and Ar plasma with 0.1 M $AgNO_3$ vapours (Fig. 4.7c). The images of the plasma displaying unique colours are given in the insets of respective figures. The pure Ar plasma, generated at 250 W microwave power, mainly consisted of colourless strikes with some shades of sea green colour. Atomic Ar and nitrogen

(N) dominated the OES spectra. The atmospheric circumstances of the synthesis were responsible for the presence of N and a little amount of oxygen (O) in the plasma. A low-intensity peak of carbon monoxide (CO) at a lower wavelength was also observed in the spectrum. The primary components of the OES spectra of pure Ar plasma measured by Melero et al. [38] at 300 W microwave power and atmospheric conditions were also Ar and N. However, contrary to our observations, they pointed out that most N exists as molecules bound to O, C, and H. This dissimilarity can be attributed to the different amounts of the elements present in the precursors used for the synthesis.

The tea tree oil vapours in the Ar plasma (operated at 250 W microwave power) showed an orange colour appearing in some parts of the plasma. The orange colour provide evidence of the occurrence of decomposition of oil vapours and graphene formation in the plasma. Despite using tea tree to form graphene, the species created were comparable to those described in the prior research on the OES spectrum where they used ethanol for this purpose [31]. The OES spectrum showed a significant contribution of C in atomic as well as molecular form. The carbon peaks mainly appeared at lower wavelengths ranging between 248 to 720 nm. The dominant species in the spectrum is C_2, which was formerly thought to be a precursor in the creation of graphene. Its existence in the spectrum is viewed as evidence that graphene was formed because of it [39, 40]. In comparison with pure Ar plasma, the decline in peak intensities of Ar and N emissions was observed. It has been previously reported that the drop in the intensity happens due to the consumption of part of the supplied energy in the dissociation of precursor i.e. oil vapours [38].

In the case of Ar plasma with 0.1 M $AgNO_3$ vapours (operated at 300 W), two strong bands of Ag near 300 nm wavelength can be observed. Other bands i.e. N and Ar have drastically descended. It suggests that the environment of the plasma was considerably different from pure

Ar or Ar with oil vapours plasma. The image of the plasma shown in the inset of Fig. 4.7c also showed comparatively different colours and mainly consisted of golden and purple colours. Since the $AgNO_3$ solution was made using distilled water, there are many water molecules in the vapors that were supplied into the tube. These vapours produced the OH peak at ~308 nm in the OES spectrum. The observation of the Ag peaks were in good accord with the previous findings, although they also found additional peaks of atomic Ag at longer wavelengths (850 nm) [41]. However, their method of synthesis seems to be distinct in that they employed Ag electrodes to create Ag NPs rather than vapours to make them.

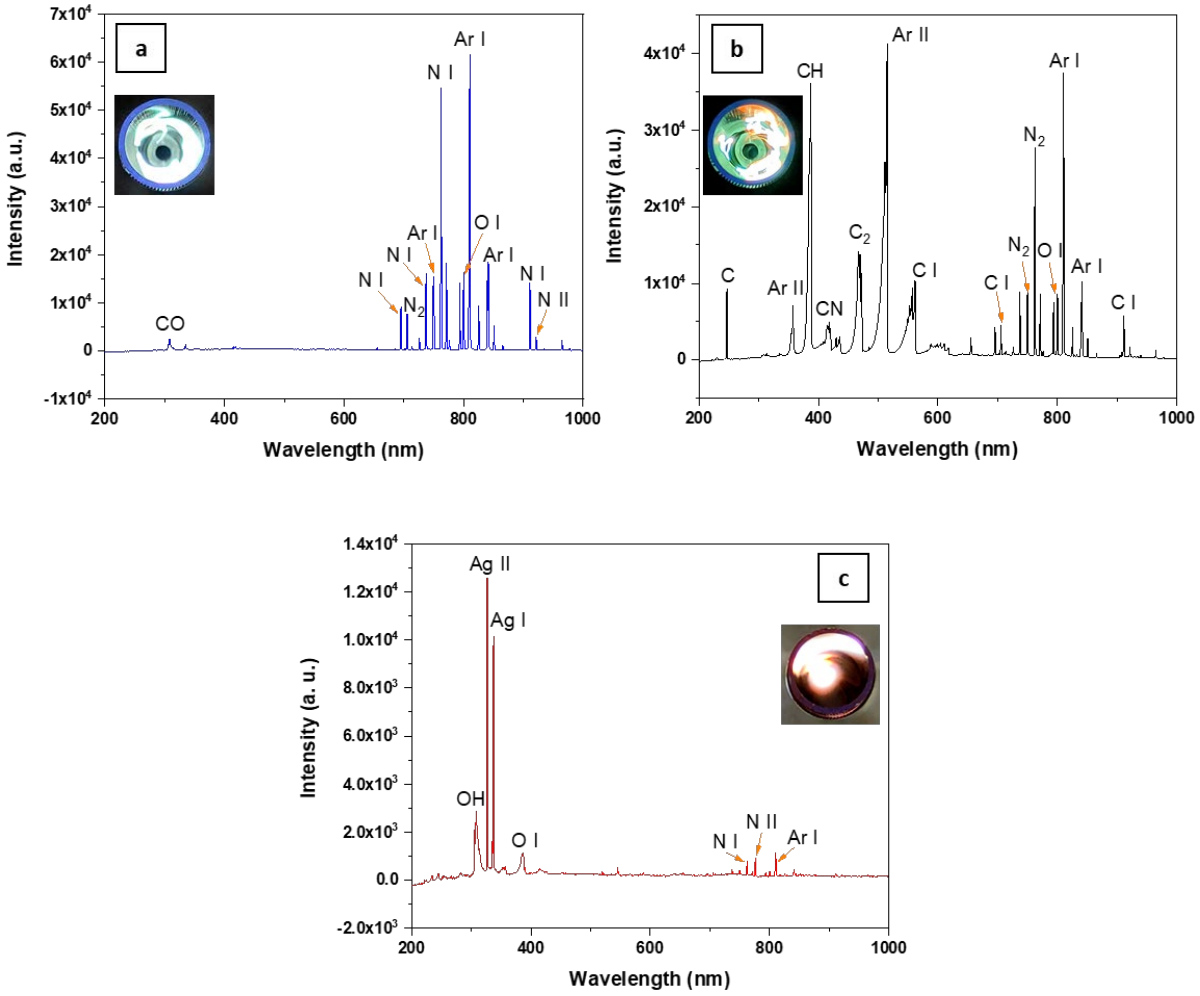

Fig 4.7: OES spectra of (a) pure Ar (b) Ar with tea tree oil vapours and (c) Ar with 0.1 M $AgNO_3$ vapours

4.4 Electrochemical detection of methyl paraben

Cyclic voltammetry (CV) is a very useful electrochemical practice for investigating redox reactions at the interface of solution and electrode. The cyclic voltammetry (CV) technique was used to investigate the electrochemical behaviour of MP at the bare SPE, graphene/SPE, and graphene-Ag nanocomposite/SPE. The bare SPE, scanned in 0.1 M PBS (pH 7.01) containing 10 µM MP, showed an oxidation peak around 0.64 V with a peak current of a small value of 0.1 µA (Fig 4.8). The graphene/SPE showed an enhanced peak current value of ~0.5 µA, which increased to ~1.4 µA in the case of graphene-Ag nanocomposite/SPE. They are shown in Fig. 4.8. Due to the irreversible nature of the process [42, 43], no reduction peaks were observed.

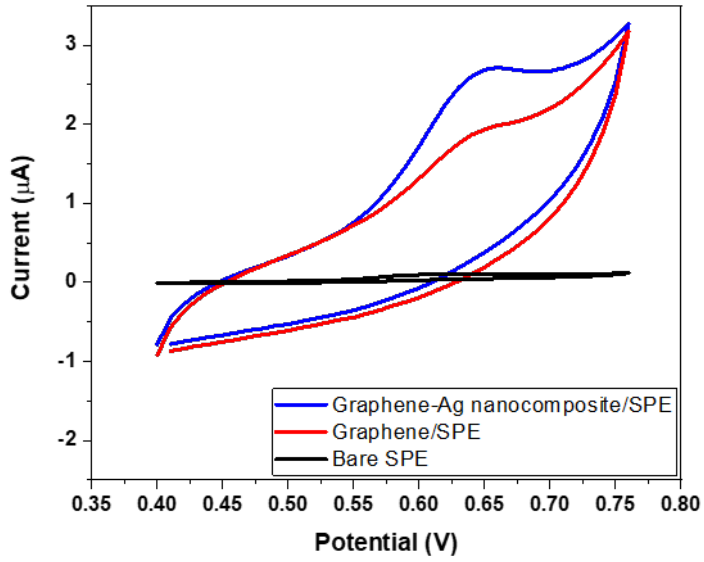

Fig 4.8: Cyclic voltammograms of (a) bare SPE, (b) graphene/SPE, (c) graphene-Ag nanocomposite/SPE in 0.1 M PBS (pH 7.01) containing 10 µM MP

Differential pulse voltammetry (DPV) was used to obtain the linear range of the calibration curve at the graphene-Ag nanocomposite/SPE sensor. The successive addition of MP into the solution showed an increased oxidation peak current. The voltammograms are presented in Fig.

4.9a. The measured peak currents were plotted against the concentration of MP to find the calibration curve. As displayed in Fig 4.9b, the peak currents were linear in the range from 20 to 260 µM, where the linear regression equation is y = 0.03385x + 6.0757 (R^2 = 0.995). The increase in concentration beyond 260 µM showed only a slight rise in peak current, which resulted in the deviation of the curve from linearity. The limit of detection (LOD) of 2.5 µM was determined by identifying the smallest amount the sensor can detect. Table 4.2 shows a comparative overview of our results with the past works. It can be noted that the proposed sensor showed wide linear range and commendable LOD.

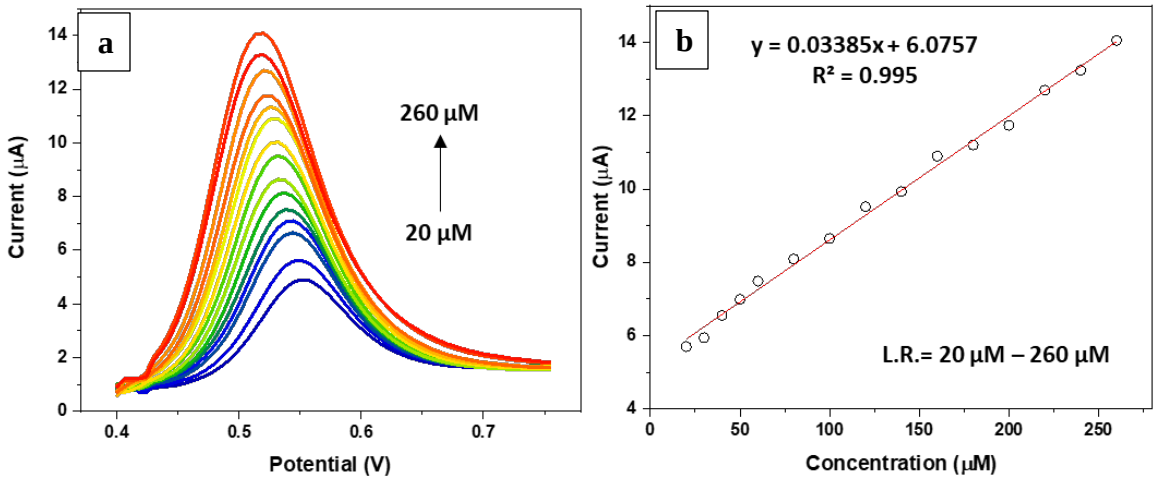

Fig 4.9: (a) Differential pulse voltammogramms of different concentrations of MP (20, 30, 40, 50, 60, 80, 100, 120, 140, 160, 180, 200, 220, 240, 260 µM) in 0.1 M PBS (pH 7.01) and (b) corresponding calibration curve

Table 4.2: Comparison of electrochemical performance of sensor for methyl paraben detection

Electrode	**Method**	**Linear range (µM)**	**Limit of detection (µM)**	**References**
AuNP/RGO/CS/GCE	SWV	0.03 - 1.3	0.0138	[44]
RGO/RuNPs/GCE	DPV	0.5 - 3	0.24	[45]
PoL/RGO/GCE	DPV	1 - 200	0.2	[46]
ZnO/GCE	SWV	20 - 120	7.25	[47]
MWCNTs/LB/GCE	LSV	1 - 80	0.4	[48]
MWCNTs/Hb/CPE	DPV	0.1- 13	0.025	[49]
Au/$(MNP/Ppy)_3$	DPV	0.0 - 131.4	0.09	[50]
graphene-Ag/SPE	DPV	20 - 260	2.5	This work

4.4.1 Repeatability, reproducibility, and stability of the sensor

The repeatability study, which is an important analytical performance, was investigated using one modified graphene-Ag nanocomposite/SPE electrode for five consecutive measurements. The peak current values are shown in Fig. 4.10a. The relative standard deviation (RSD) was calculated as 3.98 %. The recorded DPV curves are given in Fig. S4. The reproducibility of the electrode was investigated by preparing five different graphene-Ag nanocomposite/SPE electrodes. The peak current values against electrode number are presented in Fig. 4.10b. The

obtained DPV curves displayed in Fig. S5 gave an RSD of 5.13 % which was comparable with the value given in the literature [46]. Furthermore, the stability test was conducted by storing graphene-Ag nanocomposite/SPE electrode in a closed container for two weeks, which indicated that the current response retained 95 % of the initial value. The corresponding DPV curves are shown in Fig. S6.

4.4.2 Selectivity study of the sensor

The selectivity of graphene-Ag nanocomposite towards MP with interferents (oxalic acid, sodium nitrate, sodium nitrite, diuron and paraquat) was investigated. These interferents were chosen due to their potential coexistence in real samples. For this purpose, a mixture of MP and its interferents (20 µM each) was prepared in 0.1 M PBS (pH 7.01). The DPV curves of MP and its mixture with interferents are shown in Fig. S7. It was evident that the interferents had no impact on the MP signal. The sensor retained its remarkable MP selectivity even in the replicates.

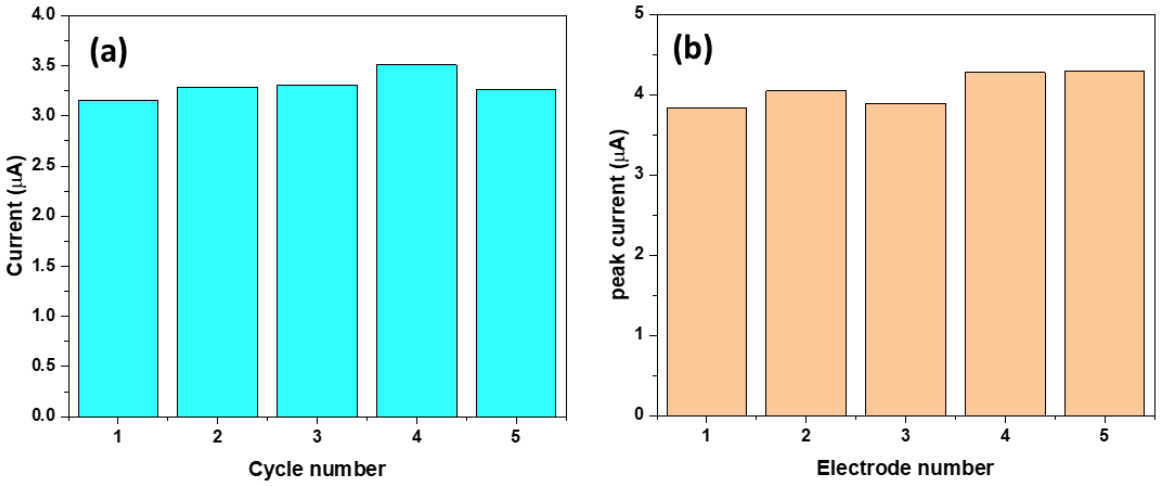

Fig 4.10: (a) Repeatability study of one graphene-Ag nanocomposite/SPE in 0.1 M PBS containing 20 µM MP. (b) Reproducibility study of five graphene-Ag nanocomposite/SPEs in 0.1 M PBS containing 20 µM MP

4.4.3 Real sample analysis

The applicability of graphene-Ag nanocomposite/SPE for the analysis of real samples was demonstrated by investigating the recoveries for the MP determination in river water. As shown in Fig. S8, upon the addition of 20 µM MP in river water, a prominent current response was observed. Whereas, the blank river water displayed no current peak. The corresponding DPV curves are shown in Fig. S6. The recovery value of 93 % makes the proposed sensor suitable for real application. In comparison with 0.1 M PBS (pH 7) containing 20 µM MP, the peak potential in river water slightly shifted from 0.55 V to a lower potential of 0.54 V. It can be attributed to the lower pH noted for river water i.e. 6.92.

4.5 Conclusion

A rapid and environmentally benign approach for synthesizing graphene-Ag nanocomposite was reported in this work. The nanocomposite was synthesized inside the atmospheric pressure microwave plasma by virtue of tea tree extract and $AgNO_3$ vapour dissociation. The formation of the nanocomposite was confirmed by XRD, which showed signature peaks related to the graphene and Ag materials. The OES spectrum recorded during the synthesis of pristine graphene showed atomic and molecular bands of C, particularly C_2 which were deemed as the precursor for graphene synthesis. Whereas, the OES spectrum of pure Ar plasma, and Ar with $AgNO_3$ vapours were mainly dominated by Ar and N, and Ag species respectively. A strong interaction between graphene and Ag NPs was confirmed through XPS spectrum, indicating a slight shift of Ag-doublet (Ag $3d_{5/2}$ and Ag $3d_{3/2}$) towards lower binding energies. The TEM images also revealed good embedment of Ag NPs with the graphene nanosheets. Interestingly, the concentration of $AgNO_3$ played a pivotal role in the determination of the size and aggregation of Ag NPs. Based on the results observed in this work, the $AgNO_3$ concentration of 0.1 M was proposed as an optimum value for well-dispersed and nano-size Ag NPs. They

are imperative for high electrocatalytic activity of graphene. The usage of graphene-Ag nanocomposite in the electrochemical detection of harmful methyl paraben showed a limit of detection of 2.5 µM and a linear range of 20 to 260 µM, which are superior to some of the results reported earlier.

Supplementary

Table S1: Comparison of our technique with the past methods to synthesize graphene-Ag nanocomposite

Nanocomposite material	**Synthesis technique for graphene material**	**Graphene-Ag nanocomposite formation**	**Sub-sets of procedure**	**Use of toxic chemicals**	**Synthesis time**	**Ref.**
Ag NPs-graphene, 2011	Modified Hummers method	Solution-based chemical method	Heating, stirring, centrifugation, drying	Yes	Several hours	[13]
Graphene-Ag 2011	Solution-based chemical method	Solution-based chemical method	Heating, ultra-sonication	Yes	< hr	[16]
Graphene-Ag NPs 2012	Modified Hummers method	Solution-based	Heating, stirring, centrifugation	Yes	> 24 hrs	[9]

		chemical method	, washing, drying			
AgNPs-GO	Modified Hummers method	Solution-based chemical method	Heating, stirring, centrifugation, washing, drying	Yes	> 24 hrs	[6]
Ag/rGO, 2014	Modified Hummers method	Solution-based chemical method & microwave irradiation	Heating, stirring, centrifugation, washing, drying	Yes	> 24 hrs	[8]
Ag/rGO, 2014	Modified Hummers method	Solution-based chemical method & sonication	Heating, stirring, sonication, centrifugation, washing, drying	Yes	Several hours	[10]
Ag/rGO, 2016	Modified Hummers method	Solution-based chemical method	Heating, stirring, sonication, washing, drying	Yes	> 24 hrs	[51]

GO-Ag NPs, 2018	Modified Hummers method	Solution-based chemical method & gamma irradiation	Heating, stirring, centrifugation, washing, drying	Yes	> 24 hrs	[7]
Ag-rGO 2019	Modified Hummers method	Solution-based chemical method	Heating, stirring, washing, drying	Yes	> 24 hrs	[12]
Graphene-Ag nanocomposite	Microwave plasma	Microwave plasma	Nil	No	Few seconds	This work

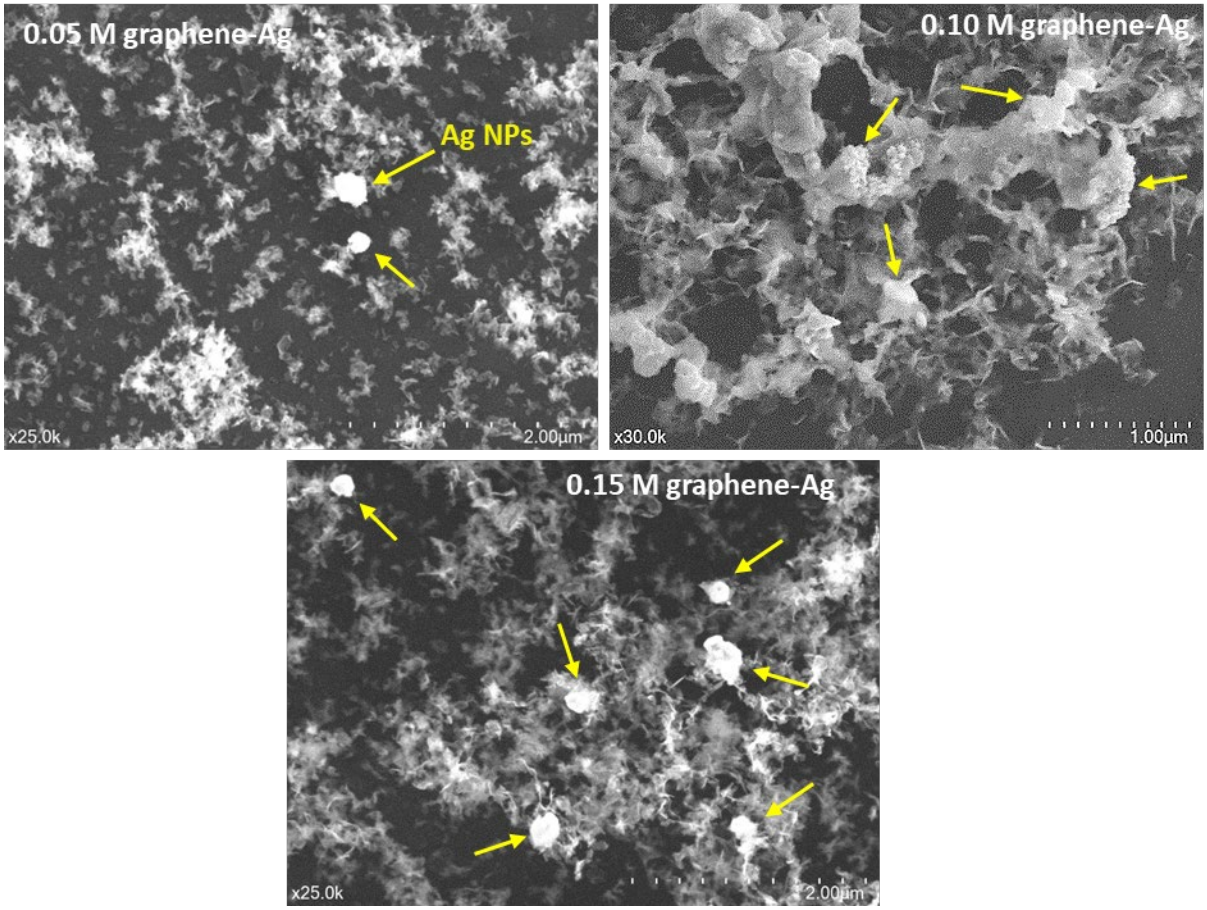

Fig. S1: SEM images of graphene-Ag nanocomposites at lower magnification

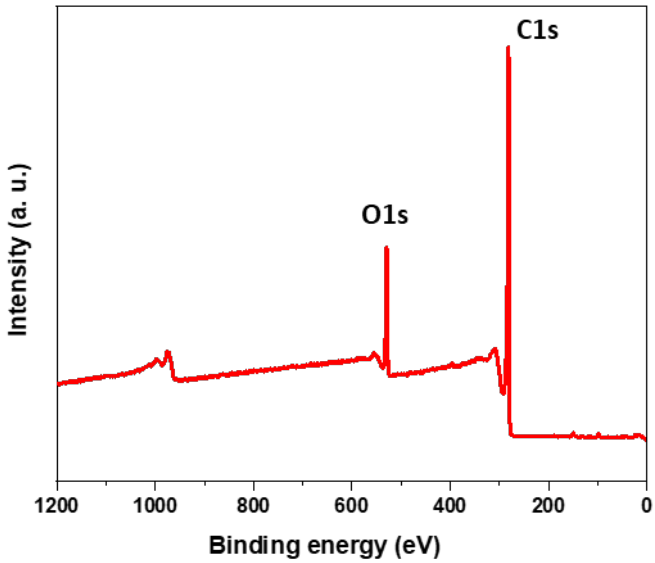

Fig. S2: XPS spectrum of pristine graphene synthesized from tea tree extract

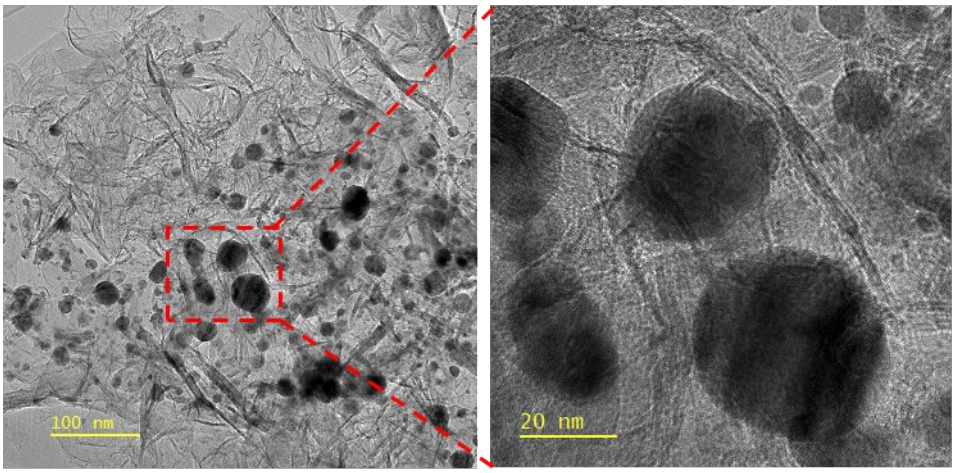

Fig. S3: TEM images of 0.15 graphene-Ag nanocomposite

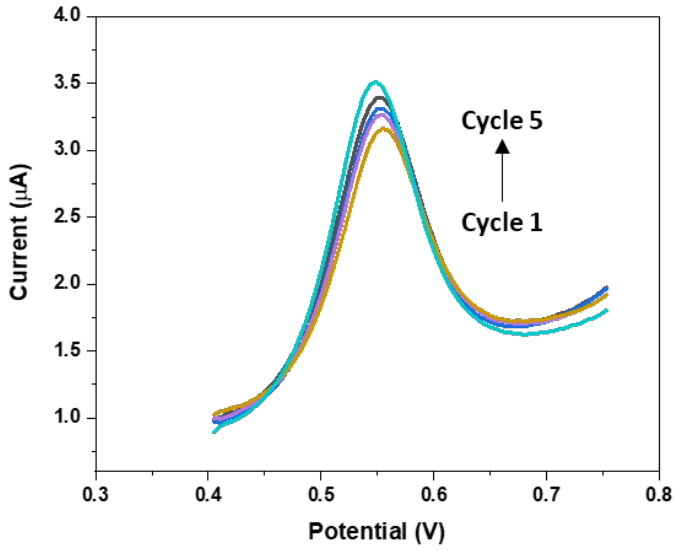

Fig. S4: Repeatability test of graphene-Ag nanocomposite/SPE in 0.1 M PBS containing 20 μM MP

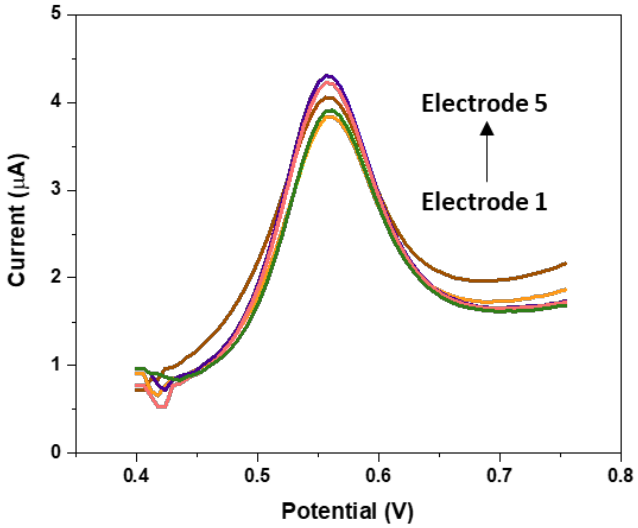

Fig. S5: Reproducibility test of graphene-Ag nanocomposite/SPE in 0.1 M PBS containing 20 µM MP

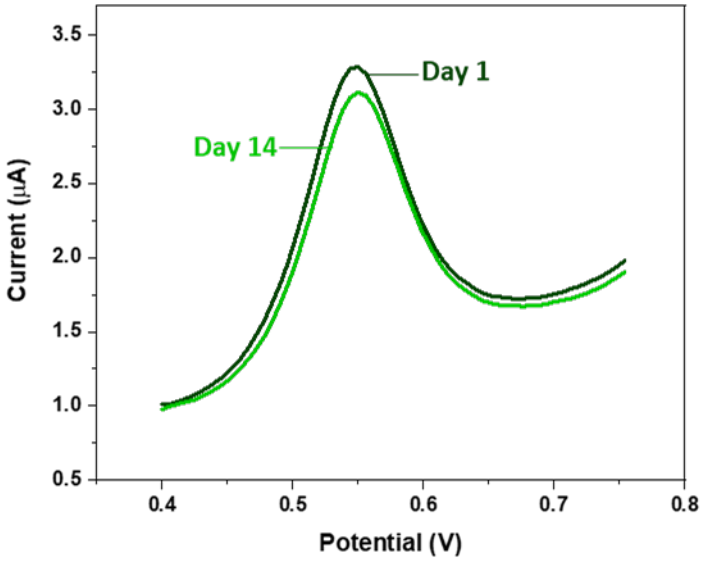

Fig. S6: Stability test of graphene-Ag nanocomposite/SPE in 0.1 M PBS containing 20 µM MP

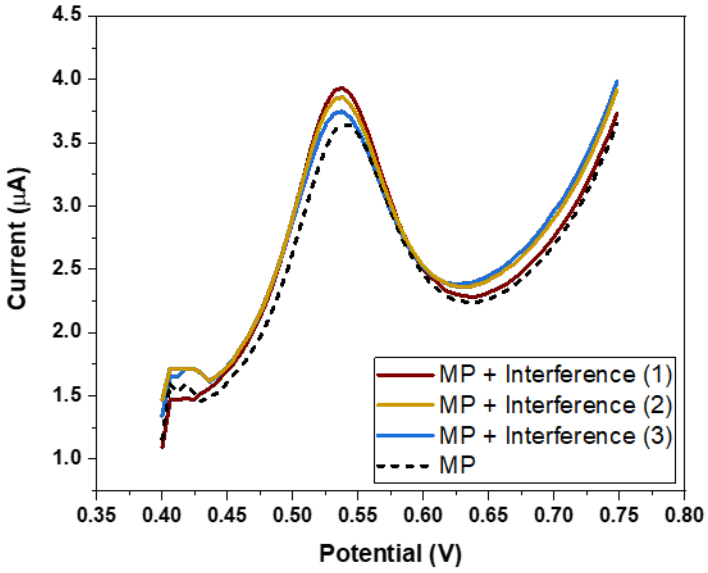

Fig. S7: Curves of MP with its interferents (oxalic acid, sodium nitrate, sodium nitrite, diuron and paraquat) (20 µM each in 0.1 M PBS pH 7.01). Figure represents three replicas

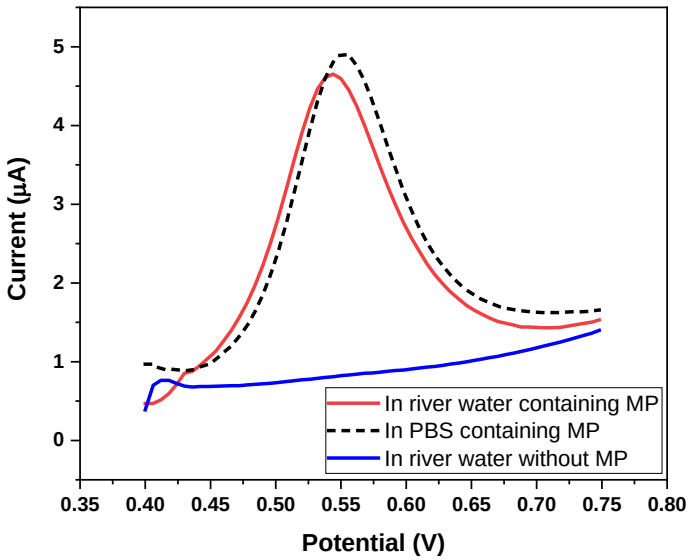

Fig. S8: DPV curves of graphene-Ag nanocomposite/SPE in 0.1 M PBS (pH 7.01) and river water (pH 6.92) containing 20 µM, and in river water without MP

References

1. Saleh, T.A. and G. Fadillah, *Recent trends in the design of chemical sensors based on graphene–metal oxide nanocomposites for the analysis of toxic species and biomolecules.* TrAC Trends in Analytical Chemistry, 2019. **120**: p. 115660.
2. Garg, K., P. Papponen, A. Johansson, N. Puttaraksa, and L. Gilbert, *Preparation of graphene nanocomposites from aqueous silver nitrate using graphene oxide's peroxidase-like and carbocatalytic properties.* Scientific reports, 2020. **10**(1): p. 1-13.
3. Krishnaraj, C., V.K. Kaliannagounder, R. Rajan, T. Ramesh, C.S. Kim, C.H. Park, B. Liu, and S.-I. Yun, *Silver nanoparticles decorated reduced graphene oxide: Eco-friendly synthesis, characterization, biological activities and embryo toxicity studies.* Environmental Research, 2022. **210**: p. 112864.
4. Kurmarayuni, C.M., B. Chandu, L.P. Yangalasetty, S.J. Gali, M. Mujahid Alam, P.N.V.V.L. Pramila Rani, and H.B. Bollikolla, *Sustainable synthesis of silver decorated graphene nanocomposite with potential antioxidant and antibacterial properties.* Materials Letters, 2022. **308**: p. 131116.
5. Ghanbari, R., R. Safaiee, M.H. Sheikhi, M.M. Golshan, and Z.K. Horastani, *Graphene Decorated with Silver Nanoparticles as a Low-Temperature Methane Gas Sensor.* ACS Applied Materials & Interfaces, 2019. **11**(24): p. 21795-21806.
6. Peng, K.-J., C.-L. Wu, Y.-H. Lin, Y.-J. Liu, D.-P. Tsai, Y.-H. Pai, and G.-R. Lin, *Hydrogen-free PECVD growth of few-layer graphene on an ultra-thin nickel film at the threshold dissolution temperature.* Journal of Materials Chemistry C, 2013. **1**(24): p. 3862-3870.
7. Zhao, X., N. Li, M. Jing, Y. Zhang, W. Wang, L. Liu, Z. Xu, L. Liu, F. Li, and N. Wu, *Monodispersed and spherical silver nanoparticles/graphene nanocomposites from*

gamma-ray assisted in-situ synthesis for nitrite electrochemical sensing. Electrochimica Acta, 2019. **295**: p. 434-443.

8. Hsu, K.-C. and D.-H. Chen, *Green synthesis and synergistic catalytic effect ofAg/reduced graphene oxide nanocomposite.* Nanoscale research letters, 2014. **9**(1): p. 1-10.
9. Yuan, W., Y. Gu, and L. Li, *Green synthesis of graphene/Ag nanocomposites.* Applied Surface Science, 2012. **261**: p. 753-758.
10. Aziz, A., H. Lim, S. Girei, M. Yaacob, M. Mahdi, N. Huang, and A. Pandikumar, *Silver/graphene nanocomposite-modified optical fiber sensor platform for ethanol detection in water medium.* Sensors and Actuators B: Chemical, 2015. **206**: p. 119-125.
11. Chen, J., B. Yao, C. Li, and G. Shi, *An improved Hummers method for eco-friendly synthesis of graphene oxide.* Carbon, 2013. **64**: p. 225-229.
12. Guo, Y., X. Yang, K. Ruan, J. Kong, M. Dong, J. Zhang, J. Gu, and Z. Guo, *Reduced graphene oxide heterostructured silver nanoparticles significantly enhanced thermal conductivities in hot-pressed electrospun polyimide nanocomposites.* ACS applied materials & interfaces, 2019. **11**(28): p. 25465-25473.
13. Xu, Z., H. Gao, and H. Guoxin, *Solution-based synthesis and characterization of a silver nanoparticle–graphene hybrid film.* Carbon, 2011. **49**(14): p. 4731-4738.
14. Ahmad, M.A., S. Aslam, F. Mustafa, and U. Arshad, *Synergistic antibacterial activity of surfactant free Ag–GO nanocomposites.* Scientific Reports, 2021. **11**(1): p. 196.
15. Zhang, Z., F. Xu, W. Yang, M. Guo, X. Wang, B. Zhang, and J. Tang, *A facile one-pot method to high-quality Ag-graphene composite nanosheets for efficient surface-enhanced Raman scattering.* Chemical Communications, 2011. **47**(22): p. 6440-6442.
16. Tang, X.-Z., Z. Cao, H.-B. Zhang, J. Liu, and Z.-Z. Yu, *Growth of silver nanocrystals on graphene by simultaneous reduction of graphene oxide and silver ions with a rapid*

and efficient one-step approach. Chemical communications, 2011. **47**(11): p. 3084-3086.

17. Çiplak, Z., N. Yildiz, and A. Çalimli, *Investigation of graphene/Ag nanocomposites synthesis parameters for two different synthesis methods.* Fullerenes, Nanotubes and Carbon Nanostructures, 2015. **23**(4): p. 361-370.
18. Wei, Y., X. Zuo, X. Li, S. Song, L. Chen, J. Shen, Y. Meng, Y. Zhao, and S. Fang, *Dry plasma synthesis of graphene oxide–Ag nanocomposites: A simple and green approach.* Materials Research Bulletin, 2014. **53**: p. 145-150.
19. Heo, U.S., D.-W. Kim, K.-S. Kim, and D.-W. Park, *A facile synthesis of anatase TiO2-Graphene nanocomposites using plasma and heat treatment.* Applied Surface Science, 2019. **474**: p. 118-126.
20. Jo, E.H., H. Chang, S.K. Kim, J.-H. Choi, S.-R. Park, C.M. Lee, and H.D. Jang, *One-step synthesis of Pt/graphene composites from Pt acid dissolved ethanol via microwave plasma spray pyrolysis.* Scientific reports, 2016. **6**(1): p. 1-8.
21. Jimenez, M., R. Rincon, A. Marinas, and M. Calzada, *Hydrogen production from ethanol decomposition by a microwave plasma: influence of the plasma gas flow.* International journal of hydrogen energy, 2013. **38**(21): p. 8708-8719.
22. Xiao, P., G. Zhu, X. Shang, B. Hu, B. Zhang, Z. Tang, J. Yang, and J. Liu, *An Fe-MOF/MXene-based ultra-sensitive electrochemical sensor for arsenic (III) measurement.* Journal of Electroanalytical Chemistry, 2022. **916**: p. 116382.
23. Zafar, M.A. and M.V. Jacob, *Synthesis of free-standing graphene in atmospheric pressure microwave plasma for the oil-water separation application.* Applied Surface Science Advances, 2022. **11**: p. 100312.

24. Liu, J., Y. Zhang, L. Zhang, F. Xie, A. Vasileff, and S.Z. Qiao, *Graphitic carbon nitride (g-C3N4)-derived N-rich graphene with tuneable interlayer distance as a high-rate anode for sodium-ion batteries.* Advanced Materials, 2019. **31**(24): p. 1901261.

25. Zafar, M.A., O.K. Varghese, F.C. Robles Hernandez, Y. Liu, and M.V. Jacob, *Single-Step Synthesis of Nitrogen-Doped Graphene Oxide from Aniline at Ambient Conditions.* ACS Applied Materials & Interfaces, 2022.

26. Zafar, M.A., Y. Liu, S. Allende, and M.V. Jacob, *Electrochemical sensing of oxalic acid using silver nanoparticles loaded nitrogen-doped graphene oxide.* Carbon Trends, 2022. **8**: p. 100188.

27. Pingale, A.D., A. Owhal, A.S. Katarkar, S.U. Belgamwar, and J.S. Rathore, *Facile synthesis of graphene by ultrasonic-assisted electrochemical exfoliation of graphite.* Materials Today: Proceedings, 2021. **44**: p. 467-472.

28. Kong, X., Y. Zhu, H. Lei, C. Wang, Y. Zhao, E. Huo, X. Lin, Q. Zhang, M. Qian, W. Mateo, R. Zou, Z. Fang, and R. Ruan, *Synthesis of graphene-like carbon from biomass pyrolysis and its applications.* Chemical Engineering Journal, 2020. **399**: p. 125808.

29. Eckmann, A., A. Felten, A. Mishchenko, L. Britnell, R. Krupke, K.S. Novoselov, and C. Casiraghi, *Probing the nature of defects in graphene by Raman spectroscopy.* Nano letters, 2012. **12**(8): p. 3925-3930.

30. do Nascimento Barbosa, A., E. Romani, C. Mendoza, M.M. da Costa, and F. Freire Jr, *Direct synthesis and characterization of graphene layers on silica glass substrates.* Materials Today: Proceedings, 2019. **10**: p. 400-407.

31. Toman, J., O. Jašek, M. Šnírer, D. Pavliňák, Z. Navrátil, J. Jurmanová, S. Chudják, F. Krčma, V. Kudrle, and J. Michalička, *On the transition of reaction pathway during microwave plasma gas-phase synthesis of graphene nanosheets: From amorphous to highly crystalline structure.* Plasma Processes and Polymers, 2021: p. e2100008.

32. Bundaleska, N., A. Dias, N. Bundaleski, E. Felizardo, J. Henriques, D. Tsyganov, M. Abrashev, E. Valcheva, J. Kissovski, and A. Ferraria, *Prospects for microwave plasma synthesized N-graphene in secondary electron emission mitigation applications.* Scientific reports, 2020. **10**(1): p. 1-13.

33. Baby, T.T. and S. Ramaprabhu, *Synthesis and nanofluid application of silver nanoparticles decorated graphene.* Journal of Materials Chemistry, 2011. **21**(26): p. 9702-9709.

34. Al-Gaashani, R., A. Najjar, Y. Zakaria, S. Mansour, and M. Atieh, *XPS and structural studies of high quality graphene oxide and reduced graphene oxide prepared by different chemical oxidation methods.* Ceramics International, 2019. **45**(11): p. 14439-14448.

35. Nair, R., H. Wu, P. Jayaram, I. Grigorieva, and A. Geim, *Unimpeded permeation of water through helium-leak–tight graphene-based membranes.* Science, 2012. **335**(6067): p. 442-444.

36. Hu, H., X. Wang, J. Wang, L. Wan, F. Liu, H. Zheng, R. Chen, and C. Xu, *Preparation and properties of graphene nanosheets–polystyrene nanocomposites via in situ emulsion polymerization.* Chemical Physics Letters, 2010. **484**(4): p. 247-253.

37. Alancherry, S., K. Bazaka, I. Levchenko, A. Al-Jumaili, B. Kandel, A. Alex, F.C. Robles Hernandez, O.K. Varghese, and M.V. Jacob, *Fabrication of Nano-Onion-Structured Graphene Films from Citrus sinensis Extract and Their Wetting and Sensing Characteristics.* ACS Applied Materials & Interfaces, 2020.

38. Melero, C., R. Rincón, J. Muñoz, G. Zhang, S. Sun, A. Perez, O. Royuela, C. González-Gago, and M. Calzada, *Scalable graphene production from ethanol decomposition by microwave argon plasma torch.* Plasma Physics and Controlled Fusion, 2017. **60**(1): p. 014009.

39. Dato, A. and M. Frenklach, *Substrate-free microwave synthesis of graphene: experimental conditions and hydrocarbon precursors.* New Journal of Physics, 2010. **12**(12): p. 125013.

40. Zafar, M.A. and M.V. Jacob, *Plasma-based synthesis of graphene and applications: a focused review.* Reviews of Modern Plasma Physics, 2022. **6**(1): p. 1-38.

41. Ocampo, I.N.D., G.M. Malapit, and R.Q. Baculi, *Ar/O2 atmospheric pressure plasma jet treatment of pure cotton fabric for antibacterial application.* Plasma and Fusion Research, 2018. **13**: p. 3406116-3406116.

42. Michalkiewicz, S., *Anodic oxidation of parabens in acetic acid–acetonitrile solutions.* Journal of Applied Electrochemistry, 2013. **43**(1): p. 85-97.

43. Hasanzadeh, M., N. Shadjou, L. Saghatforoush, R. Mehdizadeh, and S. Sanati, *Electrocatalytic oxidation of selected parabens on zinc hydroxide nanoparticles.* Catalysis Communications, 2012. **19**: p. 10-16.

44. Piovesan, J.V., E.R. Santana, and A. Spinelli, *Reduced graphene oxide/gold nanoparticles nanocomposite-modified glassy carbon electrode for determination of endocrine disruptor methylparaben.* Journal of Electroanalytical Chemistry, 2018. **813**: p. 163-170.

45. Mendonça, C.D., T.M. Prado, F.H. Cincotto, R.T. Verbinnen, and S.A. Machado, *Methylparaben quantification via electrochemical sensor based on reduced graphene oxide decorated with ruthenium nanoparticles.* Sensors and Actuators B: Chemical, 2017. **251**: p. 739-745.

46. Toan, T.T.T., *Detection of methylparaben in cosmetics by poly L–Lysine/reduced graphene oxide-based sensor.* ECS Sensors Plus, 2022. **1**(3): p. 031603.

47. Javaid, S., J. Lee, M.V. Sofianos, Z. Douglas-Moore, D.W. Arrigan, and D.S. Silvester, *Zinc oxide nanoparticles as antifouling materials for the electrochemical detection of methylparaben.* ChemElectroChem, 2021. **8**(1): p. 187-194.

48. Wang, L., Y. Li, G. Li, and B. Ye, *A new strategy for enhancing electrochemical sensing from MWCNTs modified electrode with Langmuir-Blodgett film and used in determination of methylparaben.* Sensors and Actuators B: Chemical, 2015. **211**: p. 332-338.

49. Hajian, A., J. Ghodsi, A. Afraz, O. Yurchenko, and G. Urban, *Nanomolar detection of methylparaben by a cost-effective hemoglobin-based biosensor.* Materials Science and Engineering: C, 2016. **69**: p. 122-127.

50. de Lima, L.F., C.M. Daikuzono, C.M. Miyazaki, E.A. Pereira, and M. Ferreira, *Layer-by-Layer nanostructured films of magnetite nanoparticles and polypyrrole towards synergistic effect on methylparaben electrochemical detection.* Applied Surface Science, 2020. **505**: p. 144278.

51. Shaikh, A., S. Parida, and S. Böhm, *One step eco-friendly synthesis of Ag–reduced graphene oxide nanocomposite by phytoreduction for sensitive nitrite determination.* RSC advances, 2016. **6**(102): p. 100383-100391.

Chapter 5: Synthesis of graphene from tangerine peel oil for chemiresistive sensor

The feasibility of the synthesis of graphene from natural precursor i.e. tangerine peel oil using the atmospheric pressure microwave plasma is presented in this chapter. The chapter investigates the effects of microwave power on the properties of graphene. The confirmation of the synthesis of graphene is demonstrated through state-of-the-art characterization techniques. The application of as-synthesized graphene is shown for toxic vapours sensing application.

This Chapter is submitted to the journal “RSC Sustainability” and currently under review.

M. Adeel Zafar, Yang Liu, Francisco C. Robles Hernandez, Oomman K. Varghese, Mohan V Jacob, “Rapid and sustainable synthesis of graphene for its application in the chemiresistive sensor”, RSC Sustainability.

Rapid and sustainable synthesis of graphene for its application in the chemiresistive sensor

Abstract

The commonly used plasma-enhanced chemical vapour deposition technique for graphene synthesis entails long processing time, high vacuuming and heating. Atmospheric pressure microwave plasma can synthesize freestanding graphene in a few seconds at ambient conditions. Recently, considerable research has been devoted to benefitting from this state-of-the-art method to synthesize graphene. However, the work was limited to the usage of toxic or non-renewable resources. The current work aimed to replace those precursors with one, which is environmentally benign and sustainable. We synthesized graphene from an expired tangerine peel oil, which is an abundant worldwide natural source. The Raman spectrum showed characteristic graphene-related 2D peak at microwave powers varied between 200 and 1000 W. Transmission electron microscopy revealed interstitial spacing of 0.34, which matched with the value of X-ray diffraction calculated through Bragg's law. However, marginal variations in lattice spacing owing to the presence of oxygen functional groups were also observed. Furthermore, a chemiresistive sensor, developed from the as-synthesized graphene, exhibited a promising response for the detection of vapours of ethanol, insecticide, and herbicide in the open environment.

Keywords

Atmospheric pressure microwave plasma, graphene, free-standing, chemiresistive sensor, sustainable precursor, insecticide and herbicide vapours detection

5.1 Introduction

The first successful exfoliation of monolayer graphene and the revelation of its extraordinary mechanical, electronic, thermal, and optical properties stirred extensive research activities for the synthesis as well as potential applications of graphene [1]. Certainly, the expansion and advancement of techniques to synthesize this futuristic material are crucial for the manifestation of graphene-based commercial applications. However, the technique must be sustainable, facile, and economically viable. Top-down methods such as mechanical or chemical exfoliation from graphite are either laborious or involve toxic chemicals. Bottom-up strategies such as epitaxial growth [2], chemical vapour deposition (CVD) [3], and plasma-enhanced chemical vapour deposition (PECVD) [4] are suitable for the synthesis of mono to few layers of graphene in a chemical-free environment. However, these techniques have the drawback of elaborate synthesis requirements such as the need for high vacuuming, pre-heating, and substrates [5, 6].

Recently, atmospheric pressure microwave plasma (APMP) has gained popularity due to its potential to produce graphene without the prerequisites of vacuuming, pre-heating, or substrate [7, 8]. Dato et al. [9] were the first to use the APMP to showcase the feasibility of mono and bi-layers graphene synthesis from ethanol vapours, followed by the work of Tatarova et al. [10] which entails the understanding of ethanol decomposition and resultant species inside the reactor. Bundaleska et al. [11] synthesized multilayers graphene by cracking methane at a microwave power of 1 kW. They observed that the flow rate of methane and background gas i.e. argon plays a critical role in graphene formation. In another study, Singh et al. [12] showed the effect of hydrogen supply on the graphitic nature of the graphene when added to the feedstock. A small quantity of hydrogen in the feedstock led to the formation of amorphous

carbon. Furthermore, APMP is now being employed to synthesize doped-graphene materials [8, 13].

Thus far, the focus of APMP in synthesizing graphene has remained on utilizing non-renewable resources. Unless the parent materials are sustainable and environmentally benign, the process cannot be considered renewable. Likewise, ethanol, methane, or aniline are derived from unsustainable bases and are mostly toxic or explosive. Also, the precise control of ethanol flow rate is another concern regarding APMP since its marginally higher flow rate may cause the extinction of plasma flame [14]. The usage of sustainable precursors, however, has been reported in CVD and PECVD techniques. Biomasses, botanical hydrocarbons, and food materials such as sugar [15], cookies [16], tea tree oil [17], camphor oil [18], Citrus sinensis oil [19], and geranium oil [20] are a few examples of such sustainable precursors.

The citrus reticulata, commonly known as tangerine is a naturally occurring plant material [21]. It is an economical and abundant resource, cultivated in China, Europe, the United States, and many other countries [22]. The peel of tangerine is a waste product and is not commonly used in daily life. Moreover, the extract of tangerine peel is rich in hydrocarbons and can be an excellent alternative precursor for APMP-based graphene synthesis. Although there are several constituents in tangerine peel oil, limonene happens to be its major component accounting for more than 90 % of its total weight [23]. The affordability, wide occurrence, and eco-friendly nature of the fruit product make it an ideal substitute for green feedstock for the synthesis of graphene.

The current study is intended to synthesize graphene in a sustainable, economical, and facile process. Hereby, we demonstrate the feasibility of the green synthesis of graphene from the expired essential oil of tangerine peel using the APMP. To our best knowledge, this is the first

report on the usage of a green precursor for graphene synthesis in APMP. Since the application of APMP synthesized graphene is barely reported, thus a showcase of the usage of as-synthesized graphene is also the aim of this work. We present the application of as-fabricated graphene in chemiresistive sensor for the detection of ethanol, insecticide, and herbicide vapors.

5.2 Experimental

Graphene was synthesized using downstream microwave plasma at atmospheric conditions. The primary components of the system include a 2.45 GHz microwave generator, a matching network, a cooling system, and a reaction chamber. The reaction chamber is made of quartz and carries the dimensions of 45 x 3 cm (length x outer dia.). A schematic illustration of the plasma system is shown in Fig 5.1a. To supply the precursor into the chamber, argon (Ar) gas was passed through the container of tangerine essential oil. As soon as the vapours interacted with the plasma, the colour of the plasma changed and graphene nanosheets started forming on the walls of the quartz tube (shown in Fig 5.1b). Graphene was collected on the silicon substrates to conduct further analyses. An ultra-sonicated solution of graphene in ethanol synthesized at 600 W is shown in Fig S 1. In this work, three microwave powers of 200, 600, and 1000 W were investigated, while keeping the argon gas and precursor flow rates constant at the optimum value of 3 slm. As shown in Fig 5.1c, at different microwave powers, plasma has distinguishable colours bands.

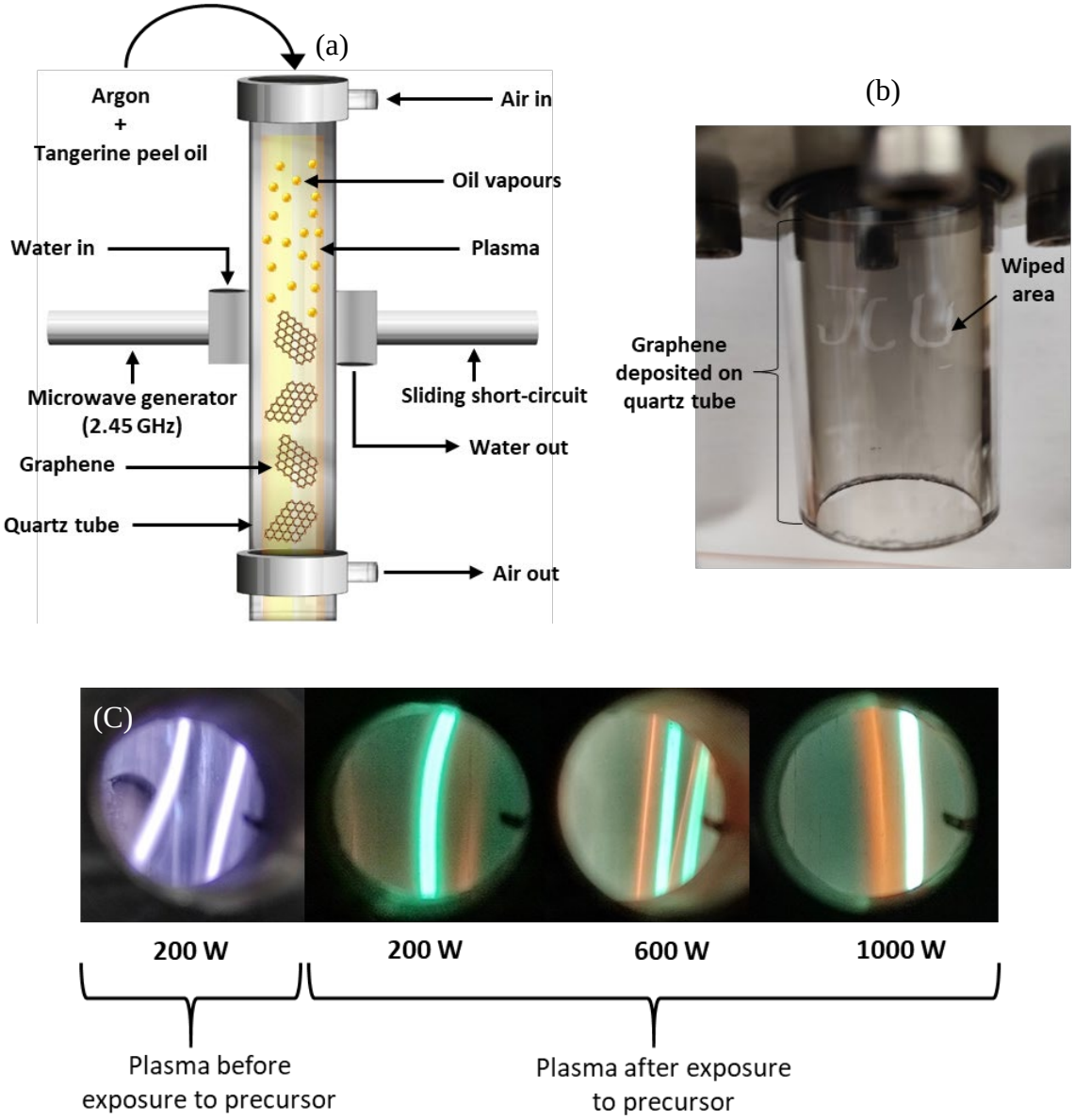

Fig 5.1: (a) Schematic illustration of atmospheric pressure microwave plasma synthesis of graphene (b) quartz tube covered with graphene after the synthesis **(c)** appearances of plasma before and after exposure to tangerine peel oil vapours at different microwave powers

The environmental responses of the graphene film deposited on glass substrate were investigated by exposing them to the insecticide, herbicide, and ethanol vapours diluted 50 % (V/V). A solution of graphene in ethanol (1 mg/mL) was drop cast on a glass substrate and was allowed to dry at room temperature. Electrical contacts were taken from the graphene film using Nichrome wires. The responses of the graphene film were monitored in resistance as a

function of time. Ambient conditions (humidity was 62 % $\pm$ 2) were used to perform all the experiments. The resulting resistance was measured using a digital multimeter (Tektronix DMM4050) at a constant voltage. For exposing the analytes to the graphene film at a constant rate, a nebulizer was utilized.

The techniques employed to study the structure and morphology of graphene as well as carry out its elemental analysis, were confocal laser Raman spectroscopy (Witec, 532 nm laser), scanning electron microscopy (SEM) (Hitachi SU 5000), and x-ray photoelectron spectroscopy (XPS) (Kratos Axis Ultra XPS with an Al Kα x-ray source). X-ray diffraction (XRD) (Bruker, D8-Advance X-ray diffractometer, Cu Kα, λ = 0.15406 nm) was used for obtaining crystallographic information on the synthesized graphene. To acquire transmission electron microscopy (TEM) images, the transmission electron microscope (Hitachi HF5000) was used. Tektronix DMM-4050 digital multimeter was employed for chemiresistive sensing measurements.

5.3 Results and discussions

The Raman spectra of the samples synthesized at different microwave powers are given in Fig. 5.2a. There were three peaks in each spectrum which are characteristic of pristine graphene or graphene-based materials. D peak (arises due to defects), G peak (related to E_{2g} vibrational mode), and 2D peak (the second-order D peak) can be seen around 1330, 1575, and 2670 cm^{-1} respectively [24]. Overall, the peak positions remained unchanged, however, differences in the intensity and peak width were observed.

The intensity of D and 2D bands relative to that of the G band i.e. I_D/I_G and I_{2D}/I_G are given in Fig 5.2b. I_D/I_G is used to indicate the degree of disorder in the graphitic structure [25]. The 200 W sample showed the highest value of I_D/I_G, which could be suggestive of defects in graphene

samples. The presence of oxygen functional groups is also responsible for augmented I_D/I_G values [26]. Based on XPS results, it was discerned that the amount of oxygen in the 200 W sample was higher than that of 600 W and 1000 W samples which accounts for higher D band intensity. Moreover, the amorphous nature of carbon observed in TEM of 200 W could also be a contributing factor in this phenomenon.

The I_{2D}/I_G along with full width half maximum (FWHM) of 2D band are indicative of the number of layers present in the graphitic structure. Generally, FWHM of ~ 30 cm^{-1} and I_{2D}/I_G of 2 were related to mono or bilayer graphene [27, 28]. Interestingly, the highest I_{2D}/I_G in our samples i.e. 0.93 was obtained at 600 W microwave power. Further increase in power led to the reduction of I_{2D}/I_G values. The I_{2D}/I_G values and overall FWHM values of less than 1 signify that our samples consisted of a few layers of graphene. The findings were also confirmed by the TEM images given below.

In comparison with ethanol-derived graphene, where FWHM is ~ 45 cm^{-1} and I_{2D}/I_G values lie within 2 to 2.6 [10], our samples showed smaller values of I_{2D}/I_G and higher values of FWHM. The study also delineated the presence of a few layers of graphene in ethanol-derived graphene which is also in good agreement with their Raman spectrum. Whereas, the number of layers in our samples was slightly greater. On the other hand, methane-derived graphene showed a very high D band, having ~ 56 % higher I_D/I_G value compared to our 600 W sample. Likewise, I_{2D}/I_G values were around 60 % lesser than our 600 W graphene samples [12].

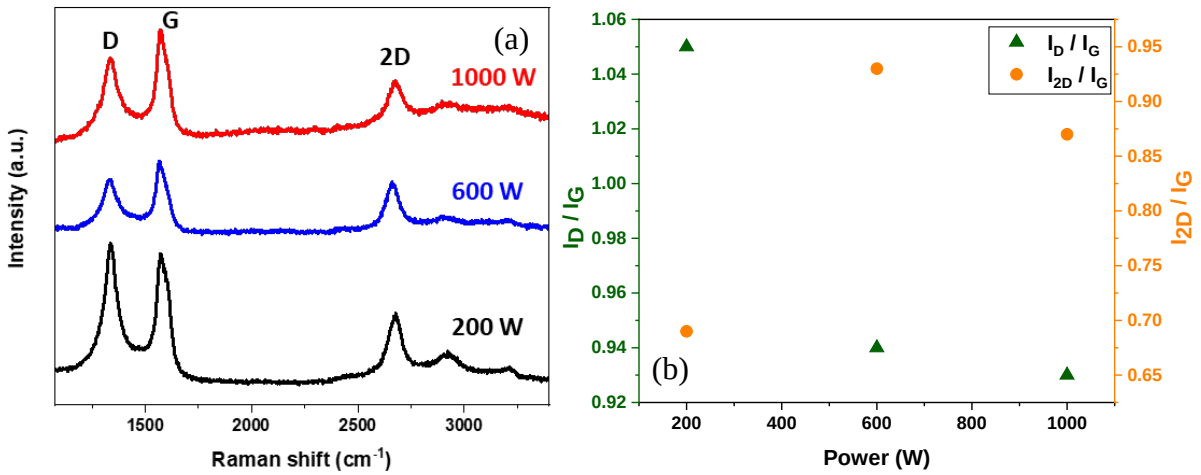

Fig 5.2: (a) Raman spectra and (b) the intensity ratios of D and 2D bands to the G band in the graphene samples, demonstrating the effect of plasma power on a synthesis

XRD pattern happens to be the hallmark of any material. Therefore, the synthesized graphene samples were also subjected to XRD characterization; the corresponding patterns are presented in Fig. 5.3. All the samples gave a consistent and prominent peak at the diffraction angle (2θ) of 26°. The location of the peak is linked with the (002) basal plane. The interlayer spacing of 0.34 nm was calculated using Bragg's law (given in supplementary) which also coincides with the TEM result. Largely, the data seems to be following the earlier findings [29, 30], which involved graphene fabrication via wet chemical method or pyrolysis.

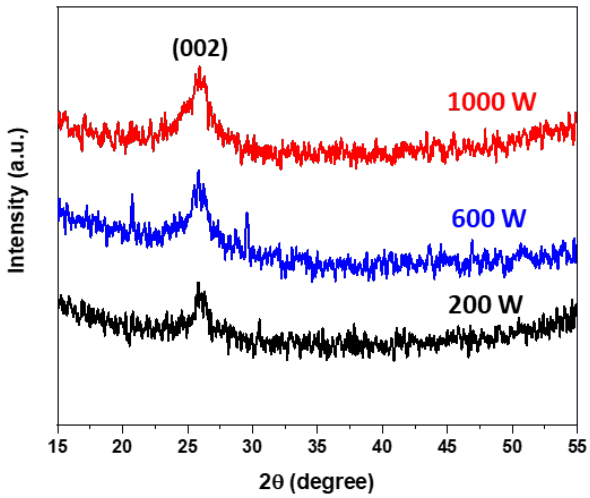

Fig 5.3: XRD pattern of graphene samples

The survey spectra shown in Fig 5.4a, substantiate the presence of carbon (C) and oxygen (O) elements at around 284 and 532 eV respectively. Nitrogen (N) in trace amounts (less than 1 %) was also noticed in all samples which were potentially contributed by N impurity in Ar gas; hence it was ignored. As expected, C turned out to be the most predominant element, while O in trivial amounts could also be observed. The 200 W sample showed comparatively high O content i.e. ~ 14 % which kept on decreasing with the increase in microwave power and vice versa for C (shown in Fig 5.4b). The existence of oxygen in the samples can be attributed to their exposure to the atmosphere. Ultimately, due to the low content of oxygen, the formation of graphene oxide was ruled out. The notion was supported by XRD patterns as well.

Upon deconvolution of C1s peaks into its constituents (shown in Fig 5.4c-e), all the samples revealed three-component peaks i.e. sp^2 (~ 284.6 eV), sp^3 (~ 285.2 eV), and C-OH (~286.1 eV). In contrast to the 600 W sample, the 200 and 1000 W samples showed intense sp^3 peaks pointing out a large number of defects in graphene structure. Considering XPS results, 600 W could be an optimum power to synthesize graphene from tangerine peel oil. The C/O ratio of ~ 16 % in our 600 W sample roughly matches that of graphene derived from ethanol (average C/O was 17 %). In C1s deconvolution of graphene, sp2 and sp3 bands were common in both the studies (tangerine peel oil and ethanol-derived graphene). The only difference was in the oxygen functional groups of the two products; the tangerine peel-derived graphene contained C-OH functional group while C-O, C=O, and epoxide oxygen functional groups were noted in ethanol-derived graphene [31].

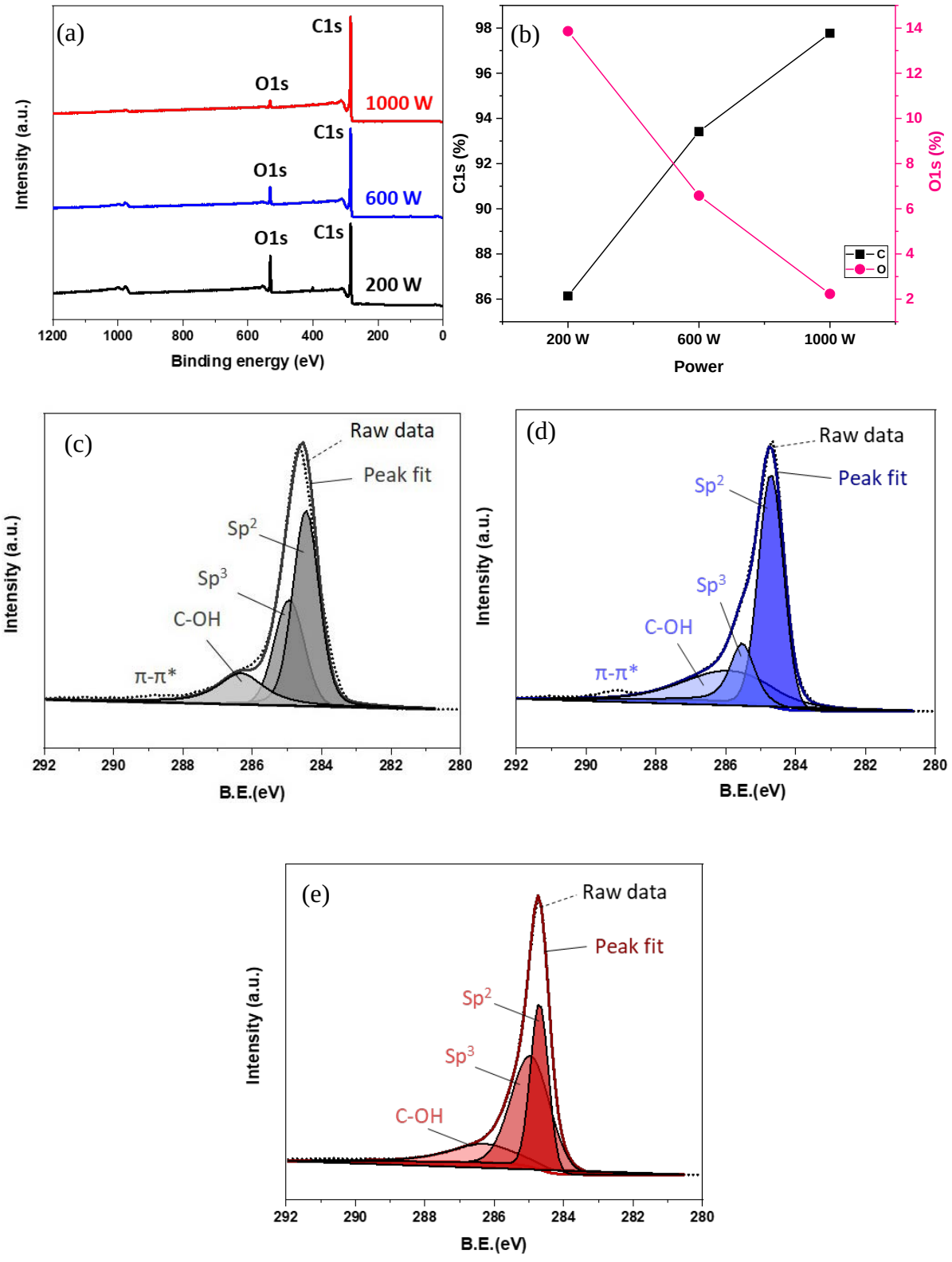

Fig 5.4: (a) Survey spectra of graphene samples (b) Percentages of carbon and oxygen vs microwave power. High-resolution C 1s XPS spectra of (c) 200 W (d) 600 W and (e) 1000 W graphene samples

The SEM images shown in Fig 5.5 revealed a structure typical of graphene. The nanosheets are vertically oriented, and have a curled-paper-like structure, entangled and aggregated. Similar SEM images of graphene have also been observed in preceding studies [8, 32].

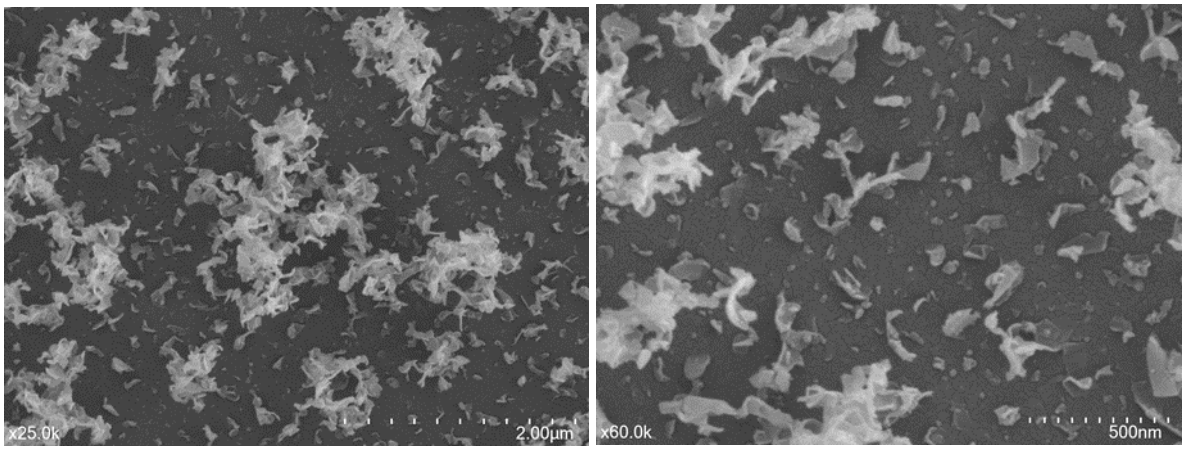

Fig 5.5: SEM images of tangerine peel oil-derived graphene nanosheets (600 W sample) at lower and higher magnifications

The graphene samples collected from the walls of the quartz tube or silicon substrate were characterized using TEM. The TEM images of the 600 W sample are given in Fig 5.6. The images of 200 and 1000 W samples can be seen in Fig S 2. Overall, 200 and 600 W samples showed few layers of graphene, whereas, the 1000 W sample displayed multilayers of graphene. However, it should also be noted that the number of layers in a single sample also varies slightly. A similar outcome was uncovered in a prior research work where graphene was synthesized from ethanol vapours [8]. The high-resolution TEM images shown in Fig 5.6 revealed the non-uniformity in the interlayer spacing. The interlayer spacing of 0.34 nm evident in the image on the left correlates with the aforementioned XRD results. An interlayer spacing of 0.40 nm can also be seen in the same 600 W sample given on the right side of Fig 5.6. This increased spacing can be ascribed to the occurrence of O atoms in the interstices creating dislocations in the graphene structures. Similarly, varying lengths of interlayer spacing can also be observed in the 200 W sample (shown in Fig S2). However, the spaces appeared to be

uniform in the 1000 W sample which corresponds to the fact that the 1000 W sample contained the least amount of O content as discussed in XPS. A brief comparison of the salient features of graphene (table 5.1) synthesized in APMP from different feedstock confirms that the comparable properties of tangerine peel oil-derived graphene are comparable to those of graphene made from other sources. Therefore it can be deduced that the strategy adopted in this work is economical, eco-friendly, and effective when it comes to finding an alternative for non-renewable and hazardous parent materials.

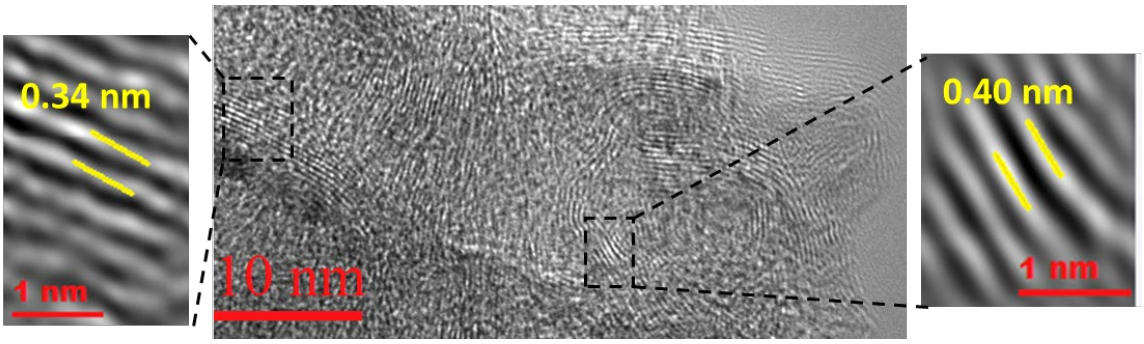

Fig 5.6: TEM images of 600 W tangerine peel oil-derived graphene sample

Table 5.1: Comparison of tangerine peel oil-derived graphene with others synthesized in atmospheric pressure microwave plasma

Precursor	**Microwave power (W)**	**Precursor flow rate (sccm)**	**I_D/I_G**	**Number of layers**	**Production rate (mg/min)**	**Ref.**
Ethanol	250	0.3	-	Mono-and bi-layers	2	[7, 9]
Ethanol	900	0.5 – 3.5	-	Few layers	2	[10]
Ethanol	200	0.0036	0.6	Multilayers	0.07	[33]
Ethanol	300	0.33	0.24	Few layers	1.33	[34]
Ethanol	300	0.048	0.35	Few to multilayers	1.45	[35]
Methane	1000	2 – 8	0.62	Multilayers	-	[11]

Methane	1200-1400	-	1.57 or 1.77	Few to multilayers	-	[12]
Tangerine peel oil	600	0.2	0.94	Few layers	1.61	This work

5.4 Chemiresistive sensing behavior of graphene

The tangerine peel oil-derived graphene synthesized at 600 W was used for developing a chemiresistive sensor by exposing it to the insecticide, herbicide, and ethanol vapours. The detailed procedure is given in the experimental section. As soon as the vapours were subjected to the sensor, a prompt decrease in the resistance of graphene was observed for all the analytes (shown in Fig 5.7). However, a slow recovery response was noted for insecticide and herbicide vapours. Whereas in the case of ethanol the recovery was very fast, and within ~ 25 seconds the sensor response was fully recovered. While insecticide and herbicide-exposed sensor took, for instance, 300 seconds to recover ~ 85 and ~ 50 % respectively. This slow recovery can be attributed to the strong binding energy between graphene and the molecules of insecticide and herbicide. A similar phenomenon was also detected by Shaik et al. [36] and Alancherry et al. [19] where graphene displayed a strong affinity for nitrogen dioxide gas and acetone vapours, respectively, thereby impeding the sensor recovery. The sensitive response of our graphene sample can be assigned to its intrinsic feature of having a large specific surface area.

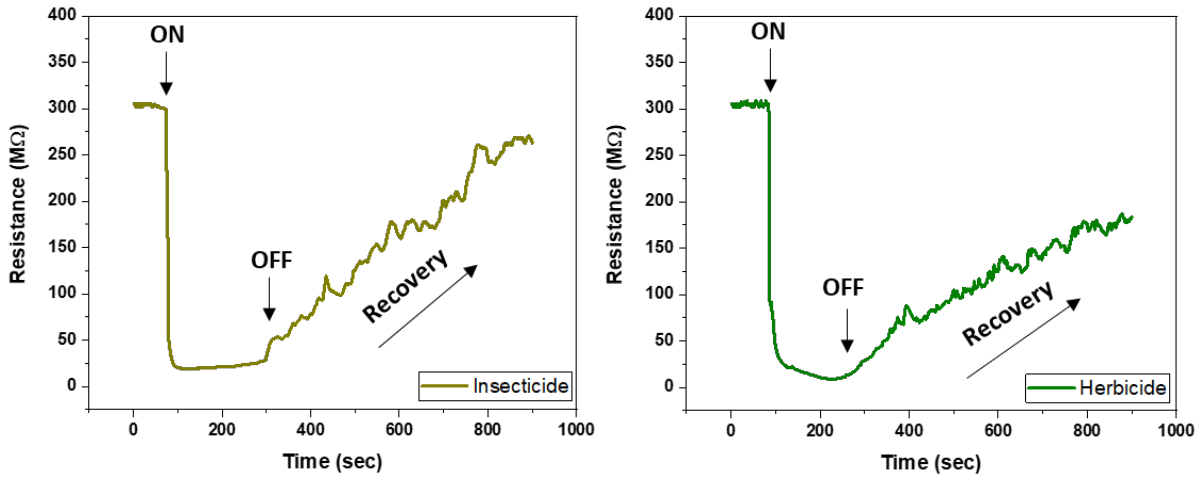

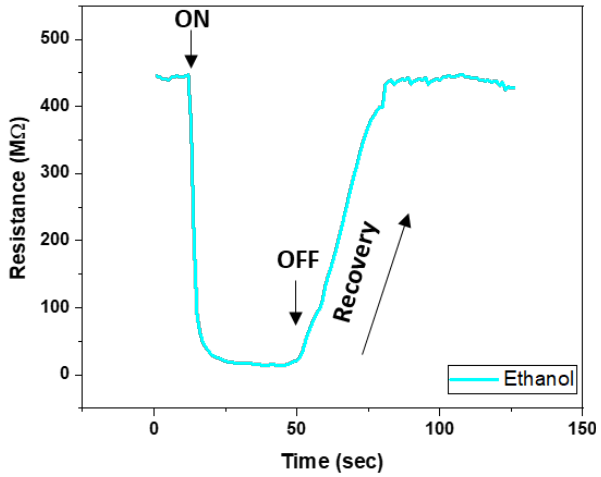

Fig 5.7: Response of tangerine peel oil-derived graphene chemiresistive device toward various chemical substances

5.5 Conclusion

In summary, the synthesis of freestanding graphene nanosheets from an expired tangerine peel oil was successfully carried out using atmospheric pressure microwave plasma. These nanosheets were predominantly composed of sp^2-hybridized carbon atoms having typical graphene structure and morphology with mild inclusions of hydroxyl oxygen functional group. The oxygen content decreases with the increase of microwave power, and hence the D band in the Raman spectrum. The interlayer spacing of 0.34 nm investigated through TEM matches with the XRD value calculated using Bragg's law. The graphene employed in chemiresistive sensor exhibited high sensitivity for insecticide, herbicide, and ethanol vapours. However, the recovery for ethanol was quite rapid as compared to that of insecticide and herbicide. In contrast to previously used non-renewable precursors, i.e. ethanol and methane, the tangerine peel oil is an abundant, sustainable and ecofriendly parent material, perfectly suited for synthesizing graphene in atmospheric pressure microwave plasma.

Supplementary

Fig. S 1: 600 W graphene solution in ethanol, ultra-sonicated for 5 minutes

Calculation of interlayer spacing using Bragg's law

According to Bragg's law:

$\lambda = 2d\sin(\theta)$

Where λ (1.54 Å) is the wavelength of the incident source (Cu), d is the distance between the adjacent graphene layers, and θ is the diffraction angle. 2θ is 26° in our work.

Thus, $d = \lambda/2\sin(\theta) = 0.154\ nm/2\sin(13°) = 0.34\ nm$

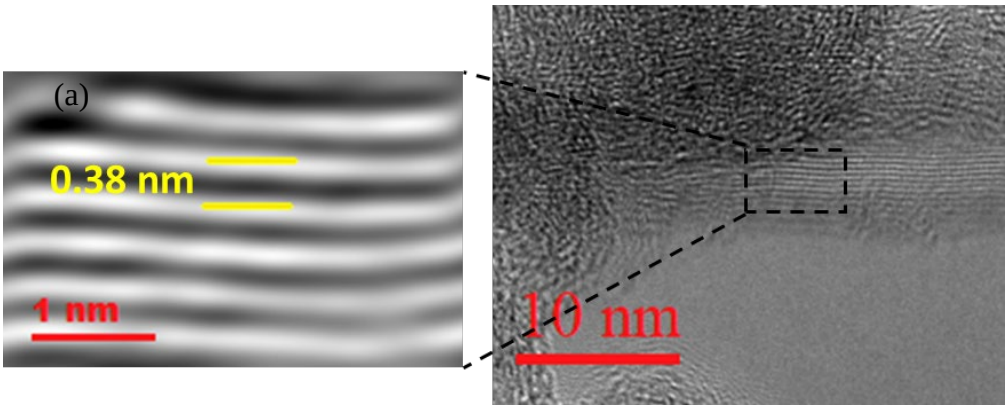

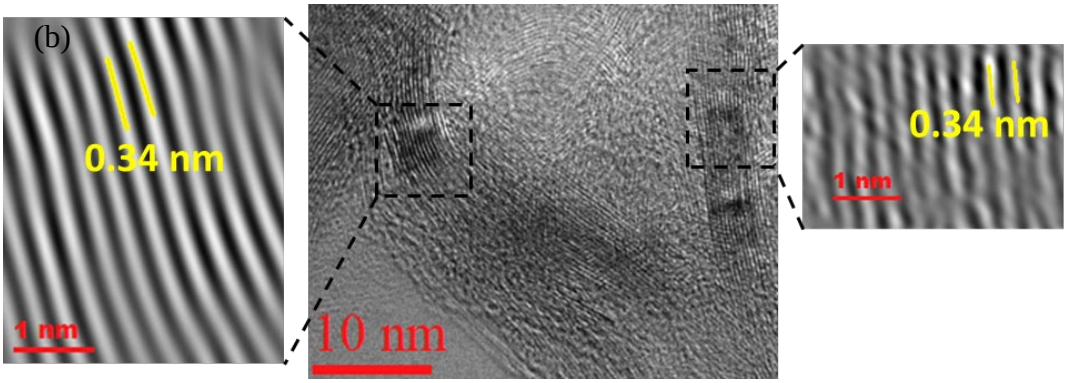

Fig. S 2: TEM images of **(a)** 200 W and **(b)** 1000 W tangerine peel oil-derived graphene samples

References

1. Lu, C.-H., K.-M. Shang, S.-R. Lee, Y.-C. Tai, and N.-C. Yeh, *Graphene on Nanoscale-Thick Au Films: Implications for Anticorrosion in Smart Wearable Electronics.* ACS Applied Nano Materials, 2022.
2. Shin, B.G., D.H. Boo, B. Song, S. Jeon, M. Kim, S. Park, E.S. An, J.S. Kim, Y.J. Song, and Y.H. Lee, *Single-crystalline monolayer graphene wafer on dielectric substrate of SiON without metal catalysts.* ACS nano, 2019. **13**(6): p. 6662-6669.
3. You, Y., M. Mayyas, S. Xu, I. Mansuri, V. Gaikwad, P. Munroe, V. Sahajwalla, and R. Joshi, *Growth of NiO nanorods, SiC nanowires and monolayer graphene via a CVD method.* Green Chemistry, 2017. **19**(23): p. 5599-5607.
4. Liu, Y. and Y. Chen, *Synthesis of large scale graphene oxide using plasma enhanced chemical vapor deposition method and its application in humidity sensing.* Journal of Applied Physics, 2016. **119**(10): p. 103301.
5. Cossutta, M., J. McKechnie, and S.J. Pickering, *A comparative LCA of different graphene production routes.* Green Chemistry, 2017. **19**(24): p. 5874-5884.
6. Devasahayam, S. and C.M. Hussain, *Thin-film nanocomposite devices for renewable energy current status and challenges.* Sustainable Materials and Technologies, 2020. **26**: p. e00233.
7. Dato, A. and M. Frenklach, *Substrate-free microwave synthesis of graphene: experimental conditions and hydrocarbon precursors.* New Journal of Physics, 2010. **12**(12): p. 125013.
8. Tatarova, E., A. Dias, J. Henriques, M. Abrashev, N. Bundaleska, E. Kovacevic, N. Bundaleski, U. Cvelbar, E. Valcheva, and B. Arnaudov, *Towards large-scale in free-standing graphene and N-graphene sheets.* Scientific reports, 2017. **7**(1): p. 1-16.

9. Dato, A., V. Radmilovic, Z. Lee, J. Phillips, and M. Frenklach, *Substrate-free gas-phase synthesis of graphene sheets.* Nano letters, 2008. **8**(7): p. 2012-2016.

10. Tatarova, E., J. Henriques, C. Luhrs, A. Dias, J. Phillips, M. Abrashev, and C. Ferreira, *Microwave plasma based single step method for free standing graphene synthesis at atmospheric conditions.* Applied Physics Letters, 2013. **103**(13): p. 134101.

11. Bundaleska, N., D. Tsyganov, A. Dias, E. Felizardo, J. Henriques, F. Dias, M. Abrashev, J. Kissovski, and E. Tatarova, *Microwave plasma enabled synthesis of free standing carbon nanostructures at atmospheric pressure conditions.* Physical Chemistry Chemical Physics, 2018. **20**(20): p. 13810-13824.

12. Singh, M., A. Sengupta, K. Zeller, G. Skoptsov, and R.L. Vander Wal, *Effect of hydrogen concentration on graphene synthesis using microwave-driven plasma-mediated methane cracking.* Carbon, 2019. **143**: p. 802-813.

13. Zafar, M.A., O.K. Varghese, F.C. Robles Hernandez, Y. Liu, and M.V. Jacob, *Single-Step Synthesis of Nitrogen-Doped Graphene Oxide from Aniline at Ambient Conditions.* ACS Applied Materials & Interfaces, 2022.

14. Jimenez, M., R. Rincon, A. Marinas, and M. Calzada, *Hydrogen production from ethanol decomposition by a microwave plasma: influence of the plasma gas flow.* International journal of hydrogen energy, 2013. **38**(21): p. 8708-8719.

15. Seo, D.H., A.E. Rider, Z.J. Han, S. Kumar, and K. Ostrikov, *Plasma Break-Down and Re-Build: Same Functional Vertical Graphenes from Diverse Natural Precursors.* Advanced Materials, 2013. **25**(39): p. 5638-5642.

16. Ruan, G., Z. Sun, Z. Peng, and J.M. Tour, *Growth of graphene from food, insects, and waste.* ACS nano, 2011. **5**(9): p. 7601-7607.

17. Ouyang, B., M.V. Jacob, and R. Rawat, *Free standing 3D graphene nano-mesh synthesis by RF plasma CVD using non-synthetic precursor*. Materials Research Bulletin, 2015. **71**: p. 61-66.

18. Sharma, S., G. Kalita, R. Hirano, Y. Hayashi, and M. Tanemura, *Influence of gas composition on the formation of graphene domain synthesized from camphor.* Materials Letters, 2013. **93**: p. 258-262.

19. Alancherry, S., K. Bazaka, I. Levchenko, A. Al-Jumaili, B. Kandel, A. Alex, F.C. Robles Hernandez, O.K. Varghese, and M.V. Jacob, *Fabrication of Nano-Onion-Structured Graphene Films from Citrus sinensis Extract and Their Wetting and Sensing Characteristics.* ACS Applied Materials & Interfaces, 2020.

20. Al-Jumaili, A., M.A. Zafar, K. Bazaka, J. Weerasinghe, and M.V. Jacob, *Bactericidal Vertically Aligned Graphene Networks Derived from Renewable Precursor.* Carbon Trends, 2022: p. 100157.

21. Kamal, G., F. Anwar, A. Hussain, N. Sarri, and M. Ashraf, *Yield and chemical composition of Citrus essential oils as affected by drying pretreatment of peels.* International Food Research Journal, 2011. **18**(4): p. 1275.

22. Spreen, T.H., Z. Gao, W. Fernandes Jr, and M.L. Zansler, *Global economics and marketing of citrus products*, in *The Genus Citrus*. 2020, Elsevier. p. 471-493.

23. Naef, R. and A. Velluz, *Volatile constituents in extracts of mandarin and tangerine peel.* Journal of Essential Oil Research, 2001. **13**(3): p. 154-157.

24. Liu, B., C.-M. Yang, Z. Liu, and C.-S. Lai, *N-doped graphene with low intrinsic defect densities via a solid source doping technique.* Nanomaterials, 2017. **7**(10): p. 302.

25. Eckmann, A., A. Felten, A. Mishchenko, L. Britnell, R. Krupke, K.S. Novoselov, and C. Casiraghi, *Probing the nature of defects in graphene by Raman spectroscopy.* Nano letters, 2012. **12**(8): p. 3925-3930.

26. Yang, H., H. Hu, Z. Ni, C.K. Poh, C. Cong, J. Lin, and T. Yu, *Comparison of surface-enhanced Raman scattering on graphene oxide, reduced graphene oxide and graphene surfaces.* Carbon, 2013. **62**: p. 422-429.

27. Boas, C.R.S.V., B. Focassio, E. Marinho, D.G. Larrude, M.C. Salvadori, C.R. Leão, and D.J. Dos Santos, *Characterization of nitrogen doped graphene bilayers synthesized by fast, low temperature microwave plasma-enhanced chemical vapour deposition.* Scientific reports, 2019. **9**(1): p. 1-12.

28. Hao, Y., Y. Wang, L. Wang, Z. Ni, Z. Wang, R. Wang, C.K. Koo, Z. Shen, and J.T. Thong, *Probing layer number and stacking order of few-layer graphene by Raman spectroscopy.* small, 2010. **6**(2): p. 195-200.

29. Wang, G., X. Shen, B. Wang, J. Yao, and J. Park, *Synthesis and characterisation of hydrophilic and organophilic graphene nanosheets.* Carbon, 2009. **47**(5): p. 1359-1364.

30. Hong, N., W. Yang, C. Bao, S. Jiang, L. Song, and Y. Hu, *Facile synthesis of graphene by pyrolysis of poly (methyl methacrylate) on nickel particles in the confined microzones.* Materials Research Bulletin, 2012. **47**(12): p. 4082-4088.

31. Tatarova, E., A. Dias, J. Henriques, A.B. do Rego, A. Ferraria, M. Abrashev, C.C. Luhrs, J. Phillips, F. Dias, and C. Ferreira, *Microwave plasmas applied for the synthesis of free standing graphene sheets.* Journal of Physics D: Applied Physics, 2014. **47**(38): p. 385501.

32. Bundaleska, N., J. Henriques, M. Abrashev, A.B. do Rego, A. Ferraria, A. Almeida, F. Dias, E. Valcheva, B. Arnaudov, and K. Upadhyay, *Large-scale synthesis of free-standing N-doped graphene using microwave plasma.* Scientific reports, 2018. **8**(1): p. 1-11.

33. Rincón, R., C. Melero, M. Jiménez, and M. Calzada, *Synthesis of multi-layer graphene and multi-wall carbon nanotubes from direct decomposition of ethanol by microwave plasma without using metal catalysts.* Plasma Sources Science and Technology, 2015. **24**(3): p. 032005.

34. Melero, C., R. Rincón, J. Muñoz, G. Zhang, S. Sun, A. Perez, O. Royuela, C. González-Gago, and M. Calzada, *Scalable graphene production from ethanol decomposition by microwave argon plasma torch.* Plasma Physics and Controlled Fusion, 2017. **60**(1): p. 014009.

35. Casanova, A., R. Rincón, J. Muñoz, C. Ania, and M. Calzada, *Optimizing high-quality graphene nanoflakes production through organic (bio)-precursor plasma decomposition.* Fuel Processing Technology, 2021. **212**: p. 106630.

36. Shaik, M., V. Rao, M. Gupta, K. Murthy, and R. Jain, *Chemiresistive gas sensor for the sensitive detection of nitrogen dioxide based on nitrogen doped graphene nanosheets.* RSC advances, 2016. **6**(2): p. 1527-1534.

Chapter 6: Synthesis of nitrogen-doped graphene oxide and its application

This chapter is divided into two sub-chapters. In the first part, a sustainable approach for the synthesis of nitrogen-doped graphene oxide (N-GO) is reported. It is shown that N-GO can now be synthesized from a single precursor i.e. aniline at a remarkably low microwave power. The confirmation of N-GO formation was carried out through various characterization techniques. In the second part, the application of as-synthesized N-GO loaded with silver nanoparticles was performed for the detection of oxalic acid.

This Chapter consists of two manuscripts, which are published as following:

1. *Zafar, M. A., Varghese, O. K., Robles Hernandez, F. C., Liu, Y., & Jacob, M. V. (2022). Single-Step Synthesis of Nitrogen-Doped Graphene Oxide from Aniline at Ambient Conditions. ACS Applied Materials & Interfaces, 14(4), 5797-5806.*

2. *Zafar, M. A., Liu, Y., Allende, S., & Jacob, M. V. (2022). Electrochemical sensing of oxalic acid using silver nanoparticles loaded nitrogen-doped graphene oxide. Carbon Trends, 8, 100188.*

6.1 Sustainable approach for the synthesis of nitrogen-doped graphene oxide

Single-Step Synthesis of Nitrogen-Doped Graphene Oxide from Aniline at Ambient Conditions

Abstract

Single-step, single-precursor synthesis of nitrogen-doped graphene oxide (N-GO) was demonstrated in this work. By choosing aniline as the sole source of carbon and nitrogen, N-GO films were fabricated using microwave plasma at a power as low as 80 W in atmospheric conditions. The aniline vapor dissociated under plasma formed islands of N-GO nanosheets on the substrates or walls of the quartz deposition chamber. The inter-planar spacing in the pristine N-GO films was observed to be lower than that of GO films, which indicated a lower concentration of oxygen and other species present in the space between the N-GO layers. The as-fabricated N-GO demonstrated superior anti-scaling and algicidal properties deemed imperative for water purification applications.

Keywords: Nitrogen-doped graphene oxide, aniline, atmospheric pressure microwave plasma, single-precursor, water purification

6.1.1 Introduction

Graphene lies top in the list of most promising 21st century materials [1, 2]. It has a two-dimensional honeycomb structure formed by two interpenetrating hexagonal Bravais lattices with sp^2-bonded carbon atoms. Some of the unique properties making graphene technologically interesting include exceptional tensile strength, excellent visible light transmittance, record high thermal conductivity, superior charge transport properties, nearly perfect impermeability to all gases, and ultra-high specific surface area [3]. It has been found useful for an extensive list of applications; however, the areas such as energy generation/storage, electronic and photonic devices, optical devices, renewable energy conversion, water purification and chemical/biological sensors are expected to be benefited substantially by the involvement of graphene [4-6].

The chemical inertness, hydrophobicity and poor solubility in aqueous solutions challenge the processability and chemical functionalization of graphene [7, 8]. However, graphene in the oxidized form as graphene oxide (GO) or reduced graphene oxide (rGO), can be used to alleviate these issues. GO is an oxidized version of graphene which is adorned with epoxide and hydroxyl (–OH) groups in basal planes, and carbonyl (C=O), alkoxy (C-O-C), and carboxylic acid (–COOH) groups at the edges of the graphene sheet [9, 10]. These oxygen-containing functional groups make the material hydrophilic and dispersible in aqueous media. [11, 12]. Moreover, GO offers a favorable matrix for further surface enhancements, especially for the doping of heteroatoms (e.g. B, N, O, P and S) [13]. Recently, nitrogen-doped GO (N-GO) and reduced graphene oxide (N-rGO) have sparked substantial interest due to the properties attributed by the unique scaffolding pattern of nitrogen and carbon atoms. The union between the lone-pair electrons of nitrogen and the π-system of graphene improve its chemical and physical properties [14], leading to a myriad of applications particularly in lithium

batteries, supercapacitors, sensors [15], and purification membranes [16]. Despite all these advantages, there are not many affordable and commercially feasible methods for the production of high quality N-GO required for devices and processes.

Considerable attempts have been made for a methodical synthesis of N-GO, however, the techniques reported until now either involve more than one precursors or require multiple stages of synthesis or both increases the cost of the process [17]. Fabrication of undoped GO itself involves toxic and corrosive chemicals and is technology intensive. 'Modified Hummers method' that utilizes strong acids and oxidants is commonly used to synthesize GO [17, 18]. The process entails numerous steps of synthesis such as dilution, mixing, oxidation, washing, centrifuging, and intense stirring [19]. On the other hand, 'chemical vapor deposition (CVD)' and 'plasma-enhanced chemical vapor deposition (PECVD)' are expensive and the processes are time-consuming. These techniques require high vacuum, high temperatures, oxidizing environment, and other post-synthesis treatment processes [20, 21]. The post-synthesis N-doping methods include thermal treatment of GO in an ammonia (NH_3) atmosphere [22], wet-chemical methods [23], treatment with nitrogen plasma [24], and a low energy N^{2+} ion sputtering [15]. Nonetheless, these techniques are complex and centered on ex-situ synthesis approaches. Ammonia is corrosive and it poses significant problems to the process chamber and the system components. The latest endeavors of N-graphene synthesis via single-step, in-situ CVD or PECVD methods [25-28] involve elevated temperatures and high power plasma that increase the production cost and cause the elimination of pyridinic nitrogen atom doping required for certain applications [29]. Such issues with the current N-GO production methods behoove us to develop a fast, cost-effective, eco-friendly, and a facile method for the synthesis of N-GO under mild conditions.

Atmospheric pressure plasma (APMP) technology utilizing microwave power is promising bottom-up materials fabrication technique which circumvent the aforementioned issues [30]. APMP avoids the need of vacuum, heating and cooling components. This technique is scalable and has the potential to manufacture nanomaterials from organic precursors without substrates. The process is simple and it consists of admitting the precursor vapor mixed with a carrier gas into the plasma chamber where the precursor bonds are broken under plasma conditions. Monolayer to a few-layer graphene nanosheets have been reported to be synthesized using this technique [31-37]. So far, the technology has been limited to the synthesis, oxidation [38-40], and N-doping [41, 42] of pristine graphene; whereas no work on single-step synthesis of GO or N-GO using APMP has been reported. Additionally, the oxidation and doping methodologies used in these approaches require high plasma power and/or additional gas/vapor precursors increasing the complexity and cost of fabrication. For instance, when nitrogen [41] or NH_3 gas [14] is used as a precursor, the required plasma power rose to the 2 kW or in this range.

Our interest was in developing a single-step, single-precursor cold plasma synthesis process for growing N-GO films at atmospheric conditions. We used only aniline as the sole precursor for both GO growth and doping. Aniline is unique with its composition consisting of nitrogen and carbon atoms and low binding energy, which helped us use a remarkably low microwave power (80W) to break the aniline molecules and achieve the N-GO growth in a single-step process. The whole procedure was carried out at normal atmosphere to harness oxygen for GO formation and with no external heating.

6.1.2 Experimental

The synthesis of N-GO was performed using downstream microwave plasma at ambient conditions. A basic schematic illustration of the setup is shown in Fig. 6.1. It mainly consists

of a microwave plasma source (2.45 GHz), quartz tube (30 mm OD), matching network, and a sliding short circuit. The microwave plasma source and the quartz tube were fitted with water- and air-cooling system respectively. Aniline (analytical grade) was utilized in its pure form as the only source of carbon and nitrogen in this experiment. To supply aniline into the quartz chamber a custom made aerosol system was developed; instead of using any additional carrier gas, the precursor was delivered along with the argon gas.

The N-GO forms instantaneously on the walls of the quartz tube once the argon-aniline mixture is introduced. Bare argon plasma showed colorless streaks, whereas, in the presence of argon-aniline mixture, the plasma glow displayed a unique colored spectrum as shown in Fig. 6.2. A microwave power up to 200 W and a fabrication time up to 4 minutes were used for optimizing the experimental conditions. Our preliminary experiments showed the formation of N-GO at a power as low as 80 W. Therefore, further experiments were done at 80 W, 150 W and 200 W. Based on the conclusions drawn from the Raman spectra (not shown), the fabrication-time was fixed at 3 minutes, argon and aniline flow-rates of 3 liters per minute (lpm) and 0.2 mL per minute respectively. The N-GO grown was collected either directly on different substrates (silicon, quartz, and a cover slip) or washed from the tube-walls with ethanol. A homogeneously dispersed N-GO flakes in ethanol can be seen in Fig. S1. The optical microscope images of N-GO collected on the silicon substrate are given in Fig. S2.

Confocal laser Raman spectroscopy (Witec, 532 nm laser), scanning electron microscopy (SEM) (Hitachi SU 5000) and Fourier transform infrared spectroscopy (FT-IR) (spectrum-100 spectrometer, Perkin Elmer, USA) were used to investigate respectively the material's structure, morphology and chemical functional groups. The crystallographic information was obtained using a Rigaku SmartLab x-ray diffractometer. The x-ray photoelectron spectroscopy (XPS) studies were performed using a Physical Electronics spectrometer (model 5700) with an

Al x-ray source. The transmission electron microscopy (TEM) images were obtained using a JEOL 2100 F machine operated at 200 kV. The electrochemical impedance spectroscopy (EIS) experiments were carried out on a PalmSense 4 potentiostat (PalmSens, Netherlands) with a conventional three-electrode system composed of a platinum auxiliary, a Ag/AgCl (saturated KCl) reference and a glassy carbon working electrode (GCE) in a 0.1 M KCl solution containing 5 mM $K_3Fe(CN)_6$. An alternating signal of 5 mV was applied to study the impedance characteristics of the samples in the frequency range 10^{-1} – 10^{5} Hz.

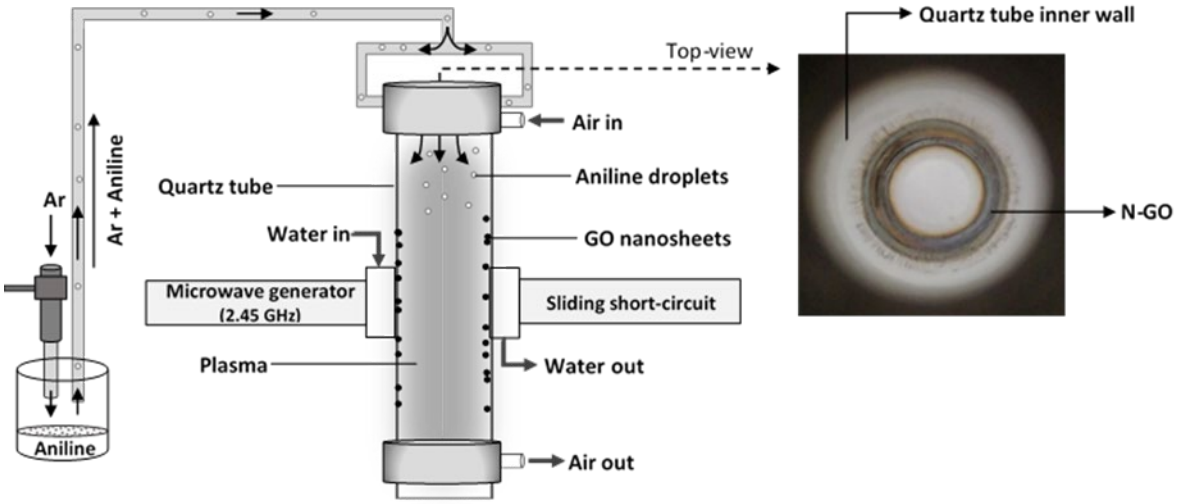

Fig 6.1: Schematic illustration of downstream microwave plasma setup and top-view of the tube showing N-GO deposited on walls

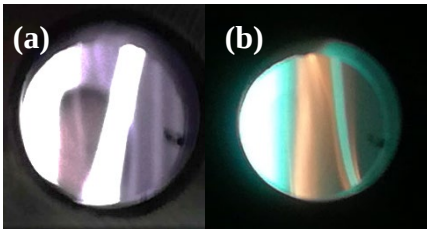

Fig 6.2: Appearance of plasma (a) in the absence of aniline and (b) after exposure to aniline

6.1.3 Results and discussions

The as-fabricated N-GO films were analyzed using Raman spectroscopy to understand the structural quality. The Raman spectra of all samples, irrespective of the plasma power used for the growth, showed three vibrational modes typical of graphene-related materials. These are represented by the D peak at ~1335 cm^{-1} (defect mode), G peak at ~1575 cm^{-1} (vertical vibration mode), and a 2D peak at ~2675 cm^{-1} (two-phonon vibration mode) [43]. The D peak arises from the scattering of phonons at the boundary of the disordered hexagonal Brillouin zone; the G peak is sourced from the in-plane C-C stretching vibration under the E2g mode [44]. It was observed that an increase in the plasma power resulted in the reduction of the intensity of the D peak. The differences in D peaks at varied plasma powers are evident in graphs shown in Fig. 6.3. Additionally, the variations in synthesis-time did not cause a substantial impact on Raman peaks (Fig. S3).

The intensity ratio of D and G peak (I_D/I_G) reflects the degree of disorder in a material. Generally, the doped graphene materials have higher ratios of I_D/I_G and they tend to rise with an increase in doping levels [23, 45]. Likewise, in the current work, the 80 W sample showed a comparatively larger value of I_D/I_G; hence indicating relatively high disorders in the structure of the synthesized material (Fig. 3b). According to studies, this disorder can be ascribed to the presence of functionalities, non-hexagonal rings, or heteroatom doping which are manifested in the form of amplified D peaks [13]. Thus, it could be deciphered that the raised content of N-doping (evident from XPS results discussed later) and functional groups in the 80 W sample were responsible for an elevated I_D/I_G ratio. A similar observation was made by Li et al. [46], where they discovered that the pyrrolic N-doped graphene yielded a greater value of I_D/I_G ratio when compared with that of pristine graphene. They attributed it to the fact that the N atoms created a sp^3-C five-atom heterocyclic ring of pyrrolic N-doped graphene by rupturing the sp^2-

C six-atom structure of graphene. Furthermore, the 80 W N-GO synthesized in our work showed a lower I_D/I_G ratio (0.93) as compared to that reported for a sample prepared using modified Hummers method (I_D/I_G = 1.62) [47]. The higher I_D/I_G ratio in modified Hummers method indicates either a higher nitrogen content (reported as 5.6 %) or possible defects in the N-GO structure.

The 2D peak has been generally recognized as the signature of the graphene and related materials in the Raman spectrum. The full width at half-maximum (FWHM) and intensity ratio between 2D and G peak, i.e., I_{2D}/I_G, are generally linked to the number of layers in graphene. The I_{2D}/I_G values of 2 or higher with FWHM ~30 cm^{-1}, and 1 to 1.5 I_{2D}/I_G ratios with FWHM ~50 cm^{-1} are usually associated with the monolayer and bilayer structures, respectively [28, 48]. In this study, the 80 W sample exhibited I_{2D}/I_G and FWHM values of 1.04 and 64 cm^{-1} respectively, indicative of multiple layers N-GO in the region from where the spectra was recorded. The comparable FWHM (66 cm^{-1}) of 2D peaks and similar I_{2D}/I_G values of 150 W and 200 W samples indicated that these samples were also multilayered N-GO. It is noteworthy that the presence of nitrogen dopants in graphene can also impart a certain effect on both D and 2D peaks. On one hand, N-doping augments the defects in graphene making the D peak more intense, on the other it enhances the electron scattering rate, which diminishes the intensity of the 2D peak [28].

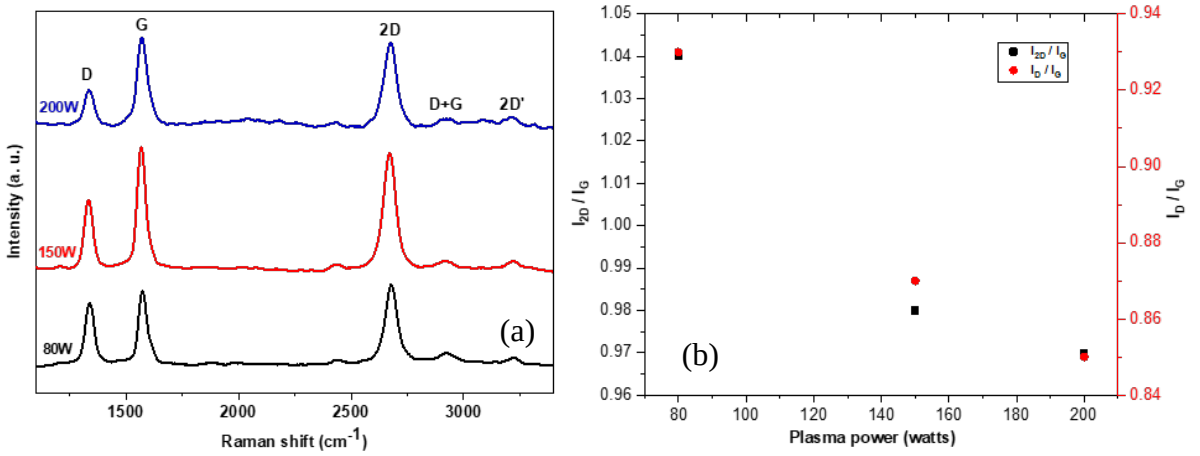

Fig 6.3: (a) Raman spectra and (b) the intnesity ratios of 2D and D peaks with respect to the G peak in the N-GO samples, representing the effect of plasma power on synthesis

The Fourier transform infrared (FTIR) spectra of all samples *i.e.* 80 W, 150 W and 200 W, appeared similar (see Fig. 6.4 and S4-a). The dips in the FTIR transmittance spectra, indicating the presence of carbon, oxygen, and nitrogen-containing functional groups endorsed the Raman spectroscopy results that the fabricated films contained N-GO. The typical peak position at 3351 cm^{-1} was assigned to the O–H stretching vibration and the two distinct peaks at 2923 cm^{-1} and 2852 cm^{-1} to the asymmetric and symmetric stretching of the C–H bond [49]. The doublet observed between 1650 cm^{-1} and 1750 cm^{-1} has been resolved and assigned to two peaks i.e. C-O (1719 cm^{-1}) and aromatic C=C (1670 cm^{-1}). The deconvoluted peaks are given in Fig. S4-b. The presence of C-O peak could be ascribed to the synthesis of 80 W N-GO at mild conditions. The higher microwave power of 200 W eliminated the doublet and showed single C=C peak (Fig. S4-a). Kumar et al. [29] also reported the reduction of oxygen functional groups in their study, where they used 500 W microwave power to simultaneously reduce and dope the GO. The peaks at 1494 cm^{-1}, 1240 cm^{-1}, and 1021 cm^{-1} were identified as the N-H, C–N, and C-O vibration modes respectively [50]. The sharp absorption peaks, centered at 748 cm^{-1} and 692 cm^{-1} were ascribed to the out-of-plane deformation vibration of N-H bonds [49].

Similar FTIR results were reported by Tao et al. [23], but the study was conducted on N-GO fabricated by the ultrasonic treatment of GO in ammonia solution.

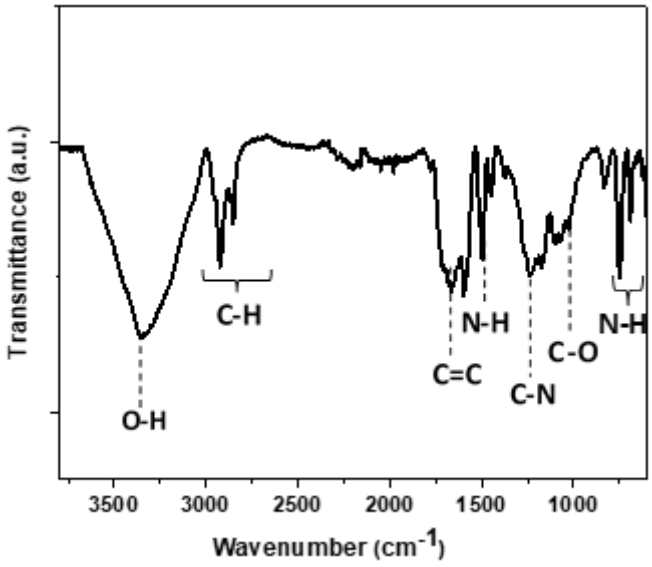

Fig 6.4: FTIR spectrum of N-GO sample synthesized at 80 W

The XPS survey scans given in Fig. 6.5 (a-c), clearly exhibit the presence of C, O, and N, verifying the presence of N-GO at all plasma powers. The peaks at 285.6, 400.8, and 532.8 eV were assigned to the C1s core level spectrum of sp^2-C, N1s spectrum of the doped N, and O1s spectrum, respectively. The variations in plasma power showed insignificant changes in the atomic percentages of C and O. However, a considerable amount of N atoms was retained in the 80 W (N: 3.55 %) sample when compared with 150 W (N: 0.84%) and 200 W (N: 1.67 %) samples, suggesting that the higher plasma power potentially led to the dissociation of C-N bonds. The doping percentage of 3.55 % N atoms achieved through this facile method was comparable to those reports where doping was introduced via multistep processes [45, 49, 51]. For instance, in modified Hummers method [47], 5.6 % of nitrogen content was obtained.

In order to comprehend the bonding configuration associated with C and N atoms, the high-resolution spectra of C1s and N1s were analyzed. The high-resolution C_{1s} spectra of 80 W, 150

W and 200 W samples are presented in figures 5-d, S 5(a) and S5(b) respectively. The peak deconvolution revealed four prominent component peaks in the 80W-C1s spectrum. The major peaks at 284.5 eV and 285.4 eV correspond to sp^2 and sp^3-C, respectively. The smaller peaks centered at 286.5 eV and 288.3 eV reflect C-N or C-O and C=O bonding respectively [28]. The presence of sp^2 C is indicative of the conjugated honeycomb lattice arrangement of graphene, while sp^3-C denotes substitution of N atoms, defects in graphene, or simply the edges of the graphene nanosheets [52].

Interestingly, the high-resolution N1s spectra of the 80 W sample, accommodating three peaks (Fig. 6.5-e) revealed different N bonding types in the graphene lattice, which are shown schematically in Fig. 6.5-f. The main peak at 401.2 eV is a signature of the graphitic N bonding, which refers to the sp^2-hybridization of N atoms with three sp^2-hybridized C neighboring atoms. Likewise, the 400.4 eV peak stands for an N-doped heterocyclic five-membered C ring, contributing to the p-system with two p-electrons. Similarly, the presence of pyridinic N bonding arising from sp^2-hybridized N atoms with two sp^2-hybridized C neighboring atoms and serving the p-system with a single p-electron, is marked by the smallest peak at 399.6 eV. Based on the deconvolution of the peaks, it was deduced that graphitic and pyrrolic N bonding were prevalent in 80 W sample, making up for 50.07 % and 38.87 % respectively of the total N-doping types. On the contrary, the content of pyridinic N-doping was only 11.06 %.

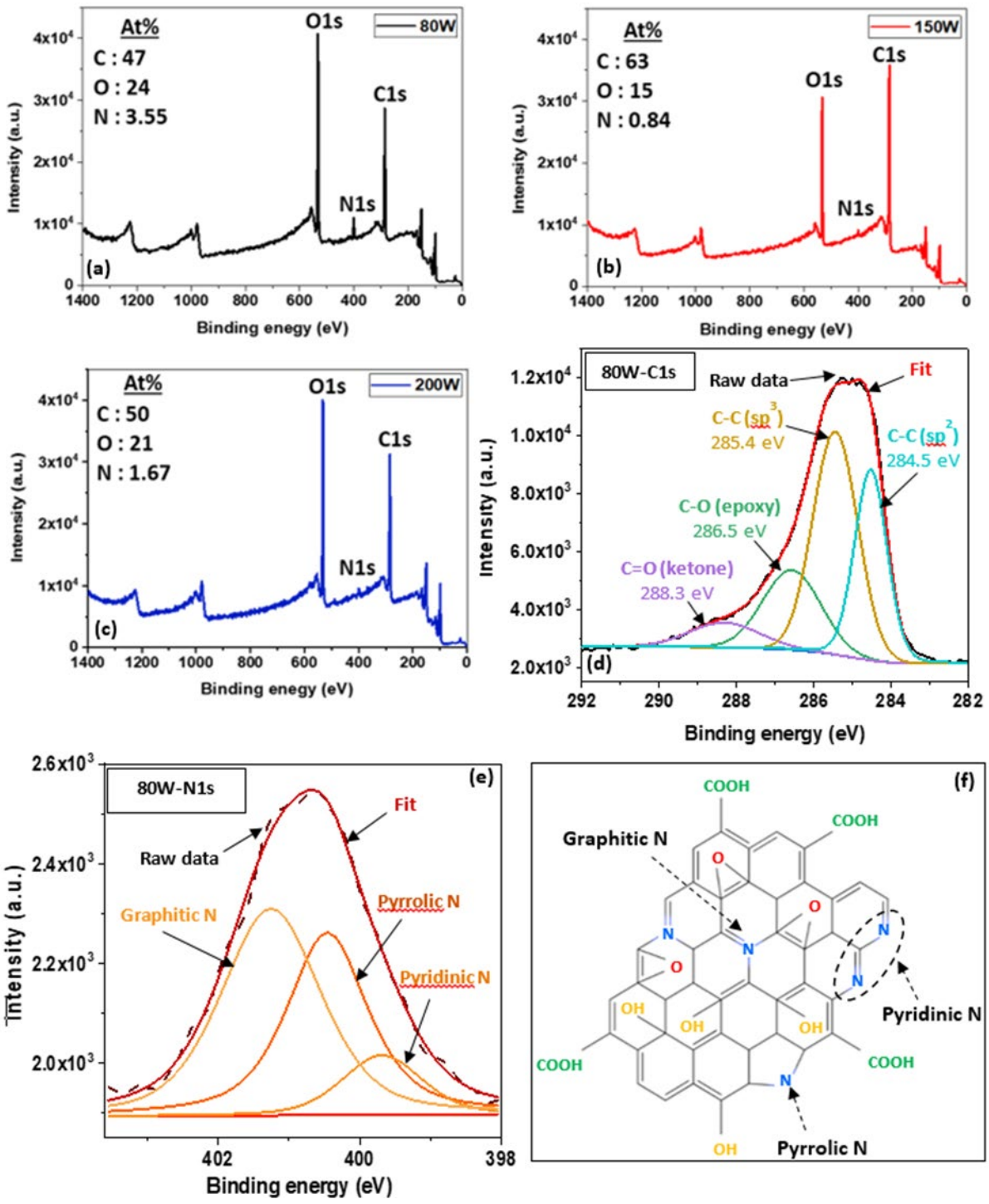

Fig 6.5: XPS survey spectra of N-GO samples synthesized at (a) 80 W (b) 150 W (c) 200 W. The deconvoluted high-resolution (d) C1s and (e) N1s peaks arising from 80W sample and (f) a schematic representation of types of N-bonding in N-GO samples are also shown.

The low and high resolution SEM images of the N-GO nanosheets grown directly on silicon substrates are shown in Fig. 6.6. As expected, the planar films were not visible in the SEM

images; however, all the samples showed three dimensional islands resembling crumpled and torn paper sheets distributed on a surface. These images could also be correlated with the optical microscope images given in Fig. S2 where the silicon surface could be seen as covered with islands. These islands consisted primarily of multilayered carbon as evidenced by the high-resolution Transmission Electron Microscopy (HRTEM) results shown in Fig. 6.7.

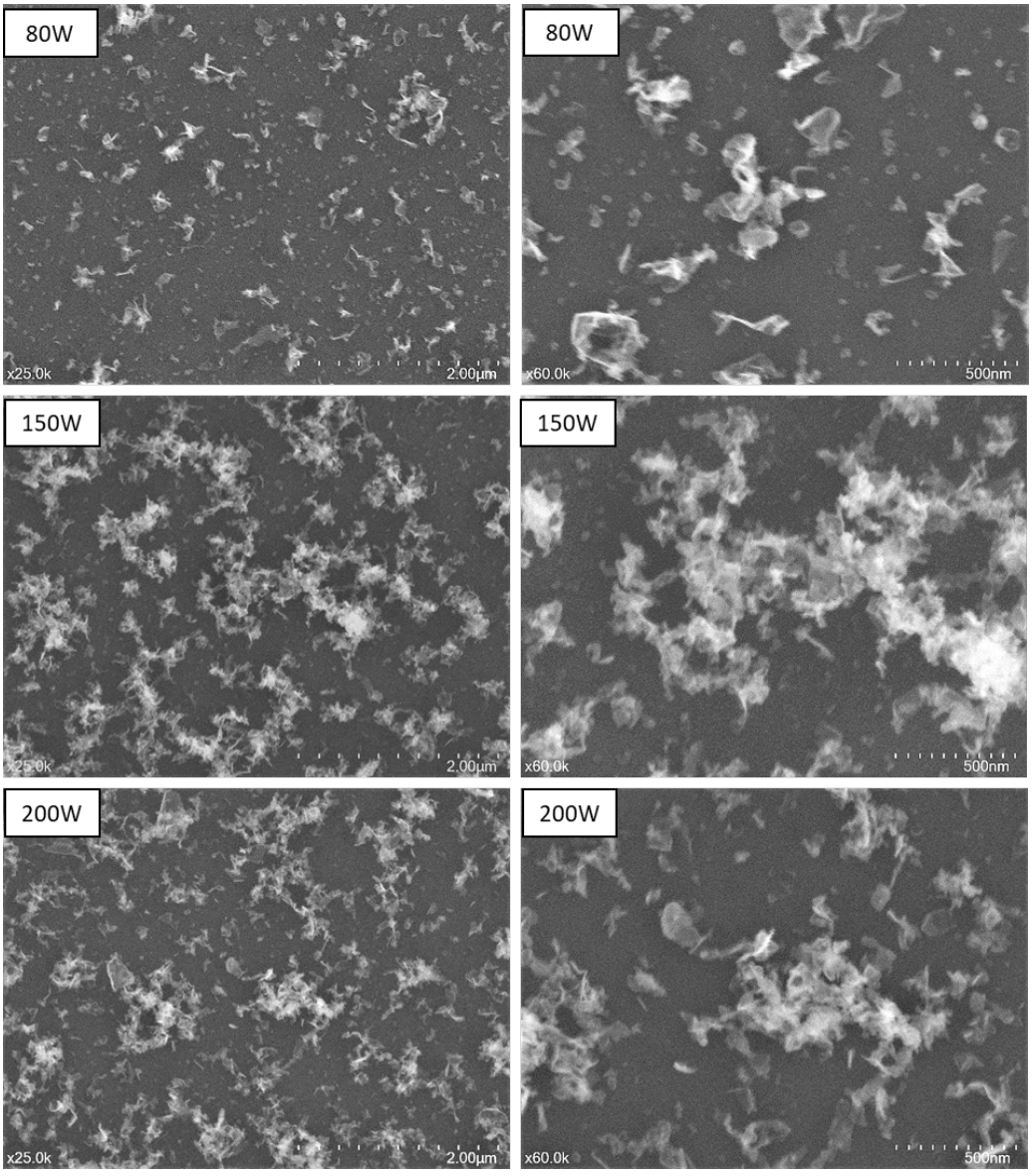

Fig 6.6: SEM images of N-GO samples synthesized at different plasma powers

The samples mechanically removed from silicon substrates were used for TEM studies. Fig. 7(a, b) show the images of an 80 W sample on a silicon (100) substrate. The high resolution

images of the selected regions in Fig. 6.7a (left) are given in Fig. 6.7a (right). Fig. 6.7a (right top & middle) images show the silicon lattice (the silicon lattice images are separately shown also in Fig. S6). A thicker poorly crystallized graphitic region could also be seen in the images (Fig. 6.7a, right bottom). Fig. 6.7a & 6.7b show respectively the multilayered films of 80 W and 150 W samples detached from the substrate. The 150 W sample appeared to have improved crystallinity. The high resolution images given in the right side of these figures showed that the inter-layer spacing was non-uniform. While the inter-layer spacing in graphene is 0.33 nm, in our samples a spacing up to 0.42 nm was visible (increased by 27 %) [53-57]. We attribute this difference in d-spacing to the presence of N and O atoms in the interstitial sites generating such large discontinuities and promoting the formation of dislocations in the graphene structure. It is perhaps interesting to see that the graphitic structures (Fig. 6.7a, right bottom) have a d-spacing within 2-3 % of that reported for graphite [58]. The observed inter-lattice spacing in our films (Fig. 6.7b and 6.7c) was significantly lower than 0.86 nm reported for graphene oxide [59].

The x-ray diffractograms (XRD) of the samples did not show any peak other than that arising from the silicon substrate (Fig. S7). While this is typical for graphene, the absence of the characteristic peak of GO at 10.2° and a lattice spacing greater than that of graphene observed in the TEM studies showed that our sample could be a reduced form of N-GO with less number of O and OH bonds in the inter-planar regions [60]. The electrical conductivity measurements showed that the samples were highly resistive, which also indicated the oxidized form of carbon present in the sample. On comparing all the results, it could be concluded that the islands seen in the optical microscope and SEM images consisted primarily of N-GO with a reduced number of inter-planar species. Nucleation of graphene oxide takes place on the substrate at the beginning of the growth process. The mismatch between silicon and N-GO lattices and the fast

film growth rate in the microwave plasma process create significant stress in the growing film. As a result, the film does not grow laterally on the substrate; rather it grows away from the substrate forming islands. From Fig. S2, it is clear that that the nucleation site density does not increase notably with increase in plasma power; however, the islands grow in size with power. Although the island formation on an initially formed mono or bi-layer N-GO similar to the Stranski-Krastanov growth process is possible, we did not get sufficient evidences to confirm this type of growth.

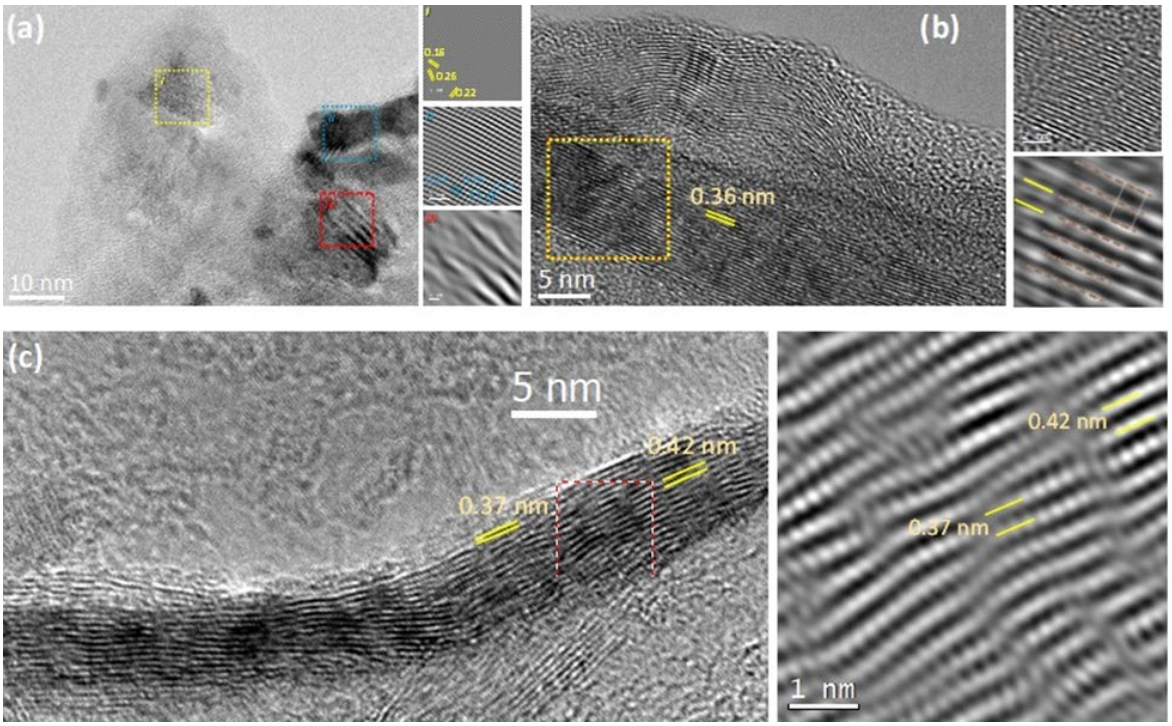

Fig 6.7: TEM images of the (a-b) 80 W and (c) 150 W films grown on silicon. The high resolution images of the regions marked in the left-side images are given in the right side of each part of the figure

Fig. 6.8 compares the EIS results of the bare GCE and the N-GO coated GCE obtained in 0.1 M KCl aqueous solution containing 5 mM $K_3Fe(CN)_6$. The plots were analysed using the Randles equivalent circuit model. It was found that the series resistance of the GCE and the N-GO coated GCE were nearly ~100 Ω, indicating that the series resistance remained unchanged

even after coating the glassy carbon electrode with the N-GO. It is in good agreement with the previous reports [61-63]. However, the charge-transfer resistance (R_{ct}), which is associated with the charge-transfer resistance across the electrode and electrolyte interface, significantly increased from 206 Ω to 1.2 kΩ after the GCE was coated by the N-GO nanosheets, demonstrating their high resistance to the electron transfer reaction at the surface.

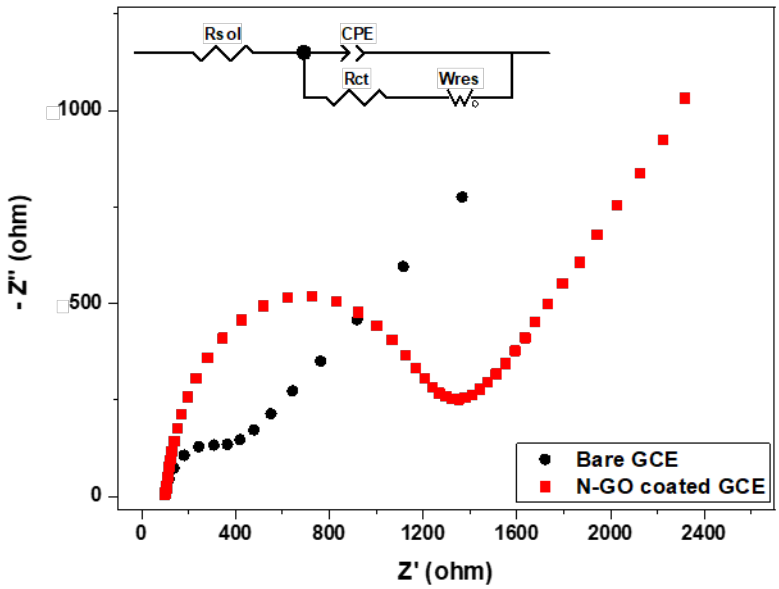

Fig 6.8: The electrochemical impedance spectroscopy (EIS) of (a) bare GCE (b) N-GO coated GCE in 0.1 M KCl aqueous solution containing 5 mM $K_3Fe(CN)_6$. The inset shows the Randles equivalent circuit model

6.1.4 Performance of N-GO membrane in water purification system

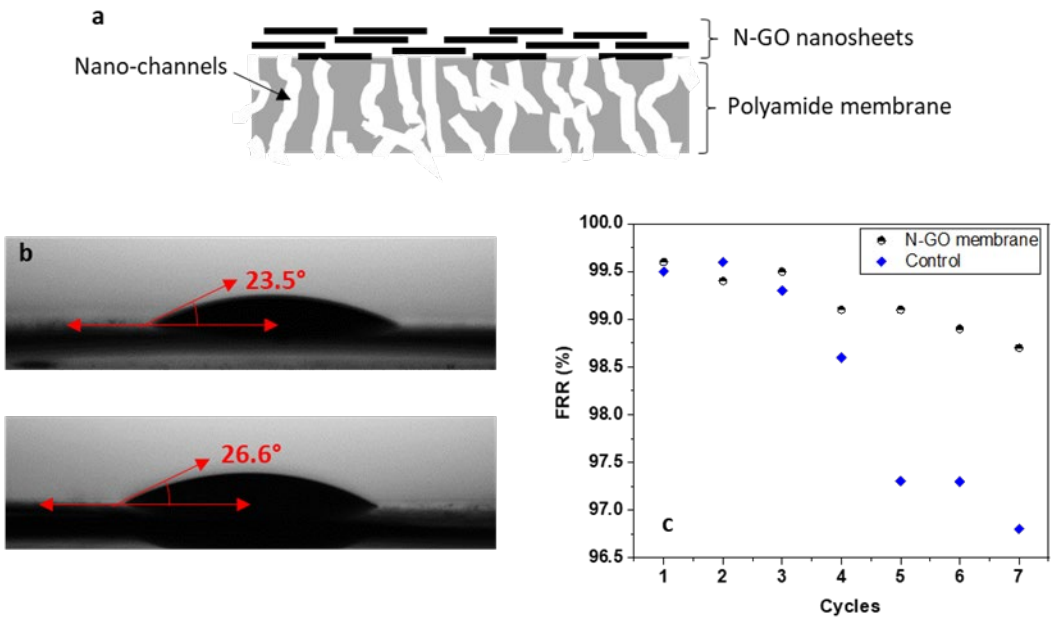

Fig 6.9: (a) Schematic presentation of N-GO coated-PA membrane (b) water contact angle of control and (c) N-GO coated-PA membrane (d) graph showing flux recovery ratio against the number of water filtration cycles

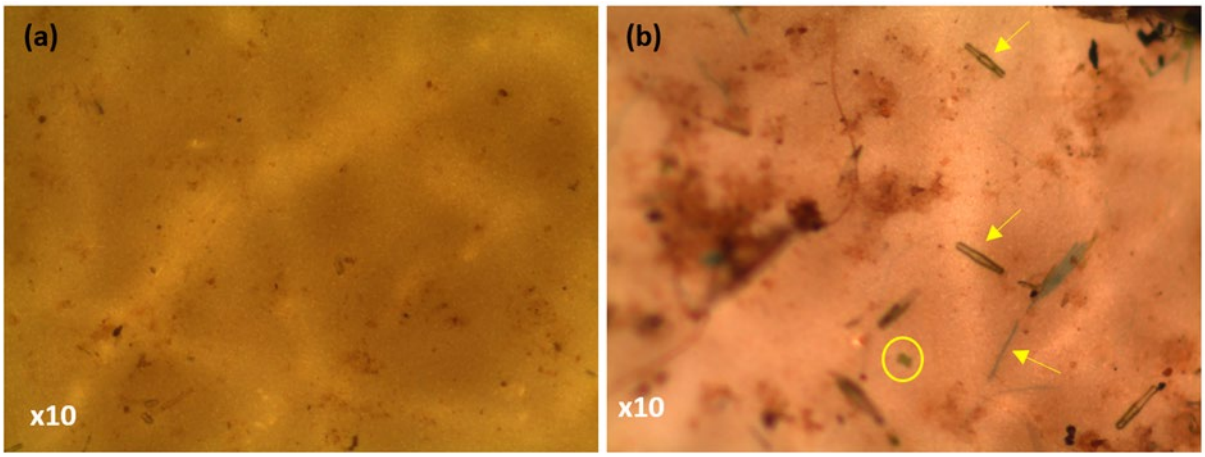

Fig 6.10: Microscopic images showing the degree of algal growth on (a) N-GO coated and (b) control polyamide membranes

The N-GO nanosheets exhibited strong potential for use in water purification membranes. Water purification has become the center of attention in research because of water scarcity and the lack of availability of safe drinking water. In order to address this issue, desalination and

wastewater recycling using polymeric membranes are considered the most promising alternative approaches. However, the “trade-off” between permeability and fouling resistance puts polymeric membranes at a disadvantage. Graphene-based materials have been employed to successfully combat this problem; however, these efforts have been limited to the study of anti-microbial activity, protein fouling, membrane flux and rejection rate, and chlorine resistance [64]. The anti-scaling and algicidal properties of such a membrane have not yet been rigorously investigated.

In this study, we casted N-GO solution on a commercially available 0.22 µm pore size hydrophilic polyamide (PA) membrane. The N-GO coated membrane is shown in Fig. S8, and a schematic illustration of the process is given in Fig. 6.9-a. The AFM images of pristine and N-GO coated membranes showed the typical surfaces that are rough (Fig. S9). Both the membranes showed an average surface roughness (Sa) of 80.8 nm, indicating trivial effects of N-GO coating on the surface morphology of pristine membrane. Moreover, a negligible increase in water contact angle, i.e. ~3° in N-GO coated-PA was observed when compared with pristine PA (Fig. 6.9-b and 6.9-c). Since the water contact angle has a direct relationship with water flux, it suggests that N-GO coating did not compromise the water flux rate. This could be accredited to the oxygen functional groups in N-GO, i.e. epoxides, carboxyl, carbonyl, hydroxyl, etc. The result is in agreement with the study performed by Choi et al. [65]. They also did not find GO coating on PA membrane was altering the water flux rate.

The anti-scaling property of N-GO coated-PA was investigated by comparing its flux recovery ratio (FRR) with that of pristine PA membrane. FRR refers to the percentage of the feed water that has been recovered. For this purpose, a sample feed solution of 1 g NaCl/L water was prepared. A specific vacuum filtration system was used for the purification experiments. The 7 cycles of purification were run, and after each cycle, membranes were thoroughly washed

with distilled water. The flux rate (J) and flux recovery ratio (FRR) were measured using equations 1 and 2 respectively.

$$J = \frac{\mathrm{V}}{\mathrm{A}} \times t \qquad (1)$$

$$FRR = \frac{\mathrm{J2}}{\mathrm{J1}} \times 100 \qquad (2)$$

Here V, A, and t are the volume (in liters) of penetrative water, the effective filtration area (19 cm^2) of the membrane, and the operation time (h) of permeation, respectively. J_1 is the flux of the previous cycle and J_2 is the flux of the next cycle.

The results obtained are shown graphically in Fig. 6.9-d. After each cycle, a slight decrease in FRR was observed in both the membranes. However, overall, the N-GO coated-PA membrane displayed better FRR, indicating comparatively less buildup of the salts. By the end of the seventh cycle of the experiment, FRR of the control PA membrane decreased below 97%, whereas, N-GO coated-PA membrane maintained a value above 98%.

The extent of algicidal activity of the synthesized N-GO was evaluated by immersing both N-GO coated and control PA membranes in pond water (located at the Palmetum botanical garden, Townsville, Australia) for 10 days. Following the designated period of exposure to fresh water algae, the samples were visualized using a compound microscope at 10X magnification. The microscopic images, shown in Fig. 6.10, revealed that in relation to pristine membrane, the N-GO coated PA membrane exhibited notable inhibitation of algae growth. The anti-biofouling ability of our N-GO films is clearly superior to those of other graphene-based materials [66, 67]. These N-GO films do not have to be converted into nanocomposites like in other cases for their use in anti-biofouling applications.

6.1.5 Conclusion

In a nutshell, N-GO nanosheets were produced from aniline in a single-step procedure using atmospheric pressure microwave plasma. A microwave power as low as 80 W could successfully dissociate aniline vapors into N-GO nanosheets, which were later collected from the walls of the quartz tube. The Raman spectrum yielded I_{2D}/I_G and FWHM values of 1.04 and 64 cm^{-1} respectively, indicative of multiple layers of N-GO sheets. Moreover, the XPS spectra revealed more than 3 % of nitrogen retention in an 80 W sample. Lastly, the N-GO-coated PA membrane showcased remarkable anti-scaling and algicidal activity without compromising the water flux rate measured through a stable water contact angle.

Supplementary

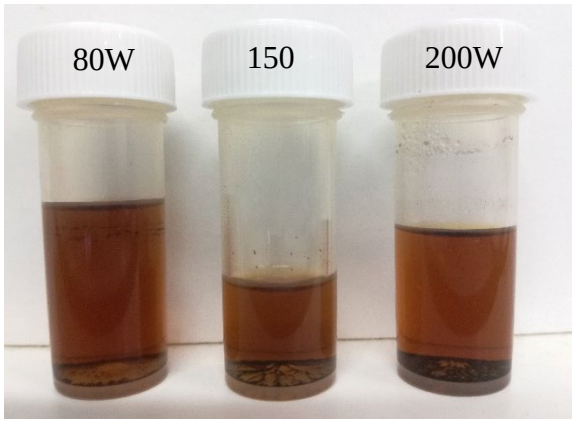

Figure S1. A well-dispersed N-GO in ethanol

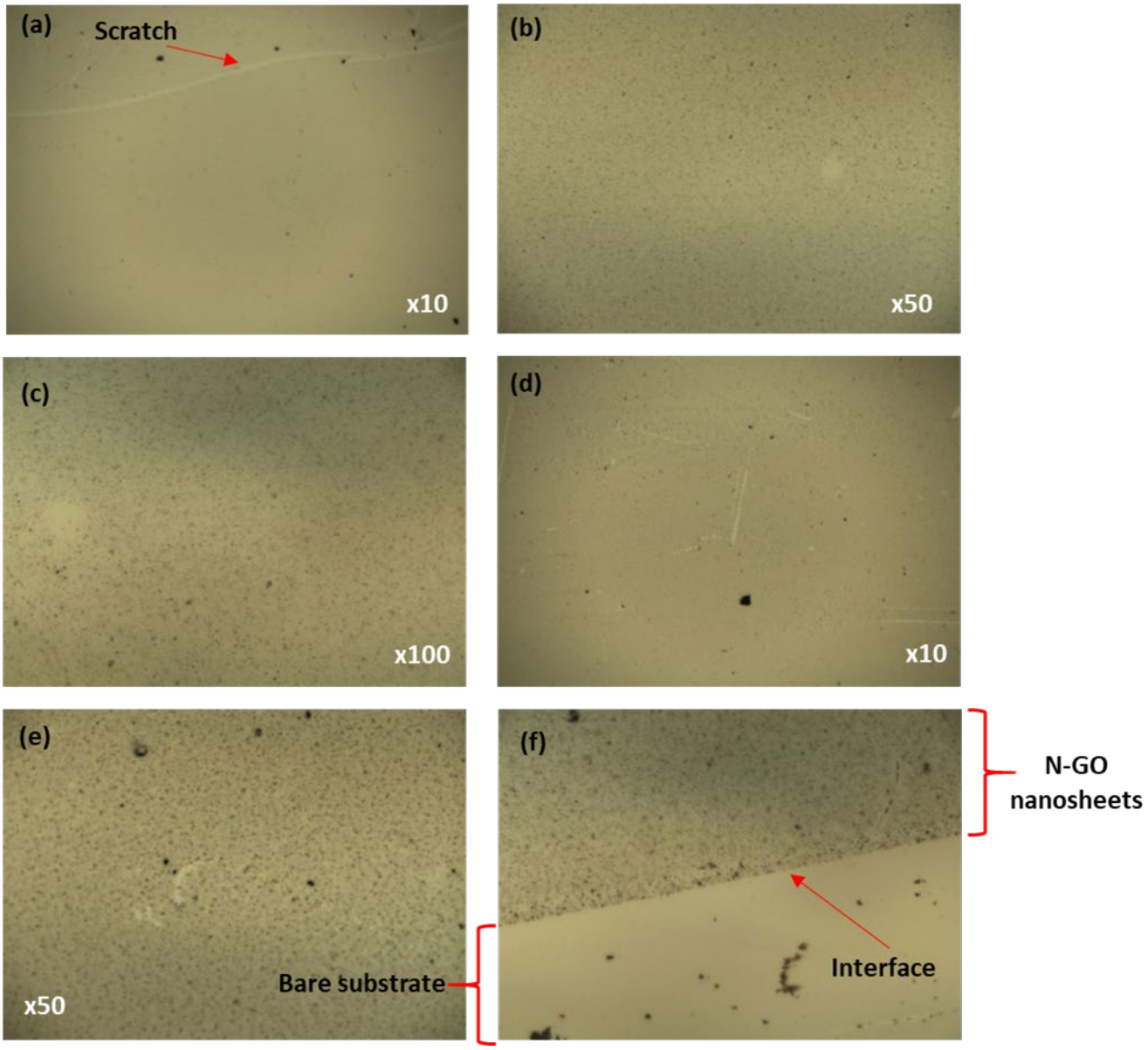

Figure S2. Microscopic images of N-GO synthesized at plasma power of **(a-c)** 80 W **(d-f)** 200 W on silicon substrate

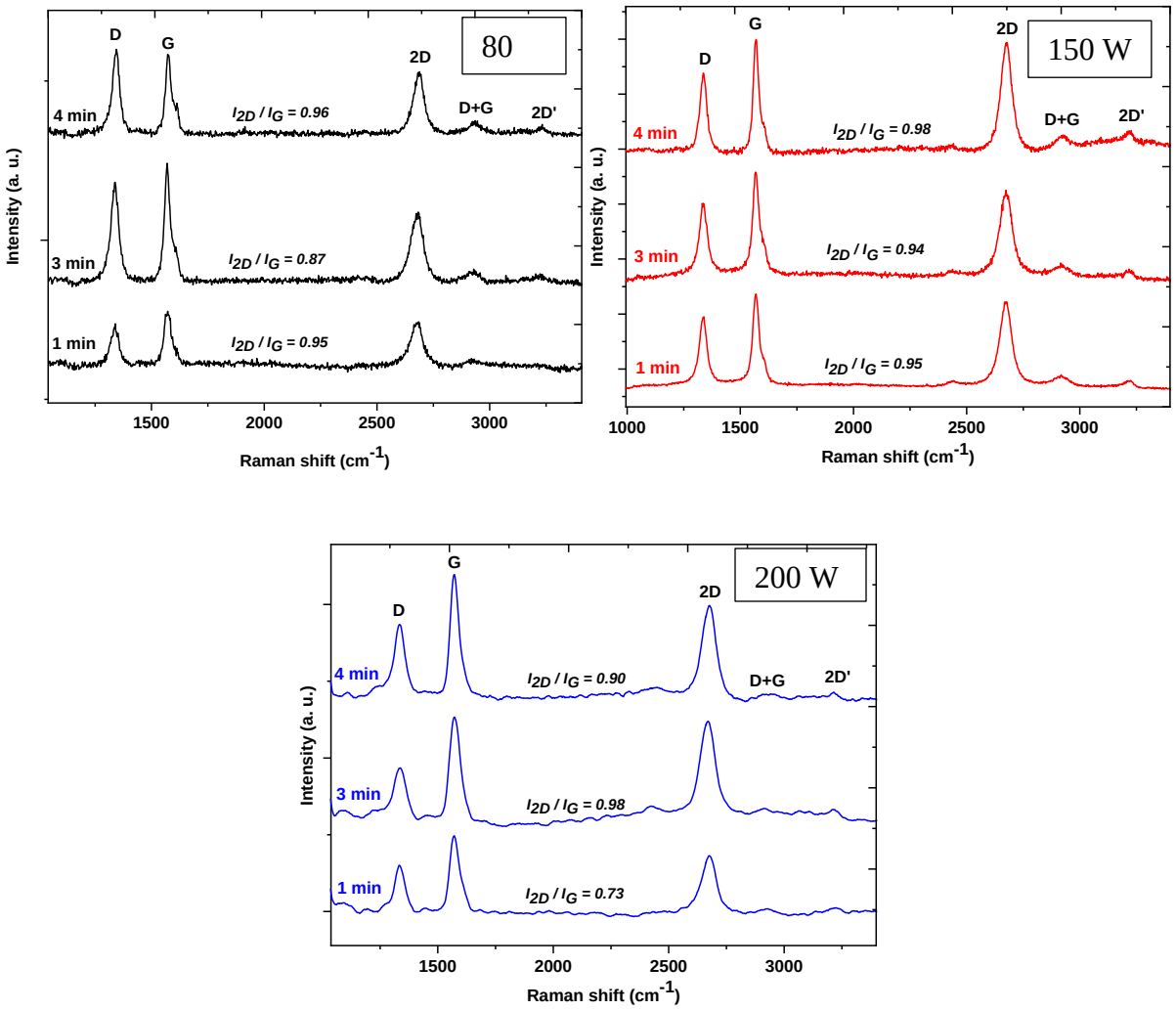

Figure S3. Raman spectra of N-GO samples showing the effects of 1, 3 and 4 min precursor supply time for 80 W, 150 W, 200 W samples

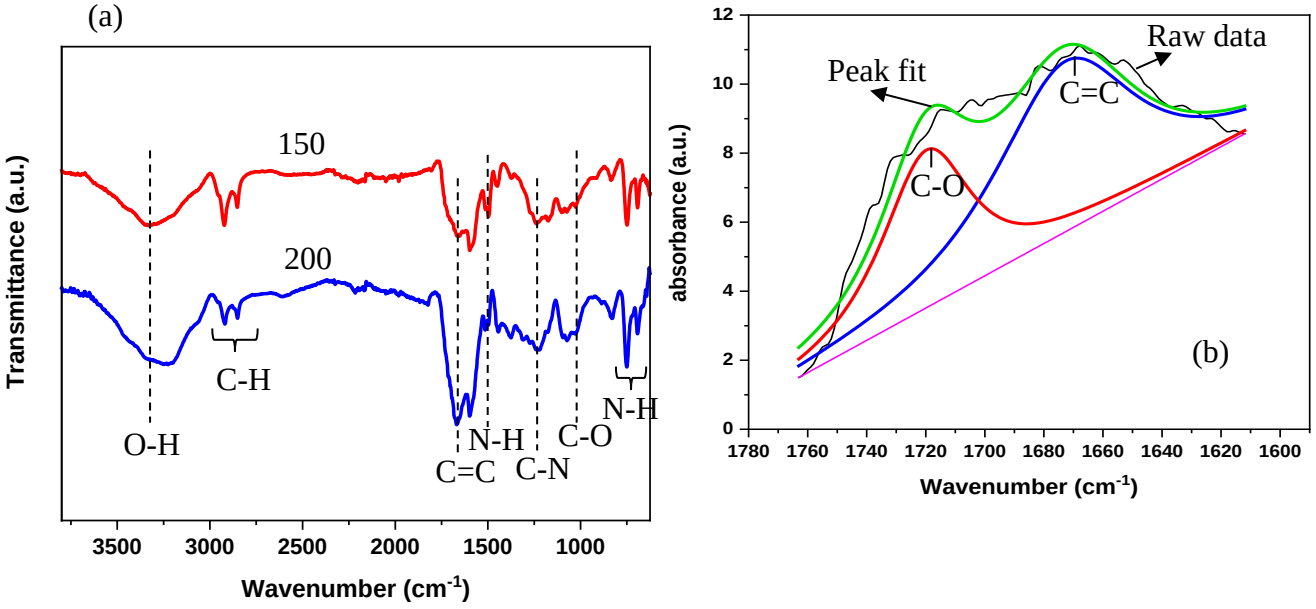

Figure S4 (a). FTIR spectrum of N-GO sample synthesized at 150 W and 200 W **(b)**

Deconvoluted peaks of FTIR spectra of 80 W sample

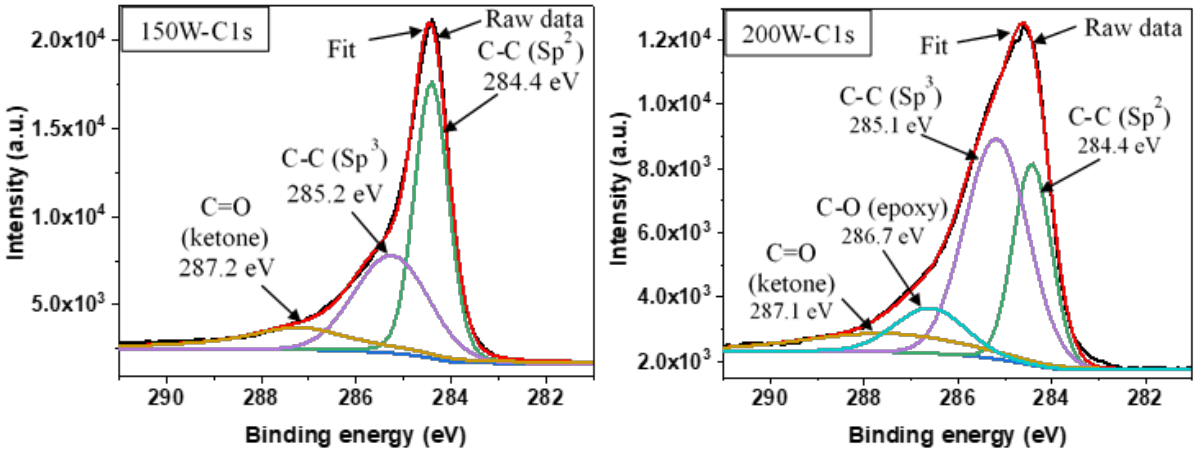

Figure S5. Deconvoluted peaks of high-resolution C1s XPS spectra of 150 and 200 W

samples

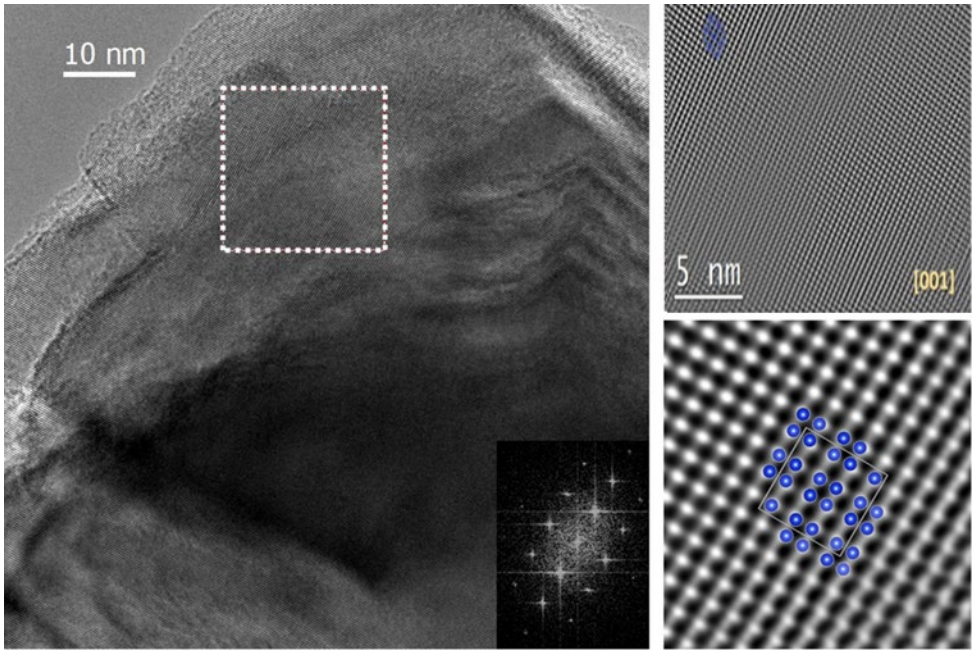

Figure S6. Low (left) and high (right) resolution images of the silicon substrate used for growing N-GO.

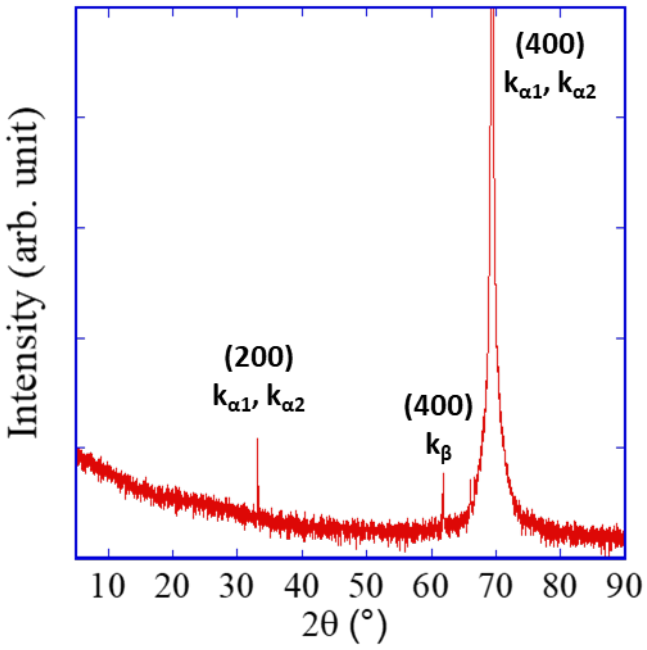

Figure S7. X-ray diffractogram of silicon (100) substrate. Only the peak from silicon is visible.

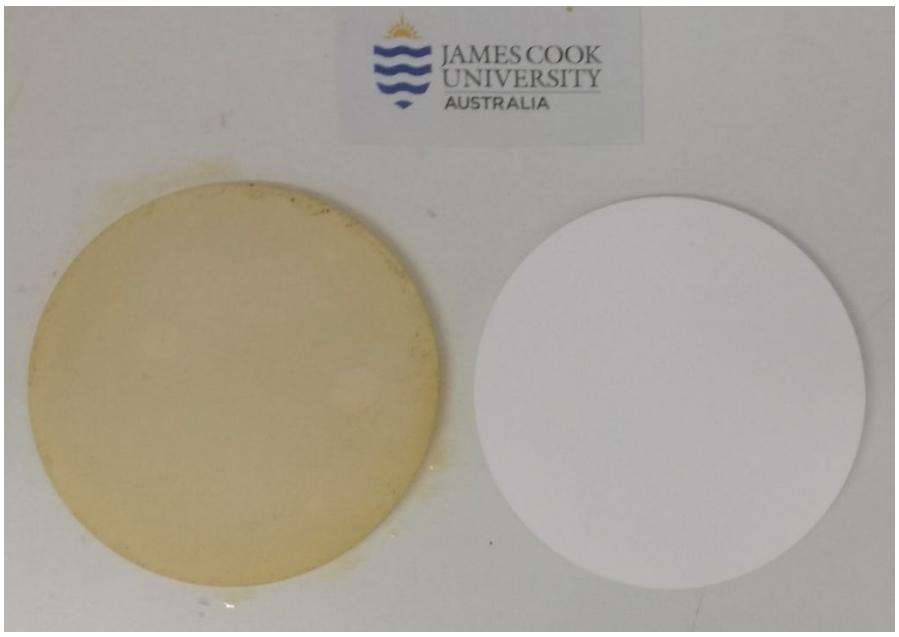

Figure S8. N-GO coated (*left*) and pristine (*right*) polyamide membrane

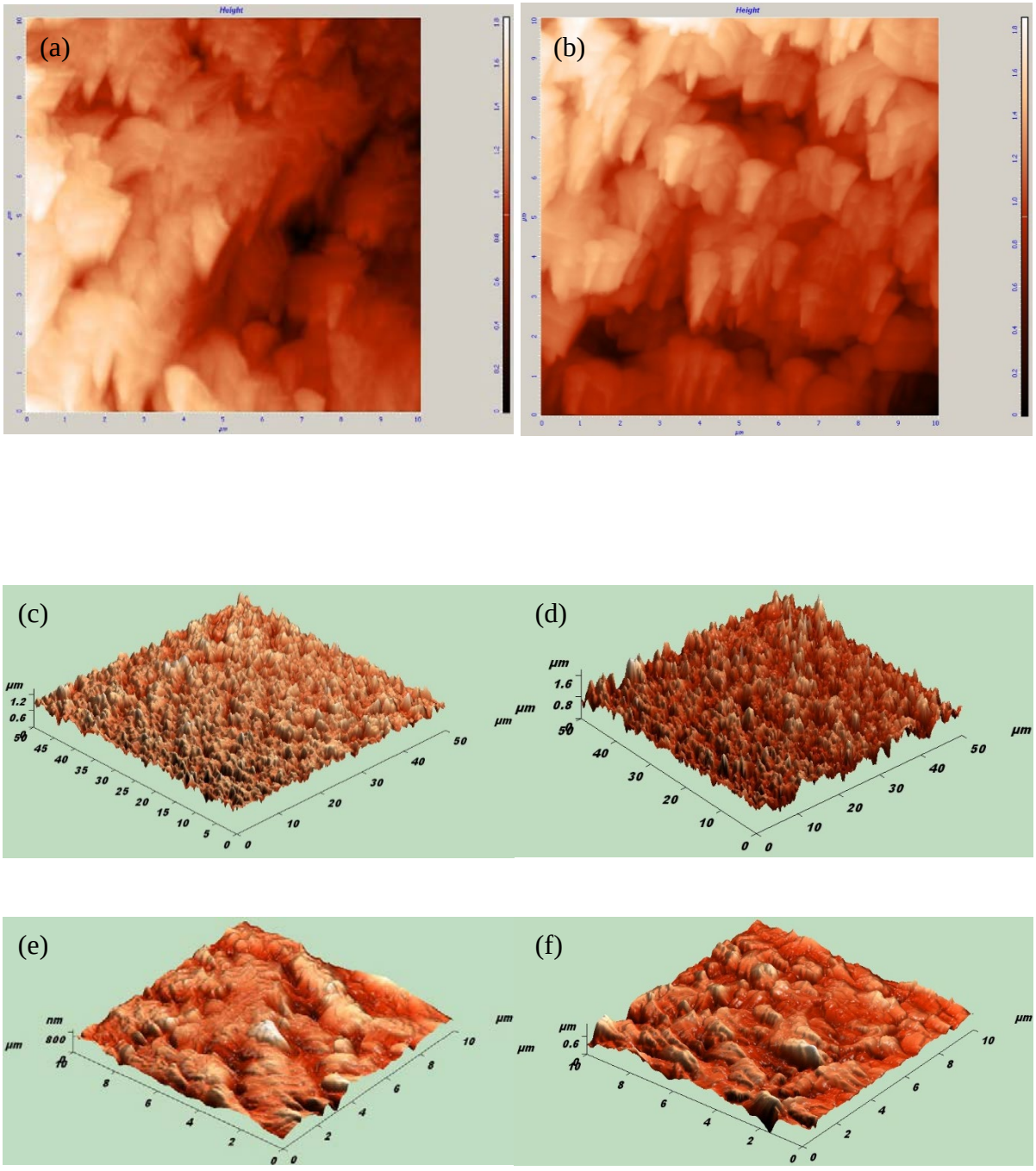

Figure S9. Results from AFM: 2D images of (a) pristine and (b) N-GO coated-polyamide membrane, 3D images of (c & e) pristine and (d & f) N-GO coated polyamide membrane

References

1. Geim, A.K. and K.S. Novoselov, *The rise of graphene*, in *Nanoscience and technology: a collection of reviews from nature journals*. 2010, World Scientific. p. 11-19.
2. Tsang, C.H.A., H. Huang, J. Xuan, H. Wang, and D. Leung, *Graphene materials in green energy applications: recent development and future perspective.* Renewable and Sustainable Energy Reviews, 2020. **120**: p. 109656.
3. Jacob, M.V., R.S. Rawat, B. Ouyang, K. Bazaka, D.S. Kumar, D. Taguchi, M. Iwamoto, R. Neupane, and O.K. Varghese, *Catalyst-Free Plasma Enhanced Growth of Graphene from Sustainable Sources.* Nano Letters, 2015. **15**(9): p. 5702-5708.
4. Singh, R.K., R. Kumar, and D.P. Singh, *Graphene oxide: strategies for synthesis, reduction and frontier applications.* Rsc Advances, 2016. **6**(69): p. 64993-65011.
5. Yang, K., J. Wang, X. Chen, Q. Zhao, A. Ghaffar, and B. Chen, *Application of graphene-based materials in water purification: from the nanoscale to specific devices.* Environmental Science: Nano, 2018. **5**(6): p. 1264-1297.
6. Cui, L., X. Chen, B. Liu, K. Chen, Z. Chen, Y. Qi, H. Xie, F. Zhou, M.H. Rümmeli, Y. Zhang, and Z. Liu, *Highly Conductive Nitrogen-Doped Graphene Grown on Glass toward Electrochromic Applications.* ACS Applied Materials & Interfaces, 2018. **10**(38): p. 32622-32630.
7. Nandanapalli, K.R., D. Mudusu, and S. Lee, *Functionalization of graphene layers and advancements in device applications.* Carbon, 2019. **152**: p. 954-985.
8. Kuila, T., S. Bose, A.K. Mishra, P. Khanra, N.H. Kim, and J.H. Lee, *Chemical functionalization of graphene and its applications.* Progress in Materials Science, 2012. **57**(7): p. 1061-1105.

9. Rodriguez-Pastor, I., G. Ramos-Fernandez, H. Varela-Rizo, M. Terrones, and I. Martin-Gullon, *Towards the understanding of the graphene oxide structure: How to control the formation of humic- and fulvic-like oxidized debris.* Carbon, 2015. **84**: p. 299-309.

10. Korkmaz, S. and İ.A. Kariper, *Graphene and graphene oxide based aerogels: Synthesis, characteristics and supercapacitor applications.* Journal of Energy Storage, 2020. **27**: p. 101038.

11. Pei, S., Q. Wei, K. Huang, H.-M. Cheng, and W. Ren, *Green synthesis of graphene oxide by seconds timescale water electrolytic oxidation.* Nature communications, 2018. **9**(1): p. 1-9.

12. Wu, Y., P. Jia, L. Xu, Z. Chen, L. Xiao, J. Sun, J. Zhang, Y. Huang, C.W. Bielawski, and J. Geng, *Tuning the Surface Properties of Graphene Oxide by Surface-Initiated Polymerization of Epoxides: An Efficient Method for Enhancing Gas Separation.* ACS Applied Materials & Interfaces, 2017. **9**(5): p. 4998-5005.

13. Li, D., X. Duan, H. Sun, J. Kang, H. Zhang, M.O. Tade, and S. Wang, *Facile synthesis of nitrogen-doped graphene via low-temperature pyrolysis: the effects of precursors and annealing ambience on metal-free catalytic oxidation.* Carbon, 2017. **115**: p. 649-658.

14. Bundaleska, N., J. Henriques, M. Abrashev, A.B. do Rego, A. Ferraria, A. Almeida, F. Dias, E. Valcheva, B. Arnaudov, and K. Upadhyay, *Large-scale synthesis of free-standing N-doped graphene using microwave plasma.* Scientific reports, 2018. **8**(1): p. 1-11.

15. Zhang, L., Y. Ye, D. Cheng, W. Zhang, H. Pan, and J. Zhu, *Simultaneous reduction and N-doping of graphene oxides by low-energy N2+ ion sputtering.* Carbon, 2013. **62**: p. 365-373.

16. Vieira, O., R.S. Ribeiro, M. Pedrosa, A.R. Lado Ribeiro, and A.M.T. Silva, *Nitrogen-doped reduced graphene oxide – PVDF nanocomposite membrane for persulfate activation and degradation of water organic micropollutants.* Chemical Engineering Journal, 2020. **402**: p. 126117.

17. Brisebois, P. and M. Siaj, *Harvesting graphene oxide–years 1859 to 2019: a review of its structure, synthesis, properties and exfoliation.* Journal of Materials Chemistry C, 2020. **8**(5): p. 1517-1547.

18. Wang, H., Q. Fu, and C. Pan, *Green mass synthesis of graphene oxide and its MnO2 composite for high performance supercapacitor.* Electrochimica Acta, 2019. **312**: p. 11-21.

19. Smith, A.T., A.M. LaChance, S. Zeng, B. Liu, and L. Sun, *Synthesis, properties, and applications of graphene oxide/reduced graphene oxide and their nanocomposites.* Nano Materials Science, 2019. **1**(1): p. 31-47.

20. Hadish, F., S. Jou, B.-R. Huang, H.-A. Kuo, and C.-W. Tu, *Functionalization of CVD grown graphene with downstream oxygen plasma treatment for glucose sensors.* Journal of The Electrochemical Society, 2017. **164**(7): p. B336.

21. Liu, Y. and Y.M. Chen, *Synthesis of large scale graphene oxide using plasma enhanced chemical vapor deposition method and its application in humidity sensing.* Journal of Applied Physics, 2016. **119**(10): p. 103301.

22. Li, X., H. Wang, J.T. Robinson, H. Sanchez, G. Diankov, and H. Dai, *Simultaneous nitrogen doping and reduction of graphene oxide.* Journal of the American Chemical Society, 2009. **131**(43): p. 15939-15944.

23. Tao, H., C. Yan, A.W. Robertson, Y. Gao, J. Ding, Y. Zhang, T. Ma, and Z. Sun, *N-Doping of graphene oxide at low temperature for the oxygen reduction reaction.* Chemical Communications, 2017. **53**(5): p. 873-876.

24. Wang, Y., Y. Shao, D.W. Matson, J. Li, and Y. Lin, *Nitrogen-doped graphene and its application in electrochemical biosensing.* ACS nano, 2010. **4**(4): p. 1790-1798.

25. Katoh, T., G. Imamura, S. Obata, and K. Saiki, *Growth of N-doped graphene from nitrogen containing aromatic compounds: the effect of precursors on the doped site.* RSC advances, 2016. **6**(16): p. 13392-13398.

26. Ito, Y., C. Christodoulou, M.V. Nardi, N. Koch, H. Sachdev, and K. Müllen, *Chemical vapor deposition of N-doped graphene and carbon films: the role of precursors and gas phase.* ACS nano, 2014. **8**(4): p. 3337-3346.

27. Zheng, B., *One-step synthesis of nitrogen-doped graphene from a sole aromatic precursor*. Materials Letters, 2019. **236**: p. 583-586.

28. Boas, C.R.S.V., B. Focassio, E. Marinho, D.G. Larrude, M.C. Salvadori, C.R. Leão, and D.J. Dos Santos, *Characterization of nitrogen doped graphene bilayers synthesized by fast, low temperature microwave plasma-enhanced chemical vapour deposition.* Scientific reports, 2019. **9**(1): p. 1-12.

29. Kumar, N.A., H. Nolan, N. McEvoy, E. Rezvani, R.L. Doyle, M.E. Lyons, and G.S. Duesberg, *Plasma-assisted simultaneous reduction and nitrogen doping of graphene oxide nanosheets.* Journal of Materials Chemistry A, 2013. **1**(14): p. 4431-4435.

30. Dato, A., V. Radmilovic, Z. Lee, J. Phillips, and M. Frenklach, *Substrate-free gas-phase synthesis of graphene sheets.* Nano letters, 2008. **8**(7): p. 2012-2016.

31. Dato, A., *Graphene synthesized in atmospheric plasmas—A review.* Journal of Materials Research, 2019. **34**(1): p. 214-230.

32. Jašek, O., J. Toman, J. Jurmanová, M. Šnírer, V. Kudrle, and V. Buršíková, *Study of graphene layer growth on dielectric substrate in microwave plasma torch at atmospheric pressure.* Diamond and Related Materials, 2020. **105**: p. 107798.

33. Tatarova, E., A. Dias, E. Felizardo, N. Bundaleski, M. Abrashev, J. Henriques, Z. Rakocevic, and L. Alves, *Microwave Plasmas Applied for Synthesis of Free-Standing Carbon Nanostructures at Atmospheric Pressure Conditions.* Journal of Magnetohydrodynamics and Plasma Research, 2016. **21**(2): p. 185.

34. Tsyganov, D., N. Bundaleska, E. Tatarova, A. Dias, J. Henriques, A. Rego, A. Ferraria, M. Abrashev, F. Dias, and C.C. Luhrs, *On the plasma-based growth of 'flowing'graphene sheets at atmospheric pressure conditions.* Plasma Sources Science and Technology, 2015. **25**(1): p. 015013.

35. Münzer, A., L. Xiao, Y.H. Sehlleier, C. Schulz, and H. Wiggers, *All gas-phase synthesis of graphene: Characterization and its utilization for silicon-based lithium-ion batteries.* Electrochimica Acta, 2018. **272**: p. 52-59.

36. Bundaleska, N., D. Tsyganov, A. Dias, E. Felizardo, J. Henriques, F. Dias, M. Abrashev, J. Kissovski, and E. Tatarova, *Microwave plasma enabled synthesis of free standing carbon nanostructures at atmospheric pressure conditions.* Physical Chemistry Chemical Physics, 2018. **20**(20): p. 13810-13824.

37. Rincón, R., C. Melero, M. Jiménez, and M. Calzada, *Synthesis of multi-layer graphene and multi-wall carbon nanotubes from direct decomposition of ethanol by microwave plasma without using metal catalysts.* Plasma Sources Science and Technology, 2015. **24**(3): p. 032005.

38. Huang, W. and S. Ptasinska, *Functionalization of graphene by atmospheric pressure plasma jet in air or H2O2 environments.* Applied Surface Science, 2016. **367**: p. 160-166.

39. Huang, C.-H. and T.-H. Lu, *Rapid oxidation of CVD-grown graphene using mild atmospheric pressure O2 plasma jet.* Surface and Coatings Technology, 2018. **350**: p. 1085-1090.

40. Liu, L., D. Xie, M. Wu, X. Yang, Z. Xu, W. Wang, X. Bai, and E. Wang, *Controlled oxidative functionalization of monolayer graphene by water-vapor plasma etching.* Carbon, 2012. **50**(8): p. 3039-3044.

41. Tatarova, E., A. Dias, J. Henriques, M. Abrashev, N. Bundaleska, E. Kovacevic, N. Bundaleski, U. Cvelbar, E. Valcheva, and B. Arnaudov, *Towards large-scale in free-standing graphene and N-graphene sheets.* Scientific reports, 2017. **7**(1): p. 1-16.

42. Tsyganov, D., N. Bundaleska, A. Dias, J. Henriques, E. Felizardo, M. Abrashev, J. Kissovski, A.B. do Rego, A. Ferraria, and E. Tatarova, *Microwave plasma-based direct synthesis of free-standing N-graphene.* Physical Chemistry Chemical Physics, 2020. **22**(8): p. 4772-4787.

43. Liu, B., C.-M. Yang, Z. Liu, and C.-S. Lai, *N-doped graphene with low intrinsic defect densities via a solid source doping technique.* Nanomaterials, 2017. **7**(10): p. 302.

44. Xie, B., Y. Chen, M. Yu, X. Shen, H. Lei, T. Xie, Y. Zhang, and Y. Wu, *Carboxyl-assisted synthesis of nitrogen-doped graphene sheets for supercapacitor applications.* Nanoscale research letters, 2015. **10**(1): p. 332.

45. Wang, M. and Y. Ma, *Nitrogen-doped graphene forests as electrodes for high-performance wearable supercapacitors.* Electrochimica Acta, 2017. **250**: p. 320-326.

46. Li, J., X. Li, P. Zhao, D.Y. Lei, W. Li, J. Bai, Z. Ren, and X. Xu, *Searching for magnetism in pyrrolic N-doped graphene synthesized via hydrothermal reaction.* Carbon, 2015. **84**: p. 460-468.

47. Du, M., J. Sun, J. Chang, F. Yang, L. Shi, and L. Gao, *Synthesis of nitrogen-doped reduced graphene oxide directly from nitrogen-doped graphene oxide as a high-performance lithium ion battery anode.* RSC Advances, 2014. **4**(80): p. 42412-42417.

48. Hao, Y., Y. Wang, L. Wang, Z. Ni, Z. Wang, R. Wang, C.K. Koo, Z. Shen, and J.T. Thong, *Probing layer number and stacking order of few-layer graphene by Raman spectroscopy*. small, 2010. **6**(2): p. 195-200.

49. Yang, W., Z. Du, Z. Ma, G. Wang, H. Bai, and G. Shao, *Facile synthesis of nitrogen-doped hierarchical porous lamellar carbon for high-performance supercapacitors.* RSC advances, 2016. **6**(5): p. 3942-3950.

50. Porwal, J., N. Karanwal, S. Kaul, and S.L. Jain, *Carbocatalysis: N-doped reduced graphene oxide catalyzed esterification of fatty acids with long chain alcohols.* New Journal of Chemistry, 2016. **40**(2): p. 1547-1553.

51. Liu, Y., L. Yu, C.N. Ong, and J. Xie, *Nitrogen-doped graphene nanosheets as reactive water purification membranes.* Nano Research, 2016. **9**(7): p. 1983-1993.

52. Wei, D., Y. Liu, Y. Wang, H. Zhang, L. Huang, and G. Yu, *Synthesis of N-doped graphene by chemical vapor deposition and its electrical properties.* Nano letters, 2009. **9**(5): p. 1752-1758.

53. Wang, Y., Z. Su, W. Wu, S. Nie, N. Xie, H. Gong, Y. Guo, J. Hwan Lee, S. Xing, and X. Lu, *Resonance Raman spectroscopy of G-line and folded phonons in twisted bilayer graphene with large rotation angles.* Applied Physics Letters, 2013. **103**(12): p. 123101.

54. Calderon, H., I. Estrada-Guel, F. Alvarez-Ramírez, V. Hadjiev, and F.R. Hernandez, *Morphed graphene nanostructures: experimental evidence for existence.* Carbon, 2016. **102**: p. 288-296.

55. Wang, Y., Z. Su, W. Wu, S. Nie, X. Lu, H. Wang, K. McCarty, S.-s. Pei, F. Robles-Hernandez, and V.G. Hadjiev, *Four-fold Raman enhancement of 2D band in twisted bilayer graphene: evidence for a doubly degenerate Dirac band and quantum interference.* Nanotechnology, 2014. **25**(33): p. 335201.

56. Calderon, H., A. Okonkwo, I. Estrada-Guel, V. Hadjiev, F. Alvarez-Ramírez, and F.R. Hernández, *HRTEM low dose: the unfold of the morphed graphene, from amorphous carbon to morphed graphenes.* Advanced structural and chemical imaging, 2016. **2**(1): p. 1-12.

57. Calderon, H., F.A. Ramirez, D. Barber, V. Hadjiev, A. Okonkwo, R.O. Olivares, I.E. Guel, and F.R. Hernandez, *Enhanced elastic behavior of all-carbon composites reinforced by in-situ synthesized morphed graphene.* Carbon, 2019. **153**: p. 657-662.

58. Belenkov, E., *Formation of graphite structure in carbon crystallites.* Inorganic Materials, 2001. **37**(9): p. 928-934.

59. Huang, H.-H., R.K. Joshi, K.K.H. De Silva, R. Badam, and M. Yoshimura, *Fabrication of reduced graphene oxide membranes for water desalination.* Journal of membrane science, 2019. **572**: p. 12-19.

60. Zhang, L., X. Yu, H. Hu, Y. Li, M. Wu, Z. Wang, G. Li, Z. Sun, and C. Chen, *Facile synthesis of iron oxides/reduced graphene oxide composites: application for electromagnetic wave absorption at high temperature.* Scientific reports, 2015. **5**(1): p. 1-9.

61. Lei, P., Y. Zhou, R. Zhu, Y. Liu, C. Dong, and S. Shuang, *Facile synthesis of iron phthalocyanine functionalized N, B–doped reduced graphene oxide nanocomposites and sensitive electrochemical detection for glutathione.* Sensors and Actuators B: Chemical, 2019. **297**: p. 126756.

62. Wang, Y., W. Cao, L. Wang, Q. Zhuang, and Y. Ni, *Electrochemical determination of 2, 4, 6-trinitrophenol using a hybrid film composed of a copper-based metal organic framework and electroreduced graphene oxide.* Microchimica Acta, 2018. **185**(6): p. 1-9.

63. Karthik, R., M. Govindasamy, S.-M. Chen, T.-W. Chen, A. Elangovan, V. Muthuraj, and M.-C. Yu, *A facile graphene oxide based sensor for electrochemical detection of prostate anti-cancer (anti-testosterone) drug flutamide in biological samples.* RSC advances, 2017. **7**(41): p. 25702-25709.

64. Mahmoud, K.A., B. Mansoor, A. Mansour, and M. Khraisheh, *Functional graphene nanosheets: The next generation membranes for water desalination.* Desalination, 2015. **356**: p. 208-225.

65. Choi, W., J. Choi, J. Bang, and J.-H. Lee, *Layer-by-layer assembly of graphene oxide nanosheets on polyamide membranes for durable reverse-osmosis applications.* ACS applied materials & interfaces, 2013. **5**(23): p. 12510-12519.

66. Guo, X., H. Yang, Q. Liu, J. Liu, R. Chen, H. Zhang, J. Yu, M. Zhang, R. Li, and J. Wang, *A chitosan-graphene oxide/ZIF foam with anti-biofouling ability for uranium recovery from seawater*. Chemical Engineering Journal, 2020. **382**: p. 122850.

67. Zhu, J., H. Zhang, R. Chen, Q. Liu, J. Liu, J. Yu, R. Li, M. Zhang, and J. Wang, *An anti-algae adsorbent for uranium extraction: l-Arginine functionalized graphene hydrogel loaded with Ag nanoparticles.* Journal of colloid and interface science, 2019. **543**: p. 192-200.

6.2 Application of nitrogen-doped graphene oxide

Electrochemical sensing of oxalic acid using silver nanoparticles loaded nitrogen-doped graphene oxide

Abstract

The adverse effects of oxalic acid (OA) on human health linked with its excessive consumption necessitates an improved sensor. Here, we demonstrate an electrochemical sensor for oxalic acid detection based on silver nanoparticles (Ag-Nps) and nitrogen-doped graphene oxide (N-GO) nanocomposite. N-GO, which was synthesized using atmospheric pressure microwave plasma has been first time employed for electrochemical application. The nanocomposite formation was confirmed through scanning electron microscopy and EDS elemental analysis. The nanocomposite-based sensor showed a higher current response, good selectivity and stability which can be attributed to the synergistic-effect of Ag-Nps and N-GO. Amperometric responses were proportional to the concentration of OA between 10 and 300 μM, and the detection limit was 2 μM.

6.2.1 Introduction

Oxalic acid (OA) is found naturally in a wide range of plants, animals, and microorganisms. The excessiveness of OA in the human body is considered risky for human health. For instance, OA can react with magnesium, potassium, and iron to form insoluble oxalate salts, and can remove calcium from the blood which leads to kidney stones or can interfere with the heart or nervous system [1, 2]. The US department of agriculture (USDA) recommends a certain limit of OA daily intake, for example, the allowed amount of OA consumption from spinach is 9.7 mg per 1 g serving [3]. Thus, the detection of OA in foods and urine garnered the significant interest of scientists.

The electrochemical method for the determination of OA, surpasses conventionally used techniques, such as spectroscopy [4, 5], chromatography [6], and enzymatic methods [7, 8] because of its low cost, fast procedure, good selectivity, and high sensitivity [9, 10]. Although many electrochemical sensors have been developed for OA detection [11], a sensing platform with inexpensive preparation and high analytical performance including high sensitivity and good stability is still highly desirable.

Graphene-based composite materials, such as Pt-Pd nanoparticles/chitosan/nitrogen-doped graphene [12], silver nanorods/graphene nanocomposite [13], Pd/rGO composite [14], gold nanoparticle/polypyrrole reduced graphene oxide [10], graphene aerogel [15], graphene (GR)-modified carbon ionic liquid electrode [16], platinum nanoparticle loaded graphene nanosheets [17], and Pd/Au Alloy Nps on ionic liquid functionalized graphene film have been investigated for OA detection [18]. Although these materials exhibited high catalytic activities towards OA oxidation, the usage of expensive metal Nps, such as Au, Pd and Pt raised the cost of the sensor. Silver nanoparticles (Ag-Nps) are promising alternatives in this respect, as they are less expensive than those precious metals and can achieve comparable electroanalytical

performance for the detection of OA. For OA detection, Ag-Nps has been used in composite with graphite [19] or graphene [13]. However, lengthy chemical synthesis procedures were utilized to make the composites [20].

In this work, we used Ag-Nps/N-GO modified GCE sensor for OA detection. N-GO which was synthesized using atmospheric pressure microwave plasma has been first time utilized in electrochemical sensor application. To make a nanocomposite of Ag-Nps with N-GO, a fast and efficient technique, i.e. electrodeposition was employed. Attributed to the synergistic-effect of Ag-Nps and N-GO for enhanced electrochemical properties, it has been shown how Ag-Nps/N-GO/GCE sensor can be an alternative to those expensive sensors used in past.

6.2.2 Materials and method

6.2.2.1 Chemicals and reagents

All chemicals were of analytical grade and were used as received. Aniline, sodium dihydrogen orthophosphate ($NaH_2PO_4.2H_2O$), disodium hydrogen orthophosphate (Na_2HPO_4), sodium hydroxide (NaOH), silver nitrate ($AgNO_3$), potassium nitrate (KNO_3), potassium hexacyanoferrate (III) $K_3[Fe(CN)_6]$, potassium chloride (KCl), ascorbic acid, and uric acid were obtained from Sigma Aldrich. Oxalic acid ($C_2H_2O_4.2H_2O$) and glucose were purchased from ChemSupply and Merck Australia respectively. Ultrapure water obtained from the Milli-Q water system was used throughout the investigation.

6.2.2.2 Instrumentation

Confocal laser Raman spectroscopy (Witec, 532 nm laser) and scanning electron microscopy (SEM) (Hitachi SU 500) were used to characterize the samples. Electrochemical experiments were performed on a PalmSens 4 (Palm Instruments BV, The Netherlands) potentiostat

equipped with a three-electrode system consisting of a glassy carbon working electrode (GCE), a platinum counter electrode, and an Ag/AgCl reference electrode. To investigate the electrochemical performance of the bare and modified GCE, electrochemical impedance spectroscopy (EIS), cyclic voltammetry (CV), and amperometric techniques were employed. CV of OA was conducted in 0.1 M phosphate buffer solution (PBS) (pH 7.0). EIS was recorded in a frequency range of 0.1 Hz to 100 kHz in a solution containing 0.1 M KCl and 5 mM $K_3[Fe(CN)_6]$.

6.2.2.3 Synthesis of nitrogen-doped graphene oxide

The synthesis of Nitrogen-doped graphene oxide (N-GO) was carried out in atmospheric pressure microwave plasma as reported earlier [21]. Aniline as a single-precursor was used to synthesize nitrogen-doped graphene oxide in a single-step. The microwave plasma system mainly consisted of a microwave generator (2.45 GHz), matching network and a quartz tube as shown schematically in Fig 4.11. Aniline was supplied from the top of the tube using a homemade aerosol system. Argon gas was used as a carrier for aniline vapours. As soon as the aniline vapours entered into the plasma glow, the breakdown started occurring which resultantly formed N-GO on the walls of the reaction chamber. The synthesis was conducted at optimized conditions of microwave power, aniline flow rate and fabrication time, i.e. 80 W, 3 litre per min and 3 min respectively. The N-GO was washed from the walls of the chamber using ethanol and was collected in a vial for the sensor application. A well-homogenised solution of N-GO in ethanol can be observed in the inset of Fig 6.11. To investigate the structure and morphology of N-GO, samples were collected directly on the silicon substrate from the reaction chamber. Further characterizations can be found in our previous work [21].

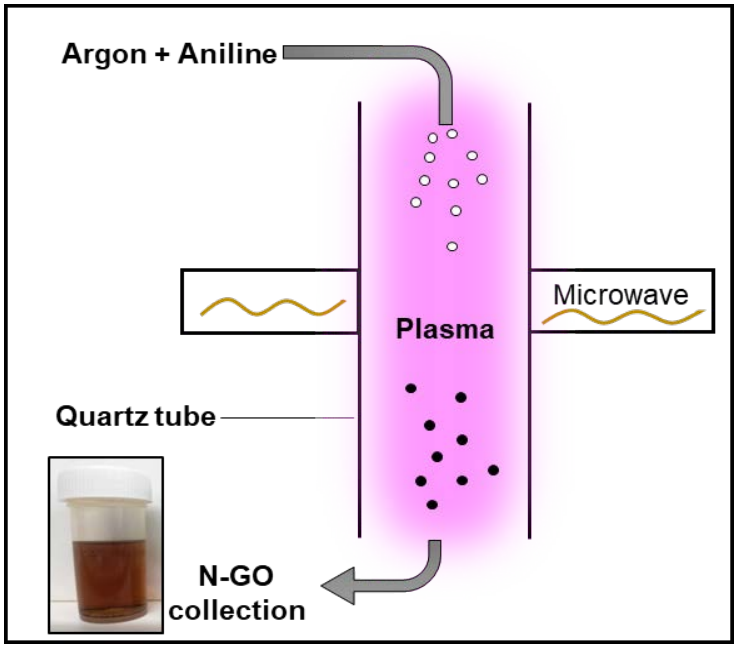

Fig 6.11: Schematic illustration of N-GO synthesis in atmospheric pressure microwave plasma

6.2.2.4 Preparation of the modified electrode

1 mg/mL solution of N-GO was prepared in ethanol for drop-casting on GCE. Before modification, GCE (3 mm diameter) was polished with 0.3 µm and 0.05 µm alumina slurry consecutively, followed by ultrasonic cleaning in ethanol and water. An aliquot of 4 µL N-GO solution was drop-casted on GCE and dried under room conditions. Electrodeposition was conducted in a 1 mM KNO_3 solution containing 0.1 mM $AgNO_3$ and at -0.2 V (vs. Ag/AgCl) potential for 350 sec. The procedure scheme is shown in Fig 6.12.

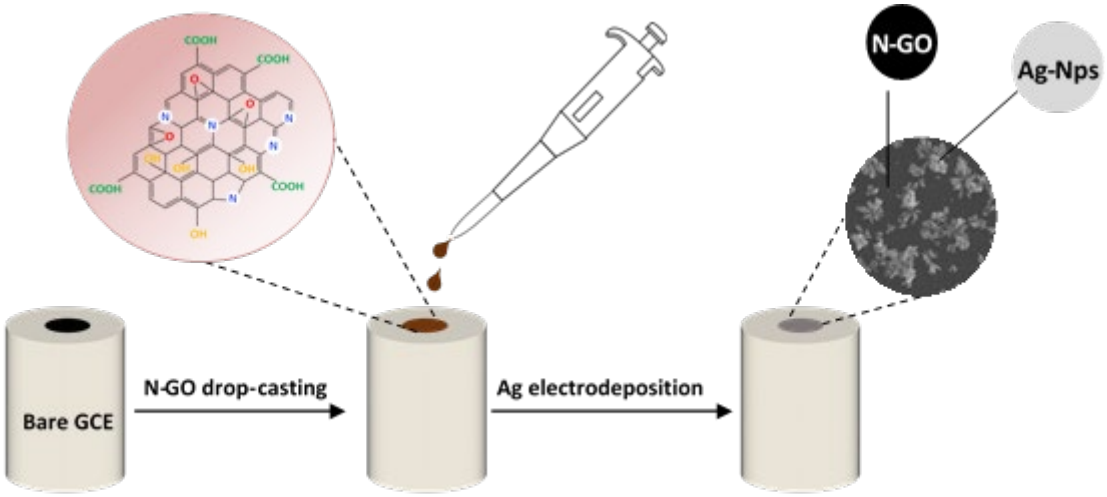

Fig 6.12: Ag-Nps/N-GO/GCE modified electrode preparation scheme

6.2.3 Results and discussion

6.2.3.1 N-GO characterization

The structural quality of N-GO nanosheets deposited on silicon substrate was analysed using Raman spectroscopy. The Raman spectrum shown in Fig 6.13a represents three vibrational modes i.e. defect mode around ~1334 cm^{-1} (D peak), vertical vibration mode around ~1576 cm^{-1} (G peak), and two-phonon vibration mode centred at ~2677 cm^{-1} (2D peak) [22]. The D peak forms due to the scattering of phonons at the boundary of the disordered hexagonal Brillouin zone; the G peak arises from the in-plane C-C stretching vibration under the E2g mode [21, 23].

The intensity ratio of D and G peaks i.e. I_D/I_G is generally ascribed to the defects in graphene. However, doping materials also contribute towards higher ratios of I_D/I_G [24, 25]. Similarly, in the present work, the N-GO indicated a relatively larger value of I_D/I_G, i.e. 0.91 [26]. According to the previous reports, this could be due to the non-hexagonal rings, functionalities, or heteroatom doping [27]. Thus, it could be interpreted that the functional groups and N-doping were responsible for a higher value of I_D/I_G. Li et al. [28] also observed that the N-doped

graphene produced a larger I_D/I_G ratio in comparison to pristine graphene. They ascribed this to the formation of sp^3-C in pyrrolic N-doped graphene consisting of five-atom heterocyclic ring.

The 2D peak is usually identified as the signature of graphene. The intensity ratio between 2D and G peaks i.e., I_{2D}/I_G and full width at half-maximum (FWHM) are usually related to the quantity of layers in graphene. The FWHM of ~50 cm^{-1} and I_{2D}/I_G values between 1 to 1.5 are commonly associated with the two layers of graphene [29, 30]. In the current work, the N-GO sample demonstrated FWHM and I_{2D}/I_G values of 68 cm^{-1} and 0.81 respectively, suggestive of multiple layers N-GO. Notably, the existence of N dopants in graphene can influence both peaks, i.e. D and 2D. N-doping enlarges the D peak on the one hand, and on the other hand, it increases the electron scattering rate, which lessens the intensity of the 2D peak. [30]. N-GO Raman spectra was compared with that of GO and rGO [31] given in the literature. The higher D peak in GO in comparison with rGO ruled out the reduction of the GO.

The SEM image of the N-GO sample deposited straightaway on a silicon substrate is displayed in Fig 6.13b. The horizontal films were not found in the image; however, the sample showed 3D islands similar to wrinkled-paper like structures spread across the surface of the substrate [21]. These islands consisted mainly of multilayered N-GO structures.

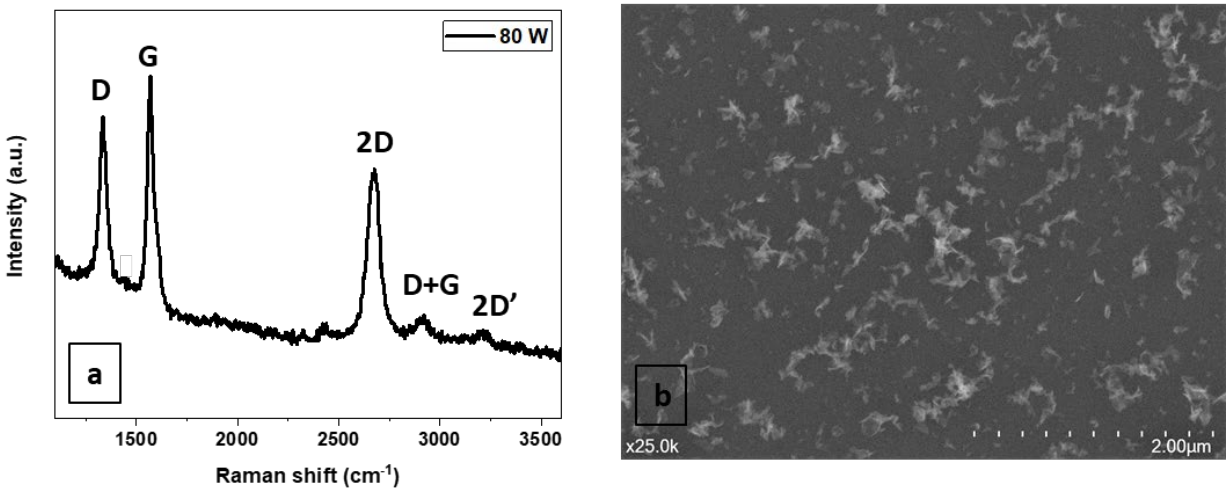

Fig 6.13: (a) Raman spectrum and (b) SEM image of N-GO sample

6.2.3.2 Electrode characterization

The surface morphology of the Ag-Nps/N-GO/GCE electrode was analysed using SEM, displayed in Fig 6.14a. Successful electrodeposition of Ag on N-GO can be observed in the images. The SEM image shows the uniformity in the distribution of Ag nanoparticles onto the N-GO/GCE electrode. The magnified image in the inset shows an aggregation of Ag-Nps, which is in good agreement with the previous reports [32, 33]. Furthermore, the presence of Ag as well as other elements, including carbon (C), oxygen (O), and nitrogen (N) which came from aniline was revealed through energy-dispersive X-ray spectroscopy (EDS). The EDS spectrum and elements percentages are delineated in Fig 6.14b.

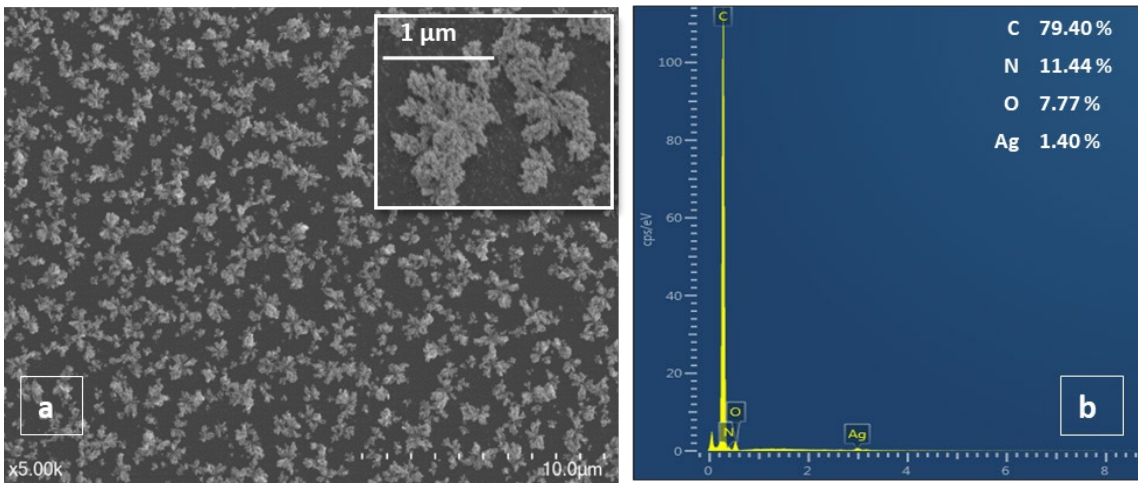

Fig 6.14: (a) SEM image (high resolution in inset) and (b) EDS of Ag-Nps/N-GO/GCE modified electrode

6.2.4 Electrochemical analysis of electrode

The electrochemical performance of the modified electrode was investigated using EIS. Fig 6.15 exhibits the Nyquist plots of bare, N-GO and Ag-Nps/N-GO modified GCE. The fitted Randles equivalent circuit is shown in the Fig 6.15 inset. The linear regions of plots at low frequencies implicate the diffusion process, whereas, semicircles at higher frequencies are associated with the electron-transfer reaction [34, 35]. The charge-transfer resistance (R_{ct}) of the bare GCE and the N-GO modified GCE was found to be 206 Ω and 1.2 kΩ, respectively, indicating the slow electron-transfer kinetics at the N-GO film surface. However, after electrodeposition of Ag-Nps on N-GO film, the R_{ct} of N-GO decreased significantly to ~653 Ω, which can be attributed to the high electrocatalytic activity of the Ag-Nps deposited at the surface of the electrode. High electrocatalytic activity of Ag-Nps is due to the large surface area, and outstanding electronic conductivity Moreover, the aggregated Ag-Nps possess porous network which facilitate the diffusion process [36].

CV was performed to investigate the electrochemical behaviour of the bare GCE, N-GO/GCE and Ag-Nps/NGO/GCE towards oxidation of 0.1 mM OA (Fig 6.16). There was an inadequate

response for OA oxidation from bare GCE, while N-GO/GCE exhibited a comparatively improved response. Noticeably, Ag-Nps/N-GO/GCE revealed a remarkable oxidation process, suggesting that Ag-Nps/N-GO/GCE considerably catalyses the OA oxidation response. It can be attributed to the synergistic effect of both Ag-Nps and N-GO. They possess excellent conductivity and enormous surface area, which can accelerate the electron-transfer kinetics and accommodate the OA molecules at the surface of the electrode [37].

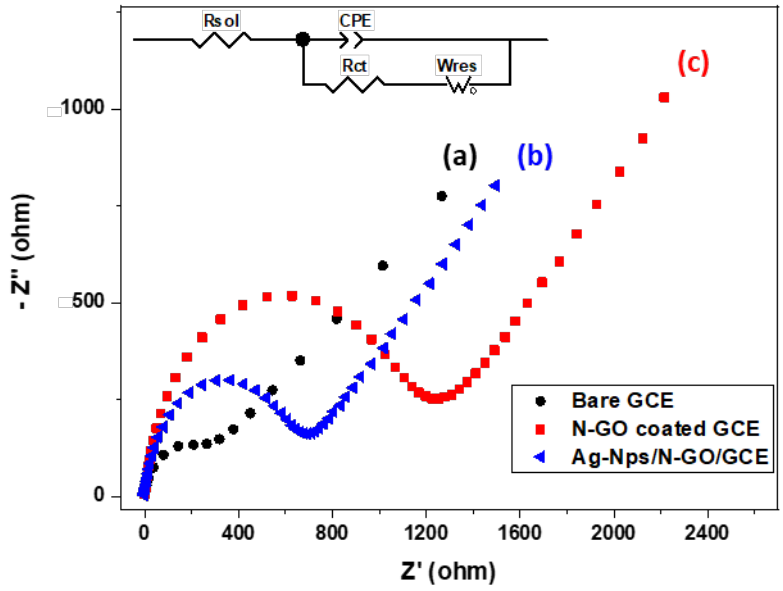

Fig 6.15: EIS spectra for (a) bare GCE (b) N-GO/GCE (c) Ag-Nps/N-GO/GCE in a solution of 0.1 M KCl and 5 mM $K_3[Fe(CN)_6]$ with the frequencies swept from 0.1 Hz to 100 kHz

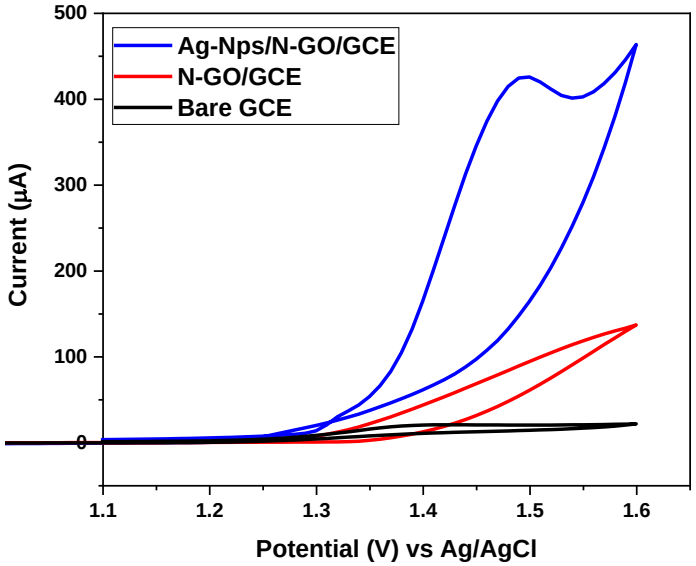

Fig 6.16: CVs of bare GCE, N-GO/GCE, and Ag-Nps/N-GO/GCE in 0.1 M PBS (pH 7) containing 0.1 mM OA, scan rate 50 mV/s

6.2.4.1 Amperometric detection of OA

Fig 6.17a exhibits the amperometric response of the Ag-Nps/N-GO/GCE on the successive addition of 2 µM to 300 µM OA into 0.1 M PBS (pH 7) stirred solution. An optimal potential of 1.2 V was used for the detection of OA owing to the highest signal-to-noise ratio. It can be observed that a fast and stable response could be obtained after each injection of OA. A calibration curve of OA concentration versus current response is displayed in Fig 6.17b. The plot shows that the Ag-Nps/N-GO/GCE can detect OA in the linear range of 10 – 300 µM; where the linear regression equation is $y = 0.0552x + 3.7385$ (R^2=0.9989). The sensor showed an excellent limit of detection of 2 µM. The commendable electroanalytical performance of the sensor can be ascribed to the combined catalytic activity of Ag-Nps and N-GO [38]. Table 6.1 shows the comparable results of the linear range and limit of detection with those of different OA sensors reported earlier.

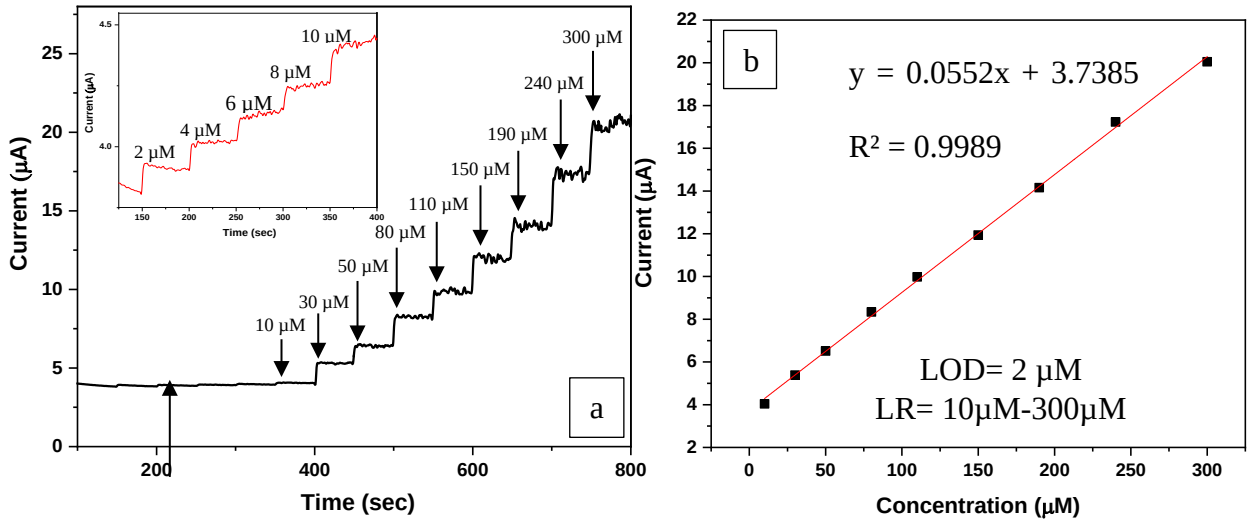

Fig 6.17: (a) Amperometric response of the Ag-Nps/N-GO/GCE in stirred 0.1 M PBS with sequential injections of OA at 1.2 V potential (b) Calibration curve showing OA current response against its concentration

Table 6.1: Comparison of the analytical performance of the electrochemical OA sensors

Electrode	Linear range	Detection limit	Reference
Porous silica-supported platinum nanoparticles/GCE	0 – 45 µM	25 nM	[3]
PdPt/GCE	10 – 4700 µM 4700 –11,800 µM	1 µM	[39]
Graphene/ Ag nanorods/GCE	3 – 30 mM	0.04 mM	[13]
Graphite/Ag/AgCl nanocomposite	10 µM – 0.75 mM	3.7 µM	[19]
Graphene aerogel	4 – 100 µM	0.8 µM	[15]
Palladium-doped mesoporous silica SBA-15 modified in carbon-paste electrode	10 – 140 µM	0.4 µM	[40]

PdAu-reduced graphene-ionic liquid/GCE	5–100 mM	2.7 mM	[18]
TiO_2 nanoparticle/MWCNT composite/GCE	0.1–1 mM, 1–100 mM	33 μM	[41]
Pt-Pd/chitosan/nitrogen doped graphene/GCE	1.5 – 500 μM	0.84 μM	[12]
Ag-doped ZSM-5 nanozeolites/CPE	16 μM – 0.18 mM and 0.18 –4.0 mM	5.5 μM	[9]
Ag-Nps/N-GO/GCE	10 – 300 μM	2 μM	This work

6.2.4.2 Reproducibility, repeatability and stability of the electrode

The reproducibility of the proposed sensor was studied by testing the current response of four Ag-Nps/N-GO/GCEs towards 0.1 mM OA. The relative standard deviation (RSD) was calculated to be 5.8%, which indicated reasonable reproducibility of the sensor. The RSD of four successive measurements of the current response at one Ag-Nps/N-GO/GCE in 0.1 mM OA solution was 3.4 %, indicating good repeatability behaviour of the proposed OA sensor. The stability tests of the sensor carried out in 0.1 mM OA after 1 and 2 weeks retained its performance and yielded 97 and 95 % respectively of the initial current values.

6.2.4.3 Interference study

The amperometric response of the Ag-Nps/N-GO/GCE electrode at an applied potential of 1.2 V was measured for 50 μM OA, followed by separate additions of 100 μM of ascorbic acid, 50 μM of glucose, and 50 μM uric acid into a stirred 0.1 M PBS solution. These interfering compounds were chosen because they are likely to coexist with OA in urine samples [1]. As

shown in Fig 6.18, a strong and fast current signal was observed at Ag/N-GO/GCE electrode after the injection of OA, however, there was on current response to ascorbic acid, glucose, and uric acid, which demonstrates the good selectivity of the proposed sensor. Additionally, again the prominent and immediate current response was detected upon the addition of 50 µM OA which can be seen at the final stage of the plot. This amperometry test demonstrates a satisfactory sensor-interference behaviour of the Ag-Nps/N-GO/GCE electrode.

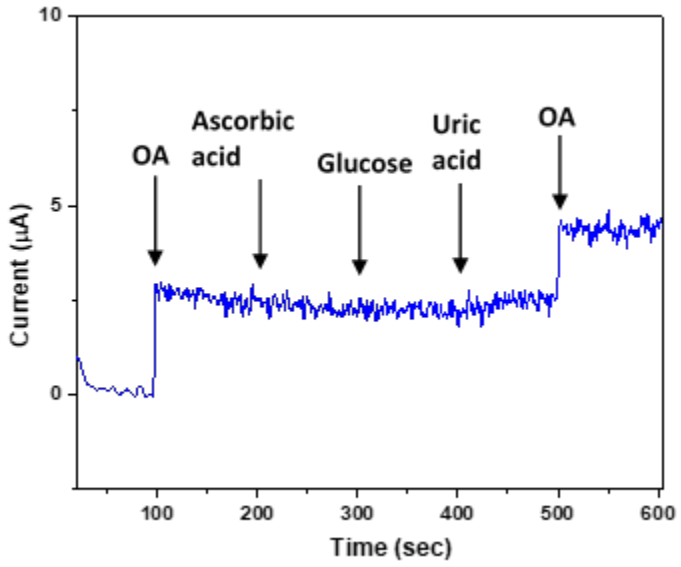

Fig 6.18: Amperometric response of Ag-Nps/N-GO/GCE towards OA (50 µM), ascorbic acid (100 µM), glucose (50 µM) and uric acid (100 µM) in 0.1 M PBS at 1.2 V

6.2.5 Conclusion

In a nutshell, the combination of Ag-Nps and N-GO for OA detection is a superior alternative to the particularly expensive metals modified electrodes. The first time usage of N-GO in this work, which was prepared through a single-step and rapid synthesis route, not only made the overall electrode preparation facile and quick but also enhanced the electrode sensing properties. Owing to the synergistic-effect of Ag-Nps and N-GO, the Ag-Nps/N-GO/GCE sensor showed a comparable linear range i.e. 10-300 µM and an excellent detection limit of 2

μM in an amperometric investigation. The admirable selectivity against ascorbic acid, glucose, and uric acid proves the superiority of the sensor. Attributed to the graphene inherent characteristics, remarkable repeatability and stability of the designed sensor have also been observed.

References

1. Mishra, P. and B.R. Bhat, *A study on the electro-reductive cycle of amino-functionalized graphene quantum dots immobilized on graphene oxide for amperometric determination of oxalic acid.* Microchimica Acta, 2019. **186**(9): p. 1-10.
2. Alizadeh, T., S. Nayeri, and N. Hamidi, *Graphitic carbon nitride (gC 3 N 4)/graphite nanocomposite as an extraordinarily sensitive sensor for sub-micromolar detection of oxalic acid in biological samples.* RSC Advances, 2019. **9**(23): p. 13096-13103.
3. Fang, Y., X. Xu, X. Guo, B. Cui, and L. Wang, *Simple and ultrasensitive electrochemical sensor for oxalic acid detection in real samples by one step co-electrodeposition strategy.* Analytical and Bioanalytical Chemistry, 2020. **412**(23): p. 5719-5727.
4. Zhai, Q.-Z., *Determination of trace amount of oxalic acid with zirconium (IV)–(DBS-arsenazo) by spectrophotometry.* Spectrochimica Acta Part A: Molecular and Biomolecular Spectroscopy, 2008. **71**(2): p. 332-335.
5. Kawamura, K., L.A. Barrie, and D. Toom-Sauntry, *Intercomparison of the measurements of oxalic acid in aerosols by gas chromatography and ion chromatography.* Atmospheric environment, 2010. **44**(39): p. 5316-5319.
6. Zhang, Y., C. Wu, J. Zhang, and S. Guo, *Mass transport effect on graphene based enzyme electrochemical biosensor for oxalic acid detection.* Journal of The Electrochemical Society, 2016. **164**(2): p. B29.

7. Rostami, S., S.N. Azizi, and S. Ghasemi, *Preparation of an efficient electrocatalyst for oxalic acid oxidation based on Ag-doped ZSM-5 nanozeolites synthesized from bagasse.* Journal of Electroanalytical Chemistry, 2017. **788**: p. 235-245.

8. Sharma, P., S. Radhakrishnan, S.S. Jayaseelan, and B.S. Kim, *Non-enzymatic Electrochemical Oxidation Based on AuNP/PPy/rGO Nanohybrid Modified Glassy Carbon Electrode as a Sensing Platform for Oxalic Acid.* Electroanalysis, 2016. **28**(10): p. 2626-2632.

9. Liu, Y., J. Huang, D. Wang, H. Hou, and T. You, *Electrochemical determination of oxalic acid using palladium nanoparticle-loaded carbon nanofiber modified electrode.* Analytical Methods, 2010. **2**(7): p. 855-859.

10. Luo, X., L. Chen, J. Yang, S. Li, M. Li, Q. Mo, Y. Li, and X. Li, *Electrochemically simultaneous detection of ascorbic acid, sulfite and oxalic acid on Pt-Pd nanoparticles/chitosan/nitrogen doped graphene modified glassy carbon electrode: A method for drug quality control.* Microchemical Journal, 2021. **169**: p. 106623.

11. Nagarajan, R.D. and A.K. Sundramoorthy, *One-pot electrosynthesis of silver nanorods/graphene nanocomposite using 4-sulphocalix [4] arene for selective detection of oxalic acid.* Sensors and Actuators B: Chemical, 2019. **301**: p. 127132.

12. Kesavan, L., A.M. Kalekar, P. Damlin, and C. Kvarnström, *Reduced graphene oxide supported palladium nano-shapes for electro-oxidation of oxalic acid.* Journal of Electroanalytical Chemistry, 2019. **847**: p. 113167.

13. Liu, D., Y. Wang, and G. Zhao, *Preparation of graphene aerogel for determining oxalic acid.* Int. J. Electrochem. Sci, 2015. **10**: p. 6794-6802.

14. Wang, X., Y. Cheng, Z. You, H. Sha, S. Gong, J. Liu, and W. Sun, *Sensitive electrochemical determination of oxalic acid in spinach samples by a graphene-modified carbon ionic liquid electrode.* Ionics, 2015. **21**(3): p. 877-884.

15. Chen, X., Z. Cai, Z. Huang, M. Oyama, Y. Jiang, and X. Chen, *Non-enzymatic oxalic acid sensor using platinum nanoparticles modified on graphene nanosheets.* Nanoscale, 2013. **5**(13): p. 5779-5783.

16. Shang, L., F. Zhao, and B. Zeng, *Electrodeposition of PdAu alloy nanoparticles on ionic liquid functionalized graphene film for the voltammetric determination of oxalic acid.* Electroanalysis, 2013. **25**(2): p. 453-459.

17. Alizadeh, T. and S. Nayeri, *Graphite/Ag/AgCl nanocomposite as a new and highly efficient electrocatalyst for selective electroxidation of oxalic acid and its assay in real samples.* Materials Science and Engineering: C, 2019. **100**: p. 826-836.

18. Abdi, G., A. Alizadeh, J. Amirian, S. Rezaei, and G. Sharma, *Polyamine-modified magnetic graphene oxide surface: feasible adsorbent for removal of dyes.* Journal of Molecular Liquids, 2019. **289**: p. 111118.

19. Zafar, M.A., O.K. Varghese, F.C. Robles Hernandez, Y. Liu, and M.V. Jacob, *Single-Step Synthesis of Nitrogen-Doped Graphene Oxide from Aniline at Ambient Conditions.* ACS Applied Materials & Interfaces, 2022. **14**(4): p. 5797-5806.

20. Liu, B., C.-M. Yang, Z. Liu, and C.-S. Lai, *N-doped graphene with low intrinsic defect densities via a solid source doping technique.* Nanomaterials, 2017. **7**(10): p. 302.

21. Xie, B., Y. Chen, M. Yu, X. Shen, H. Lei, T. Xie, Y. Zhang, and Y. Wu, *Carboxyl-assisted synthesis of nitrogen-doped graphene sheets for supercapacitor applications.* Nanoscale research letters, 2015. **10**(1): p. 332.

22. Zafar, M.A., O.K. Varghese, F.C. Robles Hernandez, Y. Liu, and M.V. Jacob, *Single-Step Synthesis of Nitrogen-Doped Graphene Oxide from Aniline at Ambient Conditions.* ACS Applied Materials & Interfaces, 2022.

23. Al-Jumaili, A., M.A. Zafar, K. Bazaka, J. Weerasinghe, and M.V. Jacob, *Bactericidal Vertically Aligned Graphene Networks Derived from Renewable Precursor.* Carbon Trends, 2022: p. 100157.

24. Tao, H., C. Yan, A.W. Robertson, Y. Gao, J. Ding, Y. Zhang, T. Ma, and Z. Sun, *N-Doping of graphene oxide at low temperature for the oxygen reduction reaction.* Chemical Communications, 2017. **53**(5): p. 873-876.

25. Wang, M. and Y. Ma, *Nitrogen-doped graphene forests as electrodes for high-performance wearable supercapacitors.* Electrochimica Acta, 2017. **250**: p. 320-326.

26. Roscher, S., R. Hoffmann, and O. Ambacher, *Determination of the graphene–graphite ratio of graphene powder by Raman 2D band symmetry analysis.* Analytical methods, 2019. **11**(9): p. 1224-1228.

27. Li, D., X. Duan, H. Sun, J. Kang, H. Zhang, M.O. Tade, and S. Wang, *Facile synthesis of nitrogen-doped graphene via low-temperature pyrolysis: the effects of precursors and annealing ambience on metal-free catalytic oxidation.* Carbon, 2017. **115**: p. 649-658.

28. Li, J., X. Li, P. Zhao, D.Y. Lei, W. Li, J. Bai, Z. Ren, and X. Xu, *Searching for magnetism in pyrrolic N-doped graphene synthesized via hydrothermal reaction.* Carbon, 2015. **84**: p. 460-468.

29. Rufino, F.C., A.M. Pascon, L.C.J. Espindola, F.H. Cioldin, D.R.G. Larrudé, and J.A. Diniz, *Definition of CVD Graphene Micro Ribbons with Lithography and Oxygen Plasma Ashing.* Carbon Trends, 2021. **4**: p. 100056.

30. Hao, Y., Y. Wang, L. Wang, Z. Ni, Z. Wang, R. Wang, C.K. Koo, Z. Shen, and J.T. Thong, *Probing layer number and stacking order of few-layer graphene by Raman spectroscopy.* small, 2010. **6**(2): p. 195-200.

31. Boas, C.R.S.V., B. Focassio, E. Marinho, D.G. Larrude, M.C. Salvadori, C.R. Leão, and D.J. Dos Santos, *Characterization of nitrogen doped graphene bilayers synthesized by fast, low temperature microwave plasma-enhanced chemical vapour deposition.* Scientific reports, 2019. **9**(1): p. 1-12.

32. Aditya, T., A.K. Nayak, D. Pradhan, A. Pal, and T. Pal, *Fabrication of MoS2 decorated reduced graphene oxide sheets from solid Mo-precursor for electrocatalytic hydrogen evolution reaction.* Electrochimica Acta, 2019. **313**: p. 341-351.

33. Basile, A., A.I. Bhatt, A.P. O'Mullane, and S.K. Bhargava, *An investigation of silver electrodeposition from ionic liquids: Influence of atmospheric water uptake on the silver electrodeposition mechanism and film morphology.* Electrochimica acta, 2011. **56**(7): p. 2895-2905.

34. Moozarm Nia, P., F. Lorestani, W.P. Meng, and Y. Alias, *A novel non-enzymatic H2O2 sensor based on polypyrrole nanofibers–silver nanoparticles decorated reduced graphene oxide nano composites.* Applied Surface Science, 2015. **332**: p. 648-656.

35. Mayedwa, N., N. Mongwaketsi, S. Khamlich, K. Kaviyarasu, N. Matinise, and M. Maaza, *Green synthesis of nickel oxide, palladium and palladium oxide synthesized via Aspalathus linearis natural extracts: physical properties & mechanism of formation.* Applied Surface Science, 2018. **446**: p. 266-272.

36. Rostami, M., G. Abdi, S.H. Kazemi, and A. Alizadeh, *Nanocomposite of magnetic nanoparticles/graphene oxide decorated with acetic acid moieties on glassy carbon electrode: A facile method to detect nitrite concentration.* Journal of Electroanalytical Chemistry, 2019. **847**: p. 113239.

37. Yuan, L., L. Jiang, T. Zhang, G. Wang, S. Wang, X. Bao, and G. Sun, *Electrochemically synthesized freestanding 3D nanoporous silver electrode with high electrocatalytic activity.* Catalysis Science & Technology, 2016. **6**(19): p. 7163-7171.

38. Li, J., D. Kuang, Y. Feng, F. Zhang, Z. Xu, M. Liu, and D. Wang, *Green synthesis of silver nanoparticles–graphene oxide nanocomposite and its application in electrochemical sensing oftryptophan.* Biosensors and Bioelectronics, 2013. **42**: p. 198-206.

39. Wang, H., H. Wang, T. Li, J. Ma, K. Li, and X. Zuo, *Silver nanoparticles selectively deposited on graphene-colloidal carbon sphere composites and their application for hydrogen peroxide sensing.* Sensors and Actuators B: Chemical, 2017. **239**: p. 1205-1212.

40. Dodevska, T. and I. Shterev, *Electrochemical non-enzymatic sensing of oxalic acid based on PdPt-modified electrodes: application to the analysis of vegetable samples.* Monatshefte für Chemie-Chemical Monthly, 2020. **151**(4): p. 495-504.

41. Raoof, J.B., F. Chekin, and V. Ehsani, *Palladium-doped mesoporous silica SBA-15 modified in carbon-paste electrode as a sensitive voltammetric sensor for detection of oxalic acid.* Sensors and Actuators B: Chemical, 2015. **207**: p. 291-296.

42. Fakhari, A.R., B. Rafiee, H. Ahmar, and A. Bagheri, *Electrocatalytic determination of oxalic acid by TiO 2 nanoparticles/multiwalled carbon nanotubes modified electrode.* Analytical Methods, 2012. **4**(10): p. 3314-3319.

Chapter 7: Conclusion

Green synthesis of graphene and graphene-based materials has been recognized as an essential part of the research to address nanotechnology and the environmental worries. In the modern nanomaterials synthesis technique, atmospheric pressure microwave plasma is suitable for producing nanomaterials at ambient conditions and does not require high heating and vacuuming. However, this technique has not been explored for sustainable synthesis, especially pertaining to renewable, cheap, and abundant feedstock. This project was designed to synthesize graphene, nitrogen-doped graphene oxide, and graphene-Ag nanocomposite from sustainable precursors in a chemical-free environment quickly and at a reduced cost. Moreover, it aimed at demonstrating the electrocatalytic properties of as-synthesized nanostructures.

7.1 Synthesis of graphene

Two separate plant extracts, namely tea tree and tangerine peel, were used to demonstrate the viability of synthesizing graphene from sustainable sources. The synthesis was carried out in atmospheric-pressure microwave plasma at a considerably low microwave power of 200 W. The confirmation of the formation of graphene was made through Raman, XPS, XRD, and TEM. The graphene nanosheets were mainly composed of sp^2-hybridized carbon atoms having typical graphene structure and morphology with mild inclusions of oxygen functional groups. The tea tree derived-graphene, employed in diuron herbicide sensing performance displayed a linear range from 20 to 1000 μM, and a limit of detection of 5 μM. The tangerine peel derived-graphene used in a chemiresistive sensor presented great sensitivity for the vapours of herbicide, insecticide, and ethanol.

7.2 Synthesis of nitrogen-doped graphene oxide

N-GO was synthesized from aniline in a single-step using atmospheric pressure microwave plasma. Aniline worked as a single source of carbon and nitrogen. Microwave power as low as 80 W effectively dissociated aniline vapors into N-GO nanosheets and deposited them on the walls of the quartz tube. The Raman spectrum showed I_{2D}/I_G and FWHM (2D peak) values of 1.04 and 64 cm^{-1} respectively, which were suggestive of the multiple layers of N-GO sheets. The XPS spectra of the 80 W sample displayed more than 3 % of nitrogen present in the graphene structure. Moreover, the N-GO-coated polyamine membrane employed in a water desalination application showed notable algicidal and anti-scaling activities without affecting the water flux rate.

N-GO in composite with Ag nanoparticles was also used for the electrochemical detection of oxalic acid. Our findings exhibited a superior linear range (i.e. 10 to 300 μM) and limit of detection (i.e. 2 μM).

7.3 Synthesis of graphene-Ag nanocomposite

The feasibility of synthesis of graphene-metal nanocomposite in microwave plasma is shown in this work. The nanocomposite was synthesized by dissociating the vapours of tea tree extract and $AgNO_3$ solution inside the plasma reactor. The formed nanocomposite was characterized by XRD, which showed signature peaks related to the graphene and Ag materials. The OES spectrum was recorded during the different stages of synthesis, which displayed different atomic and molecular bands. It included C_2, Ar, N, and Ag species. A strong interaction between graphene and Ag NPs was depicted in XPS spectrum, which showed a slight shift of Ag-doublet (Ag $3d_{5/2}$ and Ag $3d_{3/2}$) towards lower binding energies. The TEM images also confirmed a good embedment of Ag NPs with the graphene nanosheets. Interestingly, the

concentration of $AgNO_3$ played a pivotal role in the determination of the size and aggregation of Ag NPs. The $AgNO_3$ concentration of 0.1 M was proposed as an optimum value for well-dispersed and nano-size Ag NPs. The usage of graphene-Ag nanocomposite in the electrochemical detection of toxic methyl paraben exhibited a limit of detection of 2.5 µM and a linear range of 20 to 260 µM, which are superior to some of the results reported earlier.

7.4 Overall conclusion

In summary, this project addressed the rising concerns regarding the sustainability and excessive consumption of the resources for graphene synthesis. The alternative route implemented in this thesis for the synthesis of pristine graphene used natural resources such as tea tree and tangerine peel oil at ambient conditions (atmospheric pressure and no external heating). Though Microwave Source requires larger electric power, the total power requirement is relatively very small since the graphene is formed in few seconds. The rate of graphene fabrication is relatively higher, and is possible to manufacture commercial scale graphene using the sustainable sources, and the microwave plasma. This study also delineated the fast synthesis of graphene-Ag nanocomposite in atmospheric pressure microwave plasma to circumvent the previous approaches involving toxic chemicals and low production rates varying from hours to days. Furthermore, this work includes nitrogen-doped graphene oxide (N-GO) synthesis at microwave power ten times lower than the prior studies, without employing gas sources or toxic chemicals for nitrogen doping. Overall the project contributes significantly towards the development of nanomaterials using environmentally benign sources and techniques very fast, and at commercially appreciable scale.

7.5 Recommendations for future work

The reported synthesis method opened the door for an energy-efficient, environmentally friendly, and quick synthesis of graphene, and the generated graphene and graphene-based products exhibited equivalent features to any other graphene, synthesized by other approaches. However, following recommendations and future works could be additional advantages in this field:

- The production rate is an important factor in the industrialization of the process. Thus, it is important to scale up the setup for the high production of graphene. Moreover, investigate the effect of process parameters on the production rate.

- Single-layer graphene is highly desirable but very challenging to produce. Very few works in the past have reported the synthesis of single-layer graphene. It should be studied how atmospheric pressure microwave plasma can be used for a single-layer production of graphene.

- Similar to nitrogen doping of graphene in this work, doping with other heteroatoms such as boron, phosphorus, etc. should also be investigated. The process should be less energy intensive as shown for the synthesis of N-GO in this work.

- Even though aniline serves as the material's primary supply of nitrogen during the creation of N-GO, the amount of nitrogen that comes from the atmosphere should also be investigated.

- This study has shown only Ag metal nanocomposite with graphene. The possibility of synthesis with other metals such as Zn, Cu, etc. should be examined. Moreover, the

feasibility of the synthesis of bi or tri-metallic-graphene nanocomposite should be probed.

- Plant-derived graphene is a promising nanomaterial for a wide range of additional applications, including supercapacitors, antimicrobial and anticorrosion coatings. The scope will extend in the future as the research of these applications is expanded.